ESA STUDY CONTRACT REPORT

No ESA Study Contract Report will be accepted unless this sheet is inserted at the beginning of each volume of the Report

ESA CONTRACT	**SUBJECT**	**CONTRACTOR**
No 20678/07/NL/HE	**Assessment of Vegetation Photosynthesis through Observation of Solar Induced Fluorescence from Space**	**UNIVERSITY OF BOLOGNA**

*** ESA CR ( ) No**	**No of Volumes: 1** **This is volume No: 1**	**CONTRACTOR'S REFERENCE** **UNI-3540-NT-7512**

ABSTRACT:

Final report: Assessment of Vegetation Photosynthesis through Observation of Solar Induced Fluorescence from Space

The absorption of solar energy by chlorophyll in green leaves is known to be the primary process leading to vegetation photosynthesis and primary production, to carbon sequestration and, ultimately, to life on Earth. Whilst most of the absorbed energy is used in photosynthetic processes or dissipated as heat, a variable fraction is re-emitted by chlorophyll molecules at longer wavelengths, in a process known as chlorophyll fluorescence, which can be detected by advanced remote sensing techniques. Of particular relevance is the fluorescence emitted by Photosystem II (PSII), which is known to compete dynamically with photosynthetic electron transport.

Although the potential of Photosystem II (PSII) chlorophyll fluorescence as a probe of photosynthetic processes has been widely demonstrated over the last decades, the attention has generally focused on active manipulative ("pulse-saturated") techniques which are not amenable to satellite remote sensing. Recent studies, however, have demonstrated the potential of passive remote sensing techniques for the detection of solar-induced chlorophyll fluorescence (SIF) from the signal in and around the two main oxygen absorption bands (O2-A and O¬2-B), paving the way for the application of the technique to airborne and satellite remote sensing. A model of fluorescence emission and its relationship with photosynthetic processes at the leaf and canopy level (FLUORMOD) had also been developed as part of a previous project by the European Space Agency, although its applicability was limited to ideal conditions, making it unsuitable for the analysis of vegetation processes under ambient conditions.

The aim of the current project was (i) the further development of models available for the interpretation of vegetation SIF and (ii) their application over a range of vegetation types and conditions in order to demonstrate the potential of fluorescence remote sensing as a constraint for existing models of vegetation primary production.

The techniques and problems associated with the remote sensing of chlorophyll fluorescence have been first reviewed, including the confounding effects of changes in chlorophyll content; methodologies for the concurrent remote sensing of chlorophyll content have also been analyzed. Novel methods for the disentanglement of PSII fluorescence from the fluorescence signal from Photosystem I have also been developed, based on the analysis of SIF in the two main oxygen absorption bands (O2-A and O¬2-B).

Two novel algorithms have been developed for the interpretation of the solar-induced

fluorescence signal that can be measured from airborne and satellite platforms, greatly refining the previous formulation implemented in the FLUORMOD model. The proposed algorithms differ in their degree of empiricism, and manage to provide a representation that is coherent with state-of-the-art models of pulse-saturated fluorescence and leaf gas exchange. The two algorithms have been tested against detailed measurements at the leaf level under controlled conditions, demonstrating a strong and non trivial relationship between fluorescence and photochemical yield.

According to both models, the relationship between fluorescence yield and photochemical yield is not monotonic, differing under light- (negative association) or CO2-limited conditions (positive association), thus providing an elegant explanation for the contrasting results reported in the literature. Because of the parallel effects of light absorption on both processes, however, a general positive association between leaf photosynthesis and fluorescence radiance is predicted; according to the most refined model, moreover, leaf biochemistry is predicted to affect the relationship only marginally, suggesting SIF also as a general semi-empirical tool for the assessment of photosynthetic rates.

In order to scale-up the new understanding to the regional level, a novel canopy-level model of vegetation energy transfer, chlorophyll fluorescence and photosynthesis has been developed, extending the work carried under past projects and making it possible to explore the relationship between canopy fluorescence radiance and gross primary production (GPP) expected on the basis of the two leaf-level algorithms mentioned above.

Apart from the inclusion of a state-of-the-art representation of physiological and ecological processes, the newly developed SCOPE model also includes a detailed representation of thermal energy transfer and canopy TIR radiance.

A sensitivity analysis of the model has been carried out for three different vegetation types (agricultural crops, deciduous forests, evergreen coniferous forests) under different environmental conditions, making it possible to explore the generality of model predictions.

Simulations based on the two alternative leaf-level algorithms both predict a strong sensitivity of canopy fluorescence radiance to incoming radiation and the fraction of absorbed radiation, as determined by leaf area index and chlorophyll content; the fluorescence signal is also reduced under mild stress conditions, demonstrating its potential as an early indicator of stress. More interestingly, a strong relationship is predicted between canopy fluorescence and gross primary production, consistent with canopy-level observations from parallel field campaigns. Simulations based on the most advanced leaf-level algorithm predict a quasi-linear relationship between canopy SIF and GPP, which is largely insensitive to vegetation type and photosynthetic potentials. The SIF signal appears to be highly sensitive to changes in GPP (in response to chlorophyll content, LAI and light absorption, environmental conditions and photosynthetic potentials), demonstrating its suitability as a tool for the quantitative measurement of GPP from space. Modelling results appear to be consistent with experimental results from parallel field campaign, both in qualitative and in quantitative terms.

The implications of the analysis are finally discussed, and novel model advancements and applications are proposed, in combination with new experiments needed for a further quantitative test of the model at the canopy scale.

The work described in this report was done under ESA Contract. Responsibility for the contents resides in the author or organization that prepared it.	
Names of the authors:	
** NAME OF ESA STUDY MANAGER DIV: DIRECTORATE	** ESA BUDGET HEADING

* Sections to be completed by ESA

** Information to be provided by ESA Study Manager

Assessment of Vegetation Photosynthesis through Observation of Solar Induced Fluorescence from Space

Final Report

For the attention of: Mr Matthias DRUSCH – ESA contract officer

	Function	Name	Signature	Date
Prepared by	Consortium	Albert OLIOSO *(INRA, France)* Jérôme DEMARTY (*INRA, France)* Vincent GERMAIN *(NOVELTIS, France)* Wout VERHOEF *(NLR, The Netherlands)* Ismaël MOYA *(CNRS-LMD, France)* Yves GOULAS *(CNRS-LMD, France)* Giovanna CECCHI *(CNR-IFAC, Italy)* Giovanni AGATI *(CNR-IFAC, Italy)* Pablo ZARCO-TEJADA *(IAS-CSIC, Spain)* Gina MOHAMMED *(P&M Technologies, Canada)* Christiaan van der Tol *(ITC, The Netherlands)*		10/07/2009
Approved by	Project Manager	Federico MAGNANI *(DCA, University of Bologna, Italy)*		10/07/2009

ALMA MATER STUDIORUM - Università di Bologna
Via Zamboni, 33 - 40126 Bologna – Italy –
www.unibo.it

Indexing form

Customer	**ESA**	**Contract N°**	**20678/07/NL/HE**

Confidentiality codes				**Document management**	
Company / Programme		Defence			
Non-protected	☐	Non-protected	☒	None	☐
Reserved	☒	Limited diffusion	☐	Internal	☒
Confidential	☐	Defence confidentiality	☐	Customer	☐

Contractual document	**Project N°**	**Work Package**
Yes ☒ No ☐	3540	-

Assessment of Vegetation Photosynthesis through Observation of Solar Induced Fluorescence from Space

Final Report

Summary

Document			
File name	UNI-3540-NT-7512.doc	Nbr of pages	256
Project	-	Nbr of tables	23
Software	Microsoft Office Word	Nbr of figures	94
Language	English	Nbr of appendices	6

Document reference					
Internal	UNI-3540-NT-7512	Issue	1	Date	10/07/2009
External	-	Revision	0	Date	10/07/2009

Auteur(s)	**Approved by**
Consortium+ Christiaan van der Tol (ITC, The Netherlands) Jerome Demarty (INRA, France)	Federico MAGNANI

Distribution list

INTERNAL	EXTERNAL	
Name	**Name**	**Company / Organisation**
Documentation NOVELTIS	Matthias DRUSCH	ESA
Richard BRU	Albert OLIOSO	INRA, France
Vincent GERMAIN	Wout VERHOEF	NLR, The Netherlands
Frédérique PONCHAUT	Ismaël MOYA	CNRS-LMD, France
	Giovanna CECCHI	CNR-IFAC, Italy
	Giovanni AGATI	CNR-IFAC, Italy
	Pablo ZARCO-TEJADA	IAS-CSIC, Spain
	Gina MOHAMMED	P&M Technologies, Canada
	Yves GOULAS	CNRS-LMD, France

Document status

Assessment of Vegetation Photosynthesis through Observation of Solar Induced Fluorescence from Space Final Report			
Issue	**Revision**	**Date**	**Reason for the revision**
1	0	10/07/2009	Initial version
1	1	24/08/2009	Changes and corrections requested by the Agency

Acronyms

C	Carbon
C_{a+b}	chlorophyll *a+b*
CASI	*Compact Airborne Spectrographic Imager*
DVMs	Dynamic Vegetation Models
fAPAR	fraction of absorbed radiation
FI	fluorescence induction
GPP	gross primary production
LAI	leaf area index
NIR	Near Infra Red
PSII	Photosystem I (PSI) Photosystem II
ROSIS	*Reflective Optics System Imaging Spectrometer*
SIF	solar-induced fluorescence
SVAT	Soil-Vegetation-Atmosphere Transfer
TBM	Terrestrial Biogeochemical Models
VIS	Visible

Table of contents

Table of figures

fluorescence (E-F) matrix. In the present version of the SCOPE model, the E-F matrix is fixed so that fluorescence spectra could consistently deviate from field measurements. This matrix in turn depends strongly on leaf chlorophyll content and energy partioning. This can be modelled with the simple leaf model Fluspect, which uses doubling to calculate leaf optical properties; although the Fluspect model makes simple assumptions about absolute fluorescence values, it could be combined in the future with the SCOPE model. 200

Table of tables

1. INTRODUCTION

1.1. Background and approach

The increase in atmospheric CO_2 due to anthropogenic emissions, and the corresponding global warming and associated Climate Change, are known to be partly countered by the active C sequestration by natural vegetation and (to a lesser extent) agricultural crops. As an example, temperate and boreal forests in the Northern Hemisphere alone cover an area of about 2×10^7 km^2 and act as a substantial C sink (0.6-0.7 Pg C yr^{-1})(Goodale *et al.* 2002). At the European level, terrestrial vegetation is thought to absorb 7-12 % of total anthropogenic C emissions (Janssens *et al.* 2003). Far from being in equilibrium with the atmosphere, natural ecosystems absorb annually as a result of photosynthetic processes more C than is then re-emitted by plant respiration and the decomposition of plant residues (Schimel *et al.* 2001). It is therefore clear that the quantitative assessment of the contribution of photosynthetic processes to the global C balance is an important pre-requisite for the understanding of the impact of anthropogenic activities (Intergovernmental Panel on Climate Change2001).

Carbon sequestration by terrestrial ecosystems is currently investigated through an array of techniques. The inversion of atmospheric models provides a coarse picture at the continental scale (Schimel *et al.* 2001), whilst detailed information on individual ecosystems is gained from eddy-covariance measurements at a number of experimental sites across the world, as part of the FLUXNET network (Baldocchi *et al.* 2001). However, both techniques fail to provide a detailed representation of the mosaic of vegetation types and conditions encountered in the real world. New observational techniques are urgently needed to provide a link between atmospheric CO_2 observations (too broad a picture) and the detailed information on ecosystem functioning coming from experimental sites (too small footprint), through the direct measurement of land photosynthetic processes at representative regional to global scales.

The prediction of the response of vegetation to future atmospheric CO_2 and climate is also crucial for the reliable prediction of Climate Change over the next century: not only is it unsure if vegetation will continue to subtract CO_2 from the atmosphere at present rates; changes in vegetation composition and structure could also have a profound effect on surface albedo and transpirational cooling, with important feed-backs on global circulation and climate.

Mathematical models are the only tool available for the prediction of such a long-term response. Models incorporating the best available knowledge about physiological and ecological short-term processes are currently used with good success for the representation of ecosystem gas exchange (Kramer *et al.* 2002; Morales *et al.* 2005); these SVAT (Soil-Vegetation-Atmosphere Transfer) or TBM (Terrestrial Biogeochemical Models) models have been widely tested against aggregated ecosystem scalar fluxes as measured by the eddy-covariance technique over wide network experimental sites (Aubinet *et al.* 2000; Baldocchi *et al.* 2001). The amount of detail needed for their parameterisation, however, makes their large-scale application difficult.

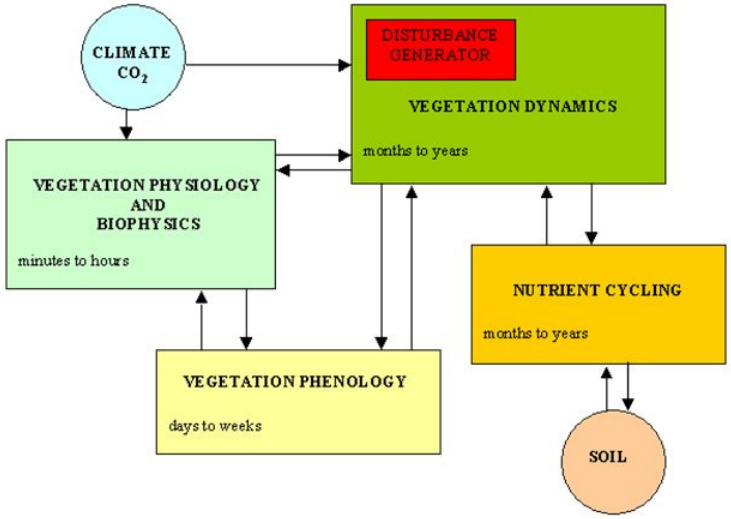

Figure 1-1. Flux diagram of a Dynamic Vegetation Model (DVM), including both short- and long-term vegetation dynamics and Carbon exchange with the atmosphere.

Other models are widely applied, often in combination with GCMs, for the representation of vegetation processes at this scale and over long periods (decades to millennia). These Dynamic Vegetation Models (DVMs) often combine a coarser representation of physiological detail with the inclusion of other ecological processes (soil dynamics, fire and disturbance, allocation …) which cannot be neglected at this time scale (Cramer *et al.* 1999; Krinner *et al.* 2005). The parameters required for these simulations are often computed internally by the model itself, through a long-term initialisation to steady-state conditions; increasingly, though, Earth-observation (EO) techniques are being used in order to reduce the uncertainties related to this initialisation process, by forcing the model with a picture of the current status of vegetation. The information retrieved by EO techniques, though, is commonly limited to the assessment of leaf area index (LAI) and of the fraction of absorbed radiation (fAPAR) that can be derived from broad-band sensors (Lawrence *et al.* 2004).

Novel advances in quantitative remote sensing, however, pave the way for the estimation of a broad new set of DVM parameters from space. In particular, an improved parameterisation of photosynthetic processes could be derived from the measurement from space of chlorophyll fluorescence.

1.1.1. Chlorophyll fluorescence as a new tool to monitor photosynthetic processes

Until now, most of the information that has been acquired by remote sensing of the Earth surface about vegetation conditions has come from reflected light in the solar domain. There is, however, one additional source of information about vegetation photosynthetic processes and gross primary production (GPP) in the optical and near-infrared wavelength range that has not yet been exploited by any satellite mission, related to the emission of fluorescence from the chlorophyll of assimilating leaves.

The fate of energy absorbed by the leaf is described in Figure 1-2. . Part of the energy absorbed by chlorophyll is not used for carbon fixation, but re-emitted at longer wavelengths as fluorescence (Govindjee 1995; Papageorgiou *et al.* 2006). Under conditions of excess light, an even larger fraction of the absorbed light is re-emitted by the plant as heat (Demmig-Adams *et al.* 2000), through the action of leaf xanthophylls and the induction of conformational changes in the pigment bed.

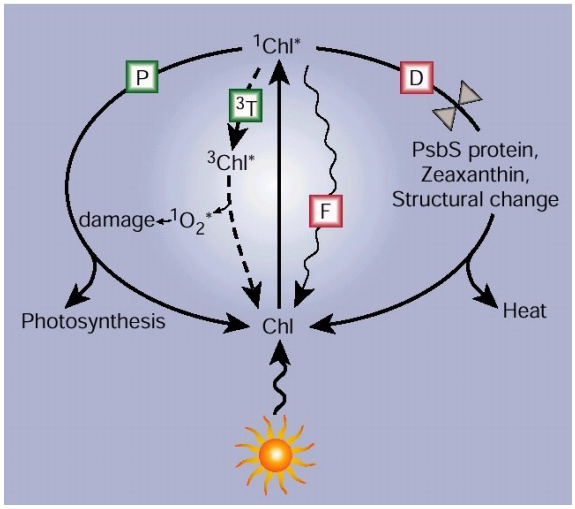

Figure 1-2. Role of chlorophyll fluorescence (F) and heat conversion (as a result of xanthophyll de-epoxidation and structural changes; D) in the dissipation of excess energy under conditions of high light or when photochemical processes (P) are impaired by stomatal limitations. Both mechanisms contribute to the prevention of the formation of chlorophyll triplets (^{3}T), which could have damaging effects on the photosynthetic apparatus.

Since the three processes (photochemistry leading to photosynthesis, fluorescence and thermal dissipation) compete against each other, the knowledge of any of them could provide precious information on the other, provided the third factor is also known (or can be neglected).

For this reason, most studies have focused until recently on a manipulative approach, known as the fluorescence induction (FI) technique (Lazar 1999). In the FI technique, photochemical processes are temporarily switched off by a saturating pulse of light, reducing the system to two components only; a robust interpretative model has long existed for this simplified system (Genty *et al.* 1989b; Kramer *et al.* 2004; Zhu *et al.* 2005).

Natural fluorescence has also been measured in laboratory studies and in the field by the laser induction technique (Rosema *et al.* 1992; Valentini *et al.* 1994; Flexas *et al.* 2000; Ananyev *et al.* 2005), but the use of active techniques in observations from space has serious technological difficulties.

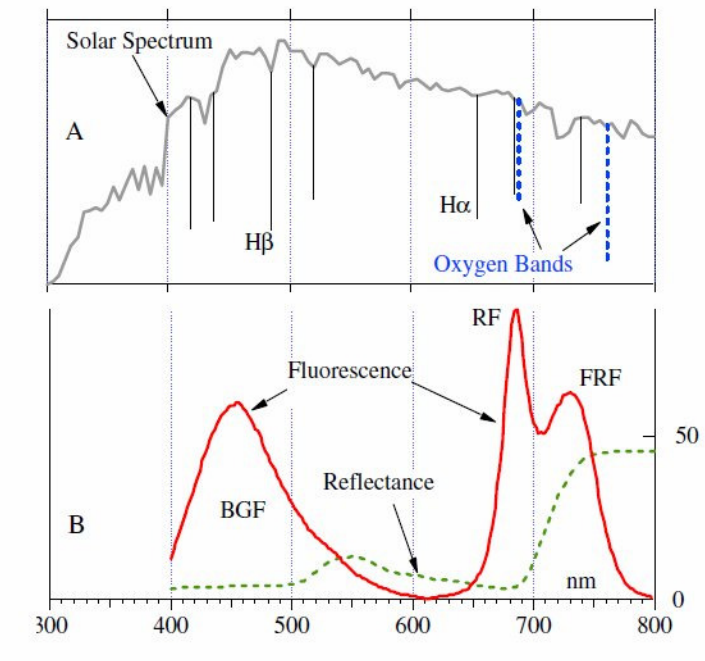

Figure 1-3. Solar spectrum and leaf reflectance in the VIS-NIR range, with the indication of a typical fluorescence spectrum (red line, panel B) and of the main lines that can be used for its remote estimation by the in-filling technique: the two Fraunhofer lines Hβ and Hα and the oxygen absorption bands O_2-B and O_2-A. From Moya *et al.* 2003.

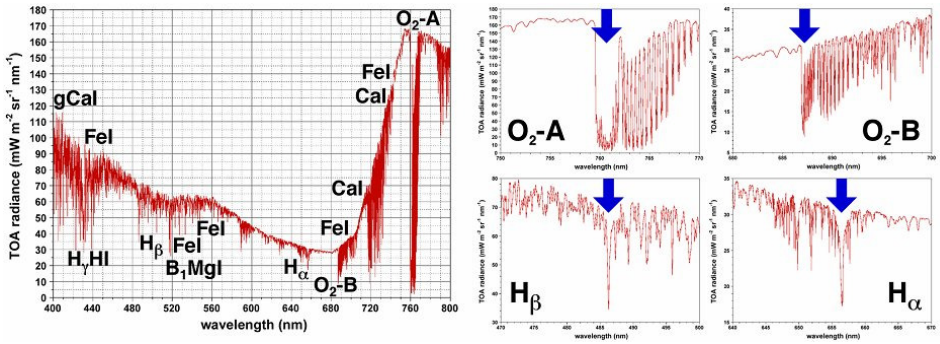

Figure 1-4. Detailed measurements of downwelling radiance in the four Fraunhofer and atmospherica absorption bands proposed in the study.

More recently, solar-induced fluorescence (SIF) has also become the subject of intense research. Whilst FI requires the manipulation of the light environment of the leaf (through the application of saturating flashes or the darkening of the leaf), SIF is a completely non-invasive technique and would therefore lend itself to the remote observation of photosynthetic processes.

The measurement of SIF by purely passive techniques makes use of the so-called Fraunhofer bands (Plascyk 1975) and of O_2 absorption of radiation in narrow regions of the spectrum, where apparent vegetation reflected radiance is mostly contributed by chlorophyll fluorescence (Figure 1-3. - Figure1-4 -).

Several studies over the last decade have demonstrated the technical feasibility of SIF measurements at the leaf and canopy level (Moya *et al.* 1992; Sailaja *et al.* 1997; Moya *et al.* 1999; Freedman *et al.* 2002; Moya *et al.* 2004; Carter *et al.* 2004; Louis *et al.* 2005; Perez-Priego *et al.* 2005; Liu *et al.* 2005; Meroni *et al.* 2006). Recent studies have also demonstrated that the weak fluorescence signal is indeed detectable from a satellite system at relevant spatial resolution and with the accuracy required by ecosystem models.

Other approaches have also been suggested for the measurement of red fluorescence, based on the shape of the reflectance spectrum in the red region, but they result in more qualitative indexes (Zarco-Tejada *et al.* 2000; Zarco-Tejada *et al.* 2003).

Apart from absolute fluorescence, several studies have also focused on the dynamics of the fluorescence spectrum, or more commonly on the ratio between red and far-red fluorescence (Lichtenthaler *et al.* 1990; Agati *et al.* 1995; Agati *et al.* 1996; Agati 1998; Agati *et al.* 2000). Apart from the effects of chlorophyll re-absorption, the ratio has been found to be responsive to several environmental factors (Figure1-5 , left), because of the differential contribution of Photosystem I (PSI) and Photosystem II (PSII) at the two wavelengths also at ambient temperature (Peterson *et al.* 2001; Franck *et al.* 2002). Recent studies at the canopy level (Louis *et al.* 2005) have also demonstrated the responsiveness of the ratio between the two fluorescence peaks to environmental factors under field conditions over a period of months (see Figure1-5, right).

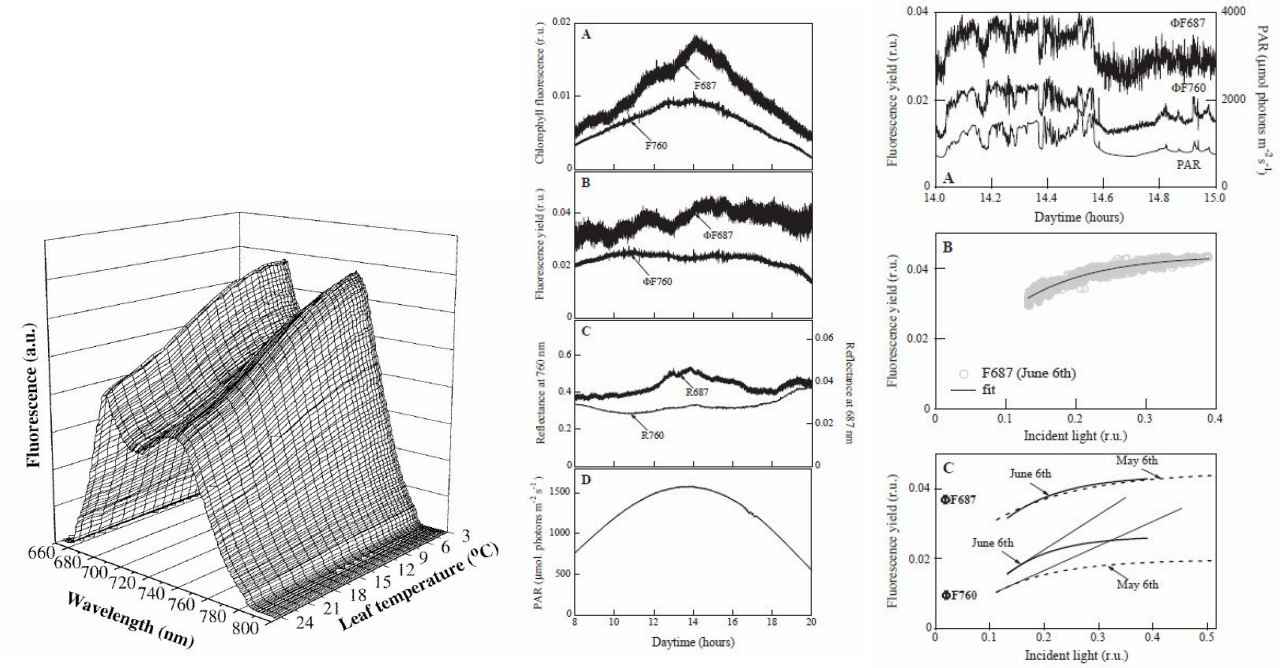

Figure 1-5. Left panel: dynamic development of the red chlorophyll fluorescence spectrum, showing the effects of leaf temperature on the mutual relationships of the two fluorescence peaks, centered at about 685 and 730-740 nm. From Agati 1998. Right panels: differential dynamics of chlorophyll fluorescence at 687 and 760 nm, as determined remotely by the partial line in-filling method during the ESA-SIFLEX campaign in Sodankyla. Also presented (right panels) is the response of fluorescence at the two wavelengths to incoming radiation in two days (May 6th, June 6th) with different environmental conditions.

Significant evidence has also accumulated over the last few years on the functional relationship between photosynthetic light-use efficiency, xanthophyll de-epoxidation state (DEPS) and hyperspectral reflectance in the green region (in particular at around 531 nm; Fig. 1.6), as captured by the Photochemical Reflectance Index (PRI) (Gamon *et al.* 1992b); although the index has been successfully applied for the remote sensing of photosynthetic processes both at the leaf (Gamon *et al.* 1997a; Tambussi *et al.* 2002) and at the canopy level (Peñuelas *et al.* 2000; Nichol *et al.* 2000b; Evain *et al.* 2004; Rahman *et al.* 2004; Louis *et al.* 2005; Fuentes *et al.* 2006), doubts still persist on the interpretation of PRI inter-specific differences and long-term dynamics (Gamon *et al.* 1999a; Guo *et al.* 2004; Weng *et al.* 2006), possibly because of the effects of leaf biochemical content (Stylinski *et al.* 2000b; Raddi *et al*. 2002).

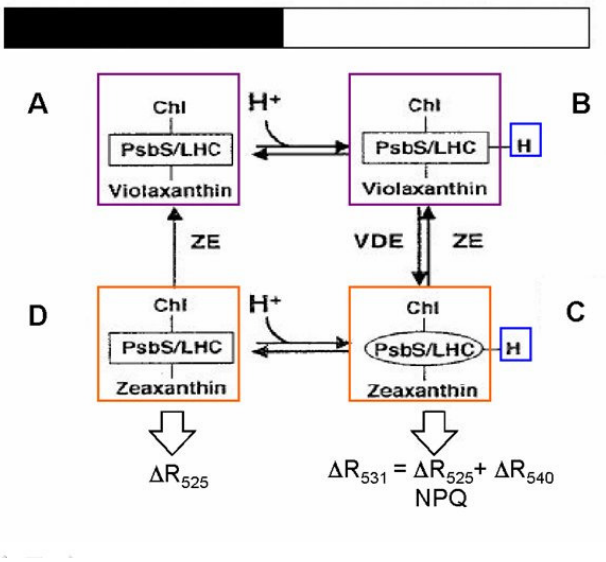

A summary model for PSII non-photochemical quenching (NPQ ; from Müller *et al.* 2001, modified).

A, in limiting light or darkness (black bar above) no quenching occurs.
B, in high light (white bar) protons bind to the PSII protein PsbS in the core antenna complex of PSII.
C, a quenching complex with different conformation, measurable as ΔR_{531} and PRI, is formed when zeaxanthin and protons are bound. Conversion of violaxanthin to zeaxanthin occurs more slowly than protonation.
D, when the light stress has ended, the PSII proteins are de-protonated readily, whereas the epoxidation of zeaxanthin to violaxanthin is slower, reflecting in the dynamics of the ΔR_{525} signal.

Figure 1-6. Summary model of the processes related to the thermal dissipation of excess energy, as a result of trans-thylakoid pH gradient and xanthophyll de-epoxidation, and of the resulting changes in leaf reflectance at 531 nm.
From Muller *et al.* (2001b), modified.

A few field campaigns have already been carried out by participants of this consortium, funded by the European Space Agency, to evaluate the potential of SIF measurements at the canopy and landscape scale. The SIF signal has been found to be detectable also from an aerial platform, and atmospheric model simulations have proved the feasibility of its measurement from space.

The propagation of the fluorescence signal through the canopy has also been the subject of a detailed study funded by the European Space Agency (Development of a Vegetation Fluorescence Canopy Model, ESTEC Contract No. 16365/02/NL/FF): in the FluorMOD model developed as part of the study (Zarco-Tejada *et al.* 2006), SIF is modelled at the leaf and canopy scale as a function of fluorescence yield and PSII/PSI stoichiometry (as well as chlorophyll content, in order to account for re-absorption effects) within the canopy. A clear understanding between these two pivotal parameters and photosynthetic processes, however, is still missing. The assumption in the model of un-stressful conditions (and therefore of a constant thermal dissipation coefficient; Rosema *et al.* 1998) make the model of little applicability under real conditions.

Other empirical and functional models have been proposed recently for the interpretation of the SIF signal in terrestrial (Agati *et al.* 2000; Medrano *et al.* 2002; Zhu *et al.* 2005) and marine ecosystems (Matorin *et al.* 2004; Laney *et al.* 2005); in combination with the significant amount of experimental evidence already available (often in laboratories involved in the present study), this would make it possible to translate space-born measurements of solar-induced fluorescence into useful information for the future application of Dynamic Vegetation Models at the global scale.

The proposed project will develop and demonstrate the tools and algorithms required to reach such a goal.

1.2. Study objectives

The key objective of this study was to analyse the applicability of vegetation fluorescence observations in addition to other biophysical variables derived from optical and thermal infrared remote sensing for regional dynamic vegetation modelling.

The study was also expected to result in a range of quantitative predictions of the link between solar-induced fluorescence, reflectance and photosynthesis at the leaf and canopy level, which could guide ongoing and future campaigns aimed at the airborne and satellite oservation of fluorescence and primary production.

The methodology originally outlined in the proposal was based on the application of two distinct models (Fig. 1.7): (i) a very detailed model of leaf and canopy photosynthesis and fluorescence (based on the FLUORMOD model, already developed as part of past ESAprojects, for the representation of the functional link between photosynthesis and fluorescence), to be included in a multi-layer canopy model and used for the simulation of expected canopy fluorescence fields and gross primary production under a range of conditions; (ii) a coarser DVM (Dynamic Vegetation Model), to be modified for the assimilation of the information coming from fluorescence remote sensing at a global scale but without a detailed representation of canopy reflectance and fluorescence. The link between the two models was to be based on the expected semi-empirical correlation between fluorescence fields and gas exchange, as derived from the application of the detailed model (e.g. between canopy fluorescence radiance and GPP or absorbed radiation, or between light-use efficiency and fluorescence efficiency). The use of predictions from the detailed model was justified by the lack at the time of any long-term experimental dataset at the canopy scale, combining parallel measurements of canopy fluorescence and GPP.

Following a detailed discussion with the Agency, the proposed methodology was later modified, since such a semi-empirical approach was not deemed to guarantee the generality of the results obtained. It was decided, on the contrary, to attempt the direct inversion of a suitable DVM (modified to include a simple representation of canopy fluorescence) on the fluorescence fields generated by the detailed model (called MLFL in the graphs), used as a proxy for the lacking measured datasets.

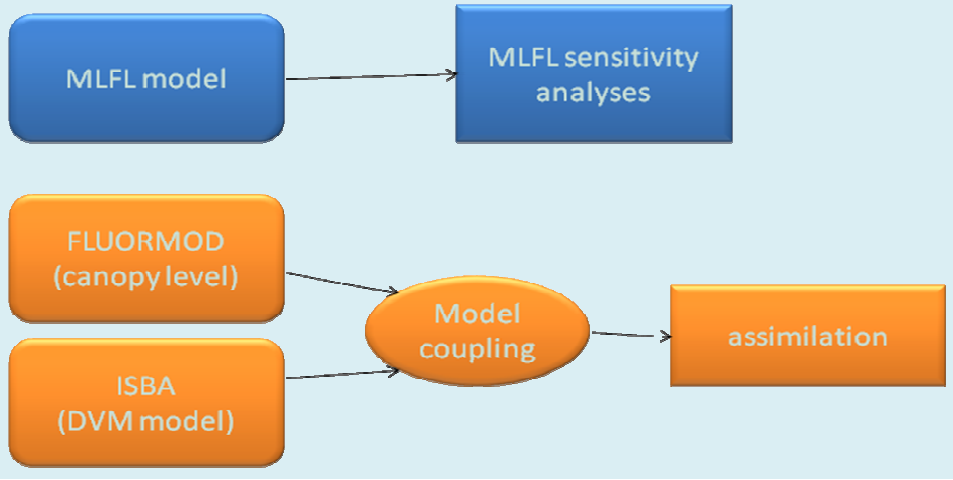

Figure 1-7. Initial simplified study logic.

An initial analysis of experimental results, derived from the literature and from ongoing, parallel experimental studies funded by the Agency (e.g. SEN2FLEX, SIFLEX, CEFLEX), however, demonstrated that the functional representation of the link between photosynthesis and fluorescence in the FLUORMOD model was not appropriate and did not provide the required level of realism under normal environmental conditions. A more detailed and realistic analysis of leaf-level processes than originally foreseen was therefore deemed desirable before the canopy-level model could be applied for the fulfillment of the original objectives.

The development and testing of an enhanced, realistic leaf-level model required an additional effort, and resulted in time and schedule constraints that led to the replacement of the assimilation activities originally foreseen by a thorough sensitivity analysis (Fig. 1.8). This new strategy has been successfully applied, the leaf level and canopy level models have been significantly improved and at the end of the project we are in a position to start assimilation studies, based on leaf- and canopy-level models which are fully consistent with available experimental evidence.

Despite these changes, a literature survey of the assimilation of remote sensing data in DVM and the possible use of fluorescence data was performed, as originally foreseen in the project. This review was based on the existing information at the beginning of the project. At that time no model allowing the establishment of the links between DVM and fluorescence signals was available and no study on the dynamic simulation of fluorescence signal, which are prerequisites for the analysis of possible implementation of data assimilation methods, were available.

Test of the simulation of fluorescence signal together with other remote sensing signals (reflectances and surface temperature) was done based on the combination of a dynamic vegetation model (ISBA-Ags) and of models simulating signals (based on SAIL, SAIL-Thermique and the newly developed SCOPE models). However due to delays in the availability of models and data this part of the study only provided preliminary results.

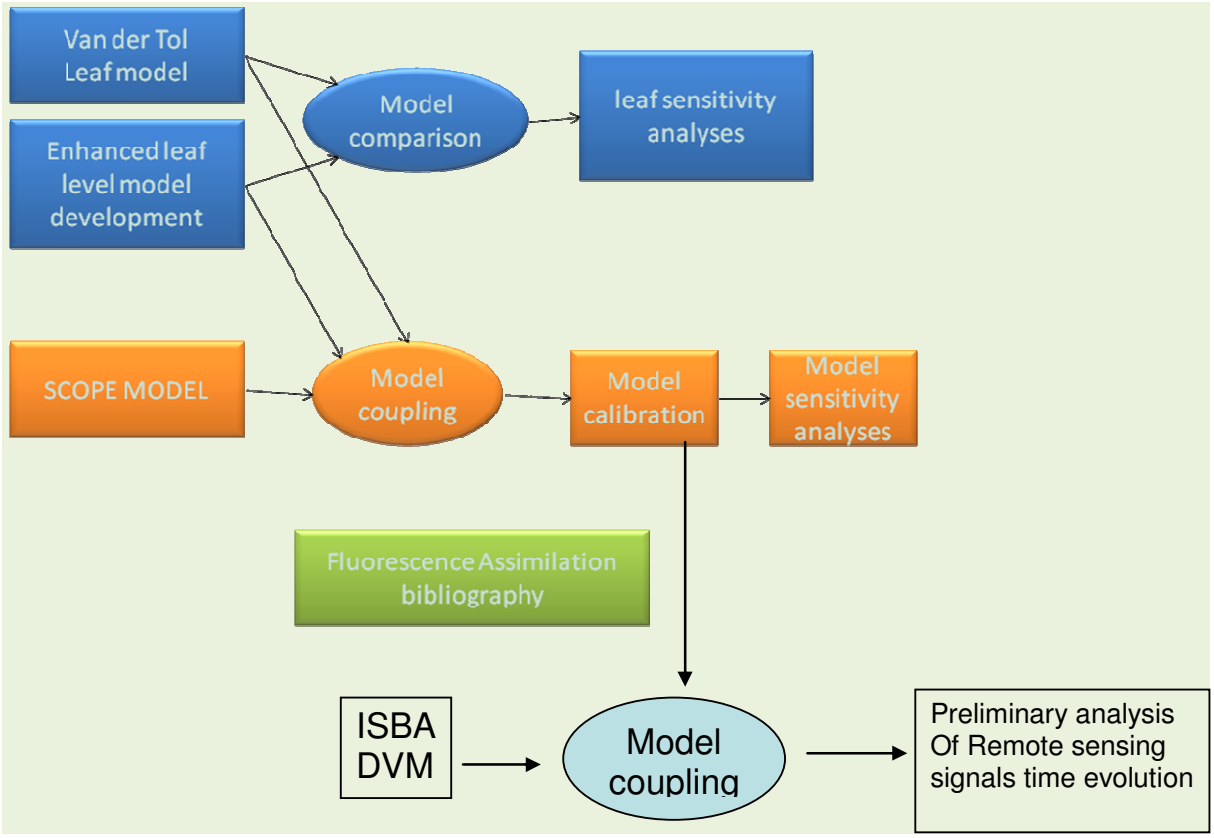

Figure 1-8. Final study logic

The initial work packages and deliveries are described in the following work breakdown structure:

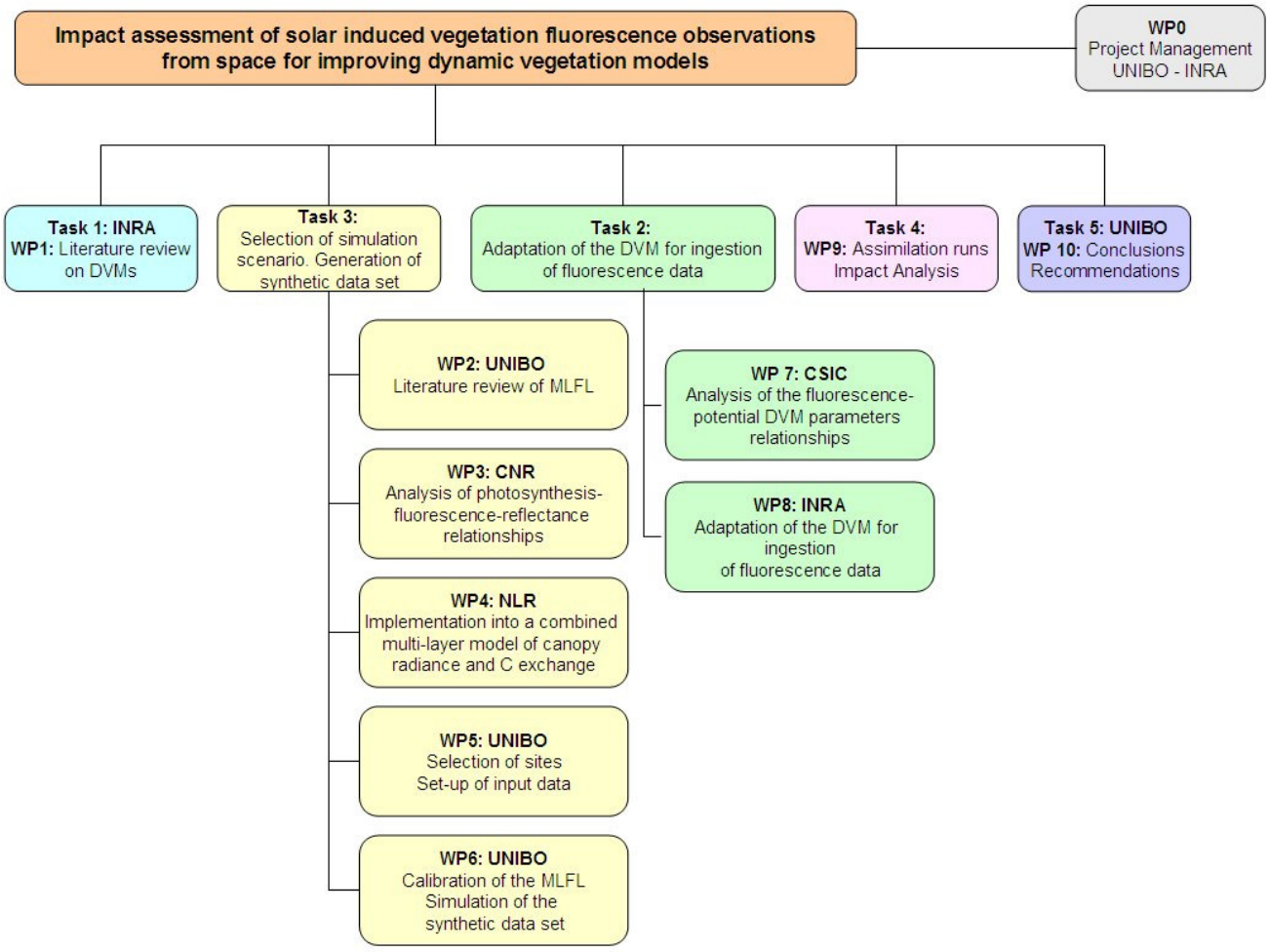

The following modified WPs are emphasized in red:

Nr.	Description	Modifications
WP 1		
DL 1.1	Description of Dynamic Vegetation Model requirements and available modelling options	
DL 1.2	Description of selected Dynamic Vegetation Model	
WP 2		
DL 2.1	Description of functional model requirements and available modelling options	
DL 2.2	Source code and description of selected functional model	
WP 3		
DL 3.1	Critical review of the state of the art concerning the relationship between fluorescence and leaf optical properties and photosynthetic parameters	

Nr.	Description	Modifications
DL 3.2	Algorithms for the inclusion of fluorescence and leaf optical propertiesin functional models at leaf level	
DL 3.3	Test of proposed algorithms against experimental data already available at the leaf level, for a limited number of species under stress conditions	
WP 4		
DL 4.1	Software to include leaf and soil thermal radiances in multi-layer model	
DL 4.2	Description of incorporation of thermal infrared radiation in canopy model	
DL 4.3	Code of multi-layer Farquhar-Leuning (MLFL) model	
DL 4.4	Modified FluorMOD model for the assimilation of functional variables from MLFL	Modified FluorMOD model for the assimilation of functional variables (single-layer for DVM) has been canceled because the maturity of the models was not sufficient to perform assimilation.
WP 5		
DL 5.1	Database of eddy-covariance measurements and environmental parameters for each selected site	
WP 6		
DL 6.1	Database of MLFL model parameters for each selected PFT	
DL 6.2	Dataset of simulated annual canopy gap exchange at the selected sites	
DL 6.3	Dataset of simulated canopy radiance (inclusive of reflectance and fluorescence) for selected days at the canopy site	
WP 7		
DL 7.1	Review of parameters that can be extracted from canopy fluorescence model	
DL 7.2	Review of parameters that can be extracted from canopy reflectance model	
DL 7.3	Algorithms for assimilation of remote-sensing derived biophysical parameters into a dynamic vegetation model	DL 7.3 was canceled during kick off meeting.
WP 8		WP8&9 have been canceled and replaced by WP 11 and WP12
DL 8.1	Technical report: description of the modified Dynamic Vegetation Model	
WP 9		

Nr.	Description	Modifications
DL 9.1	Report on the impact of fluorescence assimilation on DVM predictive results (diagnostic mode)	
DL 9.2	Report on the impact of fluorescence assimilation on DVM predictive results (diagnostic mode)	
WP 10		
DL 10.1	Summary analysis: canopy fluorescence fields and relationship with canopy gas-exchange	
DL 10.2	Summary analysis: impact of fluorescence assimilation on DVM predictive ability	DL10.2 is replaced by DL10.4 consisting of the comparison of the fluorescence models
DL 10.3	Recommendations: future needs for the preparation of a space-borne SI vegetation fluorescence mission and for the exploitation of the resulting data	

The new work package list is presented hereunder.

Nr.	Description	
WP 1		
DL 1.1	Description of Dynamic Vegetation Model requirements and available modelling options	
DL 1.2	Description of selected Dynamic Vegetation Model	
WP 2		
DL 2.1	Description of functional model requirements and available modelling options	
DL 2.2	Source code and description of selected functional model	
WP 3		
DL 3.1	Critical review of the state of the art concerning the relationship between fluorescence and leaf optical properties and photosynthetic parameters	
DL 3.2	Algorithms for the inclusion of fluorescence and leaf optical propertiesin functional models at leaf level	
DL 3.3	Test of proposed algorithms against experimental data already available at the leaf level, for a limited number of species under stress conditions	
WP 4		
DL 4.1	Software to include leaf and soil thermal radiances in multi-layer model	
DL 4.2	Description of incorporation of thermal infrared radiation in canopy model	
DL 4.3	Code of multi-layer Farquhar-Leuning (MLFL) model	

WP 5		
DL 5.1	Database of eddy-covariance measurements and environmental parameters for each selected site	
WP 6		
DL 6.1	Database of MLFL model parameters for each selected PFT	
DL 6.2	Dataset of simulated annual canopy gap exchange at the selected sites	
DL 6.3	Dataset of simulated canopy radiance (inclusive of reflectance and fluorescence) for selected days at the canopy site	
WP 7		
DL 7.1	Review of parameters that can be extracted from canopy fluorescence model	
DL 7.2	Review of parameters that can be extracted from canopy reflectance model	
WP 10		
DL 10.1	Summary analysis: canopy fluorescence fields and relationship with canopy gas-exchange	
DL 10.3	Recommendations: future needs for the preparation of a space-borne SI vegetation fluorescence mission and for the exploitation of the resulting data	
DL 10.4	Comparison of the two fluorescence models improved during the project	WP10 : DL10.2 is replaced by DL10.4 consisting of the comparison of the fluorescence models
WP11	Advanced leaf reflectance and fluorescence model	WP11 consisting of the elaboration of an advanced leaf reflectance and fluorescence model. To deliverable are identified: DL11.1 model description and DL11.2 model code.
DL 11.1	Model description	
DL 11.2	Model code	
WP 12	DVM sensitivity analysis	WP12 consists of the sensitivity analysis with DL12.1 report on DVM sensitivity analysis
DL 12.1	DVM sensitivity analysis report	

1.3. Description of Dynamic Vegetation Model requirements and available modelling options

1.3.1. Review of existing Dynamic Vegetation Models (DVMs)

The goal of the following sections is to provide a short overview of existing DVMs and to present some of the studies which have been carried out on data assimilation in DVMS (or DVM components). Many information was extracted from the studies by Kucharik *et al.* (2006), Cramer *et al.* (1999), Olioso *et al.* (2005), Gibelin *et al.* (2006) and Demarty *et al.* (2007).

1.3.1.1. Importance of DVM and data assimilation in the FLEX context

Until now, most of the information that has been acquired by remote sensing of the Earth surface about vegetation conditions has come from reflected light in the solar domain. There is, however, one additional source of information about vegetation photosynthetic processes and gross primary production (GPP) in the optical and near-infrared wavelength range that has not yet been exploited by any satellite mission, related to the emission of fluorescence from the chlorophyll of assimilating leaves, and consequently to the photosynthesis. Other information not yet exploited can be found in the Photochemical Reflectance Index, PRI, which is related to xanthophyll cycle (in what follows, the term 'fluorescence signal' will associated PRI and fluorescence *s.s.* signals). Photosynthesis is a dynamic process that is influenced by many factors (light, water, nutrients, plant types, management practices etc.), so a true characterization is only possible with continuous measurement and is quite difficult to achieve on the basis of satellite observation without combination with modelling studies. Dynamic Vegetation Models (DVMs), simulating vegetation dynamics should be then used to "assimilate" the fluorescence information in a proper way. The data assimilation concept would probably require model modification/adaptation to allow them to use fluorescence signal as an input, linked to photosynthesis parameters already used in the models through different input parameterisations.

1.3.1.2. Review of DVMs

DVMs is a recent class of models that has emerged in the last decade (Foley *et al.*, 1996, 1998; Friend *et al.*, 1997; Woodward *et al.*, 1998; Kucharik *et al.*, 2000; Cramer *et al.*, 2001; Bachelet *et al.*, 2003; Bonan *et al.*, 2003; Sitch *et al.*, 2003; Hickler *et al.*, 2004; Krinner *et al.*, 2005). These models range in complexity from empirical formulations to quasi-mechanistic models that integrate biogeography, soil biogeochemistry, and soil–vegetation–atmosphere transfer (SVAT) components into the same framework, allowing for vegetation characteristics (e.g., leaf area index, height, biomass and type, root biomass, and albedo), soil moisture, and nutrient availability to respond to atmospheric forcing (climate and carbon dioxide) and land management change. They are currently being used to investigate the magnitude and geographical distribution of energy and mass exchanges, of the vegetation production, as well as at local, regional and global scales (in this last case, we speak of DGVMs for Dynamic Global Vegetation Models). More 'specific' models, such as crop models, as constructed by agronomist (e.g. Brisson *et al.* 2003, Williams *et al.* 1989), forest dynamic models (e.g. Dufrêne *et al.* 2005, Loustau *et al.* 2005), or 'interactive vegetation' SVAT models (Ji 1995, Calvet *et al.* 1998a, Lu *et al.* 2001, see also Arora 2002), present many features similar to general types of Dynamic Vegetation Models, while simulating more specific processes (grain, fruit or wood production, energy exchanges as Land Surface parameterization in the frame of atmospheric modelling studies…). Such models may however be considered as being part of the DVM family as they include the two way interactions between canopy growth and development, climate and soil (the use of remote sensing data as presented below is often more advanced with such types of models than with more standard DVMs).

Generally, in the last generation of DVMs, individual tree, grass, and shrub species are typically grouped into generic plant functional types (PFTs; such as "temperate deciduous tree"), whose spatial distribution is determined by bioclimatic rules and by competition for light and water resources. However, a few approaches simulate competition between individual plants that occurs at finer scales (Smith *et al.*, 2001). These dynamics give rise to simulated "biome" types (e.g., savannah, temperate deciduous forest, boreal evergreen coniferous forest). In addition, DVMs have been mainly developed in order to be coupled with Global Climate Models (GCMs) (Foley *et al.*, 1998; Delire *et al.*, 2003, 2004); in "coupled mode" these models can explicitly represent the bi-directional feedbacks between vegetation and climate. Although some formulations in coupled DVM-GCMs are simplified relative to ecosystem-scale models (e.g., vegetation dynamics, cf. Hickler *et al.*, 2004; Moorcroft, 2003), and the spatial resolution of the "coupled mode" is relatively coarse, the explicit links between ecological processes and the atmosphere in DVMs represent a considerable step forward (Arora, 2002; Hickler *et al.*, 2004), and DVMs are now currently indispensable for the study of biome distribution, ecosystem function, and climate feedbacks in the context of both global climate change and land use change (Foley *et al.*, 2000).

Many recent studies deal on DVM validation at continental to global scales (e.g., Kucharik *et al.*, 2000; Lucht *et al.*, 2002; Bachelet *et al.*, 2003; Bonan *et al.*, 2003; Sitch *et al.*, 2003; Gordon *et al.*, 2004; Gerten *et al.*, 2004; Hickler *et al.*, 2004). In these studies, simulated land cover, hydrology, and global carbon balance have been evaluated with land observations, satellite data, or other model outputs (Cramer *et al.*, 2001). A small number of published studies have also evaluated DVM water, carbon, and energy balance at the individual field scale (Delire and Foley, 1999; El Maayar *et al.*, 2001, 2002; Sitch *et al.*, 2003). Comparisons of DVM simulated plant phenology with field observations are rarely made, but have recently been performed using satellite information (Lüdeke *et al.*, 1996; McCloy and Lucht, 2004; Kim and Wang, 2005; Piao *et al.*, 2007).

1.3.1.3. Assimilation of remote sensing data in DVMs

Remote sensing earth observations provide useful information on plant canopy processes that may be used for driving or constraining DVMs (including crop, forest and interactive SVAT models) over large areas. The models may be operated without a systematic use of remote sensing data by intrinsically providing the means for interpolating energy and water fluxes or biomass production between remote sensing data acquisitions. This is important since remote sensing data acquisitions may be infrequent. Moreover, it is uneasy to implement procedures to use data acquired by one or a large range of remote systems, differing in wavelength domains, acquisition time or geometry. Remote sensing information on plant canopy processes is not direct because it results from the interaction of radiation with soil surface and plant canopy. It is then necessary to use specific radiative transfer models for interpreting these interactions and for relating plant and soil characteristics to remote sensing signals. These models range from very complex models to simplified approaches based on empirical relationships. For example, numerous relationships were established between spectral reflectances and LAI (Leaf Area Index), by means of vegetation indices; they can be used for estimating LAI that is then fed into DVMs. LAI is a key biophysical variable simulated in DVMs because of its close relationship with vegetation structure and its impact on the exchanges of CO_2, water vapour and energy by vegetation canopies (Myneni *et al.*, 2002). Moreover, it is routinely derived from satellite observations acquired in optical domain (MODIS, MERIS, VEGETATION) and currently used to drive DVMs (Hazarika *et al.*, 2005; Liu *et al.*, 1997, Demarty *et al.*, 2007) or to optimize their parameters (Rayner *et al.*, 2005; Kaminski *et al.*, 2002). Some examples of method to assimilate LAI in DVMs may be found, for example, in Delécolle *et al.* (1992), Clevers *et al.* (2002), Sellers *et al.* (1996), Olioso *et al.* (2005 and 2006). An example of positive impact of contraining DGVMs assimilating global MODIS-LAI on the simulation of global phenology and global carbon fluxes is presented in Demarty *et al.* (2007).

As suggested by the previous examples, until now, most of the studies devoted to assimilation of remote sensing data into vegetation models focused on the use of visible and near infrared reflectances, or in some cases on microwave measurements (see also the articles of Moulin *et al.*

1998, Inoue *et al*. 1998, Clevers *et al*. 2002, Verhoef and Bach 2003, Wigneron *et al*. 2002). Indeed, these measurements give information on vegetation structure and biomass seasonal dynamics. Thermal infrared (TIR) may also provide significant information on vegetation processes when water limitations occur, but the assimilation of TIR data requires that the resolution of energy balance is performed either by the model, or as a 'pre-processes' (e.g. Soer 1980, Taconet and Vidal-Madjar 1988, Carlson *et al*. 1990, Camillo 1991, Olioso *et al*. 1996, 1999, Moran *et al*. 1996, Cayrol *et al*. 2000, Olioso *et al*. 2005, Droogers and Bastiaanssen 2002, Schuurmans *et al*. 2003).). The use of passive microwave data has been emphasized in the last year in particular in relation to the SMOS mission. Works by Calvet *et al*. (1998b) or Wigneron *et al*. (1999) investigated the possibility to assimilate surface soil moisture data in preparation to the possible assimilation of SMOS derived soil moisture. The coupling of ISBA-Ags to a radiative transfer model at L-band made it possible to extend such studies to real microwave emission data (Wigneron *et al.,* 2002). Emitted microwave observations were also used to analyse surface soil moisture by Entekhabi *et al*. (1994) and Reichle *et al* (2001). Finally relatively few studies have analyzed the possible complementary assimilation of various wavelengths (Camillo 1991, Bouman 1992, Clevers and van Leeuwen 1996, Moran *et al.* 1996, Olioso *et al.* 1999, Cayrol *et al.* 2000, Olioso *et al.* 2001, 2005, Droogers and Bastiaanssen 2002).

1.3.1.4. The possible use of remote sensed fluorescence signals

The possibility to use fluorescence information for monitoring vegetation at canopy scale and hence for constraining DVMs has been proposed for a long time (e.g. Baret *et al*. 1988, Méthy *et al*. 1994) but until now no studies has been performed in this way. Potential relationships that have been obtained in the field show for example that fluorescence or PRI information could be related to light use efficiency, photosynthesis and stomatal processes or chlorophyll content. However information at canopy scale is only sparse and not yet well established (examples of relationships can be found in Evain *et al*. 2004, Rosema *et al*. 1998, Peñuelas and Inoue 2000, Nichols *et al*. 2006, McFarlane *et al*., 1980, Louis *et al*. 2005, Inoue and Peñuelas 2006; see also the FLEX-DVM Deliverable 3.1.1 by Zarco-Tejada & Mohammed 'Steady-State Fluorescence and Chlorophyll'). Application from airborne or satellite remote sensors is even sparser but present results indicates the potential of using fluorescence signals over large areas (e.g. Fuentes *et al*. 2006, Asner *et al*. 2005, Drolet *et al*. 2005, Suarez *et al*. 2008). The possibility of ingestion of fluorescence, or PRI, information in DVMs, necessits that better basis and understandings of the relationships between remote signals and canopy processes are developed. The development of a model integrating the processes influencing fluorescence or PRI signals at canopy scale is required in order to better understand the combined impacts of plant physiological processes and canopy structure on signals (modelling studies by Méthy *et al*. (1991, 1994), Rosema *et al*. (1991), Olioso *et al*. (1992), Verhoef (2005), Zarco-Tejada *et al*. (2006) have shown that canopy structure has a strong effect on fluorescence signal at canopy level). Field experiment makes it possible to follow vegetation processes together with remote signals along the phenological cycle. Increasing the number of such experiments is required (fluorescence data at the canopy scale are still very few due to the lack of adequate instrumentation, while PRI information can be derived from field or in-flight spectroradiometers). At the time of writing, information level on the possible use of remote fluorescence or PRI measurements for assimilation in DVMs is very low and only some first guess proposals can be done.

- If well established relationships between signals and light use efficiency can be derived, they might be used for informing on the canopy biomass production in combination with a standard fAPAR estimation (some large scale or ecosystem DVM, working at the monthly or decadal time steps, have a potential for using such information: e.g. Potter *et al*., 1993, Haxeltine *et al*., 1996, Goetz *et al*., 2000);

- If well established relationships between plant parameters (e.g. chlorophyll content) and signals (e.g; fluorescence ratios) can be derived, they might be used for deriving information on plant nitrogen content or "photosynthetic enzymes" content (for example as summarized in the 'Vcmax' parameter in the classical Farquhar's photosynthesis model). These might be used for informing process models accounting for the nitrogen cycle (such as standard crop models: STICS, Brisson *et al*. (2003); EPIC, Williams *et al*., 1989) or which are including biochemical description of photosynthesis (such as Farquhar's description which is now included in many DVMs as for example ORCHIDEE (described in mode details below), CASTANEA and GRAECO two forest dynamic models (Dufrêne *et al*. 2005, Loustau *et al*. 2005)…;
- If a model able to simulate remotely sensed signals is developed, it would be possible to adapt a DVM in order to provide signal simulation along the phenological cycle, and then to implement procedure to assimilate remote sensing data. This option may be very interesting for the use of solar induced fluorescence signals since it may give access to information on non-photochemical quenching by the assimilation of the time evolution of measured signals (as it may be determined by comparison of signals at various solar irradiance and in relation to stomatal behaviour in the case of water stress (Evain *et al* 2004, Flexas *et al* 2000)). The assimilation of remote sensing data offers the possibility for exploiting various remote sensing signals together and a mathematical framework making it possible to include information on measurement and model errors in the analysis;

1.3.2. Examples of DVM: ISBA-Ags and ORCHIDEE

In this section, we present the ISBA-Ags and ORCHIDEE DVMs used by the French research community. These two models have been developed by large research groups and benefit from permanent improvements. They were basically developed for being interfaced with atmospheric models in meteorological (ISBA) and climate studies (ISBA and Orchidee). Orchidee has a stronger focus on climate studies and emphasizes carbon cycle problematics. Recent and new versions of ISBA, ISBA-A-gs (Calvet *et al*. 1998a, Gibelin *et al*. 2006) and ISBA-CC (Gibelin *et al*. 2008) have now a correct assessment of the carbon cycle. ISBA-A-gs and ORCHIDEE are both able to simulate the dynamic of vegetation in terms of leaf area index and biomass (from a physiological description of the photosynthetic processes). These two models have been currently used in numerous studies and validated against both in situ eddy covariance towers and global datasets (e.g. satellite maps of biophysical variables) (see reference list at the end of Section B for ISBA and Ciais *et al*. (2005) for ORCHIDEE). Methods to assimilate various remote sensing products have been also developed and implemented within these two models, using either existing field campaigns (Calvet *et al*. 1998b, Wigneron *et al*. 2002, Olioso *et al*. 2005, Inoue and Olioso 2006, Munoz-Sabater *et al*., 2007) or either global fields of biophysical products derived from MODIS data (Demarty *et al*., 2007).

1.3.2.1. ORCHIDEE

The ORCHIDEE (ORganizing Carbon and Hydrology in Dynamic EcosystEms) model has been developed at IPSL (France) (Krinner *et al*.; 2005). It is heavily based on three different existing models, consisting of (1) an hydrological and energy module from SECHIBA SVAT model (Ducoudré *et al*., 1993) , (2) a new carbon module, called

ORCHIDEE

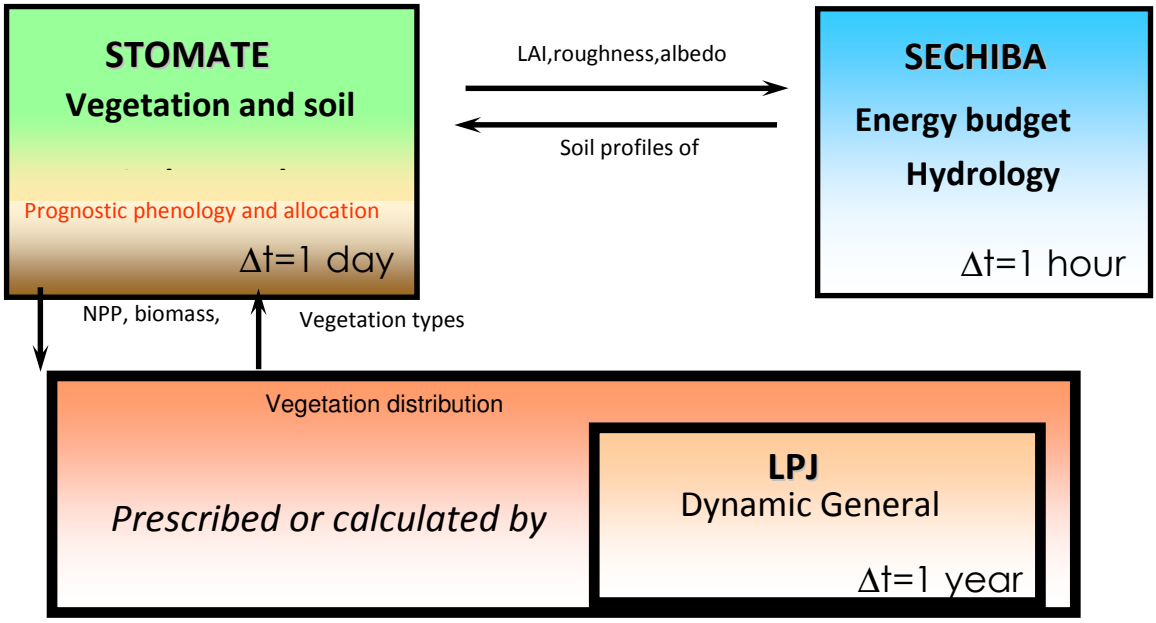

STOMATE, allowing simulating photosynthesis, carbon allocation, litter decomposition, soil carbon dynamics, maintenance and growth respiration and phenology and (3) parameterizations of vegetation dynamics from the Lund-Potsdam-Jena (LPJ) DGVM (Sitch *et al.*, 2003) in order to simulate fire, sapling establishment, light competition, tree mortality, and competition between species. As a consequence, the ORCHIDEE model explicitly simulates the phenomena of the terrestrial carbon cycle that are linked to vegetation and soil decomposition processes but also changes in vegetation distributions in response to climate change as well as short time scale interactions between the vegetated land surface and the atmosphere. It simulates carbon cycling on time scales ranging from hours to centuries including the slow carbon reservoirs of the soil and the dynamics of ecosystems after disturbance.

The carbon balance of each ecosystem is determined by photosynthesis, respiration and disturbances (harvest, fires). The plant and soil carbon reservoirs need to be initialized by running the model to equilibrium (i.e. spin up procedure). The seasonal onset and senescence of vegetation activity are calculated prognostically from climate (Botta *et al.*, 2000) and for 12 plant functional types (PFTs), which are tropical broad-leaved evergreen trees, tropical broad-leaved raingreen trees, temperate needleleaf evergreen trees, temperate broad-leaved evergreen trees, temperate broad-leaved summergreen trees, boreal needleleaf evergreen trees, boreal broad-leaved summergreen trees, boreal needleleaf summergreen trees, C_3 grass natural and agricultural, and C_4 grass natural and agricultural. In every grid element the different PFTs can coexist, the fraction of the element occupied by each PFT being either calculated (if the LPJ vegetation dynamic is activated) or prescribed (without vegetation dynamic). The fractional area occupied by agricultural PFTs is always prescribed (i.e. vegetation dynamics does not act on the agricultural fraction of the grid element).

In ORCHIDEE grasses cannot grow below trees. This idealizing assumption simplifies several parameterizations, for example photosynthesis, transpiration and light competition. Carbon dynamics is described through the exchanges of carbon between the atmosphere and the different carbon reservoirs in plants and soils. There are 3 reservoirs in living plants (leaves, roots, sapwood above and below ground, heartwood above and below ground, fruits and a plant carbohydrate reserve), 3 reservoirs in the soil (active, slow and passive soil carbon) and 4 in dead biomass (structural and metabolic litter above and below the surface). The litter and soil carbon reservoirs are treated separately on the agricultural and natural part of each grid cell. Within each of these two parts of a

grid cell (agricultural and natural) the PFTs are supposed to be well mixed so that the soil carbon is not calculated separately below each PFT. The parameterizations of litter decomposition and soil carbon dynamics are essentially taken from Century (Parton *et al.*, 1988).

ORCHIDEE must be forced using meteorological fields compatible in spatial resolution with the vegetation map. Moreover, it can be run in different configurations, depending on the type of problem to be addressed. It can be run in stand-alone mode, that is forced by climatologically or experimental data (global or local) and it can be run coupled to a GCM. The vegetation dynamics can be de-activated, so that ORCHIDEE can be run with a prescribed vegetation distribution. Additionally, STOMATE can be de-activated entirely or partly. In the second case the parameterizations of photosynthesis and stomatal conductance still operate, so that energy and water exchanges through the leaf surface can be modelled more realistically than in the first case, while the leaf area index is prescribed (it is calculated when the carbon module is fully activated). In its normal version the model makes no use of satellite input data that would force the state of the vegetation, so that the leaf and vegetation cover, with their seasonal and interannual variability, are entirely simulated by the model when meteorological forcing data are available.

1.3.2.2. ISBA-A-gs

The ISBA-A-gs model has been developed at Météo-France (Calvet *et al.*, 1998a; Calvet and Soussana, 2001, Calvet 2000, Calvet *et al.* 2004). It is based for the physical processes (energy balance, soil water and atmospheric processes) on the standard ISBA version (Interactions between Soil, Biosphere and Atmosphere, Noilhan and Planton, 1989; Noilhan and Mahfouf, 1996). It is used as a land surface model in climate and weather forecast systems. This model solves the surface energy balance and the soil water balance with a five minute time step. The soil is described by one bulk reservoir corresponding to the maximum root zone (including a thin surface layer and regardless to actual root development) as proposed by Deardorff (1978), the various 'water and heat transfer coefficients' depending on soil texture. Drainage below the root zone has been introduced by Mahfouf and Noilhan (1996). The main surface variables simulated by ISBA are the surface temperature, the soil moisture in the root zone, the surface soil moisture and the energy fluxes. We may note that only one energy balance equation is solved, but that a separation of soil evaporation and plant transpiration is done on the basis of the vegetation fraction cover.

The first version of ISBA-A-gs (Calvet *et al.* 1998a) uses a physiological stomatal resistance scheme to describe photosynthesis and its coupling with stomatal resistance at the leaf level (from Jacobs *et al.* 1996, Jacobs 1994). The computed net vegetation assimilation is used to feed a simple growth sub-model, and to predict the density of the vegetation cover. Three main 'ecophysiological' parameters are introduced in ISBA-Ags: leaf life expectancy (τ_M) and effective biomass per unit leaf area (α.) in the growth sub-model, and a mesophyll conductance (g_m). ISBA-Ags is able to simulate water budget, energy and mass fluxes (CO_2, sensible and latent heat fluxes, etc.) and leaf area index (LAI). Thus, the model is able to adapt the simulations of vegetation growth in response to changes in the environmental conditions (precipitation distribution, irrigation, water storage of the soil moisture in the root-zone, atmospheric CO_2 concentration, etc.) and, in contrast to ISBA, ISBA-Ags can be considered as an 'interactive-vegetation SVAT model' (or dynamic). The last developed versions have introduced the impact of leaf nitrogen content on plant growth and various behaviors in reaction to water deficit ('drought avoiding' and 'drought tolerant' plants). ISBA-A-gs parameters may be calibrated for a specific experiment (ex. Calvet *et al.* 1998a, Inoue et Olioso 2006, Calvet *et al.* 2007). For being used at the global scale, Gibelin *et al.* (2006) have proposed a tabulation of the parameters for 9 different PFTs.

ISBA-A-gs has been used in several data assimilation experiments (Calvet *et al.* 1998b, Wigneron *et al.* 2002, Olioso *et al.* 2005, Inoue and Olioso 2006, Munoz-Sabater *et al.* 2007). As shown in the Fig. 1.9 below, it has been coupled to several radiative transfert (RT) models in order to simulate remote sensing signals and implement remote sensing data assimilation procedure. The interactive vegetation module can be de-activate in order to force the model with LAI data (Olioso *et al.* 2005), making it possible to map surface processes from remote sensing maps of LAI (Olioso *et al.* 2006).

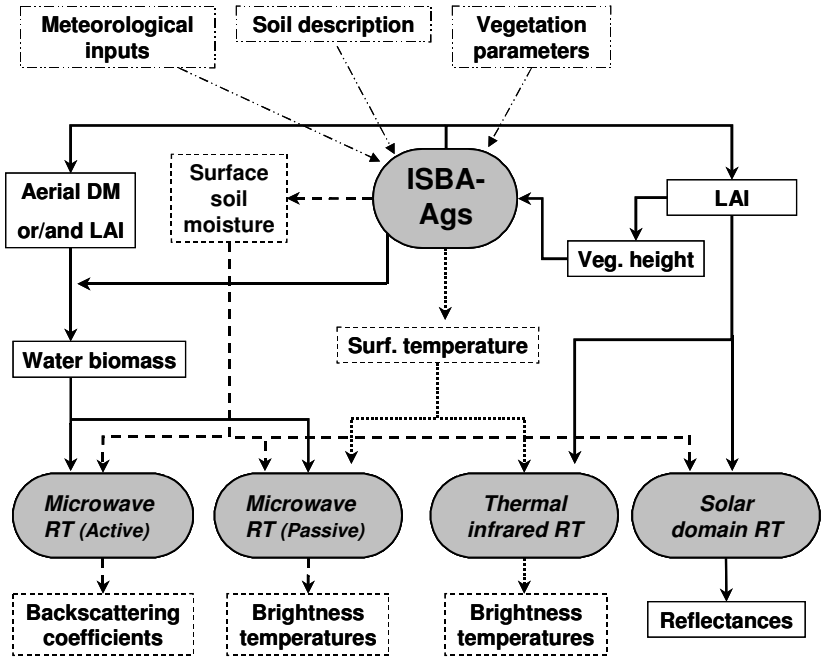

Figure 1-9. Presenting the coupling between ISBA-Ags and radiative transfert (RT) models (from Olioso *et al.* 2005)

1.3.2.3. Elements for choosing a DVM in the FLEX-DVM study

As shown above, a large range of DVM models exists. For the present study a pragmatic choice had to be made in order to account for the following points:

- available time is low so that the modelling experience of the participant has to be considered (the use of an 'external' model would require an adaptation period);
- knowing that at the moment the exploitation of fluorescence signals is at its real beginning, the use of a very complex model may not be required; a simple representation of vegetation dynamics may be enough considering however that the main processes influencing fluorescence signals are described by the model;
- the chosen model must have the potential for being coupled to a remote sensing signal simulation model and to implement simple assimilation procedures;
- the computer environment should be simple in a first step (run on PC, simple source code) and the model should be freely available from the owning Institution.

Eventually, the choice was done to use the ISBA-Ags model which presents the advantages of simulating the main required processes and which has already been used in several assimilation studies. ORCHIDEE was also considered, but it requests a high computing environment and assimilation procedures were not yet very developed.

2. REMOTE SENSING OF SOLAR-INDUCED FLUORESCENCE

2.1. Estimation of chlorophyll fluorescence

2.1.1. Red edge indices related with chlorophyll fluorescence emission

Indices related to fluorescence maxima at 685 and 740 nm are considered potentially useful, in addition to the spectral curvature index $R685^2/(R675 \cdot 690)$ (Zarco-Tejada *et al.,* 2000a;b; 2002a) to study the relationship of canopy reflectance with chlorophyll fluorescence (CF): i.e., R680/R630, R685/R630, R687/R630 and R690/R630, R685/R655, $R683^2/(R675 \cdot R691)$, D730/D706, where D represents derivation spectra.

A summary of such potentially valuable optical indices from reflectance and derivative spectra, grouped into 4 categories based on the spectral region and the type of parameter used, is provided in Zarco-Tejada *et al.* (1999a; 1999b).

At the laboratory level, results in a diurnal study showed that optical indices R680/R630, R685/R630, R687/R630 and R690/R630 achieved determination coefficients r^2=0.93, r^2=0.94, r^2=0.92, and r^2=0.91, respectively with Fv/Fm, the apparent quantum yield of Photosystem II for photochemical processes. Indices sensitive to changes in the reflectance curvature also showed correlations with diurnal changes in Fv/Fm (r^2=0.95) (Zarco-Tejada *et al*, 2000a;b). The effects of fluorescence emission in the red edge region were observed in experiments from *Acer saccharum* M. in the laboratory after dark adaptation and after 3 minutes of illumination (Fig. 2.1). The differences in reflectances at 680-690 nm and 730-750 nm are observed due to changes in chlorophyll fluorescence.

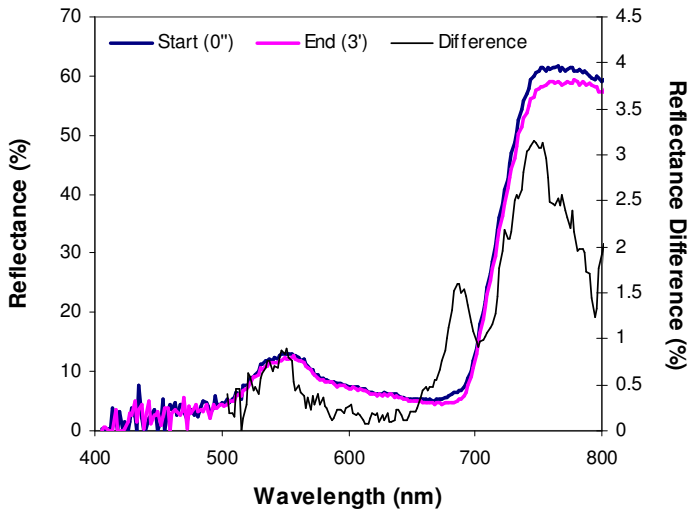

Figure 2-1- Changes in apparent leaf reflectance following 3' exposure of a dark-adapted Acer saccharum leaf to light. The reflectance change centered at 530 nm can be attributed to xanthophyll de-epoxidation and conformational changes and provides the basis for PRI (Photochemical Reflectance Index). The larger changes in apparent reflectance at about 680 690 nm and 730-750 nm are the result of the onset of chlorophyll fluorescence.

At the canopy level using CASI airborne imagery, red edge indices were assessed for detection of chlorophyll fluorescence (Table 2-1). Several optical indices had a strong determination coefficient r^2 with Fv/Fm at the canopy level with CASI data. These include red edge spectral derivative indices D730/D706 and DP21, with r^2 = 0.81 and 0.83, respectively, which however, also showed correlation with chlorophyll a+b content at r^2 = 0.49 and 0.4, respectively. Canopy structural effects on red edge indices for fluorescence detection varied depending on the type of index. Derivative indices were less sensitive to canopy structure and viewing geometry than structural VIS/NIR indices (Zarco-Tejada *et al.*, 1999b): the comparison between $R683^2/(R675 \cdot R691)$ and DP21 ($D_{\lambda p}/D_{703}$) indicates that the curvature index used for fluorescence detection is not influenced when structure or viewing geometry are accounted for by the canopy reflectance models.

Table 2-1- Determination coefficients obtained in chlorophyll a+b and Fv/Fm estimations applying relationships from SAIL and Kuusk CR models to hyperspectral CASI data collected over *Acer saccharum* M. study sites, Algoma (Ontario, Canada).

Optical Index	r^2 Chl a&b/cm^2	r^2 CF Fv/Fm
D730/D706	0.49	0.81
*DP21 ($D_{\lambda p}$/D703)	0.4	0.83
Curvature $R683^2/(R675 \cdot R691)$	0.18	0.7
R685/R655	-	0.52
PRI (R570-R539)/(R570+R539)	-	0.4

* *DP21 ($D_{\lambda p}$/D703) is defined as the derivative of the reflectance at the inflection point in the red edge spectral region ($D_{\lambda p}$) over the derivative at 703nm (D703).*

2.1.2. Derivative analysis and spectral difference in the red edge region for CF detection

Zarco-Tejada *et al.* (2000b; 2001a; 2003) suggested that a *double-peak* feature at 690-710 nm spectral region seen in the derivative reflectance was possibly due to the combined effects of fluorescence emission and low chlorophyll *a+b* (C_{a+b}) content on stressed vegetation, providing potentially important applications in vegetation stress detection using passive hyperspectral remote sensing methods. Two different methods are proposed to extract the fluorescence signal from canopy-level reflectance using derivatives and spectral difference calculations: i) the first method consisted in the calculation of the reflectance difference between two times at which fluorescence emissions are different. This method "extracts" the fluorescence change between the two times at which reflectance is collected (Zarco-Tejada *et al.,* 2000a); ii) calculation of derivative reflectance enables the detection of subtle changes due to fluorescence emission in the red edge region while minimizing other confounding effects. Derivative indices used are D_{705}/D_{722}, D_{730}/D_{706}, DP22 ($D_{\lambda p}/D_{720}$), DPR1 ($D_{\lambda p}/D_{\lambda p+12}$), where λ_p is the inflexion point of the reflectance spectrum in the red edge spectral region. Changes in the derivative spectra (Figures below) were associated with water and heat stress conditions, observing the recovery after the diurnal experiment (Zarco-Tejada *et al.*, 2003).

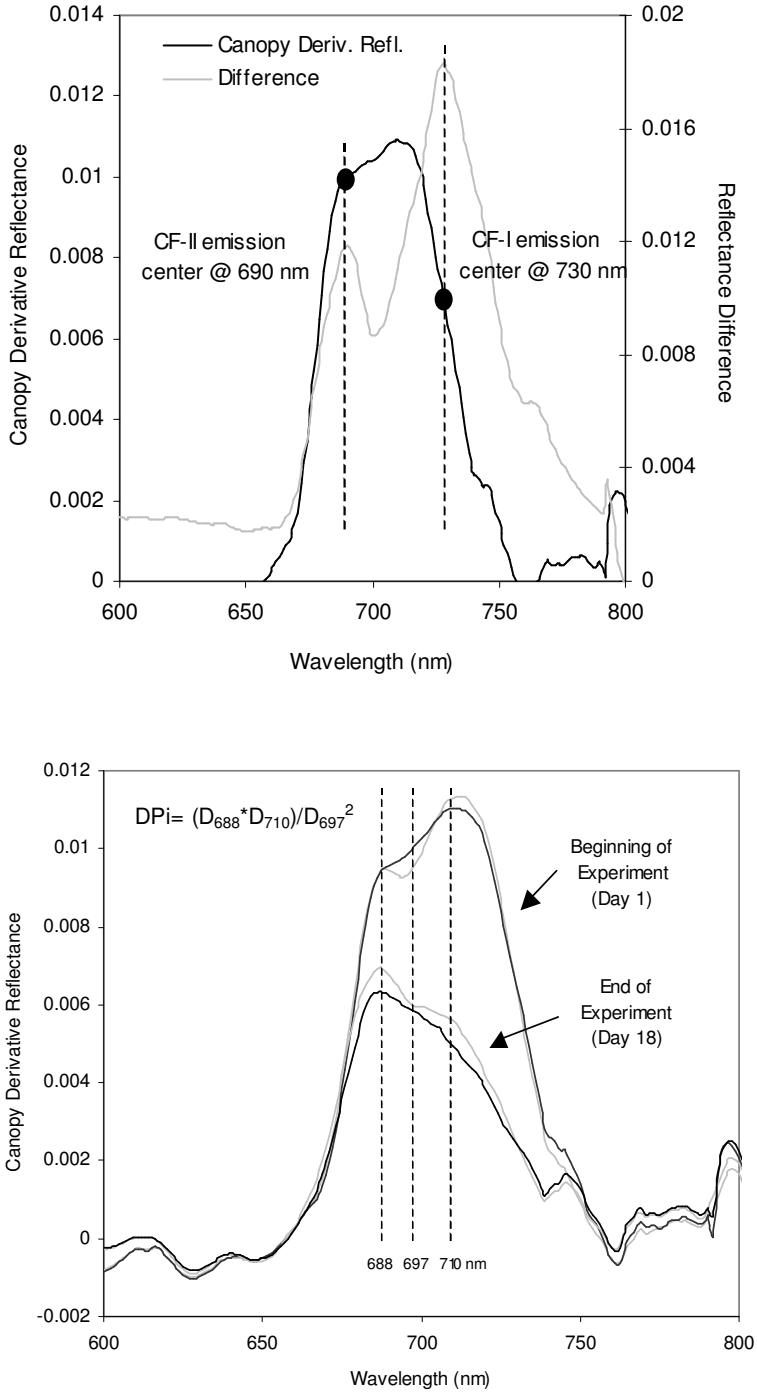

Figure 2-2. Demonstration of the spectral derivative method for the extraction of a fluorescence signal from apparent canopy-level reflectance. Top graph: demonstration of canopy derivative reflectance and fluorescence emission bands in an artificial Acer negundo seedling canopy. Bottom graph: observed changes in the apparent canopy reflectance spectrum of the Acer negundo canopy at the start and end of a stress experiment. Black and gray lines refer to times of low and high fluorescence, respectively. The overimposed effects of changes in chlorophyll content and fluorescence are apparent; the proposed DPi index enables to extract the fluorescence signal alone. From Zarco-Tejada *et al.* 2003

The double-peak index based on derivative analysis demonstrated a successful relationship with steady-state fluorescence emission (Figure 2-3.) and assimilation (Dobrowski *et al.,* 2005). Two optical indices calculated from canopy derivative reflectance are suggested as they demonstrate to be directly related to the steady-state fluorescence emission in vegetation. DPi, calculated as $(D_{688}{\cdot}D_{710})/D_{697}^2$, and the area of the *double-peak* feature, A_{dp}, showed to track Ft (steady-state fluorescence at time t) variation during both short and long-term stress induction stages. Moreover, the reflectance difference calculation, the *double-peak* feature, and the proposed new optical indices, were able to track fluorescence recovery after depression induced by temperature and humidity. Relationships found between steady-state fluorescence measured with a fluorometer and the *double-peak* optical indices DPi (r^2=0.67) and A_{dp} (r^2=0.77) during the course of a laboratory experiment (18-day trial) demonstrated the validity of these indices for tracking fluorescence variation. The relationship found between DPi and Ft at the beginning (r^2=0.97) and the end of the trial (r^2=0.88) demonstrated that the index closely tracks steady-state Ft variation during depression and subsequent recovery.

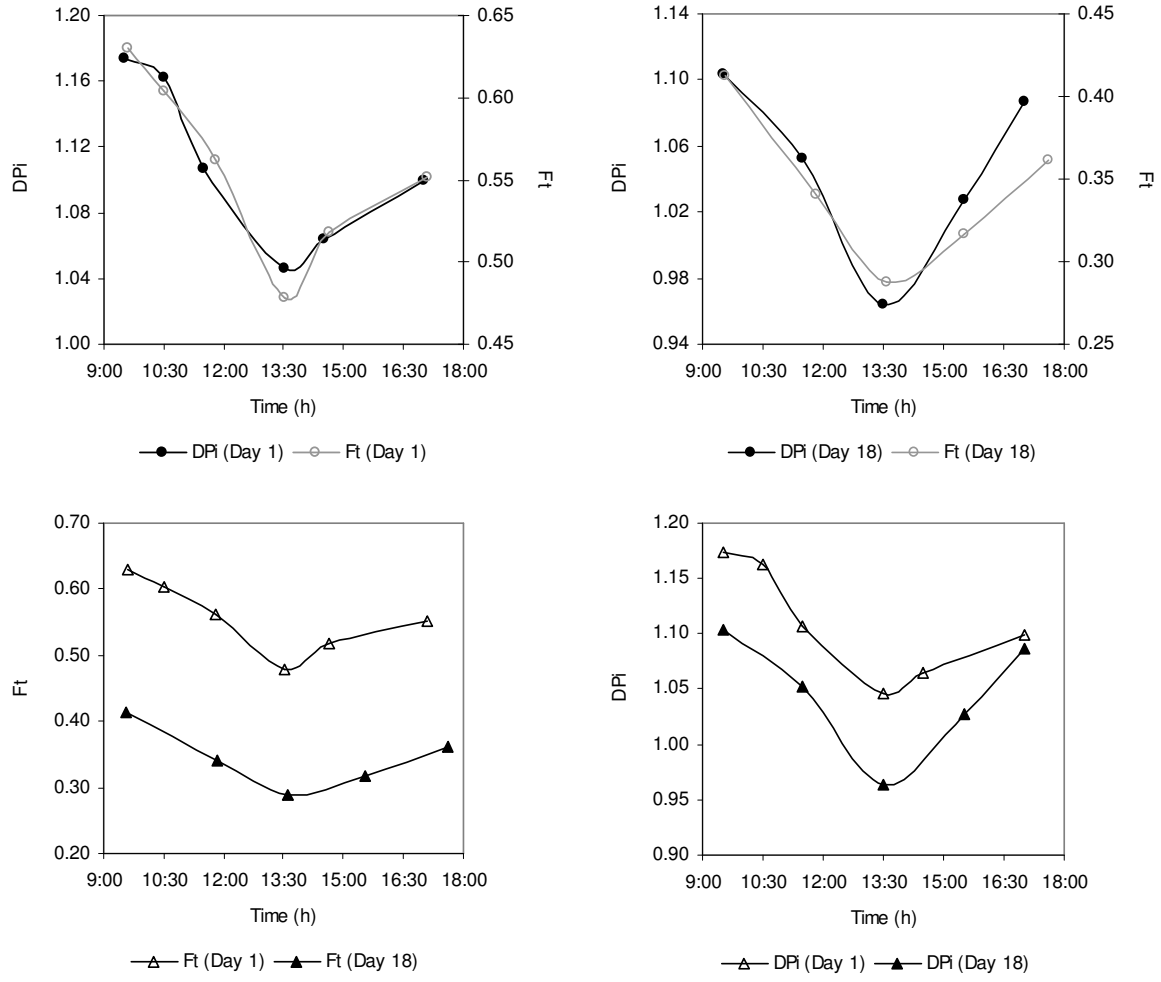

Figure 2-3. Demonstration of the potential of the spectral derivative method for tracking steady-state fluorescence emission by passive remote-sensing techniques. Concurrent daily changes in steady-state fluorescence (Ft, as measured by a PAM-2000 modulated fluorometer) and the DPi index during the course of a temperature and humidity stress experiment in an artificial Acer negundo canopy; data correspond to the first (top left) and last day (top right) of the 18-day trial. Variations of Ft (bottom left) and DPi (bottom right) at the beginning and end of the experiment show that both Ft and DPi decrease their values due to the long-term effects induced during the 18-day experiment. From Zarco-Tejada *et al.* 2003

2.1.3. Detecting CF using the O_2-A fluorescence *infilling* method

A very promising method to detect fluorescence emission is based on the Fraunhofer absorption lines, also known as the *infilling* method. Previous studies such as the measurements of solar-induced natural fluorescence in vegetation canopies were reported by McFarlane *et al.* (1980) who measured solar-induced fluorescence in a crop canopy using the H-α Fraunhofer line at 656 nm, and Carter *et al.* (1990, 1996a) using the H-α and O_2-B lines in leaf measurements. Recent studies provide evidence for fluorescence *in-filling* of the O_2-A atmospheric oxygen absorption band at 760 nm, as a detectable feature in the radiance spectra at the near-canopy levels (Moya *et al.*, 2004; Evain *et al.*, 2004; Perez-Priego *et al.*, 2005; Liu *et al.*, 2005). At the airborne and far-field scales, Maier *et al.* (2002) and Zarco-Tejada *et al.* (2002c) found evidence for the detection of the solar-induced fluorescence signal on apparent reflectance obtained from airborne sensors *Reflective Optics System Imaging Spectrometer* (ROSIS) and *Compact Airborne Spectrographic Imager* (CASI) based on the *in-filling* of fluorescence in the 760 nm atmospheric oxygen absorption band. Experiments conducted with narrow band spectrometers (0.065 nm FWHM) (Perez-Priego *et al.,* 2005) demonstrated that the observed fluorescence *in-filling* in the O_2-A band at 760.5 nm was able to detect and track water stress status in orchard trees. The figure below shows the spectral irradiance (a,b) and crown radiance measurements (c,d) showing the O_2-A and O_2-B absorption bands collected with the narrow-band HR2000 spectrometer in the field. Calculation of reflectance in the red edge spectral region (e,f) from irradiance (a,b) and vegetation radiance spectra (c,d) generates a *peak* due to the fluorescence *in-filling* emission at the O_2-A band.

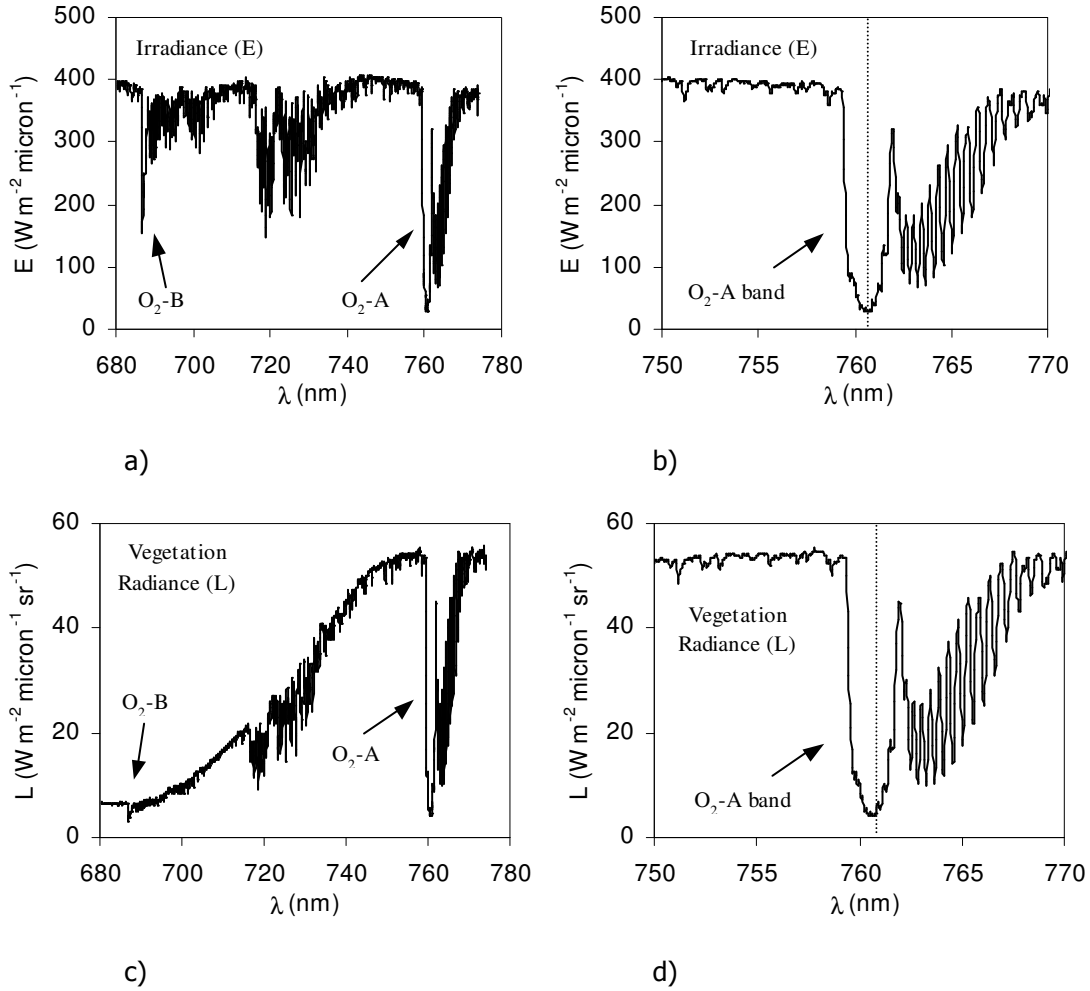

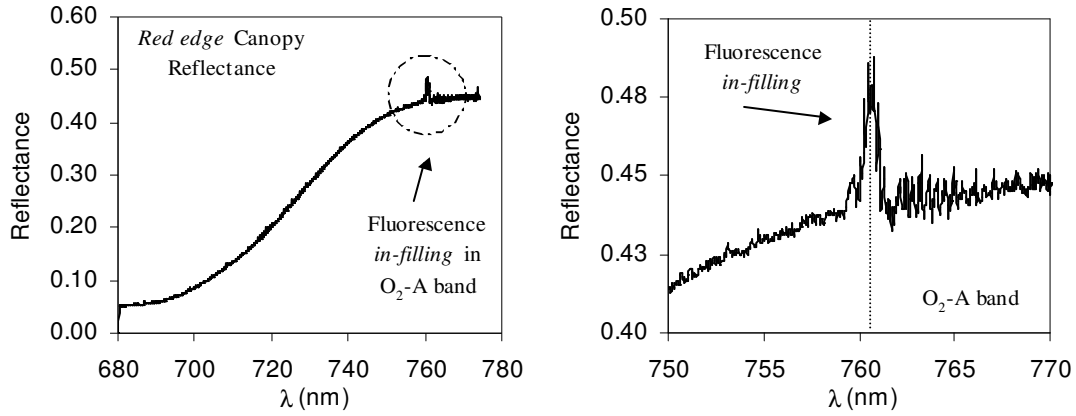

e) f)

Figure 2-4. Figure 2.4 Detection of the solar-induced fluorescence signal by the in-filling of fluorescence in the 760 nm atmospheric oxygen absorption band, based on canopy radiance measurements with a narrow band spectrometers (0.065 nm FWHM; Perez-Priego *et al.*, 2005). Spectral irradiance (a,b) and crown radiance measurements (c,d) showing the O2 A and O2-B absorption bands collected with the narrow-band HR2000 spectrometer in the field. Calculation of reflectance in the red edge spectral region (e,f) from irradiance (a,b) and vegetation radiance spectra (c,d) generates a peak due to the fluorescence in filling emission at the O2-A band. Left- and right-hand side graphs only differ for their spectral range.

The amplitude of the 760 nm peak demonstrated a link between Ft and *in-filling* of the 760 nm apparent reflectance at the crown level on individual trees (r^2=0.61) (Perez-Priego *et al.*, 2005), suggesting that natural fluorescence was detected through reflectance spectra on all trees under different water stress conditions. Results obtained at canopy level for water stress monitoring through fluorescence detection are in agreement with studies conducted by Meroni *et al.* (2005) at the leaf level, and with canopy results by Moya *et al.* (2004), showing that fluorescence emission can be detected at the leaf level and on a corn canopy under diuron herbicide penetration using the O_2-A band.

2.2. Correction of fluorescence for chlorophyll content effects

2.2.1. Influence of chlorophyll content on fluorescence and fluorescence spectra

Chlorophyll content is arguably the single greatest factor affecting steady-state chlorophyll fluorescence ratios derived from red and far-red fluorescence (R/FR). In a review of the variability of the CF emission ratio R/FR of leaves, Buschmann (2007) concluded that the ratio depends mainly on chlorophyll content, to a lower degree also on photosynthetic activity, and to a relatively low extent on the optical characteristics and arrangements of cells in the leaf tissue. An important external factor is excitation wavelength of incident light (Lichtenthaler and Babani 2004). It has been estimated that 92% or more of the variation in the ratio F685/F735 in leaves during development or at damage and stress events is determined by variations in chlorophyll content and corresponding changes in the optical properties of leaves (Gitelson *et al.* 1998).

Chlorophyll content exerts its control over R/FR fluorescence mainly through re-absorption of fluorescence. (Note: Absorption by chlorophyll also influences bands at 531 nm, 551 nm, and 667 nm (Drolet *et al.* 2005). Re-absorption is much stronger in the red wavelengths around 680-690 nm than in the far red region around 735 nm (Lichtenthaler and Rinderle 1988). Generally, as chlorophyll content increases, chlorophyll fluorescence decreases in the red region. Thus, chlorotic leaves have higher fluorescence compared to deep green foliage (Lichtenthaler and Babani 2004, Lictenthaler and

Rinderle 1998). Also, sun leaves have lower steady-state red fluorescence (Fs) than shade foliage, a function of higher F690 re-absorption in thicker leaves with higher chlorophyll in the sun. So that, while increasing chlorophyll content does produce overall more CF, it is not evident from casual measurement of CF because of this re-absorption phenomenon.

With increasing chlorophyll, the relative proportion of the F690 band continuously decreases (Lichtenthaler and Babani 2004). This is true for leaves and green algae suspensions of various algal densities. With autumnal senescence, the R/FR ratio increases and shifts towards shorter wavelengths as a result of leaf chlorosis (a blue shift of 6 nm or so is not uncommon among several woody species when chlorophyll content is lower than 10 μg/cm2). In addition, F690/F735 was shown to rise during desiccation of poikilochlorophyllous plants as chlorophyll content decreased, and was considered a reliable indicator of chlorophyll breakdown in these plants (Csintalan *et al*. 1998).

Louis *et al*. (2005) found an increase in F760 with increasing chlorophyll content, likely a result of the lower tendency for re-absorption at this wavelength. Theirs was a canopy-level study of the boreal forest species Scots pine during spring recovery.

The relatively strong relationship between chlorophyll content and CF emission ratio has allowed the R/FR ratio to be proposed as an actual measure of chlorophyll content; F740/F685 has also been used successfully in a preliminary study of ginkgo trees at 60 m distance (Saito *et al.* 2000). The relationship of chlorophyll content to F690/F735 has been reported to be an inverse curvilinear one (Buschmann 2007, Gitelson *et al.* 1998, Babani and Lichtenthaler 1996). In other leaf-level work, F735/F700 was found to be at least linearly proportional to chlorophyll content (Gitelson *et al.* 1999).

Normal leaf values of F690/F735 are 0.85 to 1.05 (Lichtenthaler and Rinderle 1988). Early stress is identified when the ratio exceeds 1.1, and more severe stress when it exceeds 1.2, all reflecting changes in chlorophyll content and eventually photosynthetic conversion declines. Over various species, very low chl (a+b) produces an F690/F740 of 8 to 10, i.e., no partial re-absorption, which has been confirmed for a variety of tree species (Buschmann 2007, Lichtenthaler and Babani 2004).

The sensitivity of the R/FR ratio is high when chlorophyll content is less than 250 mg/m^2, and sensitivity decreases at chlorophyll greater than 300 mg/m^2 (Gitelson *et al*. 1998). Hence, when chlorophyll is high (as in deep green plants), changes in the ratio might be more indicative of the influence of factors other than chlorophyll.

In considering the R/FR ratio as an indicator of chlorophyll content, it should be recognized that not just leaf chlorophyll may be involved. The chlorophyll content per unit bark area can be as high as in leaves (Solhaug and Haugen 1998). For example, the bark of aspen contains 17-40% of whole tree chlorophyll (the phellem transmits 35-55% of incident light) (Kharouk *et al*. 1995).

Blue light excitation produces higher F690/F740 because blue light-excited CF is less re-absorbed in the upper cell layers of the leaf (Lichtenthaler and Babani 2004, Lichtenthaler and Rinderle 1988). With blue excitation light the red short-wavelength fluorescence is higher as compared to an excitation by green or orange light, owing to the lesser penetration of blue light beyond the superficial layers of the leaf and consequently the lower chance of re-absorption. With green (ca. 550 nm) or orange light (ca. 600 nm) that is not absorbed by carotenoids penetration is deeper into the green leaf mesophyll, and fluorescence is also emitted deeper inside the leaf from where it may be strongly re-absorbed on its way to the leaf surface.

There are several papers on the possible effects of PS I on the R/FR ratio measured at room temperature (Buschmann 2007). For example, the increase of CF with decreasing temperature of leaves from 23ºC to 4ºC was more pronounced at the long-wavelength fluorescence band than at the short-wavelength band, causing a decrease in the ratio by approximately 25% (Agati 1998). This effect has been attributed to a higher increase of the PS I fluorescence than that of PS II (Agati *et al*. 2000). The contribution of PS I fluorescence is reported to occur mainly in the range of 705-725 nm (Lombard and Strasser 1984).

2.2.2. Correction of fluorescence for chlorophyll content (re-absorption)

Given that chlorophyll content has such a strong influence on steady-state R/FR fluorescence ratios, it is important to consider whether it is possible to remove the effect of chlorophyll content through some form of correction which yields a true indication of fluorescence without the effects of re-absorption.

At the leaf level, Gitelson *et al*. (1998) retrieved the actually emitted CF spectrum and the R/FR ratio based on simultaneous measurement of the absorption and reflectance spectra of the same leaf (Gitelson *et al*. 1998). The CF emission spectrum was corrected at each wavelength for re-absorption by means of non-absorbed radiation, as follows:

$f_\lambda = l\, F_\lambda / (R+T)_\lambda$

where l is constant, f is retrieved (or true) fluorescence, F is measured fluorescence, R is reflectance, and T is transmittance.

The shape of the retrieved CF at 685 and 735 nm was found to be very similar to that of strongly diluted chlorophyll *a* in solution, only the position of the emission maxima was different (673 nm of Chl *a* in ethanol solution, and 685 nm in leaves). The leaves used in these experiments were from beech (*Fagus sylvatica* L.), elm (*Ulmus minor* Miller), and a wild vine shrub (*Parthenocissus tricuspidata* L.). Leaves had a broad range of green colour, with chlorophyll contents from 70 to 670 mg/m^2 (Gitelson *et al*. 1998). For leaves in different stages of development and pigment content, the retrieved CF at 685 nm and 735 nm was found to be virtually linearly proportional to chlorophyll content. The absorption at 685 nm reached 90-95% at a chlorophyll content > 250 mg/m^2 whereas it was just over 50% at the lowest chlorophyll content. Leaf absorption at 735 nm was small (average value 15%) and its variation did not exceed 5.5%. The correction of the F685/F735 ratio for re-absorption removed almost all of its dependence on chlorophyll content. The average value of the corrected ratio with high chlorophyll content was about eight times higher for all leaves studied than that of the uncorrected F685/F735 ratio.

Two further approaches for correction were suggested by Agati *et al*. (1993) and Ramos and Lagorio (2004). While Gitelson's method was developed empirically, the latter two were physical approaches involving interaction between light and matter. All three methods were tested by Cordón and Lagorio (2006) to estimate the re-evaluated ratio F690/F735 corrected for re-absorption of CF, and very different results were obtained. The corrected ratio F690/F735 for the same *Ficus benjamina* leaf was:

13 ± 1.3 according to the method of Gitelson *et al*. (1998),

2.04 ± 0.20 according to the method of Ramos and Lagorio (2004), and

1.41 ± 0.14 according to the method of Agati *et al*. (1993).

The latter two ratios are considered too low to be realistic (Buschmann 2007), as it has already been shown that in leaves with very low chlorophyll content or in diluted chloroplast suspensions, where re-absorption is minimal, considerably higher values of at least 5 are obtained. Consequently, the theoretical assumptions made by Agati *et al*. (1993) and Ramos and Lagorio (2004) for the correction of the R/FR fluorescence ratio are suggested to be incorrect (Buschmann 2007).

The implication of the work of Gitelson and colleages is that the R/FR ratio may be satisfactorily corrected to account for re-absorption by chlorophyll. One qualification that could be made in the interpretation of that work is that there was a slight trend evident in their data for an increase in the corrected R/FR ratio with increasing chlorophyll content (see Gitelson *et al*. 1998: their Figure 2-4C) suggesting that assessment of chlorophyll content is useful for this determination. A calibration could be undertaken with a sample of leaves in a given study situation to include chlorophyll content, measured fluorescence, transmittance, and reflectance, in order to derive a corrected R/FR ratio as a function of chlorophyll content. This would be especially valuable in situations involving coniferous species with needle-shaped, evergreen foliage as such species were not included in their study. Periodic measures of chlorophyll content may also be needed.

2.2.3. Estimation of chlorophyll content from reflectance

Zarco-Tejada *et al*. (2004) examined the potential to estimate needle chlorophyll content from airborne hyperspectral optical data through inversion of linked leaf level and canopy level radiative transfer models. The study focused on several sites of jack pine (*Pinus banksiana* Lamb.) in Canada, where field, laboratory, and airborne data were collected over two consecutive years. Airborne hyperspectral CASI data of 72 bands in the visible and near-infrared region and 2m spatial resolution were collected from 20x20 m study sites. Needle chlorophyll content could be estimated at the leaf level (r^2=0.4) by inversion of the PROSPECT leaf model from needle reflectance and transmittance spectra collected with a special needle carrier apparatus coupled to a Li-Cor 1800 integrating sphere. The forest stands had LAI>2, and the high spatial resolution hyperspectral reflectance allowed the use of the SPRINT canopy reflectance model coupled to PROSPECT for needle chlorophyll content estimation by model inversion. The optical index R750/R710 was used as the merit function in the numerical inversion to minimize the effect of shadows and LAI variation in the mean canopy reflectance from the 20 × 20 m plots. Estimates of needle pigment content from airborne hyperspectral reflectance using this linked leaf-canopy model inversion methodology showed an r^2=0.4 and RMSE=8.1 µg/cm^2 when targeting sunlit crown pixels with pigment content ranging between 26.8 and 56.8 µg/cm^2 (1570–3320 µg/g).

In another study, Zarco-Tejada *et al*. (2005) examined chlorophyll *a* and *b* (C_{ab}) estimation at leaf and canopy levels in *Vitis vinifera* L. Field and airborne data were collected for 24 vineyards in northern Spain, with the *Compact Airborne Spectrographic Imager* (CASI), the *Reflective Optics System Imaging Spectrometer* (ROSIS) and the *Digital Airborne Imaging Spectrometer* (DAIS-7915) hyperspectral sensors. A total of 103 study areas of 10 × 10 m were used, and measurements included chemical analysis of leaf pigment concentration, leaf reflectance and transmittance. Several narrow-band vegetation indices were calculated from leaf reflectance spectra, and the PROSPECT leaf optical model was used for inversion using the extensive database of leaf optical properties. Results showed that the best indicators for chlorophyll content estimation were narrow-band hyperspectral indices calculated in the 700–750 nm spectral region (r^2 ranging between 0.8 and 0.9), with poor performance of traditional indices such as the *Normalized Difference Vegetation Index* (NDVI). Results for other biochemicals indicated that the *Structure Insensitive Pigment Index* (SIPI) and the *Photochemical Reflectance Index* (PRI) were more sensitive to carotenoids C_{x+c} and chlorophyll–carotenoid ratios C_{ab} / C_{x+c} than to chlorophyll content C_{ab}. Chlorophyll *a* and *b* estimation by inversion of the PROSPECT leaf model on *V. vinifera* L. spectra was successful, yielding a determination coefficient of r^2 = 0.95, with an RMSE = 5.3 µg/cm^2. The validity of leaf-level indices for chlorophyll content estimation at the canopy level in *V. vinifera* L. was studied using the *scaling-up* approach that links PROSPECT and rowMCRM canopy reflectance simulation to account for the effects of vineyard structure, vine dimensions, row orientation and soil and shadow effects on the canopy reflectance. The index calculated as a combination of the *Transformed Chlorophyll Absorption in Reflectance Index* (TCARI), and the *Optimized Soil-Adjusted Vegetation Index* (OSAVI) in the form TCARI/OSAVI was the most consistent index for estimating C_{ab} on aggregated and pure vine pixels extracted from 1 m CASI and ROSIS hyperspectral imagery. Predictive relationships were developed with a PROSPECT–rowMCRM model between C_{ab} and TCARI/OSAVI as function of LAI, using field-measured vine dimensions and image-extracted soil background, row-orientation and viewing geometry values. Prediction relationships for C_{ab} content with TCARI/OSAVI were successfully applied to the 103 study sites imaged on 24 fields by ROSIS and CASI airborne sensors, yielding r^2 = 0.67 and RMSE = 11.5 µg/cm^2.

Recently, canopy chlorophyll (and carotenoid) concentration was studied in a boreal mixedwood forest in Canada, using hyperspectral and lidar data (Thomas *et al*. 2007). Mixedwood forests are quite complex spatially. The study tested over 30 indices categorized by Visible and/or NIR Indices, Red-Edge Reflectance Indices, and Derivative Indices (Table 2-2). First, canopy scale application of hyperspectral reflectance and derivative indices were used to estimate chlorophyll concentration. Second, lidar data was used to identify structural metrics related to chlorophyll concentration. Third, lidar metrics and hyperspectral indices were combined to determine if chlorophyll concentration

estimates could be further improved. Of the hyperspectral indices considered, two derivative indices worked well. The derivative chlorophyll index (DCI) $\delta_{(705)}/\delta_{(722)}$ (Zarco-Tejada *et al*. 2002a) (r^2=0.79) and the red-edge inflection point λ_p (Zarco-Tejada *et al*. 1999a) (r^2=0.78) were good predictors of chlorophyll concentration when mixed-species plots were included in analysis. Integrating mean lidar first return heights for the 25th percentile with the hyperspectral DCI index further strengthens the relationship to canopy chlorophyll concentration (r^2=0.84 for mixed species, the coefficient being much higher if only a single species is considered (r^2=0.94).

Table 2-2. - Indices tested for determination of canopy chlorophyll concentration in Thomas *et al*. (2007).a,b

Visible and/or NIR Indices	**Description**	**Reference**
R_{551}/R_{680}	Narrow-band Greenness Index	Zarco-Tejada *et al*. 1999a
$(R_{430})/(R_{680})$	Simple Ratio Pigment Index	Peñuelas *et al*. 1995
$(R_{680}-R_{430})/(R_{680}+R_{430})$	Normalized Pigment Chlorophyll Index	Peñuelas *et al*. 1994
$(R_{695})/(R_{420})$	Carter Index	Carter 1994
$0.5*(120*(R_{650}-R_{550})-00*(R_{670}-R_{550}))$	Triangular Vegetation Index	Broge and Leblanc 2000
$Lic1=(R_{800}-R_{680})/(R_{800}+R_{680})$ $Lic2=(R_{440})/(R_{690})$	Lichtenthaler indices	Lichtenthaler *et al*. 1996
$PRI1=(R_{528}-R_{567})/(R_{528}+R_{567})$ $PRI2=(R_{531}-R_{570})/(R_{531}+R_{570})$	Photochemical Reflectance Index	Gamon *et al*. 1992
$(R_{800}-R_{450})/(R_{800}+R_{650})$	Structure Intensive Pigment Index	Peñuelas *et al*. 1995
Red-Edge Reflectance Indices		
$TCARI/(1+0.16)(R_{800}-R_{670})/(R_{800}+R_{670}+0.16)$	TCARI/OSAVI TCARI=3MCARI overcomes sensitivity to soil reflectance	Rondeaux *et al*. 1996 Haboudane *et al*. 2002
$(R_{700}-R_{670})-0.2(R_{700}-R_{550})(R_{700}/R_{670})$	Modified chlorophyll absorption index MCARI counteracts background influences	Kim *et al*. 1994 Daughtry *et al*. 2000
$(R_{750})/(R_{710})$	Zarco-Tejada & Miller	Zarco-Tejada *et al*. 2001b
$(R_{750}-R_{705})/(R_{750}+R_{705})$	Modified NDVI, designed to detect leaf chlorophyll content	Gitelson and Merzlyak 1996
$(R_{600}-R_{699})/(R_{500}-R_{599})$	Chlorophyll and pigments	Gamon and Surfus 1999
$G\&M1=R_{750}/R_{550}$ $G\&M2=R_{750}/R_{700}$	Designed for the measurement of chlorophyll content in plant leaves	Gitelson and Merzlyak 1997
$R_{min(650-700)}$ $R_{max(700-770)}$	Chlorophyll fluorescence, red-edge	Zarco-Tejada *et al*. 1999a
$Vog1=(R_{740})/(R_{720})$ $Vog2=(R_{734}-R_{747})/(R_{715}+R_{726})$ $Vog3=(R_{734}-R_{747})/(R_{715}+R_{720})$	Vogelmann indices	Vogelmann *et al*. 1993; Zarco-Tejada *et al*. 1999a
$(R_{695})/(R_{760})$	Carter Index	Carter *et al*. 1996b

Derivative Indices	**Description**	**References**
λ_p	Red edge inflection point. Chlorophyll fluorescence and pigments (calculated as red-edge wavelength where $d^2R/dw^2=0$	Zarco-Tejada *et al*. 1999b
$DPR_1=\delta_{\lambda p(680-750)}/\delta_{\lambda p+12}$ $DPr_2=\delta_{\lambda p(680-750)}/\delta_{\lambda p+22}$ $DP2_1=\delta_{\lambda p(680-750)}/\delta_{703}$ $DP2_2=\delta_{\lambda p(680-750)}/\delta_{720}$	Double peak derivative indices for chlorophyll fluorescence and pigments	Zarco-Tejada *et al*. 2003
$\delta_{(705)}/\delta_{(722)}$	Derivative chlorophyll index (DCI)	Zarco-Tejada *et al*. 2002a,b
$\delta_{max(680-750)}$	Maximum 1st derivative for red-edge	Thomas *et al*. 2006
$\delta_{max(500-600)}$	Maximum 1st derivative for green	Thomas *et al*. 2007
$\delta_{min(500-600)]}$	Minimum 1st derivative for green	Thomas *et al*. 2007

[a] R denotes reflectance.

[b] δ denotes magnitude of the first derivative, *dR/dw*

3. ANALYSIS OF ABSOLUTE VALUES OF SOLAR-INDUCED FLUORESCENCE

3.1. Factors affecting absolute SIF values

For many years the SIF variation has been measured during a diurnal cycle and confronted with photosynthetic activity (Valentini *et al.* 1995; Cerovic *et al.* 1996; Rosema *et al.* 1998; Flexas *et al.* 2000; Evain *et al.* 2002; Evain *et al.* 2004; Louis *et al.* 2005). Most of the measurements were at the leaf level, owing to the very few instruments capable to determine the fluorescence at the canopy level. In the following the more representative results are emphasised.

The SIF daily cycle follows a "M" shaped variation with a more or less marked minimum an solar noon. The minimum depends on several parameters including plant species and light intensity. On healthy plants variation between maximum and minimum SIF is about 50% of the minimum. Under constraint the variation can reach 100%. This is the case of draught conditions, as a result of a decrease of the minimum SIF value, under maximum illumination conditions.

Stationary fluorescence alone doesn't allow to calculate the electron transfer rate of PSII (ETR) in the absence of the Fo and Fm' information (i.e. fluorescence measurements on the leaf either dark-aclimated or exposed to a brief pulse of saturating light). Furthermore there is still an important gap between ETR and photosynthesis (CO2 assimilation) (see Figure 4 in Cerovic *et al.* 1996) as photorespiration may account for up to 40% of ETR in C3 species (majority of deciduous plants and trees). Under drought conditions ETR is still 50% of its value under watered conditions whereas photosynthesis is almost zero.

At the canopy level the situation is more complex due to the particular light climate of each specific leaf. As a result the averaged SIF value may differ from the SIF at leaf level by more than 40%. Two set of passive fluorescence measurements done in outdoor conditions have been reported in the literature. The first reported a time series of simultaneous SIF measurements at 687 and 760 nm from a 10 m tower above a corn field that was subject during several days to a progressive drought (Evain *et al.* 2002). SIF was averaged over a 4 hours period around solar noon. No significant fluorescence yield change was detected until the end of the experiment when the Chl content started to decrease. A similar experiment was carried out with the same instrumentation over the boreal pine forest, during spring recovery of the photosynthetic activity (Louis *et al.* 2005). Although the CO_2 assimilation changed during the time series of the measurement from almost zero to the full summer capacity, SIF yield at 760 nm alone showed a small increase at the end of the campaign while SIF yield at 687 nm stays constant.

3.2. Novel algorithms for the inclusion of fluorescence and leaf optical properties in functional models of leaf photo-synthesis

Chlorophyll fluorescence has been widely used over recent decades as a powerful tool for the assessment of photosynthetic processes (Govindjee 1995; Adams III *et al.* 2004). Although several models have been developed for the interpretation of the resulting signal (Genty *et al.* 1989a; Lavergne *et al.* 1995; Hendrickson *et al.* 2004; Kornyeyev *et al.* 2007), these generally only apply to pulse-saturated fluorescence, where the information provided by ambient fluorescence is complemented by the signal after a pulse of saturating light. A model for the interpretation of ambient fluorescence has been proposed by Rosema (1998), but it is admittedly limited to ideal conditions rarely encountered in the field.

Based on available evidence and on the strong background of available models of pulse-saturated fluorescence, two novel models have been developed as part of the project, aimed at the representation of the functional link between electron transport and photosynthetic processes, on the one hand, and ambient fluorescence on the other (van der Tol *et al.* 2008; Magnani *et al.* 2009). The two models, which share several features but differ in their assumptions and predictions, will be briefly presented here and tested against available experimental data.

3.2.1. The van der Tol-Verhoef-Rosema model

The proposed model describes the relationship between fluorescence and photosynthesis at leaf level. A photon absorbed by a leaf can be dissipated as heat, or used for photochemistry, or emitted as fluorescence. The probability of each depends on biochemical and environmental conditions. For the interpretation of the chlorophyll fluorescence signal, it is necessary to describe the relationship between fluorescence and photochemistry as a function of these conditions.

The relationship between steady state fluorescence and photochemistry under low light conditions is reasonably well understood (Genty *et al*. 1989a; Rosema *et al*. 1998). With increasing irradiance, the fraction of energy used for fluorescence increases and the fraction used for photochemistry decreases (Maxwell *et al*. 2000). Thus at low light intensity, a negative correlation exists between the probability of fluorescence and photochemistry.

The relationship is different for high light conditions. With increasing irradiance and moisture stress, chlorophyll fluorescence and photochemistry both drop due to deactivation of antennae to prevent damage by harmful radicals formed in those conditions (Gilmore *et al*. 1992; Maxwell *et al*. 2000). Thus at high light intensity and stress, a positive correlation exists between fluorescence and photochemistry.

Because the relationship between fluorescence and photochemistry in unstressed and in stressed conditions is different, the interpretation of the fluorescence signal is not straightforward. An observed increase in fluorescence may be interpreted either as an increase or a decrease of photochemistry, depending on the micro-environment of the observed vegetation. Both effects have been observed (Flexas *et al*. 2000). This has given rise to the discussion of whether chlorophyll fluorescence is a measure of photosynthesis or of stress factors (Maxwell *et al*. 2000). One needs to know the micro-environment before the translation from a chlorophyll fluorescence measurement to actual photosynthesis can be made.

The chapter presents a model for the relationship between chlorophyll fluorescence and photosynthesis at leaf level as a function of environmental conditions. The model is based on previously developed models for photosynthesis (Farquhar *et al*. 1980; Collatz *et al*. 1992) and chlorophyll fluorescence (Genty *et al*. 1989a; Rosema *et al*. 1998). Coupled models for chlorophyll fluorescence and photosynthesis have been developed before (He *et al*. 1996). The new element of the model presented here is that fluorescence during stressed conditions is quantified as well.

The sensitivity of chlorophyll fluorescence and photosynthesis to radiation, temperature, humidity and soil moisture content at different times of the day is studied. This model is tested against measurements of chlorophyll fluorescence and photosynthesis carried out in a laboratory experiment. In the future, this model can be used to produce diurnal cycles of fluorescence and photosynthesis, and to determine the optimum time of day for taking fluorescence measurements.

3.2.1.1. Coupling photosynthesis and fluorescence

The model presented in this section is based on the existing theory of chlorophyll fluorescence and photosynthesis. For vegetation of the C3 photosynthetic pathway, the model of Farquhar and co-workers (Farquhar *et al*. 1980; Bernacchi *et al*. 2002) is used. In section 3 the model is extended to vegetation of the C4 photosynthetic pathway, for which the model of Collatz *et al*. (Collatz *et al*. 1992) is used.

The model of Farquhar and co-workers describes photosynthesis as the result of two coupled processes: (1) regeneration of RuP2 (ribulose-1,5-bisphosphate, the five-carbon acceptor of CO2), which depends on concentrations of ATP and NAPDH (adenosine tri-phosphate and reduced nicotinamide adenine tinucleotide phosphate, respectively: the final high-energy products of light photosynthetic reactions), and thus on light, and (2) the maximum carboxylation rate at RuP2 saturated conditions in the presence of sufficient light. This depends on the enzyme concentration. The first is referred to as light limitation, the second as enzyme limitation. In practice, it appears to be sufficient to model both processes as if they were independent and estimate actual photosynthesis as the minimum of the two corresponding rates of photosynthesis.

Regeneration of RuP2 depends on the harvest of photons for photochemistry by antennae complexes of two photosystems (PS II and PS I). The harvest in unstressed, low light conditions is calculated using the models of Genty *et al*. (Genty *et al*. 1989a) and Rosema *et al*. (Rosema *et al*. 1998). These models are based on a number of assumptions.

First, the sum of the probabilities of an absorbed photon to result in fluorescence Φf, photochemistry Φp and heat dissipation Φd is unity:

$$\Phi_p + \Phi_f + \Phi_d = 1 \qquad \text{(Eq. 3-1)}$$

Second, open and closed photosystems are distinguished. Closed photosystems are photosystems which recently (during the last ~10-4 s) absorbed a photon. The antennae of these photosystems can absorb photons, but they do not contribute to photochemistry. From these assumptions, the following relationship between fluorescence and photochemistry can be derived (Genty *et al*. 1989b; Rosema *et al*. 1998):

$$\Phi_p = 1 - \frac{\Phi_f}{\Phi_{fo}}\left(1 - \Phi_{po}\right) \qquad \text{(Eq. 3-2)}$$

Where subscript 'o' denotes open photosystems. The higher the irradiance, the more photosystems will be closed. In literature, this process is referred to as photochemical quenching (Maxwell *et al.* 2000).

Third, Φp is proportional to the fraction of open photosystems ζp:

$$\Phi_p = \zeta_p \Phi_{po} \qquad \text{(Eq. 3-3)}$$

Fourth, electron transport for photochemistry J (μmol m^{-2} s^{-1}) from charged photosystems is proportional to the number of closed photosystems (1-ζ_p) and to a maximum rate of electron transport, if all photosystems are closed J_{max} (μmol m^{-2} s^{-1}):

$$J = \left(1 - \zeta_p\right) J_{\max} \qquad \text{(Eq. 3-4)}$$

If photon yield for photochemistry and electron transport from the photosystems are in equilibrium, then:

$$J = \Phi_p Q / 2 \qquad \text{(Eq. 3-5)}$$

Where Q is the rate of absorbed photons (μmol m^{-2} s^{-1}), and the number 2 denotes that half of the photons is absorbed by PS II (and used for J), and the other half by PS I (and used for NADPH). Photochemical quenching (the fraction of open photosystems) can now be solved from Eqs 3-5:

$$\zeta_p = \frac{2J_{\max}}{2J_{\max} + \Phi_{po} Q} \qquad \text{(Eq. 3-6)}$$

The six equations above describe the relationship between fluorescence and electron yield for photosynthesis. The electron yield can be used directly in the model of Farquhar and co-workers to calculate actual photosynthesis. Parameter J_{max} is used in order to be consistent with the model of Farquhar. Equations 1-6 are commonly used in literature, although the use of symbols may vary.

Table 3-1. List of model parameters, with units and description

Symbol	Unit	Description
A	µmol $m^{-2}s^{-1}$	Net carbon dioxide used for leaf photosynthesis
C	µmol m^{-3}	Carbon dioxide concentration in the mesophyll
h	µmol m^{-3}	Size of the proton pool
h_m	µmol m^{-3}	Size scaling parameters of the proton pool
J	µmol $m^{-2}s^{-1}$	Electron transport rate
J	µmol $m^{-2}s^{-1}$	Unstressed electrion transoirt rate
J_{max}	µmol $m^{-2}s^{-1}$	Maximum electron transport rate
K_c	µmol m^{-3}	Michaelis-Menten coefficient for carbon dioxide
K_o	µmol m^{-3}	Michaelis-Menten coefficient for oxygen
K_r	µmol m^{-3}	Michaelis-Menten coefficient for RuP2
O	µmol m^{-3}	Oxygen concentration in the mesophyll
Q	µmol $m^{-2}s^{-1}$	Rate of absorbed photochemically active photons
R	µmol $m^{-2}s^{-1}$	Size of the RuP2 pool
t	s	Time
V_c	µmol $m^{-2}s^{-1}$	Gross carboxylation rate
V_{cc}	µmol $m^{-2}s^{-1}$	Enzyme limited carboxylation rate
V_{cj}	µmol $m^{-2}s^{-1}$	Light limited carboxylation rate
$V_{c\,max}$	µmol $m^{-2}s^{-1}$	Maximum carboxylation capacity
Φ		Ratio of oxygenation over carboxylation
ϕ_d		Probability of heat dissipation
Φ_d		Probability of heat dissipation of activated photosystems
ϕ_f		Probability of chlorophyll fluorescence
Φ_f		Probability of chlorophyll fluorescence of activated photosystems
Φ_{fo}		Probability of chlorophyll fluorescence of open photosystems
ϕ_p		Probability of photochemistry
Φ_p		Probability of photochemistry activated photosystems
Φ_{po}		Probability of photochemistry of open photosystems
ζ_n		Deactivation reduction factor
ζ_p		Photochemical reduction factor

The model presented so far does not explain all the variations in chlorophyll fluorescence observed in field and laboratory experiments. During stressed conditions (drought, high irradiance and high temperature), chlorophyll fluorescence decreases (Cornic *et al.* 1991; Flexas *et al.* 2000; Flexas *et al.* 2002), whereas the equations above only predict an increase of fluorescence with increasing irradiance. In literature, the quenching effect during stress is often referred to as slowly-relaxing non-photochemical quenching (NPQ), although deactivation of antennae would be a more appropriate term (Rosema *et al.* 1998). Open photosystems are deactivated by zeaxanthin, which is formed in high concentrations when the pH in the lumen (the interior of the thykaloid, the organelle where light reactions take place) is low (Schreiber *et al.* 1990; Osmond *et al.* 1999; Maxwell *et al.* 2000; Müller *et al.* 2001b). Deactivation is a mechanism designed to prevent the plant from damage caused by reactive intermediates produced under conditions of excess light. This also acts to regulate energy harvest for photosynthesis (Osmond 1994). Rosema *et al.* (Rosema *et al.* 1998) attribute the deactivation of antennae to light and drought stress, but do not provide a mechanistic model to quantify its effect as a function of environment. In the next section, deactivation is modelled as a function of environmental conditions.

3.2.1.2. Quantifying deactivation of antennae

To quantify the deactivation of antennae, use is made of the fact that deactivation is a function of the pH of the lumen. A low pH induces reversible conversion of violaxanthin into zeaxanthin in leaves. Zeaxanthin enhances the dissipation of absorbed energy as heat ϕ_d and decreases ϕ_f and ϕ_p (Gilmore *et al.* 1992).

It is assumed that deactivation of antennae reduces fluorescence and photochemistry to ϕ_f and ϕ_p by the same reduction factor ζ_n:

$$\zeta_n = \frac{\phi_f}{\Phi_f} = \frac{\phi_p}{\Phi_p} \qquad \text{(Eq. 3-7)}$$

Capital letters are used for unstressed conditions, and small letters for stressed conditions. The equivalent of Eq 3-2 for the relationship between photochemical yield and fluorescence in stressed conditions is:

$$\phi_p = \zeta_n \left(1 - \frac{\Phi_f}{\Phi_{fo}} \left(1 - \Phi_{po} \right) \right) \qquad \text{(Eq. 3-8)}$$

It is now clear that in order to calculate photochemical yield from fluorescence, the deactivation factor ζ_n has to be known.

The equivalent of Eq 3-5 for electron yield for photosynthesis in stressed conditions j (μmol m^{-2} s^{-1}) is:

$$j = \phi_p Q / 2 = \zeta_n \zeta_p \Phi_{po} Q / 2 \qquad \text{(Eq. 3-9)}$$

The pH in the lumen plays an important role in the regulation of photosynthesis. On the one hand, there is evidence that deactivation of antennae is caused by a low pH in the lumen (as discussed above). On the other hand, the protons in the lumen are needed for the production of ATP, an energy compound which is used for the regeneration of RuP2 (Müller *et al.* 2001b). By having this double role, the proton concentration in the lumen forms the connection between electron transport as calculated with the equations above (negative effect), and carboxylation as calculated with the model of Farquhar and co-workers (positive effect).

Photosynthesis is usually calculated as the minimum of two separate processes, in reality, it is limited by both at the same time. In the coupled equation (Eq 2 of Farquhar *et al.*, 1980), carboxylation is both enzyme and light (RuP2) limited:

$$V_c = V_{c\max}\frac{C}{C + K_c\left(1 + O/K_o\right)}\frac{R}{R + K_r'} = V_{cc}\frac{R}{R + K_r} \qquad \text{(Eq. 3-10)}$$

Where $V_{c\max}$ is the maximum carboxylation capacity of Rubisco (μmol m^{-2} s^{-1}), K_c and K_o the Michaelis-Menten coefficients for carbon dioxide and oxygen (μmol m^{-3}), C an O the concentrations of carbon dioxide and oxygen in the mesophyll (μmol m^{-3}), R the RuP2 concentration integrated (μmol m^{-3}), K_r the Michaelis Menten coefficient for RuP2 (μmol m^{-3}), and V_{cc} the enzyme limited rate of carboxylation (μmol m^{-2} s^{-1}).

It is assumed that the RuP2 pool, the ATP pool and the proton pool are in equilibrium. This is a reasonable approximation, albeit a rather coarse one (ATP is used for other processes besides the regeneration of RuP2, and the regeneration of RuP2 depends on other factors such as the production of NAPH as well). Using this assumption, the RuP2 concentration can be replaced with the proton concentration:

$$V_c = V_{c\max}\frac{C}{C + K_c\left(1 + O/K_o\right)}\frac{h}{h + \left(4 + 4\Phi\right)K_r} \qquad \text{(Eq. 3-11)}$$

Where h is the proton concentration in the lumen (μmol m^{-3}), Φ the ratio of carboxylation to oxygenation and the number 4 denotes that the minimum requirement for carboxylation or oxygenation is 4 moles of electrons and 4 moles of protons per mol converted carbon dioxide or oxygen. It is implicitly assumed that RuP2 regeneration is limited by ATP production, which is governed by PS II. The role of NADPH is not considered. NADPH is produced when a second photon is absorbed by PS I. Excess NADPH can be recycled to produce additional excited electrons and protons (Munekage *et al.* 2004). This contribution to the proton pool has been neglected.

An expression for deactivation can be derived by solving the mass balance of the proton pool in the lumen. This mass balance is:

$$D\frac{\partial h}{\partial t} = j(h,t) - (4 + 4\Phi)V_c(h,t) \qquad \text{(Eq. 3-12)}$$

where t is time (s) and D (m) a coefficient to convert from a concentration into a volume density per unit of leaf surface (the volume of the lumen per unit of leaf surface area).

The first term on the right hand side of Eq. 3-12 is the electron (and proton) yield of PS II (Eq. 3-9), and the second term is the use of protons for the production of ATP, and eventually for carboxylation. This term is a function of the proton pool itself (Eq 3-11).

In order to solve the differential equation for the proton pool (Eq. 3-12), function $\zeta_n(h)$ needs to be known, due to the fact that the proton and electron yield j depends on ζ_n. This function should meet the following criteria:

$$\lim_{h\downarrow 0}\zeta_n = 1 \quad \& \quad \lim_{h\to\infty}\zeta_n = 0 \qquad \text{(Eq. 3-13)}$$

Two examples of simple functions which meet these criteria are:

$$\zeta_n = 1 - e^{-h_m/h} \quad , \quad \zeta_n = e^{-h/h_m} \qquad \text{(Eq. 3-14)}$$

Where h_m (μmol m^{-3}) is a size parameter for the proton pool. Based on the reaction equations in the xantophyll cycle (the pH dependent reversible conversion of violaxanthin into zeaxanthin), one could model ζ_n as a function of the proton pool size more realistically. However, this is not feasible for practical applications.

With Equations 6,8,9,11,12 and 14, the evolution of carboxylation, fluorescence and deactivation can be calculated numerically, using appropriate parameter values, initial conditions and input. Absorbed radiation Q and internal carbon dioxide concentration C are the driving (environmental) variables.

The model can be simplified by assuming that the proton pool is in steady state $(\partial h/\partial t = 0)$. Then, by some rearranging:

$$\zeta_n = \frac{V_c(h)}{J/(4+4\Phi)} = \frac{V_c(h)}{V_{cj}} \qquad \text{(Eq. 3-15)}$$

Where V_{cj} (μmol m^{-2} s^{-1}) is the light limited carboxylation rate of the original Farquhar model. Eq. 3-15 implies that in steady state, deactivation of antennae is the ratio of actual over potential light limited carboxylation. In other words, the function of deactivation is to match the supply of excited electrons by photosystems with the use of excited electrons for photosynthesis. When the proton pool is not a in steady state, then the proton pool delays the response of deactivation to light.

The model can be simplified further, by considering only the two limiting cases of the model of Farquhar and co-workers. Calculating only the limiting cases has the advantage that parameters h_m and K_r', and Eq 3-14 are not necessary. Instead, only the extremes of Eq 3-13 are used. If the proton concentration is small:

$$\lim_{h\downarrow 0} \zeta_n = 1 \qquad \text{(Eq. 3-16)}$$

And thus (from Eq 15):

$$\lim_{h\downarrow 0} V_c = V_{cj} = \frac{P_o \zeta_p Q}{4+4\Phi} \qquad \text{(Eq. 3-17)}$$

which is the light limited rate of carboxylation of the original photosynthesis model. If the proton pool is large:

$$\lim_{h\to\infty} \frac{h}{h+K} = 1 \qquad \text{(Eq. 3-18)}$$

And thus (from Eq 11)

$$\lim_{h\to\infty} V_c = V_{cc} = V_{c\max} \frac{C}{C + K_c(1 + O/K_o)} \qquad \text{(Eq. 3-19)}$$

which is the enzyme limited rate of carboxylation of the original Farquhar model.

If only the two limiting cases are considered, then deactivation is (from Eq 3-15):

$$\zeta_n = \min\left(1, \frac{V_{cc}}{V_{cj}}\right) \qquad \text{(Eq. 3-20)}$$

Eq. 3-20 is a simple way to calculate deactivation of antennae from the original model of Farquhar and co-workers. The model makes it possible to calculate photosynthesis and chlorophyll fluorescence in different conditions. The term 'stressed conditions' for conditions in which deactivation occurs is not sufficiently specific, since here it includes all conditions in which photosynthesis is enzyme limited rather than light limited. These conditions include high light levels as well as low carbon dioxide concentrations in the mesophyll, caused by for example stomatal closure. When only the two extreme cases are considered, then deactivation occurs only in light limited conditions. In the dynamic (Eq 3-12) or steady state (Eq 3-15) model, the transition between light and enzyme limitation is gradual, and deactivation also occurs when photosynthesis is co-limited by light and enzymes. The concentration of carbon dioxide in the mesophyll can be calculated from gas exchange using models for stomatal and mesophyll conductance. Stomatal resistance is mainly a function of actual photosynthesis, vapour pressure deficit in the ambient air and soil water potential. Numerous conceptual and empirical functions for stomatal conductance are available (Cowan 1977; Ball *et al.* 1987; Leuning 1995; Wang *et al.* 1998).

3.2.1.3. Extension to C4 vegetation

In vegetation of the C4 photosynthetic pathway, the carboxylation process as described by Eq 3-10 takes place in the bundle sheath (where carbon dioxide is concentrated). The higher carbon dioxide concentration reduces photorespiration losses. Carbon dioxide is concentrated in the bundle sheath using a series of reactions: fixation of carbon dioxide by PEP-carboxylation in the mesophyll, transportation to the bundle sheath cells, and de-carboxylation (Collatz *et al.* 1992). In equilibrium, the transportation of carbon dioxide towards the bundle sheath cells (minus leakage) equals the carboxylation rate in the bundle sheath cells. If we know the equilibrium carbon dioxide concentration in the bundle sheath, then photosynthesis of C4 vegetation can be calculated by replacing carbon dioxide concentration in the mesophyll C with the concentration in the bundle sheath.

Some of the excited electrons are used for PEP-carboxylation in the mesophyll. If the fraction of electrons used for the reactions in the mesophyll is x, then (Massad *et al.* 2007):

$$J_{C4} = (1-x)J \qquad \text{(Eq. 3-21)}$$

In practice, a value of x=0.4 can be used (Massad *et al.* 2007).

The carbon dioxide concentration in the bundle sheath is usually unknown. It can be calculated by assuming the carboxylation rate in the bundle sheath is equal to the PEP-carboxylation rate in the mesophyll minus leakage of carbon dioxide from the bundle sheath to the mesophyll.

3.2.2. Testing the van der Tol-Verhoef-Rosema model

Figure 3-1, Figure 3-2, Figure 3-3 illustrate the behaviour of the modelled processes under different conditions. Figure 3-1and Figure 3-2 are model simulations, whereas Figure 3-3 shows a comparison of the model with laboratory measurements. Because absorbed radiation Q and carbon dioxide concentration in the mesophyll C are the driving variables, these figures focus on the response of the model to these two variables.

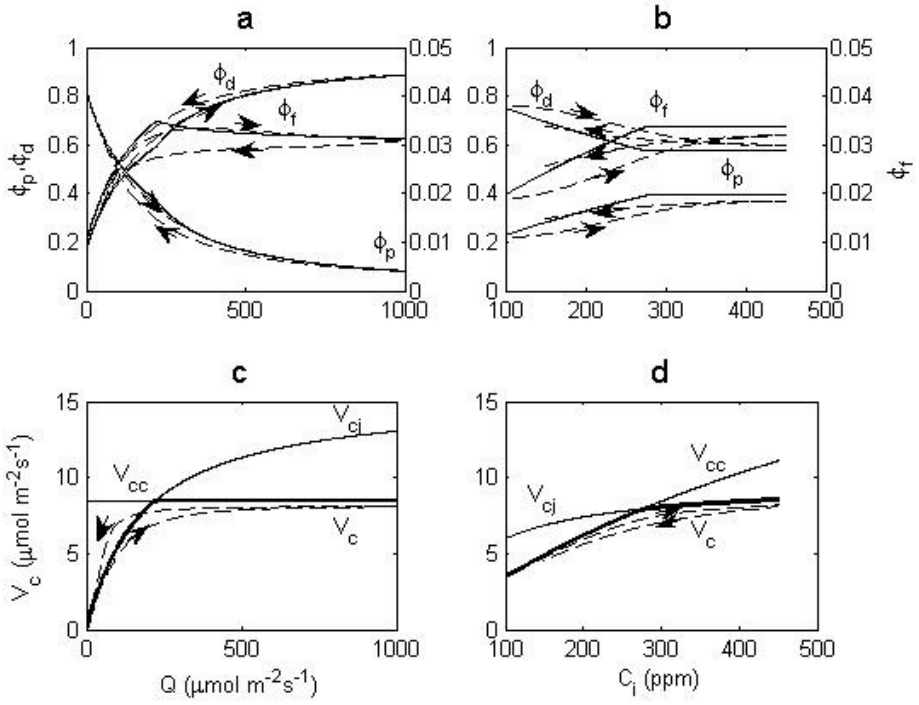

Figure 3-1 - Example of fractions of absorbed light used for photosynthesis ϕ_p, chlorophyll fluorescence ϕ_f, and heat dissipation ϕ_d as functions of (a) absorbed PAR Q at high C (300 ppm) and (b) carbon dioxide concentration C at moderate light intensity (Q=200 μmol m^{-2}s^{-1}). The solid lines are the two limited cases, and the dashed lines the situation for which the size of the proton pool is numerically calculated with Eq 12. The arrows indicate the direction of the response to increasing and decreasing Q and C; (c-d) for the same simulations, actual carboxylation rate calculated with the numerical solution of Eq 12 (dashed lines), and for the two asymptotes of the Farquhar model: electron limited V_{cj} and enzyme limited V_{cc} and the minimum of the two in bold.

Figure 3-1 shows modelled probabilities of fluorescence ϕ_f, photochemistry ϕ_p and heat dissipation ϕ_d, and enzyme and light limited carboxylation V_{cc} and V_{cj} as a function of the two driving variables, notably absorbed radiation Q and carbon dioxide concentration in the mesophyll C. Fluorescence ϕ_f is plotted on a different scale, because it is an order of magnitude smaller than ϕ_p and ϕ_d.

Figure 3-1a shows that the probability for photochemistry ϕ_p drops and the probability for fluorescence ϕ_f initially rises with increasing irradiance (solid lines). This is the result of photochemical quenching, i.e. closing of photosystems. Fluorescence ϕ_f increases with irradiance until carboxylation becomes enzyme limited, then decreases as a result of deactivation of antennae. The decrease is only moderate if the carbon dioxide concentration is high (as in Figure 3-1a).

Plotting the same quantities versus internal carbon dioxide concentration C shows the following (solid lines in Figure 3-1b). Once C drops below the point where enzyme and light limited carboxylation are equal, both fluorescence and photochemistry decrease with decreasing C. It is worth noting that this response is independent of the cause of the reduction in C. For example, the model would predict the same response for an increasing ambient carbon dioxide concentration as for a relief from stress (which both causes a higher C). Flexas *et al.* (2002) indeed reported that when severely stressed leaves were exposed to high carbon dioxide concentrations, a total or partial reversion of water stress effects on photosynthesis and deactivation resulted.

The solid lines in Figure 3-1 represent the two limiting cases of the model of Farquhar and co-workers, whereas the dashed lines represent a numerical solution of the differential equation for the proton pool (Eq 3-12). For the dashed lines, the response to a variation in light or carbon dioxide concentration is delayed, and the transition between the enzyme and light limited stage is gradual. Deactivation does not only occur in the enzyme limited case, but also in the light limited case. The time delay depends on the choice of the pool size parameter h_m. Whether this hysteresis should be taken into account, has to be studied experimentally in the future.

Figure 3-2 illustrates the combined effect of radiation and carbon dioxide concentration. This figure shows relative chlorophyll fluorescence (Figure 3-1a) and photochemistry (Figure 3-1b) as functions of absorbed PAR Q for high C (bold lines) and low C (fine lines). Both photochemistry and fluorescence are lower in the case of low C (which can be the result of, for example, water shortage or a high atmospheric vapour pressure deficit) than in the case of high C (sufficient water and high atmospheric vapour pressure deficit). This agrees with observations of Flexas *et al.* (2000), who reported that increasing vapour pressure deficit decreases stomatal conductance, internal carbon dioxide concentration, and fluorescence. Fluorescence at high irradiance decreases with increasing stress (lower C), and the irradiance at which the maximum fluorescence occurs decreases with increasing stress (Figure 3-2a). Both of these phenomena have been experimentally observed (Flexas *et al.* 2002).

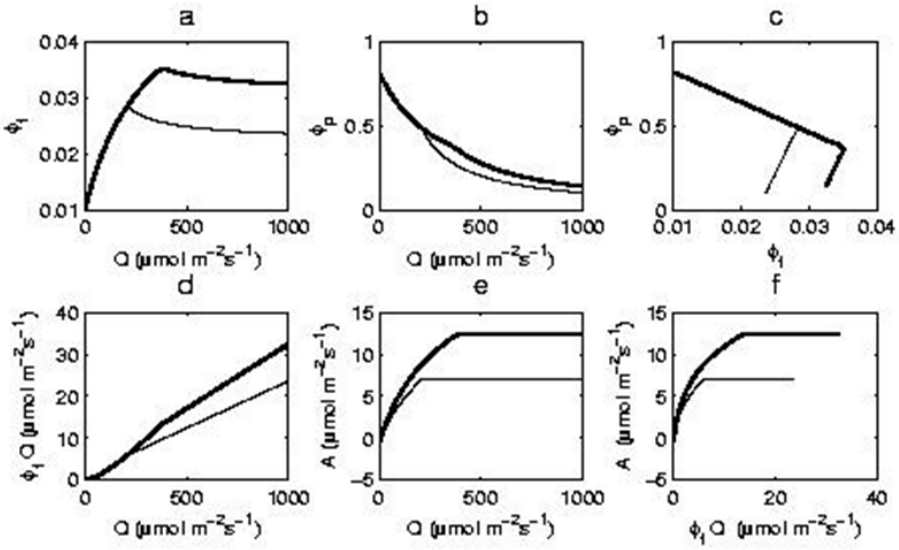

Figure 3-2 - Upper graphs: example simulations of (a) chlorophyll fluorescence ff and (b) photosynthetic yield ϕ_f as functions of absorbed PAR Q, and (c) ϕ_p versus ϕ_f. Lower graphs: (c) total fluorescence $\phi_f Q$ and (3) net photosynthesis A versus Q; and total fluorescence $\phi_f Q$ versus net photosynthesis A. In all graphs, the bold line denotes a high internal carbon dioxide concentration C, and the fine line a low C.

Figure 3-2c shows the probability of photochemistry versus the probability of fluorescence. This figure clearly illustrates the problem interpreting the fluorescence signal. As long as photosynthesis is light limited (ζ_n=1), a unique, negative relationship between relative fluorescence and photochemistry exists. In the enzyme limited case the relationship becomes positive. As a result, multiple photosynthesis values are possible at a single fluorescence value, depending on whether the vegetation is in the light or enzyme limited phase. The point where the relationship reverses is a function of carbon dioxide concentration C.

The lower graphs (Figure 3-2d-f) show (instead of the probability of fluorescence and photochemistry) total fluorescence and net photosynthesis versus absorbed radiation. Figure 3-2e and Figure 3-2f show that even in the light limited case (low Q), the relationship between total fluorescence and photosynthesis depends on C. The cause of the difference in photosynthesis between low and high C

(the bold and the fine line) is a difference in photorespiration. As a result, the higher the carbon dioxide concentration is, the higher the ratio of photosynthesis/fluorescence. This effect has been described before by Flexas *et al*. (2000).

In Figure 3-3, the model is compared to literature data: laser-induced measurements of chlorophyll fluorescence of water stressed poplar trees (*Populus nigra*) in a growth cabinet (Rosema *et al.* 1998). The intensity of the laser was low enough to prevent disturbing steady state conditions. Diurnal cycles (5 days) of photosynthesis, chlorophyll fluorescence and irradiance are available. Air temperature and humidity were controlled at 20 °C and 70% during the day, and 18 °C and 70% during the night. Photosynthesis was measured by pumping air from the cabinet to a gas analyser. Photosynthesis was measured for the whole cabinet. Because leaf area was not known, the values could not be calculated per unit of leaf surface. For this reason, only the shape of the diurnal cycle is used, instead of the absolute values. The experiment is described in detail in Rosema *et al*. (1998).

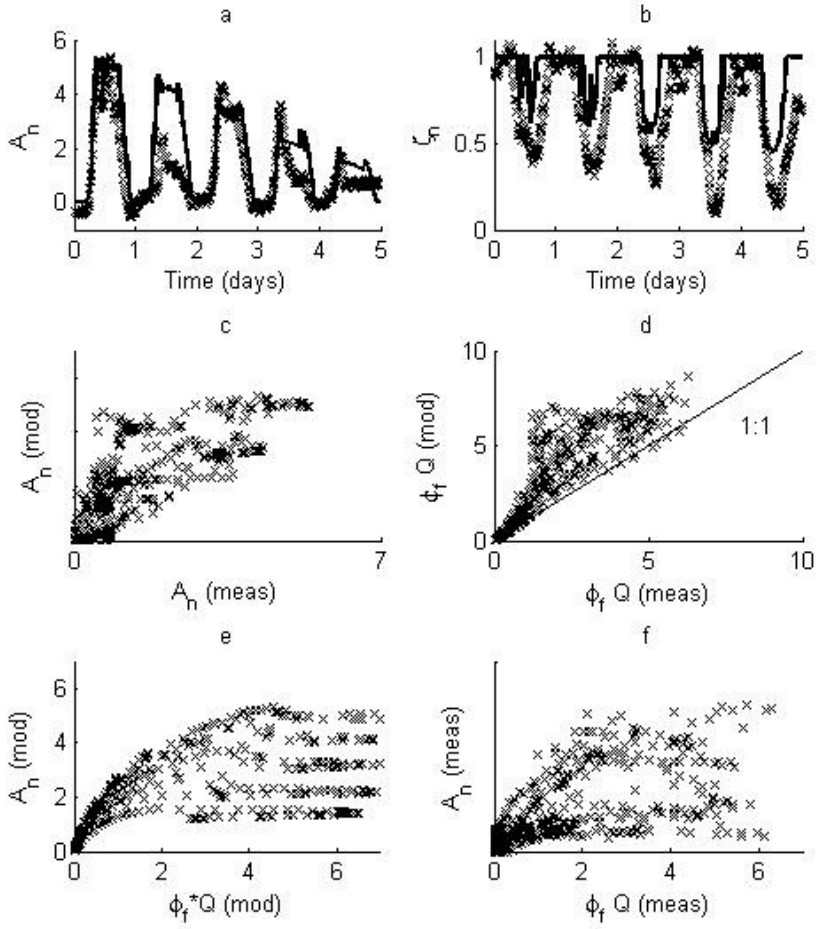

Figure 3-3 - (a) Modelled and measured net photosynthesis versus time of the experiment of Rosema *et al*. (1998); (b) modelled an 'measured' deactivation factor ζ_n, where measured ζ_n is the ratio of measured steady sate fluorescence over calculated potential fluorescence; (c) modelled versus measured photosynthesis; (d) modelled versus measured total fluorescence; (e) measured relationship between fluorescence and photosynthesis; (f) modelled relationship between fluorescence and photosynthesis. Measured photosynthesis is in relative units, because the rates per unit leaf area were unknown.

Photosynthesis for a leaf was calculated with the model for the two limiting cases. Irradiance was used as a proxy for absorbed irradiance Q, and internal carbon dioxide concentration C was calculated from the ambient concentration and vapour pressure deficit with the stomatal conductance model of Wang and Leuning (Wang *et al.* 1998). For mesophyll conductance, a value of 0.1 mol m^{-2} s^{-1} bar^{-1} was used (Loreto *et al.* 1992). Due to lack of additional information about the light and carbon dioxide response of photosynthesis, and stomatal regulation of the leaves, a-priori values for parameters the photosynthesis model ($V_{c\ max}$ = 60 μmol m^{-2} s^{-1} and J_{max} = 150 μmol m^{-2} s^{-1}) and the stomatal conductance model (a = 9, D_0 = 1.6 kPa, and water stress parameter f_w linearly decreasing from 1 to 0.7 during the 5 days) were used. Because the absolute rates of photosynthesis are unknown, and a-priori values for the parameters were used, it only tests whether the relationship between photosynthesis and fluorescence under different light conditions is modelled realistically.

Figure 3-3a shows modelled and measured photosynthesis versus time. Since the absolute level of photosynthesis was not known, the measurements have been scaled so that the maximum measured and modelled photosynthesis during the first day match. Modelled diurnal cycles of photosynthesis correlate reasonably well with measurements (Figure Figure 3-3c), except for the second day (Figure 3a). Figure 3b shows modelled and 'measured' diurnal cycles of deactivation, where measured deactivation is the ratio of measured fluorescence over modelled potential fluorescence. In the experiment, ζ_n gradually decreases with increasingly dry conditions. The model also shows a gradual decrease of ζ_n with increasing soil water stress (decreasing parameter f_w of the stomatal conductance model). During the whole experiment, deactivation is underestimated. The experiment provides insufficient information to verify whether the underestimation is caused by the parameter values chosen or by the model itself. Because the model for the extreme cases was used, no deactivation in light-limited conditions was predicted.

Figure 3-3c and Figure 3-3d show measured versus modelled photosynthesis and total fluorescence. The squared correlation coefficients for measured versus modelled photosynthesis is R^2 = 0.68 and for total fluorescence R^2 = 0.84. Figure 3-3e and Figure 3-3f show the modelled and measured relationship between total chlorophyll fluorescence photosynthesis. For both the modelled and measured relationship, a hyperbolic curve can be fitted through the highest photosynthesis values at each chlorophyll fluorescence interval. This hyperbolic equation is described by Eqs 3-1 to 3-6. The values below the hyperbolic shape are conditions of deactivation of antennae, and consequently lower than potential fluorescence and photosynthesis. In those conditions, carbon dioxide concentration in the mesophyll is lower, and photosynthesis is further decreased by relatively higher photorespiration losses. Apart from the hyperbolic shape that is visible in both the model and the measurements, the data forms a seemingly random cloud of points. This cloud of points can be interpreted when the process of deactivation of antennae is quantified using a model for stomatal regulation and the model of Farquhar and co-workers for enzyme and light limited photosynthesis. In this case, the reduction was mainly caused by the decreasing soil moisture parameter f_w.

Figure 3-3 indicates that the model is able to reproduce observed diurnal cycles of steady state chlorophyll fluorescence and photosynthesis, and that the most important mechanisms are included in a realistic way. The data used here are insufficient to satisfactorily validate the underlying assumptions. To validate the model, light and carbon dioxide response curves of photosynthesis of individual leaves at several stages of drought stress are necessary, preferably for multiple agricultural crops. Despite the limitations of the current study, the model provides a conceptual basis for further development and testing.

The model presented here was developed for the leaf level. When the model is scaled to canopy level, the inhomogeneity of irradiance may cause the relationships to be different, and possibly even effectively simpler than at leaf level.

3.2.2.1. Sensitivity analysis

The sensitivity of modelled net photosynthesis A and relative fluorescence ϕ_f to absorbed PAR Q, internal carbon dioxide concentration C and photosynthetic capacity $V_{c\,max}$, was calculated numerically using meteorological data from 11 typical summer days in the Netherlands, at 9 AM, 11 AM, 1 PM and 3 PM. The meteorological input was collected for various purposes during a campaign above a Spruce forest (52°15'N,5°41'E) between 10 and 20 June 2006. The sensitivity analysis was carried out for a hypothetical leaf, not necessarily for the forest where the measurements were carried out. Irradiance was used instead of absorbed radiation, i.e. calculations were carried out for a horizontal leaf with an emissivity of 1.

Table 3-2 shows the change in total fluorescence and photosynthesis as a percentage of a small change in absorbed radiation A, photosynthetic capacity $V_{c\,max}$ and internal carbon dioxide concentration C. The sensitivity to electron transport capacity J_{max} was not calculated separately, but a fixed ratio of J_{max}:$V_{c\,max}$ = 2.5 was assumed. Each value in the table represents the average fluorescence or photosynthesis calculated from 11 days of input variables, at the times specified. For photosynthetic capacity, a value of $V_{c\,max}$ = 50 μmol $m^{-2}s^{-1}$ was used, and C was calculated from vapour pressure deficit using the model of Cowan (1977) for stomatal conductance, using λ = 500 μmol μmol^{-1} for the marginal water cost of photosynthesis.

Table 3-2. Percent of change of modelled photosynthesis and chlorophyll fluorescence as a result of a change of a small variation of the input *I*: $100 \cdot \frac{\delta A}{\delta I}\frac{\bar{I}}{\bar{A}}$ and $100 \cdot \frac{\delta \phi_f}{\delta I}\frac{\bar{I}}{\bar{A}}$, for the following input: absorbed radiation *Q*, carbon dioxide concentration in the mesophyll *C*, and maximum carboxylation capacity $V_{c\,max}$. The values are averages for 11 days of meteorological input for summer days in The Netherlands, at the specified time of the day.

Parameter	*Q*	*C*	$V_{c\,max}$ or J_{max}
Photosynthesis			
9 AM	24	39	38
11 AM	0	110	94
1 PM	0	111	93
3 PM	0	113	92
Fluorescence ϕ_f			
9 AM	9	24	-25
11 AM	-7	71	7
1 PM	-6	71	6
3 PM	-7	72	7

The sensitivity to input parameters differs between morning and afternoon, and also between photosynthesis and fluorescence. The sensitivity to absorbed radiation is highest in the morning for relative fluorescence and photosynthesis. The sensitivity of chlorophyll fluorescence and photosynthesis to C is higher in the afternoon than in the morning, although both photosynthesis and fluorescence are sensitive to C by 11 AM. Moreover, the ratio of $\delta A/\delta C$: $\delta\phi_f/\delta C$ does not change after 11 AM. The combination of a relatively low sensitivity to Q, a high sensitivity to C, and a constant $\delta A/\delta C$: $\delta\phi_f/\delta C$ mean that fluorescence measurements after 11 AM are suitable for detection of the effects of water stress and vapour pressure deficit. For most of the day, chlorophyll fluorescence is positively correlated with photosynthesis. The fact that the correlation coefficient is rather consistent implies that variations in chlorophyll fluorescence can be used as a proxy for those in photosynthesis.

The reason is that, for most of the time, variations in photosynthesis and chlorophyll fluorescence are dominated by deactivation, which is assumed to affect both in the same way. The fluorescence signal around noon is dominated by variations of C (stomatal regulation or stress). The largest variations in C usually occur around noon and in the afternoon (Wilson *et al.* 2003).

The sensitivity of fluorescence to maximum carboxylation capacity $V_{c\ max}$ is low, except in the early morning. Thus only early morning values are suitable to detect variations of maximum carboxylation capacity. However, photosynthesis is sensitive to maximum carboxylation capacity throughout the day. For the calculation of actual photosynthesis, $V_{c\ max}$ is a necessary parameter. This implies that only variations of actual photosynthesis, not the absolute level, can be estimated with an afternoon measurement of fluorescence. The sensitivity of chlorophyll fluorescence to photosynthetic capacity switches sign: $\delta\phi_f/V_{c\ max}$ is negative during the morning and positive during the late morning and afternoon, whereas $\delta A/\delta_{\ max}$ is always positive. This makes it particularly difficult to obtain information about maximum carboxylation capacity in the late morning.

3.2.2.2. Conclusions

The model predicts that total chlorophyll fluorescence correlates with actual photosynthesis in the late morning and in the afternoon. This makes fluorescence the most direct measure for instantaneous vegetation growth that is currently available for remote sensing. Absolute rates of photosynthesis, however, would be difficult to determine according to the model, because afternoon fluorescence is insensitive to maximum carboxylation capacity (whereas photosynthesis is proportional to this parameter). Early morning values of fluorescence are sensitive to maximum carboxylation capacity, but also to radiation and stress factors, which makes an early morning measurement of fluorescence difficult to interpret. Variation in fluorescence and photosynthesis in the afternoon are caused by deactivation of antennae and stomatal regulation. These variations are most profound in the later morning and early afternoon (Wilson *et al.* 2003).

The detailed model in which the concentration of proton in the lumen is calculated can be simplified by assuming steady state conditions and neglecting co-limitation of photosynthesis by light and enzymes (i.e. ignoring hysteresis in the response of deactivation to light). It is expected that the simplified version of the model contains sufficient detail to interpret large scale observations. In some leaf level experiments, the dynamic model may be used.

The current model is limited as it was developed for the leaf scale. In order to apply the model for the interpretation of above-canopy measurements of chlorophyll fluorescence, scaling from leaf to canopy with a radiative transfer model is necessary.

3.2.3. The Magnani model

The chapter proposes a further development of the leaf-level model of the A-SIF relationship. IN particular, a central assumption of the van der Tol-Verhoef-Rosema model about the parallel quenching of photochemistry and fluorescence by heat dissipation is relaxed. The fate of energy in PSII and the competition between the three processes, on the contrary, are represented in mechanistic terms, based on the latest understanding from pulse-saturated and time-resolved fluorescence studies and models.

3.2.3.1. Assumptions

We consider a population of N photosystem II (PSII) units, where each PSII has a given amount of *Chl a*, *Chl b* and xanthophyll molecules, as well as associated quinone and plastoquinone pools. Apart from xanthophyll de-epoxidation state, all other stoichiometries are assumed constant. The quinone and plastoquinone pools are treated together, since the analysis of the redox state of the different quinone pools falls outside the scope of the present study. Consequently, we represent the different forms as a single pool of quinone-equivalent molecules, capable of accepting one electron each. Finally, the system of N PSII units is assumed to follow a lake-type organisation model (Kitajima *et al.* 1975; Dau 1994; Bernhardt *et al.* 1999) and excitons can move freely between PSII units. Although PSII units are known to be only partly interconnected in higher plants (Lazar 1999), the lake model has been demonstrated to yield almost indistinguishable results (Kramer *et al.* 2004).

The formation of chlorophyll triplet states is considered part of the constitutive heat dissipation component. Moreover, photoinhibitory NPQ is not yet included in the model. Finally, the state-transition form of NPQ, which is much smaller than the pH-dependent form (Krause *et al.* 1991), is not considered here for simplicity reasons.

3.2.3.2. Processes

In the proposed model, pigment molecules and quinone-equivalents shift from a base (*OFF*) to an excited (*ON*) state after accepting a photon, an exciton or an electron, returning to the OFF state after losing it. Excitation transfer between *Chlb* and *Chla* is known to be unidirectional and to occur in the order of picoseconds (Dau 1994; Amerongen *et al.* 2003). As a result, at the time scale considered, *Chl b* operates only in light absorption and excitons are always assumed to be located on *Chl a* molecules. From excited *Chl a* molecules, excitons can follow different paths (Figure 3-4): it can be re-emitted as fluorescence, lost as constitutive heat, dissipated by pH-dependent heat dissipation processes (non-photochemical quenching) or captured by an oxidized quinone-equivalent. Finally, the reduced quinone-equivalents can be re-oxidized by the downstream electron transport, returning to the *OFF* state.

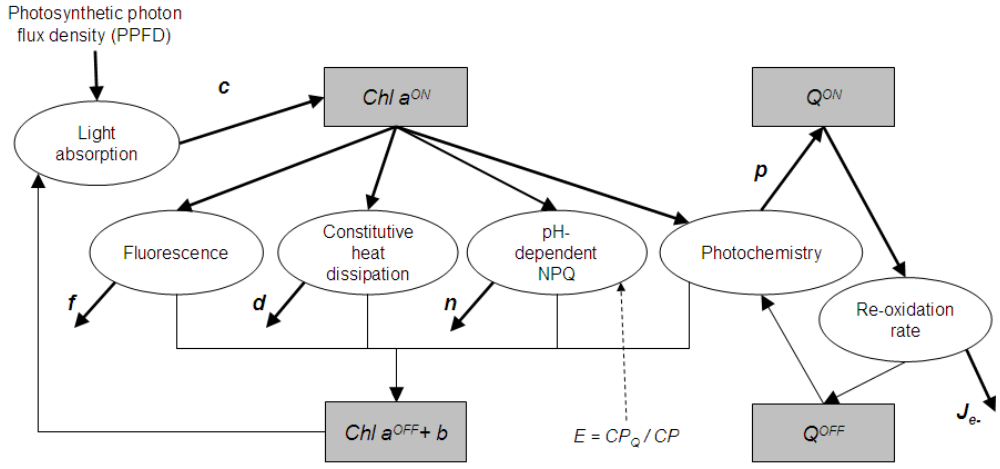

Figure 3-4. Scheme of light energy capture and dissipation in photosystem II. Rectangular boxes represent density of a substance in an energy state, circles represent processes. The flow of energy is represented by thick lines, state transitions by continuous thin lines; dashed lines represent an influence. $Chla^{ON}$ and $Chla^{OFF}$ represent the density of chlorophyll a molecules carrying an exciton or in the ground state, respectively. Q^{ON} and Q^{OFF} are the density of quinone-equivalents in a reduced and oxidized state, respectively. E is the fraction of core antenna complexes in a quenched state. f, d, n, p and J_{e-} are the rate of fluorescence, constitutive heat dissipation, pH-dependent non-photochemical heat dissipation, reduction of the quinone-equivalent pool (photochemistry) and electron transport, respectively. From Porcar-Castell *et al.* (2006, modified).

3.2.3.3. Dynamic equations

The rate of light energy capture (*c*, mol m^{-2} s^{-1}) is determined by light intensity (*I*) and the number of chlorophyll molecules in the ground state:

$$c = \alpha \cdot I \cdot \left(Chla^{OFF} + Chlb^{OFF} \right) \quad \text{(Eq. 3-22)}$$

where I is the photosynthetical photon flux density (PPFD) at the leaf surface (mol m^{-2} s^{-1}), ChlaOFF and ChlbOFF are numbers of Chla and Chlb molecules in the ground state (mol m^{-2}) calculated from PSII stoichiometry and number of PSII units and α is a light absorption parameter (m^2 mol^{-1}). Excitation transfer between Chlb and Chla is unidirectional and occurs in the order of picoseconds (Dau 1994). Therefore, at the time scale considered, Chlb molecules are assumed to operate only in light absorption and excitons are assumed to be always located on Chla (i.e. $Chlb^{OFF}$ = Chlb).

The rate of constitutive heat dissipation (d) (mol m^{-2} s^{-1}) is linearly proportional to the number of excitons ($Chla^{ON}$):

$$d = k_d \cdot Chla^{ON} \quad \text{(Eq. 3-23)}$$

where k_d (s^{-1}) is the rate constant for heat dissipation. Likewise, the rate of fluorescence (*f*) (mol m^{-2} s^{-1}) is:

$$f = k_f \cdot Chla^{ON} \quad \text{(Eq. 3-24)}$$

where k_f (s^{-1}) is the rate constant for fluorescence.

The rate of heat dissipation (*n*; mol m^{-2} s^{-1}) is assumed to be proportional to the number of excitons and to the fraction of inner antenna complexes in a quenched state (*E*):

$$n = k_n \cdot E \cdot Chla^{ON} \quad \text{(Eq. 3-25)}$$

where k_n (s^{-1}) corresponds to the rate constant of heat energy dissipation. The fraction of inner antenna complexes in a quenched state, in turn, will itself be a function of xanthophyll de-epoxidation state and of lumen pH (Gilmore *et al.* 1998b), as described in a following section.

The efficiency of photochemistry varies according to the redox state of the plastoquinone pool: when the pool of plastoquinone is totally reduced, the rate of photochemistry is zero and this rate is at its maximum when the plastoquinone pool is totally oxidized. The rate of photochemistry (*p*; mol m^{-2} s^{-1}) is therefore proportional to the oxidized fraction of the quinone-equivalent pool (*Q*), which is analogous to the commonly referred to fraction of open reaction centres (Kramer *et al.* 2004):

$$p = k_p \cdot Q \cdot Chla^{ON} = k_p \cdot \frac{Q^{OFF}}{Q^{OFF} + Q^{ON}} \cdot Chla^{ON} \quad \text{(Eq. 3-26)}$$

where k_p (s^{-1}) is a rate constant associated with photochemical processes and Q^{ON} and Q^{OFF} are the number of quinone equivalents in a reduced and oxidized state, respectively.

The rate of electron transport to PSI (J_{e-} ; mol m^{-2} s^{-1}) determines the rate at which the quinone-equivalent pool is re-oxidized, and will be proportional to the number of quinone equivalents in a reduced state. Under steady-state conditions, this must be equal to the rate of photochemistry (*p*), which determines the rate of reduction of the quinone-equivalent pool:

$$J_{e-} = \gamma \cdot Q^{ON} = p \quad \text{(Eq. 3-27)}$$

where γ (s^{-1}) is the rate constant for the re-oxidation of the quinone-equivalent pool. Under steady-state conditions, the rate of light capture must equal energy dissipation (by photochemistry, fluorescence or heat):

$$c = d + f + n + p \quad \text{(Eq. 3-28)}$$

By combining Eqns. 22-28, electron transport rate can be estimated from the following quadratic equation:

$$J_{e-} = \frac{-\beta_2 \pm \sqrt{\beta_2^{\,2} - 4 \cdot \beta_3}}{2}$$

$$\beta_2 = -\gamma \cdot Q^{TOT} \cdot \frac{\left(\alpha \cdot I + k_d + k_f + k_n \cdot E + k_p\right)}{k_p} - \alpha \cdot I \cdot \left(Chla + Chlb\right) \quad \text{(Eq. 3-29)}$$

$$\beta_3 = Q^{TOT} \cdot \gamma \cdot \alpha \cdot I \cdot \left(Chla + Chlb\right)$$

Of the two possible solutions, the only one yielding $J_{e-} = 0$ for $I = 0$ is:

$$J_{e-} = \frac{-\beta_2 - \sqrt{\beta_2^{\,2} - 4 \cdot \beta_3}}{2} \quad \text{(Eq. 3-30)}$$

From Eqns. 22-26, the number of excited chlorophyll molecules can be estimated as:

$$Chla^{ON} = \frac{\left(Chla + Chlb\right)}{1 + \frac{k_d + k_f + k_n \cdot E + k_p \cdot Q}{\alpha \cdot I}} \quad \text{(Eq. 3-31)}$$

Under saturating light conditions (i.e. for I →∞), all chlorophyll molecules will be in an excited state. By combining Eqns. 26 and 27, the maximum electron transport rate ($J_{e-}^{\max}$) can be then expressed as:

$$J_{e-}^{\max} = \lim_{I \to \infty} J_{e-} = \frac{\gamma \cdot Q^{TOT} \cdot k_p \cdot \left(Chla + Chlb\right)}{\gamma \cdot Q^{TOT} + k_p \cdot \left(Chla + Chlb\right)} \quad \text{(Eq. 3-32)}$$

3.2.3.4. Modelling chlorophyll fluorescence

By combining Eqns. 24 and 31, fluorescence rate can be expressed as:

$$f = k_f \cdot \frac{\alpha \cdot I \cdot \left(Chla + Chlb\right)}{k_d + k_f + k_n \cdot E + k_p \cdot Q} \quad \text{(Eq. 3-33)}$$

and the fluorescence yield (ΦF, fraction of absorbed photons dissipated as fluorescence) as:

$$\Phi F = \frac{k_f}{k_d + k_f + k_n \cdot E + k_p \cdot Q} \quad \text{(Eq. 3-34)}$$

In a dark-acclimated leaf, xanthophyll de-epoxidation can be assumed to be fully dissipated so that $E = 0$. The quinone-equivalent pool will also be fully oxidized ($Q = 1$; all reaction centres are open), so that the fluorescence yield (ΦF_o) of such a dark-adapted leaf (as typically measured by a modulated fluorometer under a dim measuring light) will be (Krause *et al.* 1991):

$$\Phi F_o = \frac{k_f}{k_d + k_f + k_p} \quad \text{(Eq. 3-35)}$$

After exposing the leaf to a brief pulse of saturating light, the quinone-equivalent pool can be assumed to be fully reduced ($Q = 0$; all reaction centres are closed), and the maximum dark-acclimated fluorescence yield (ΦF_m) can be expressed as (Krause *et al.* 1991):

$$\Phi F_m = \frac{k_f}{k_d + k_f} \qquad \text{(Eq. 3-36)}$$

Since the maximum fluorescence yield for molecules associated with photosystem II in vivo is typically 10% (Barber *et al.* 1989), and the rate constant for fluorescence is 6.7×10^7 s^{-1} (Rabinowich *et al.* 1969), the rate constant for constitutive heat dissipation (k_d) can be estimated from Eq. 36.

From Eqns. 27 and 29, the yield of photochemistry of a dark-acclimated leaf ($\Phi PSII$) can be expressed as (Krause *et al.* 1991):

$$\Phi PSII = \frac{k_p}{k_d + k_f + k_p} \qquad \text{(Eq. 3-37)}$$

Since $\Phi PSII$ has a typical value of 0.84 in healthy leaves (Schreiber *et al.* 1987), the value of the rate constant for photochemistry (k_p) can be estimated from Eq. 37.

Values for all rate constants are presented in Figure 3-5.

From Eqns. 25 and 27, fluorescence rate can be represented as a function of electron transport rate:

$$f = \frac{k_f}{k_p} \cdot \frac{\gamma \cdot Q^{TOT} \cdot J_{e-}}{\gamma \cdot Q^{TOT} - J_{e-}} \qquad \text{(Eq. 3-38)}$$

where $\gamma \cdot Q^{TOT}$ is the electron transport rate that could be expected if all the quinone-equivalent pool were in a reduced state (i.e. if all reaction centres were closed).

From Eq. 32, the preceding relationship for chlorophyll fluorescence can be expressed in terms of maximum electron transport rate as:

$$f = k_f \cdot \frac{1}{\left(\frac{1}{J_{e-}} - \frac{1}{J_{e-}^{\max}}\right) \cdot k_p + \frac{1}{(Chla + Chlb)}} \qquad \text{(Eq. 3-39)}$$

This expression can be combined with the semi-empirical approach proposed by van der Tol *et al.* (2008) for the representation of leaf and canopy fluorescence as a function of key environmental parameters.

Alternatively, the model can be combined with a detailed representation of electron transport and ATP-ase regulation (Magnani *et al.*, submitted) for a process-based representation of light photosynthetic processes.

Let I_a (µmol photons m^{-2} s^{-1}) be the amount of light energy absorbed by PSII units. Fluorescence yield can then be computed from Eq. 3-17 as:

$$\Phi F = \frac{f}{I_a} = k_f \cdot \frac{1}{\left(\frac{I_a}{J_{e-}} - \frac{I_a}{J_{e-}^{\max}}\right) \cdot k_p + \frac{I_a}{(Chla + Chlb)}} \qquad \text{(Eq. 3-40a)}$$

The equation can be re-stated in terms of photochemical PSII quantum yield ($\Phi P = J_{e-} / I_a$) as:

$$\Phi F = \Phi P \cdot \frac{k_f}{k_p} \cdot \frac{1}{1 - \frac{J_{e-}}{\gamma \cdot Q^{TOT}}} \qquad \text{(Eq. 3-41b)}$$

Table 3-3. - Values of the rate constants of fluorescence (k_f), constitutive heat dissipation (k_d), pH-dependent non-photochemical heat dissipation (k_n), photochemistry (k_p) and plastoquinone pool re-oxidation (γ).

Rate constant or parameter	Value	Source
k_f (s^{-1})	6.7×10^7	Rabinowich and Govindjee (1969)
k_d (s^{-1})	6.03×10^8	Eq. 3-14
k_p (s^{-1})	3.52×10^9	Eq. 3-15
k_n (s^{-1})	2.92×10^9	Porcar-Castell *et al.* (2006)
γ (s^{-1})	2.74	Porcar-Castell *et al.* (2006)

3.2.4. Testing the Magnani model

The aim of the work described in this document was the thorough test of the mathematical model of leaf steady-state fluorescence and photosynthesis developed as part of the project and described in detail in the preceding chapter, henceforth referred to as Magnani model (Magnani *et al.* 2009).

Although the sensor specifications relevant for the project refer to the passive measurement of solar-induced fluorescence (SIF) by the Fraunhofer-line in-filling method, detailed measurements at the leaf level under controlled conditions using this technique are not currently available. Measurements of modulated chlorophyll fluorescence using commercial instrumentation have been therefore used as a reliable substitute. Although an active technique is not amenable to satellite measurements, modulated fluorescence has a long record in ecophysiological studies, which has however relied so far on a combination of steady-state and pulse-saturated fluorescence measurements.

In the following document, the correspondence of modulated and solar-induced fluorescence measurements will be first discussed. A qualitative test of the Magnani model based on literature data will be then presented. Finally, the model will be quantitatively tested against leaf-level data recently collected with this specific purpose under controlled environmental conditions.

3.2.4.1. Interpretation of PAM modulated fluorometer steady-state measurements

Commercial instrumentation for the measurement of chlorophyll fluorescence by the amplitude-modulated technique has been available for over 20 years (Schreiber *et al.* 1987; Logan *et al.* 2007). Although not amenable to remote-sensing, this active measurement technique present some advantages over the measurement of solar-induced fluorescence, which make it more suitable to ecophysiological measurements under controlled conditions. In particular, the active nature of the measurement (described below in some detail) makes for a more straightforward measurement of fluorescence over the entire spectrum of chlorophyll emission; moreover, measurements do not have to be taken under natural light conditions (which are on the contrary needed with the Fraunhofer line in-filling method), making it easier to carry out experiments under controlled environmental conditions.

The interpretation of the results obtained by the amplitude-modulated technique, however, requires some clarification.

In this technique (exemplified in Figure 3-1, which describes one such commercial fluorometer, the Walz PAM-2000), fluorescence is excited by very brief but strong light pulses from light-emitting diodes. With the PAM-2000, these pulses are 3 μsec long and repeated at a frequency of 600 or 20000 Hz. The LED light passes a short-pass filter (λ < 670 nm) and the photodetector is protected by a long-pass filter (λ > 700 nm), so as to avoid any interference between the reflected measuring light

and the fluorescence signal. A highly selective pulse amplification system ignores all signals except the fluorescence excited during the 3 μsec measuring pulses. As a result, the measured fluorescence is the fluorescence radiance induced by the modulated measurement light.

The amplitude-modulated technique described above has been traditionally applied in combination with the pulse-saturated technique, for which well-established interpretative models have long been available (Kitajima *et al.* 1975; Genty *et al.* 1989a; Kramer *et al.* 2004; Kornyeyev *et al.* 2007), focusing on the relationship between fluorescence under background light (F_s), dark-acclimated (F_o) and light-saturated conditions (F_m, F_m'), rather than on the information content of F_s itself.

As a result, the fluorescence signal is not calibrated radiometrically and no quantitative information is provided about the measurement light.

However, since the measurement pulses are of constant intensity (under constant settings) and so brief as not to interfere with PSII status, the F_s signal can be assumed to be proportional to fluorescence yield (Φ_f) under background light conditions, which can be therefore estimated albeit only in arbitrary units (a.u.).

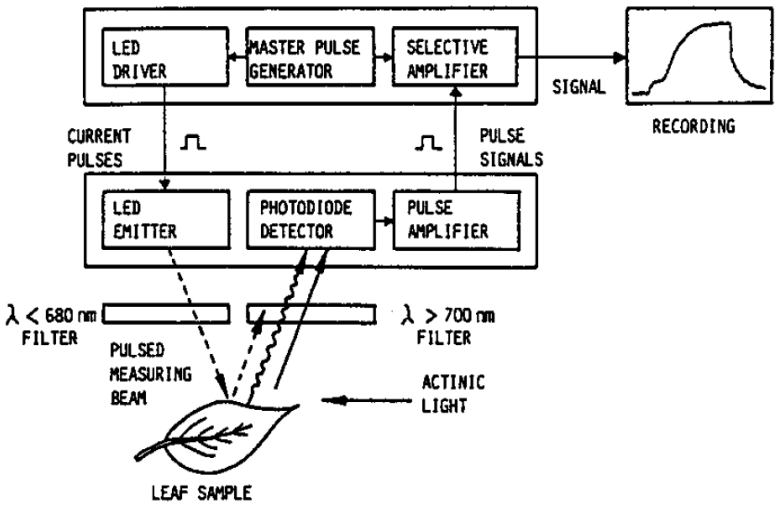

Figure 3-5. Scheme of the PAM-2000 modulated fluorometer (Heinz Walz Gmbh, Effeltrich, Germany). Fluorescence is excited by very brief but strong light pulses from light-emitting diodes. With the PAM-2000, these pulses are 3 μsec long and repeated at a frequency of 600 or 20000 Hz. The LED light passes a short-pass filter (λ < 670 nm) and the photodetector is protected by a long-pass filter (λ > 700 nm) and a heat absorbing filter. A highly selective pulse amplification system ignores all signals except the fluorescence excited during the 3 μsec measuring pulses. As a result, the measured fluorescence is the fluorescence radiance induced by the modulated measurement light. Since the measurement pulses are of constant intensity and so brief as not to interfere with PSII status, the signal can be assumed to be proportional to fluorescence yield under background light conditions.

3.2.4.2. Qualitative test of the model: comparison with literature data

A first qualitative test of the Magnani model has been carried out against data derived from the detailed study of Flexas *et al.* (2002). *Vitis vinifera* plants were exposed to different levels of water stress, and the response to light of leaf photosynthesis measured together with modulated chlorophyll fluorescence (Figure 3-2). Fluorescence measurements were normalized for pre-dawn fluorescence so as to reduce the variability among leaves associated with differences in absorbance, although differences were admittedly quite small. Measurements were also taken on leaves exposed to saturating CO2, so as to eliminate any stomatal limitations of photosynthesis as a result of drought (Figure 3-3).

A selection of results is presented in Figure 3-7 and Figure 3-8, together with a qualitative comparison of the experimental patterns with those expected from model predictions.

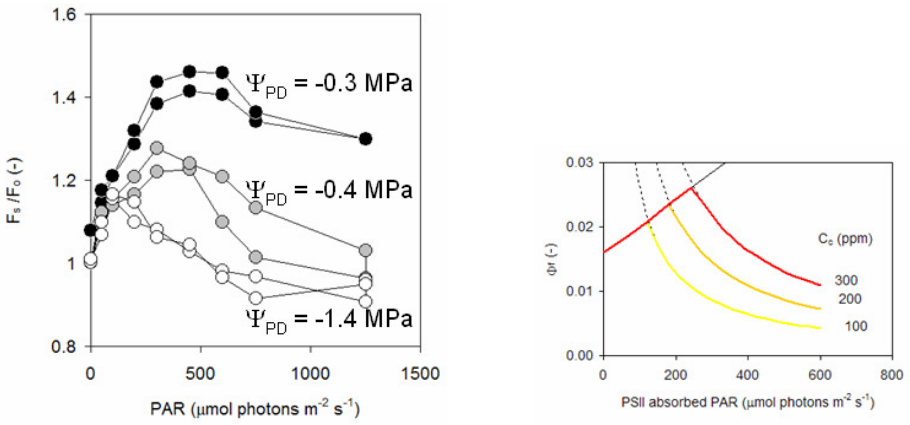

Figure 3-6. Leaf modulated fluorescence (F_s) in response to changes in incoming light (PAR, photosynthetically active radiation) and stomatal limitations resulting from drought (Ψ_{PD}, pre-dawn leaf water potential); from Flexas *et al.* (2002). The signal had been normalized by pre-dawn steady-state fluorescence (F_o). For a qualitative comparison, the predicted response of fluorescence yield (Φ_f) to changes in PAR and intercellular CO_2 concentration (C_i, indicative of stomatal limitations) according to the Magnani model is presented in the inset on the right.

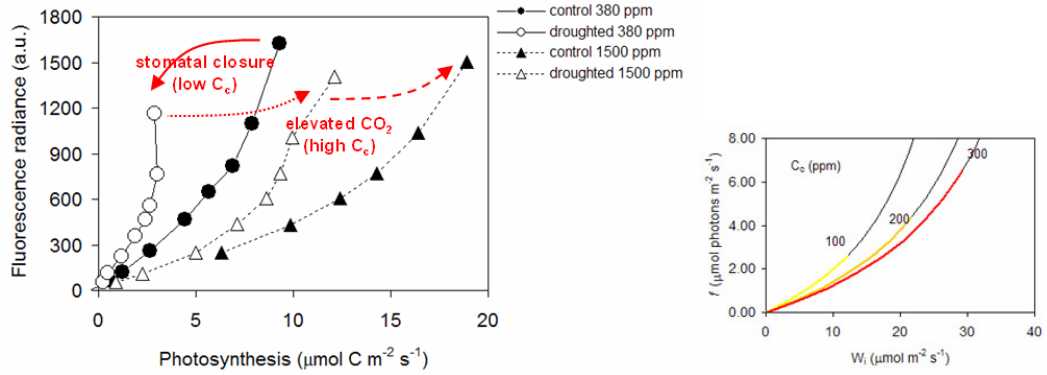

Figure 3-7. Relationship between estimated fluorescence radiance and leaf photosynthesis in *Vitis vinifera* (Flexas *et al.* 2002). Points within a series correspond to different light intensities. Different series correspond to contrasting treatments: leaves under ambient CO2 concentration (380 ppm) in well-watered (black dots) and droughted plants (white circles); triangles correspond to the same plants exposed to a saturating CO_2 concentration (1500 ppm), which would have relieved any stomatal imitations of photosynthesis. The residual difference between droughted and control plants indicates a sustained non-stomatal limitation of photosynthesis in response to drought. For a qualitative comparison, the predicted response of fluorescence radiance (*f*) to changes in PAR and intercellular CO_2 concentration (C_i, indicative of stomatal limitations) according to the Magnani model is presented in the inset on the right.

In response to increasing irradiance, fluorescence yield is shown to present a peaking response, first increasing up to a maximum and then declining for increasing light levels. This is in contrast with the pattern of PSII photochemical yield (data not shown), which presents on the contrary a monotonic decline with increasing light. The onset of the fluorescence yield decline is anticipated under drought conditions (more negative values of predawn water potential), resulting in lower values of fluorescence yield (and fluorescence radiance). This pattern is well captured by the model (right panel in Figure 3-7), which predicts an earlier decline in fluorescence yield under conditions of higher stomatal limitations (as evidenced by the lower level of CO_2 concentration at carboxylation sites, C_c).

When considering fluorescence radiance (as estimated from F_s and incoming irradiance, and therefore also expressed in arbitrary units), they can be seen to be sharply reduced by drought and stomatal closure (Figure 3-8), although to a lower extent than photosynthetic rates (resulting therefore in a higher slope of the relationship). Relieving stomatal limitations by exposing the leaf to saturating CO2 result in an increase in fluorescence radiance and a decline in the slope of the relationship with photosynthesis. This is in good agreement with model predictions, as demonstrated by the inset on the right for increasing values of C_c (decreasing stomatal limitations).

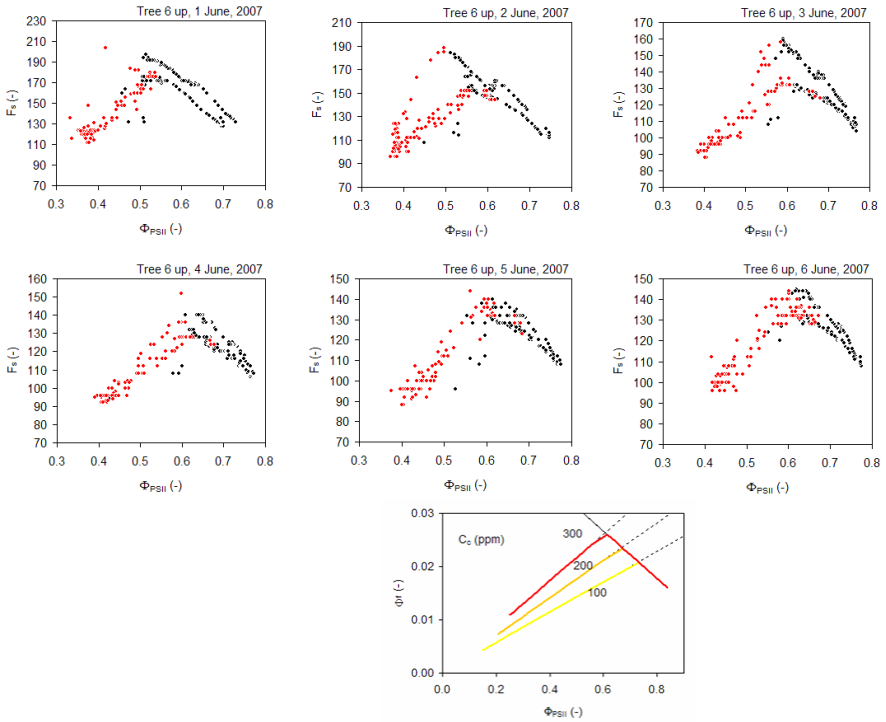

Figure 3-8. Diurnal changes in steady-state modulated fluorescence (F_s) as measured on *Pinus sylvestris* needles using the MoniPAM field modulated fluorometer (Porcar-Castell *et al.* 2008 and unpublished data). Black dots correspond to measurements under light-limited conditions (PAR < 600 µmol m^{-2} s^{-1}), red dots to CO_2-limited conditions. For a qualitative comparison, the predicted response of fluorescence yield (Φ_f) to changes in PAR and intercellular CO_2 concentration (C_i, indicative of stomatal limitations) according to the Magnani model is presented in the inset on the right.

A second qualitative test of the Magnani model comes from a comparison with long-term F_s measurements on *Pinus sylvestris* needles using the new MoniPAM system (Heinz Walz Gmbh, Effeltrich, Germany) at the Hyytiala experimental site in Finland (Porcar-Castell *et al.* 2008). The published data have been complemented with ancillary data kindly provided by the Authors; a more thorough quantitative comparison of model predictions with this extended dataset is under way.

Even in the absence of gas exchange measurements of photosynthesis, useful information can be derived from modulated fluorescence alone, through a comparison of fluorescence yield (Φ_f), as derived from steady-state fluorescence F_s, and PSII photochemical yield (Φ_{PSII}), as derived from the commonly used pulse-saturated parameter $\Delta F'/F_m'$ (= $1 - F_s/ F_m'$).

The relationship between the two yields over a number of days is presented in Figure 3-4. . As expected from the model, a non-monotonic relationship is always observed, with a negative association between the two yields in the morning and late afternoon under light-limited conditions (black symbols) and a positive association on the contrary in the middle of the day under conditions limited by stomatal closure and CO_2 availability (red symbols). The variable slope of the positive correlation over the middle of the day is presumably related to different temperatures, as predicted by the model (data not shown).

3.2.4.3. Quantitative test of the model: combined measurements of leaf photosynthesis and fluorescence under controlled conditions

In order to test in a more quantitative way the predictions of the model, photosynthetic rates and fluorescence parameters have been measured under controlled conditions on individual leaves of *Arbutus unedo*, an evergreen schlerophyllous Mediterranean species for which a background of information is already available (Schreiber *et al.* 1987; Baraldi *et al.* 2008).

Individual leaves were enclosed in the broadleaf cuvette of a LiCor Li-6400 infrared gas analyzer (LI-Cor Inc., Lincoln, NE, USA) and acclimated to high light conditions using a dichroic halogen lamp connected to a stabilized energy source. The fiberoptics probe of a PAM-2000 modulated fluorometer (Heinz Walz Gmbh, Effeltrich, Germany) also pointed at the surface of the leaf through a sealed opening in the leaf cuvette. Environmental conditions experienced by the leaf were varied as depicted in Figure 3-9, changing first light levels in steps (whilst keeping ambient CO_2 constant) and then air CO_2 concentrations in the cuvette (under constant high irradiance). The leaf was kept for at least 15 minutes at each level of light and CO_2, in order to ensure full acclimation.

Measurements were repeated with the same experimental setup on three leaves.

A selection of results for one leaf is presented in Figure 3-10, which shows the response of fluorescence yield (Φ_f), PSII photochemical yield (Φ_{PSII}) and photosynthetic rates to individual environmental factors *ceteris paribus*.

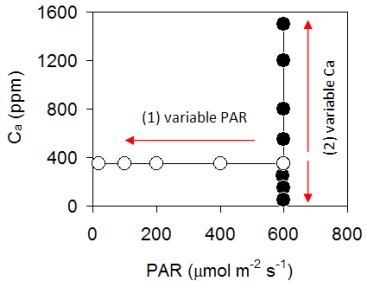

Figure 3-9. Schematic representation of the measurement protocol applied on *Arbutus unedo* leaves under controlled conditions. (1) incoming irradiance from a dichroic halogen lamp was modulated through a stabilized power source between 600 and 20 µmol m^{-2} s^{-1}, whilst maintaining the leaf under ambient CO_2 concentration (380 ppm) inside the LiCor Li-6400 cuvette. (2) CO_2 concentration inside the Li-6400 cuvette was then reduced to 50 and increased to 1500 ppm whilst maintaining irradiance constant at 600 µmol m^{-2} s^{-1}.

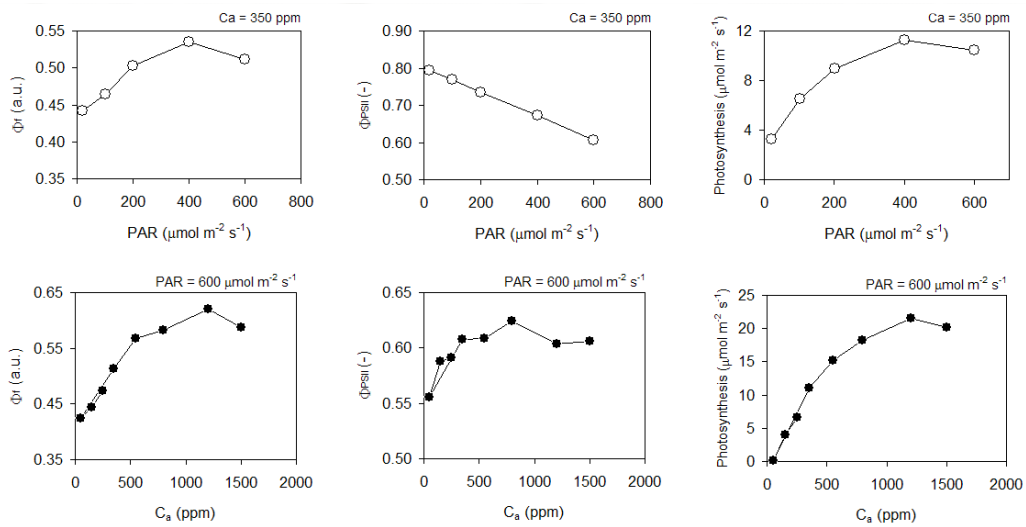

Figure 3-10. - Response of fluorescence yield (Φ_f), PSII photochemical yield (Φ_{PSII}) and photosynthetic rates to changes in irradiance (PAR, photosynthetically active radiation) under constant CO_2 (white circles, top graphs) or in ambient CO_2 concentration (C_a) under constant irradiance (black dots, bottom graphs) in an *Arbutus unedo* leaf.

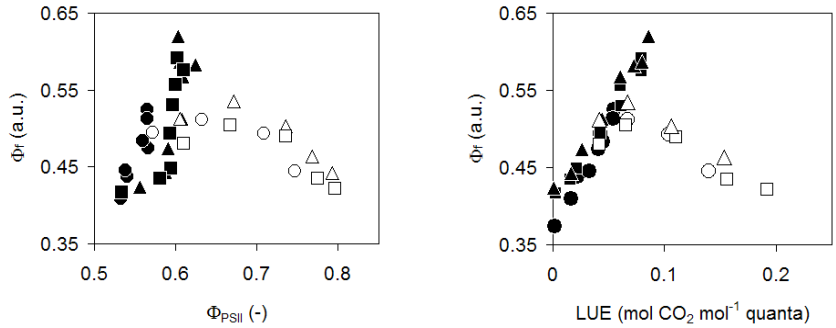

Figure 3-11. Parallel changed in fluorescence yield (Φ_f), PSII photochemical yield (Φ_{PSII}) and photosynthetic light-use efficiency (LUE) in response to changes in irradiance under constant CO_2 (white symbols) or to changes in ambient CO2 under constant irradiance (black symbols). Different symbols refer to three *Arbutus unedo* leaves measured under the same experimental conditions.

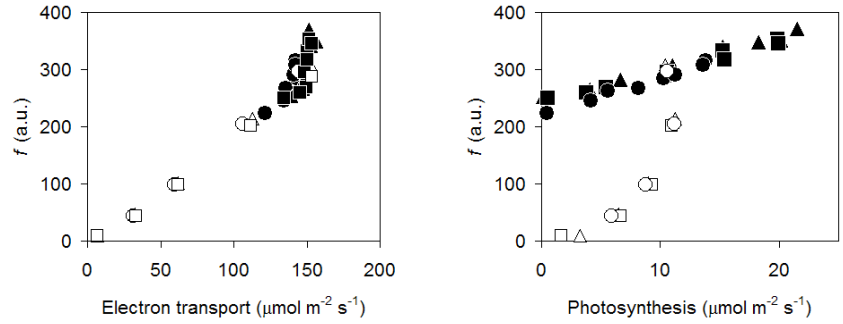

Figure 3-12. Parallel changes in fluorescence radiance (*f*), PSII electron transport rates and photosynthesis in response to changes in irradiance under constant CO_2 (white symbols) or to changes in ambient CO2 under constant irradiance (black symbols). Different symbols refer to three *Arbutus unedo* leaves measured under the same experimental conditions.

The relationship between fluorescence yield and PSII photochemical yield (left graph) and photosynthetic light-use efficiency (right graph) for three leaves is presented in Figure 3-11. As expected, a markedly different relationship is observed under light-limited conditions (with irradiance increasing to saturating values; white symbols) or conditions of variable CO_2 under saturating irradiance (black symbols), with a negative and a positive association, respectively, with both Φ_{PSII} and LUE. Also interesting is the very close resemblance of the relationship for the three leaves. The corresponding relationship for estimated fluorescence radiance, electron transport and photosynthetic rates is presented in Figure 3-12.

A high coherence among leaves is also apparent in the relationship between estimated fluorescence radiance, electron transport and photosynthesis (Figure 3-13). A single relationship is observed in the case of PSII photochemical yield (left graph), irrespective of whether changes in fluorescence and photochemical yield are brought about by irradiance or CO_2. In the comparison with photosynthesis, on the contrary, a markedly different pattern is observed depending on the environmental parameter being modulated, as a result of the effects of photorespiration on net photosynthetic rates in C_3 plants.

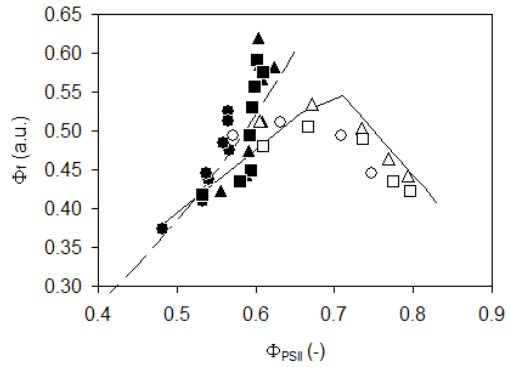

Figure 3-13. Quantitative test of the Magnani model against the leaf-level data of fluorescence yield (Φ_f) and PSII photochemical yield (Φ_{PSII}) described in Figure 3-12. The continuous line corresponds to simulated changes in irradiance under constant CO_2; the dashed line corresponds to changes in atmospheric CO_2 under constant irradiance. All photosynthetic and fluorescence parameters were derived from the literature, except for maximum photosynthetic potential and a fluorescence scaling factor accounting for PAM-2000 measurement light intensity.

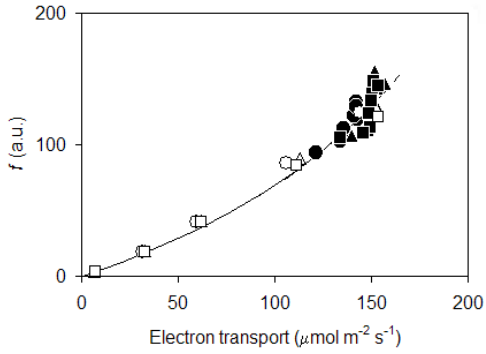

Figure 3-14. Quantitative test of the Magnani model against the leaf-level data of fluorescence radiance (*f*) and electron transport rates described in Figure 3-13. The continuous line corresponds to simulated changes in irradiance under constant CO_2; the dashed line corresponds to changes in atmospheric CO_2 under constant irradiance. All photosynthetic and fluorescence parameters were derived from the literature, except for maximum photosynthetic potential and a fluorescence scaling factor accounting for PAM-2000 measurement light intensity.

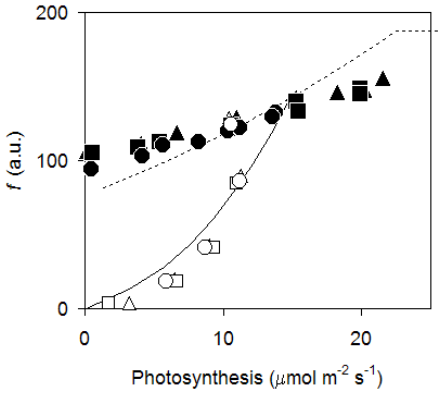

Figure 3-15. Quantitative test of the Magnani model against the leaf-level data of fluorescence radiance (*f*) and photosynthetic rates described in Figure 3-8. . The continuous line corresponds to simulated changes in irradiance under constant CO_2; the dotted line corresponds to changes in atmospheric CO_2 under constant irradiance. All photosynthetic and fluorescence parameters were derived from the literature, except for maximum photosynthetic potential and a fluorescence scaling factor accounting for PAM-2000 measurement light intensity.

A quantitative comparison of experimental data with predictions from the Magnani model is presented in Figure 3-14 to Figure 3-16 for fluorescence yield and fluorescence radiance. In all cases, all model parameters for fluorescence and photosynthetic processes were derived from the literature (Rabinowich *et al.* 1969; Farquhar *et al.* 1980; Bernacchi *et al.* 2001; Bernacchi *et al.* 2003), apart from the estimate of potential carboxylation rates (and associated potential electron transport rate; Leuning 1997) and a fluorescence scaling factor accounting for PAM-2000 measurement light intensity. The very good agreement between model predictions and experimental data is apparent from the figures presented, lending a strong support to the prediction of the relationship between fluorescence fields and gross primary production at canopy level through the SCOPE model, as planned as part of the current project.

Additional experiments under controlled conditions are under way in order to obtain an even more robust test of the Magnani model.

3.2.5. Comparison of proposed A-SIF models

A summary of model predictions in response to a wide interval of environmental and physiological parameters is presented in Figure 3-17. Similar results are obtained in response to changes in temperature and leaf chlorophyll content.

A positive association between fluorescence and photosynthesis is predicted by both models. The relationship, however, appears to be tighter according to the Magnani model, but to depend to a large extent upon the interaction between parameters in the Tol model. In particular, leaf photosynthetic potential (captured by the parameter V_{cmax}, assumed proportional also to maximum electron transport rate J_{max}) appears to have a strong effect on photosynthesis, as expected, but not on leaf fluorescence. This contrast with the more mechanistic Magnani model, where J_{max} is an explicit term in the relationship between fluorescence and electron transport rate, so counter-balancing the effect of V_{cmax}.

Preliminary tests against experimental data appear to agree with predictions by the Magnani model (see DL 3.3.2 Test of proposed algorithms against experimental data already available at the leaf level: SIF and photosynthesis: absolute SIF values).

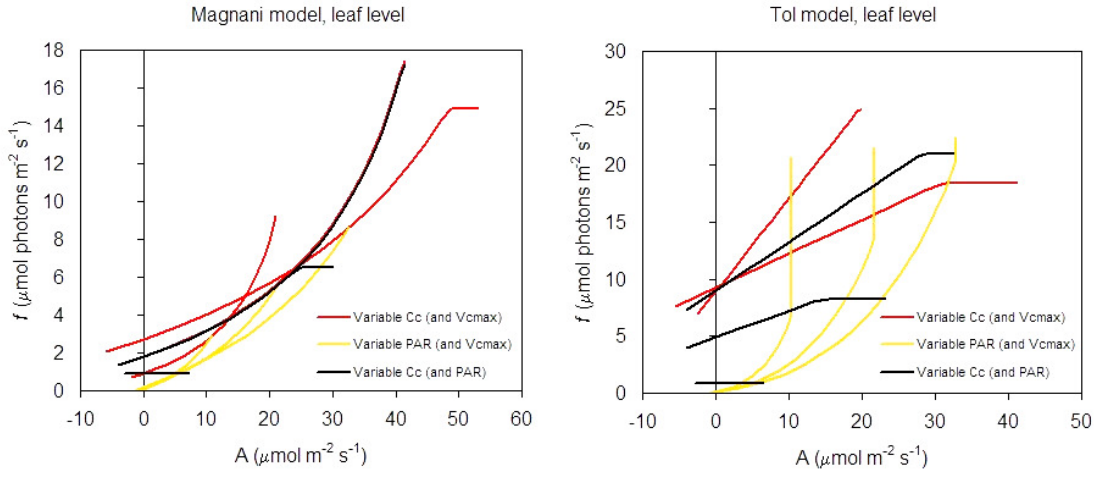

Figure 3-16. Simulated values of leaf photosynthesis (A) and PSII fluorescence (*f*) in response to a wide range of environmental parameters (PAR, photosynthetically active radiation: 0-1200 μmol m^{-2} s^{-1}; C_c, CO_2 concentration at carboxylation sites, indicative of air CO_2 and stomatal closure: 20-620 ppmv) and leaf photosynthetic potential (V_{cmax}, maximum carboxylation rate: 50-150 μmol m^{-2} s^{-1}). Results are presented based both on the Magnani and on the van der Tol model.

3.2.6. Modelling electron transport, fluorescence and xanthophyll de-epoxidation state

A more complex model of energy fate and electron transport, chlorophyll fluorescence and xanthophyll de-epoxidation state has been also developed as part of the project, in order to be able to assimilate in the proposed modelling scheme all the information that could be obtained from the proposed satellite sensor. Apart from solar-induced fluorescence, other indices have been proposed over the last few years for the remote sensing of photosynthetic processes. The Photochemical Reflectance Index (PRI), in particular, has been proposed as an effective tool for the measurement of xanthophyll de-epoxidation state and photosynthetic light-use efficiency, both at leaf (Gamon *et al.* 1997a; Gamon *et al.* 1999a; Peguero-Pina *et al.* 2008) and at canopy level (Rahman *et al.* 2004; Drolet *et al.* 2008). Although not yet implemented at the canopy scale, the model could provide in the future an interesting tool for the remote sensing of vegetation photosynthesis and productivity.

3.2.6.1. Background: the Photochemical Reflectance Index

Under conditions of excess excitation energy, the acidification of the chloroplast lumen determined by light-driven proton pumping is known to activate the enzyme responsible for the reversible de-epoxidation of the carotenoid violaxanthin into antheraxanthin and finally zeaxanthin. In turn, antheraxanthin and zeaxanthin are responsible for the non-radiative dissipation of excess light, by inducing in conjunction with low lumen pH a conformational change in light-harvesting complexes (Müller *et al.* 2001a; Holt *et al.* 2005). In so doing, xanthophyll de-epoxidation reduces ε (photosynthetic light-use efficiency) below its maximum potential value and protects, at the same time, the photosynthetic machinery from photodamage. Since all carotenoids are pigments, the change in the composition of the xanthophyll pool induces a slight shift in leaf color, and has been therefore detected by spectroscopic means as a change in leaf reflectance at 531 nm (Gamon *et al.* 1990). Detailed studies, however, demonstrate that the 531 nm signal results in reality from the superimposition of a fast- and a slow relaxing component, attributable to zeaxanthin content and to conformational changes in protein-chlorophyll complexes, respectively, and centered at about 525 and 540 nm (Bilger *et al.* 1989a). The processes involved are summarizd in Figure 3-17. .

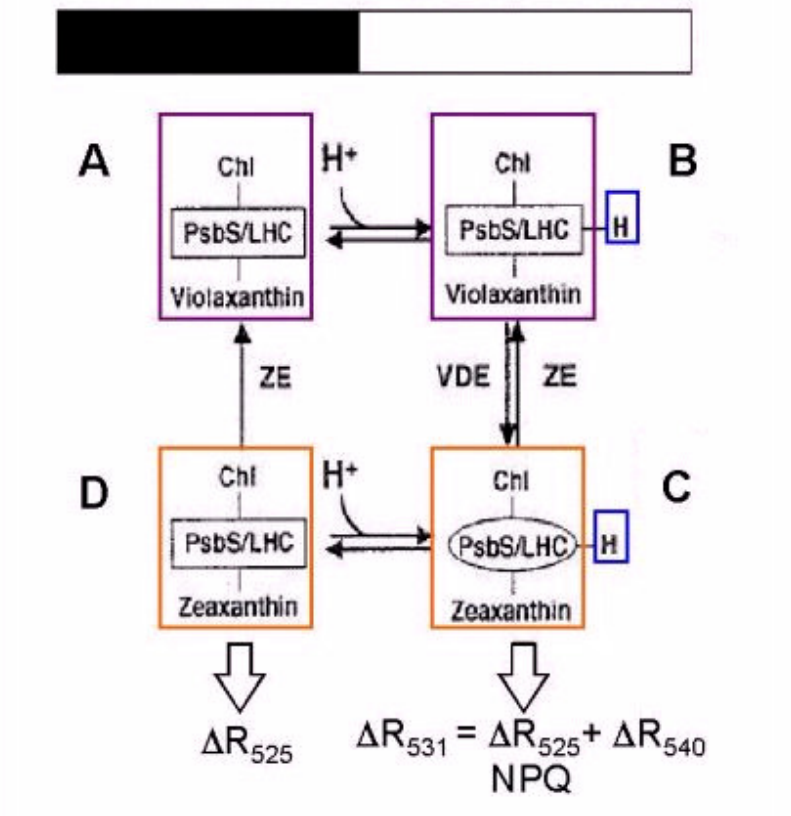

Figure 3-17. A summary model for non-photochemical quenching (NPQ; from Müller *et al.* 2001, modified). A, in limiting light or darkness, no quenching occurs (black bar above). B, in high light (white bar) protons bind to the PSSII protein PsBS and LCH. C, a quenching complex with different conformation, measurable as ΔR_{531} and PRI, is formed when zeaxanthin occurs more slowly than protonation. D, when the light stress has ended, the PSII proteins are de-protonated readily, whereas the epoxidation of zeaxanthin to violaxanthin is slower, reflecting in the dynamics of the ΔR_{525} signal

The possibility that NPQ and therefore ε could be directly estimated from these reflectance changes by RS techniques was originally proposed by Gamon *et al.* (Gamon *et al.* 1990). This later resulted in the development of the Photochemical Reflectance Index (PRI), defined as the normalised difference of leaf reflectance at 531 and 570 nm (Gamon *et al.* 1992a; Gamon *et al.* 1997b).

Several studies have since reported a strong link between PRI and ε both at the leaf (e.g. Carter 1998; Gamon *et al.* 1999b; Evain *et al.* 2004) and at the canopy level (Nichol *et al.* 2000a; Rahman *et al.* 2004; Garbulsky *et al.* 2008), although a lack of correlation has also been observed under extreme drought conditions (Penuelas *et al.* 1994).

Most recently, the index has also been applied to RS data for the estimation of canopy light-use efficiency at the regional level (Drolet *et al.* 2008).

Despite the empirical evidence relating PRI to photochemical processes, however, a quantitative explanation is still missing. The relationship between excess energy and NPQ has been the object of detailed models (Gilmore *et al.* 1998a; D'Haese *et al.* 2004), which consider the separate effects of pH gradients and xanthophyll de-epoxidation state on energy dissipation. As already mentioned, however, PRI results from the superimposition of the two signals and a technique for their deconvolution under field conditions is still missing.

As a result, short-term changes in the index are strongly related to xanthophyll de-epoxidation state, but PRI absolute values appear to be related also to other factors (Gamon *et al.* 1999c) and have been empirically correlated to leaf photosynthetic potentials (Stylinski *et al.* 2000a), possibly because of a functional link with total leaf xanthophyll pool size.

3.2.6.2. Model description

Leaf photosynthesis is the primary process behind vegetation gross primary production and life on earth and its modelling has received a great deal of attention over the last decade.

Photosynthesis is composed of light- (light energy capture and conversion into chemical energy) and dark reactions (storage of chemical energy in stable C-based compounds). However, whilst biochemically-based models of dark reactions have been available for more than 20 years (Farquhar *et al.* 1980), light reactions are generally represented in a purely empirical way (Long *et al.* 2003).

Although operationally effective, empirical models are not able to represent intermediary steps which are amenable to RS observation (e.g. chlorophyll fluorescence)

Detailed information is available, however, on individual steps of light capture, electron transport and ATP production, fluorescence emission, as schematically represented in Figure 3-18. The present model will try and combine this body of information into a simple process-based model of photosynthetic light reactions and sloar-induced fluorescence

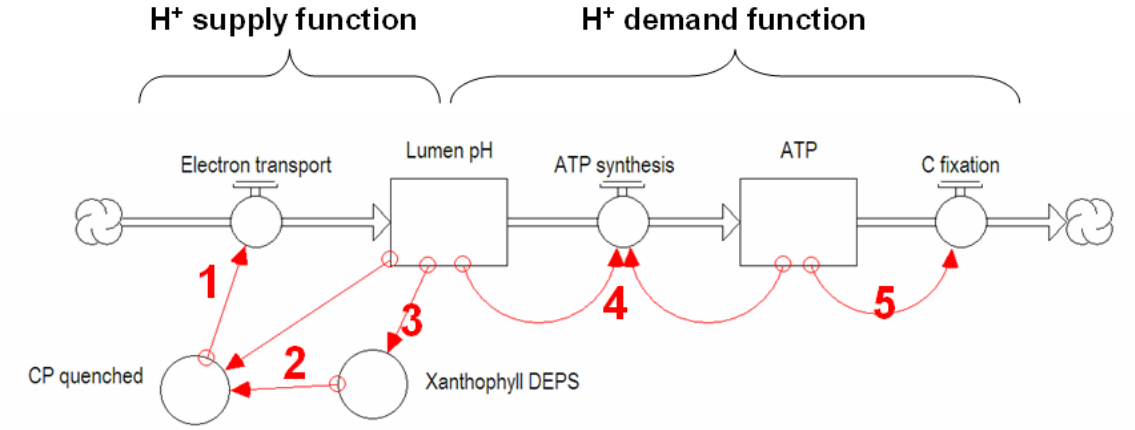

Figure 3-18. Schematic representation of the key processes involved in energy utilisation and photosynthetic electron transport. Based on the central role of thylakoid lumen pH, processes are grouped in a H^+ supply function (representing the response of H^+ influx into the thylakoid lumen to lumen pH) and a H^+ demand function (representing the use of H^+ for ATP generation as a function of lumen pH).

3.2.6.3. Step 1. CP quenching and energy dissipation

Step one has been described in detail in section 3.2.3.

3.2.6.4. Step 2. Site activation, zeaxanthin binding and CP quenching

The fraction of quenched CPs is known to be a function of lumen pH and zeaxanthin concentration per PSII (Gilmore *et al.* 1994). To quantitatevely incorporate the effects of the pH on the xanthophyll cycle-dependent Chl *a* fluorescence quenching, we assume that protonation of carboxyl groups on the lumenal side of the PSII inner core antenna proteins is necessary for the reversible activation of the binding site for Z. Following Gilmore *et al.* (1998b), the protonation steps are represented using the simple scheme:

$$H^+ + CP - \underset{(W)}{COO^-} \xleftrightarrow{pK} CP - \underset{(X)}{COOH} \qquad \text{(Eq. 3-42)}$$

where W in parentheses represents the binding site for Z and X is the protonated binding site, with a high binding affinity for Z, and pK is an affinity coefficient, with value of approximately 4.5.

The pH dependence of the frequency of the two states of the binding site is given by the Henderson-Hasselbach equation:

$$pH = pK + \log\frac{W}{X} \qquad \text{(Eq. 3-43)}$$

All Z molecules are assumed to compete for the binding site, and to bind to it in a fully reversible way:

$$Z + CP - \underset{(X)}{COOH} \xleftrightarrow{K_z} Z - CP - \underset{(Y)}{COOH} \qquad \text{(Eq. 3-44)}$$

where Y represents the fraction of sites bound to Z. The equilibrium constant Ka is given by:

$$K_a = \frac{Y}{X \cdot Z} \qquad \text{(Eq. 3-45)}$$

A value of about 2.5 for the equilibrium constant Ka has been proposed by Gilmore *et al.* (1998b).

By combining the preceding equations, the fraction *p* of CPs that are bound to zeaxanthin and therefore actively quenching can be expressed as:

$$p = \frac{CP_Q}{CP} = \frac{Y}{W + X + Y} = \frac{K_a \cdot Z \cdot 10^{pK-pH}}{1 + 10^{pK-pH} \cdot \left(1 + K_a \cdot Z\right)} \qquad \text{(Eq. 3-46)}$$

where CP_Q is the number of CPs in the quenched state and CP the total number of CPs.

3.2.6.5. Step 3. Lumen pH and xanthophyll de-epoxidation

The de-epoxidation of violaxanthin into antheraxanthin and zeaxanthin is controlled by the activity of the enzyme violaxanthin de-epoxidase (VDE). This lumen-localized enzyme requires ascorbate as a cofactor and shows a pH optimum of about 5.2 (Eskling *et al.* 1997). The activation of VDE at low pH seems to be accompanied by the binding of the enzyme to the membrane (Hager *et al.* 1994). Both processes of VDE activation and VDE binding to the membrane show a high cooperativity with respect to the proton concentration (Pfundel *et al.* 1993), so that the dependence of xanthophyll de-epoxidation state upon lumen pH can be represented by a Hill equation:

$$\log\frac{Z}{Z_{\max} - Z} = n_H \cdot \log\left[H^+\right] - \log K_d = -n_H \cdot pH_l - \log K_d \qquad \text{(Eq. 3-47)}$$

where Z is the number of zeaxanthin molecules per PSII, Z_{max} is its maximum value under conditions of maximum quenching, n_H is the so-called Hill coefficient and K_d is a dissociation constant. Jahns and Heyde (1999) provided for n_H and log K_d a value of 5.6 and -34.2, respectively, in good agreement with the results of Pfundel and Dilley (1993).

The maximum value of xanthophyll DEPS under conditions of full lumen acidification has been reported to approach 90% (Eskling *et al.* 1997); if nVAZ is the total number of VAZ (zeaxanthin +antheraxanthin + violaxanthin) molecules per CP, Zmax can be expressed as:

$$Z_{\max} = DEPS_{\max} \cdot n_{VAZ} = 0.9 \cdot n_{VAZ} \qquad \text{(Eq. 3-48)}$$

A value of 8 has been proposed for the parameter n_{VAZ} (Gilmore *et al.* 1998b). The distinct role of antheraxanthin and zeaxanthin as quenchers of Chl *a* fluorescence has been neglected for the sake of simplicity.

3.2.6.6. Step 4. ATP synthesis

Several alternative models have been proposed over recent years for the representation of ATP synthesis, as affected by lumen pH and other biochemical parameters (Schönknecht *et al.* 1995; Pänke *et al.* 1996; Pänke *et al.* 1999; Jain *et al.* 2000; Xing *et al.* 2005), ranging from the simplistic to

the very complex. A suitable compromise between simplicity and detail appears the model of ATP-synthase activity proposed by Panke and Rumberg (1999), which duly represents the role of transmembrane pH gradient, as well as the back-regulation exerted on ATP synthesis by the concentration of ATP, ADP and inorganic phosphate (Takizawa *et al.* 2008).

The model (schematically represented in Figure 3-19) focuses on the role of the elastic element of ATP-synthase, realized by the stalk-like subunit γ, whose function is energy transduction between F0 and F1 taking into account the H/ATP coupling ratio of four. Fitting parameters are the rate constants and the torsional rigidity of γ, which have been adjusted by the Authors according to the experimental results where the influence of transmembrane ΔpH on the rates of ATP synthesis/hydrolysis is put to the test. An analysis of available data demonstrates that the input and output of torsional energy are regulated by purely statistical principles, giving rise to the amount of transiently stored energy to be sliding, depending on ΔpH.

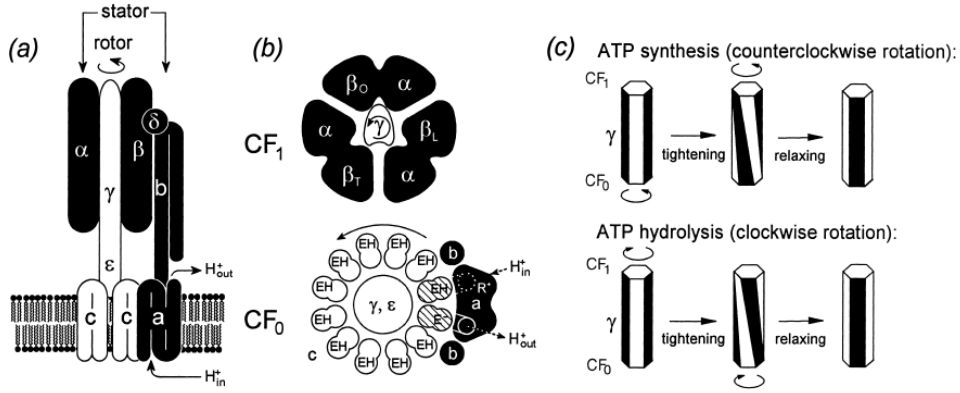

Figure 3-19. Scheme of ATP synthase activity. (a) The eastic element γ accumulates rotational energy generated by CFo before it is transferred to CF1. (b) Cross-sections of CF0 and CF1 seen from above. Anticlockwise rotation corresponds to ATP synthesis. (c) Visualization of the sequence of torsional states of the elastic element γ during ATP synthesis/hydrolysis. From Panke and Rumberg (1999)

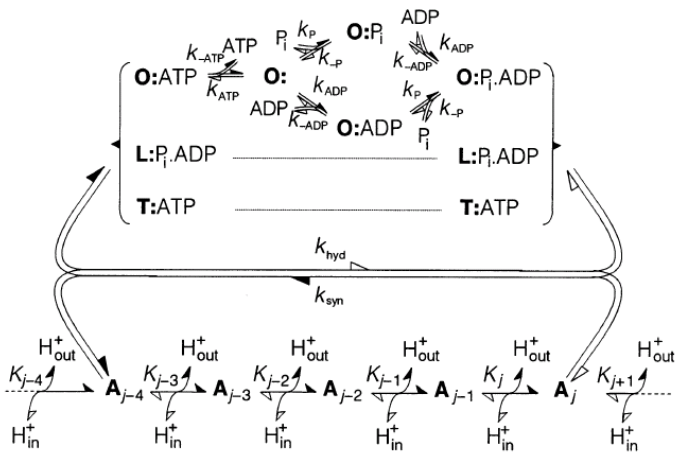

Figure 3-20. Schematic presentation of the binding change mechanism for ATP synthesis/hydrolysis as described in the text. Solid arrows refer to synthesis of ATP and open arrows to hydrolysis. Symbols Aj refer to the torsional states of subunit γ.

The rate of the five state transitions represented schematically in Figure 3-20. Figure 3-22 can be represented by a set of five equations, which is amenable to an analytical solutions.

$$
\begin{aligned}
&k_{syn}\cdot X_{O:P.ADP}+k_{ATP}\cdot ATP\cdot X_{O:}-\left(k_{hyd}+k_{-ATP}\right)\cdot X_{O:ATP}=0\\
&k_{-ATP}\cdot X_{O:ATP}+k_{-P}\cdot X_{O:P}+k_{-ADP}\cdot X_{O:ADP}-\left(k_{ATP}\cdot ATP+k_{P}\cdot P_i+k_{ADP}\cdot ADP\right)\cdot X_{O:}=0\\
&k_{ADP}\cdot ADP\cdot X_{O:}+k_{-P}\cdot X_{O:P.ADP}-\left(k_{-ADP}+k_{P}\cdot P_i\right)\cdot X_{O:ADP}=0\\
&k_{ADP}\cdot ADP\cdot X_{O:P}+k_{P}\cdot P_i\cdot X_{O:ADP}+k_{hyd}\cdot X_{O:ATP}-\left(k_{-ADP}+k_{-P}+k_{syn}\right)\cdot X_{O:P.ADP}=0\\
&X_{O:ATP}+X_{O:}+X_{O:P}+X_{O:ADP}+X_{O:P.ADP}=1
\end{aligned}
\qquad \text{(Eq. 3-49)}
$$

where X_i and k_i are the concentration and rate constants for each individual step.

The net rate of ATP production is represented as the difference between the rate constant for ATP synthesis and hydrolisis, each multiplied by the corresponding concentration:

$$\nu = k_{syn}\cdot X_{O:P.ADP}-k_{hyd}\cdot X_{O:ATP} \qquad \text{(Eq. 3-50)}$$

The rate constant for ATP synthesis is represented as:

$$k_{syn}=k^{\circ}_{syn}\cdot D \qquad \text{(Eq. 3-51)}$$

whilst the corresponding value for ATP hydrolisis is:

$$k_{hyd}=k^{\circ}_{hyd}\cdot D\cdot\exp\left(4\cdot\Delta\mu/RT\right) \qquad \text{(Eq. 3-52)}$$

where k°_{syn} and k°_{hyd} are specific binding rate constants for ATP synthesis and hydrolisis, respectively, and the factor D corresponds to:

$$D=\sum_{j=-\infty}^{\infty}p_j\cdot\exp\left[8\cdot\alpha\cdot\kappa\cdot\left(j-2\kappa\right)/RT\right] \qquad \text{(Eq. 3-53)}$$

and the parameter α is:

$$\alpha=\frac{1}{2}\cdot N_A\cdot M^{*}\cdot\left(\frac{2\pi}{12}\right)^2 \qquad \text{(Eq. 3-54)}$$

The probability p_j of a definite torsional state A_j in Eq. 71 is calculated as:

$$p_j=\frac{\exp\left[-\left(\Delta\mu\cdot j+\alpha\cdot j^2\right)/RT\right]}{\sum_{j=-\infty}^{\infty}\exp\left[-\left(\Delta\mu\cdot j+\alpha\cdot j^2\right)/RT\right]}=\frac{\exp\left[-\left(\Delta\mu\cdot j+\alpha\cdot j^2\right)/RT\right]}{\sum_{j=j_{peak}-3}^{j_{peak}+3}\exp\left[-\left(\Delta\mu\cdot j+\alpha\cdot j^2\right)/RT\right]} \qquad \text{(Eq. 3-55)}$$

Finally, the Gibbs energy which is stored primarily in the transmembrane H^+ gradient and which is available during H^+ transport from inside to outside is described by the electrochemical potential difference for H^+ according to:

$$\Delta\mu=-2.3\cdot RT\cdot\Delta pH+F\cdot\Delta\Psi\approx-2.3\cdot RT\cdot\Delta pH \qquad \text{(Eq. 3-56)}$$

where $\Delta pH=pH_{out}$ - pH_{in} denotes the outside-minus inside pH difference and $\Delta\Psi$ the corresponding electrical potential difference.

The position of the peak in the Gaussian curve representing the dependence of p_j upon the torsional number γ can be expressed as:

$$j_{peak} = -\Delta\mu / 2\alpha \qquad \text{(Eq. 3-57)}$$

Further details on the ATP-synthase model and its test against experimental data can be found in Panke and Rumberg (1999).

Table 3-4. Description of parameters involved in the representation of ATP synthesis and proposed values

Symbol	Definition	Value	Units	Source
k_{ATP}	rate constants of ATP association	$2.08 \cdot 10^{6}$	$mol^{-1}\ s^{-1}$	1
k_{-ATP}	rate constants of ATP dissociation	$2.70 \cdot 10^{2}$	$mol^{-1}\ s^{-1}$	1
k_{P}	rate constants of P association	$8.10 \cdot 10^{5}$	$mol^{-1}\ s^{-1}$	1
k_{-P}	rate constants of P dissociation	$2.03 \cdot 10^{3}$	$mol^{-1}\ s^{-1}$	1
k_{ADP}	rate constants of ADP association	$8.90 \cdot 10^{6}$	$mol^{-1}\ s^{-1}$	1
k_{-ADP}	rate constants of ADP dissociation	$4.90 \cdot 10^{2}$	$mol^{-1}\ s^{-1}$	1
$k_{syn}°$	specific binding site rate constant, synthesis	$1.15 \cdot 10^{-3}$	s^{-1}	2
$k_{hyd}°$	specific binding site rate constant, hydrolisis	$4.5 \cdot 10^{5}$	s^{-1}	2
M^{*}	torsional rigidity of γ (elastic element)	$3.0 \cdot 10^{-20}$	J	2
κ	position of the binding site transition state	0.6	-	2
R	universal gas constant	8.314	$J \cdot K^{-1} \cdot mol^{-1}$	
T	absolute temperature	298.3	K	
F	Faraday constant	96485.3	coulomb mol^{-1}	
N_A	Avogadro's number	$6.022 \cdot 10^{23}$	mol^{-1}	

[1] from Pänke & Rumberg (1996); [2] from Pänke & Rumberg (1999)

3.2.6.7. Step 5. ATP consumption in the Calvin cycle

The relationship between ATP (and ADP) concentration, photosynthesis and stomatal closure will be represented by considering the stoichiometry of ATP use in the Calvin cycle and treating photosynthesis as an irreversible enzymatic reaction with two substrates (ATP and CO2; Laisk & Eichelmann 1989). Ignoring for the time being the effects of photorespiration, carboxylation rates can be then expressed as:

$$V = V_m \cdot \frac{ATP \cdot C_c / (K_{ATP} K_C)}{1 + ATP / K_{ATP} + C_c / K_C} \qquad \text{(Eq. 3-58)}$$

By inverting the equation above, the ATP concentration required to drive the photosynthetic process can be computed as a function of CO_2 concentration at carboxylation sites (C_c)

$$ATP = \frac{V \cdot K_{ATP} \cdot (K_C + C_c)}{C_c \cdot V_m - V \cdot K_C} \qquad \text{(Eq. 3-59)}$$

By imposing a known stoichiometry between ATP synthesis and dark photosynthetic rates, and accounting for the back-regulation exerted by ATP concentration on ATP-synthase activity (see Eq. 3-49), the two preceding equations can be solved to provide an estimate of leaf photosynthetic rates under imposed conditions.

Table 3-5. Summary of parameters involved in the representation of dark photosynthetic processes

Symbol	Definition	Units	Source
K_{ATP}	rate const. of substrate association for ATP	mol m^{-2}	Laisk & Eichelmann (1989)
K_C	rate constants of substrate association for CO2	ppmv	Laisk & Eichelmann (1989)
C_c	CO2 concentration at carboxylation sites	ppmv	
V	carboxylation rate	µmol m^{-2} s^{-1}	
V_m	maximum carboxylation rate	µmol m^{-2} s^{-1}	

3.2.6.8. Representation of leaf PRI

As already discussed, changes in the 531 nm reflectance signal that constitutes the basis of the Photochemical Reflectance Index result from two different components: a slower component associated to xanthophyll de-epoxidation state and a fast component associated with conformational changes and CP quenching (Bilger *et al.* 1989b; Brugnoli *et al.* 1992; Mohanty *et al.* 1995). The PRI signal is therefore proposed to be the sum of three components:

$$PRI = PRI_0 + a \cdot CP_Q + b \cdot Z$$

where PRI_o is a baseline value of the index and *a* and *b* are two suitable empirical parameters.

3.2.6.9. Model predictions

As described in the initial scheme, the model defines a supply and a demand function, related to the production and to the utilisation of H^+ as a result of electron transport and ATP production, respectively. Both steps will be regulated by lumen pH. Under steady-state conditions, H^+ production and utilisation will correspond to each other, i.e. the operational status of the photosynthetic apparatus will correspond to the intersection of the supply and demand functions, as demonstrated in Figure 3-21. .

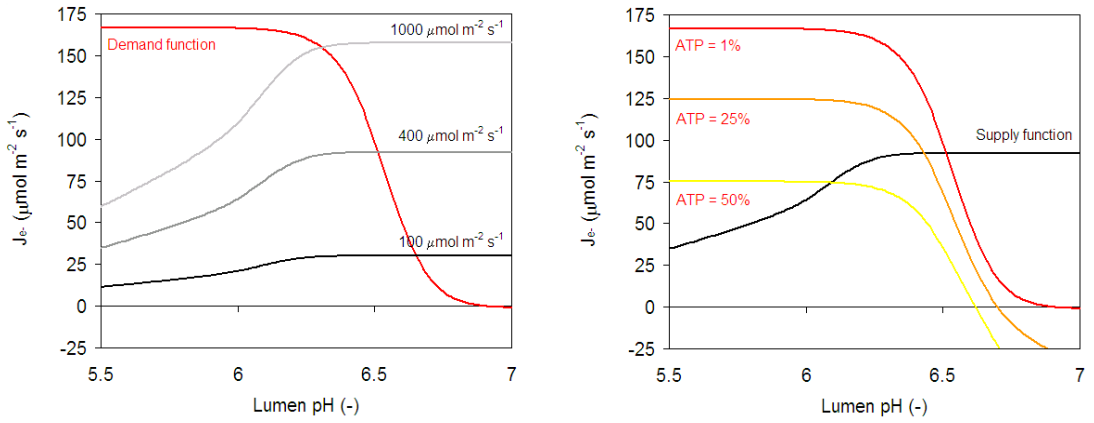

Figure 3-21. Response of H^+ production (supply function) and utilisation for ATP production (demand function) in response to three different light levels (left) and to different stomatal limitations, corresponding to different ATP/ADT ratios (right). The operational status of the photosynthetic apparatus will correspond to the intersection of thedemand and supply functions.

A demonstration of model applications and predictions in response to a range of internal and external parameters is presented in Figure 3-24. The corresponding changes in fluorescence yield and in PRI are compared against each other in Figure 3-25, in order to demonstrate the different information content of these two indices of photosynthetic processes.

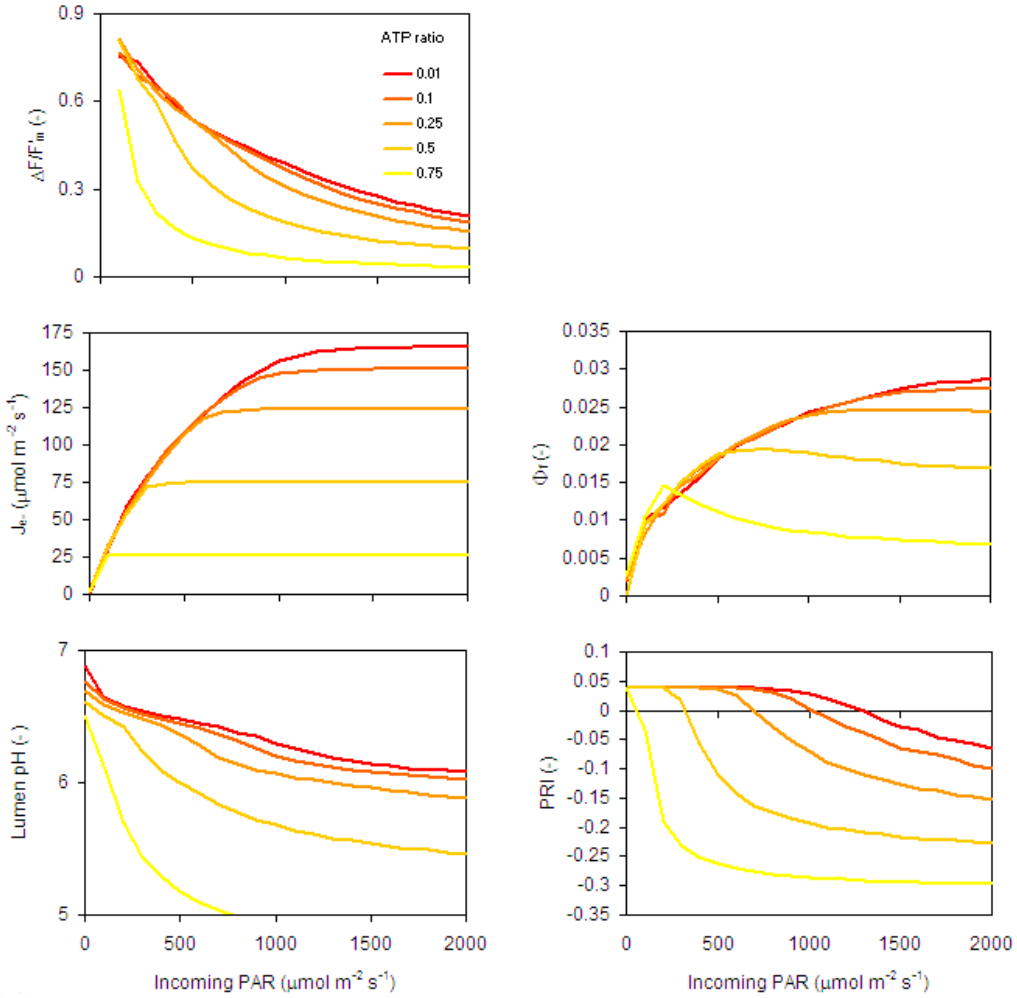

Figure 3-22. Simulated response of several photosynthetic parameters to a combination of changes in incoming photosynthetically active radiation (PAR) and stomatal limitations, corresponding to different ATP/ADT ratios. Simulations are presented for PSII apparent quantum yield ($\Delta F/F_m'$ = photochemical efficiency), electron transport rate (J_{e-}), lumen pH, fluorescence yield (Φ_f) and the Photochemical Reflectance Index (PRI).

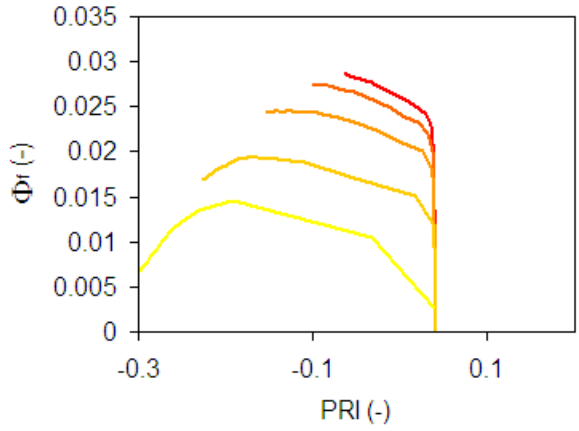

Figure 3-23. Comparison of simultaneous changes in fluorescence yield (Φ_f) and the Photochemical Reflectance Index (PRI) in response to changes in incoming PAR and stomatal limitations, as described in Figure 3-6. .

3.3. Estimation of canopy photosynthesis from canopy reflectance through the Photochemical Reflectance Index: potential and limitations

Apart from the direct measurement of vegetation chlorophyll fluorescence, which is the main topic of the present study, use of the Photochemical Reflectance Index (PRI), a remote sensing index based on the measurement of canopy hyperspectral reflectance in the visible domain (531-570 nm), has been proposed and widely applied in recent years for the assessment of vegetation photosynthetic light-use efficiency (LUE) and photosynthetic rates. The physiological basis of the PRI index has already been reviewed in the preceding chapter, where a novel leaf-level model has been presented which integrates the process-based representation of both PRI and SIF. The information content of the two signals, which can be both extracted from canopy radiance in the VIS-NIR region, has also been demonstrated to be non-redundant.

In the present chapter, a brief review of PRI application is presented, in order to demonstrate its potential and limitations, and therefore the need for its combination with the measurement of solar-induced fluorescence for a more direct and precise assessment of photosynthetic rates.

3.3.1. Importance of LUE in photosynthetic models

Estimation of photosynthesis or primary productivity from remotely sensed absorbed solar radiation requires knowledge of light use efficiency (LUE), which indicates the efficiency of a vegetative canopy to use light for fixing carbon (Drolet *et al*. 2006).

Models used to express photosynthetic productivity, or carbon gain, include the following (Gamon and Qiu 1999):

$$\text{Photosynthetic rate} = \text{APAR} * \varepsilon,$$

where, APAR indicates the quantity of absorbed photosynthetically active radiation, and ε represents photosynthetic light- (or radiation) use efficiency.

$$\text{Primary productivity} = \Sigma\text{APAR} * \varepsilon,$$

where, primary productivity is often expressed as net primary productivity (NPP), usually meaning accumulated biomass integrated over a growing season, APAR is the absorbed PAR or the annual integral of radiation absorbed by vegetation, and ε represents the average light (or radiation) use efficiency (Cavender-Barea and Bazzaz 2004). APAR can be further defined as the product of photosynthetically active radiation (PAR) and the fraction of that irradiance that is absorbed by vegetation (F_{APAR}), and expression of net primary productivity (NPP) derived as follows:

$$\text{NPP} = \text{PAR} * F_{APAR} * \varepsilon,$$

While respiration is not explicitly included in these models, it can be incorporated either into ε or as a separate coefficient. Estimation of APAR is often done using the relationship between Normalized Difference Vegetation Index (NDVI) (or other appropriate reflectance index) and F_{APAR}, such that NPP can be expressed as a function (*f*) of NDVI, PAR, and ε:

$$\text{NPP} = f(\text{NDVI} * \text{PAR} * \varepsilon)$$

Early models assumed LUE to be constant, but more recently, calculations have incorporated adjustments for temperature and moisture stress, e.g., using look-up tables to relate these environmental variables to LUE for various vegetation types (Grace *et al*. 2007). However, it has become increasingly clear that such approaches are not robust, and that more direct measures of LUE are needed, given the complexities of ecosystem photosynthetic responses (Drolet *et al*. 2005, 2006).

Canopy LUE can be measured directly using data from eddy covariance flux towers (Drolet *et al.* 2005, 2006) or it may be estimated using spectral indices.

3.3.2. Photochemical reflectance index, light use efficiency, and photosynthesis

The photochemical reflectance index (PRI) was introduced by Gamon and colleagues in the 1990s as an index of xanthophyll (carotenoid) cycle activity, which is sensitive to changes in light use efficiency (Gamon *et al.* 1992, Peñuelas *et al.* 1995b, Gamon *et al.* 1997). PRI has now become a widely applied surrogate for light use efficiency. The fact that it can be measured remotely is a significant advantage. It is usually expressed as:

$$PRI = (R_{531} - R_{570}) / (R_{531} + R_{570}),$$

where, R_{531} represents reflectance at 531 nm (the xanthophyll cycle band) and R_{570} reflectance is used as a reference, using narrow-band (± 2 nm) reflectance. Based on relationships often observed between PRI and photosynthetic rates, Rahman *et al.* (2001) proposed the following equation:

$$CO_2 \text{ uptake} = f(\text{sPRI} * \text{NDVI})$$

where, sPRI is a scaled value of PRI ranging from 0 to 1, calculated algebraically as sPRI = (PRI +1)/2.

Although PRI measured from space will be a small signal, it is apparently discernible. Various commercial imaging spectrometers offer sufficiently high spectral resolution to accurately measure PRI. Table 3-6 lists examples.

Table 3-6. Operational hyperspectral imaging spectrometers capable of measuring PRI with high accuracy.
(Source: Grace et al. 2007).

Name	Full name	Manufacturer	Bands	λ range (and full width at half maximum) (nm)
AAHIS	Advanced Airborne Hyperspectral Imaging System	SETS Technology	288	432-832 (6)
AISA	Airborne Imaging Spectrometer for Applications	Specim Ltd.	286	450-900 (1.56-9.36)
AVIRIS	Airborne Visible / Infrared Imaging Spectrometer	NASA, JPL	224	400-2450 (9.4-16)
CAESAR	CCD Airborne Experimental Scanner for Applications in Remote Sensing	NLR	12	520-780 (10-30)
CASI	Compact Airborne Spectrographic Imager	Itres Research	288	430-870 (2.9)
CHRIS	Compact High Resolution Imaging Spectrometer	Sira Optics UK and BNSC	63	400-1050 (2.3-12)
CIS	Chinese Imaging Spectrometer	Shanghai Institute of Technical Physics	91	400-12500 (10-1000)
EPS-A	Environmental Probe System	GER Corp.	32	400-12000 (10-variable)

Name	Full name	Manufacturer	Bands	λ range (and full width at half maximum) (nm)
FLI/PMI	Fluorescence Line Imager / Programmable Multispectral Imager	Moniteq Ltd.	228	430-805 (2.5)
FTVFHSI	Fourier-Transform Visible Hyperspectral Imager	Kestrel Corp., FIT	256	440-1150 (5-10)
HYDICE	Hyperspectral Digital Imagery Collection Experiment	Naval Research Laboratory	210	413-2504 (7.6-14.9)
MERIS	Medium Resolution Imaging Spectrometer	ESA	15	400-1050 (2.5-20)
MODIS	Moderate Resolution Imaging Spectrometer	NASA	36	415-14240 (10-500)
ROSIS	Reflective Optics System Imaging Spectrometer	DLR, GKSS, MBB	84 / 30	450-850 (4-12)
TRWIS III	TRW Imaging Spectrometer	TRW Inc.	384	300-2500 (5-6.25)
VIFIS	Variable Interference Filter Imaging Spectrometer	University of Dundee	60	440-890 (10-18)
VIMS-V	Visible Infrared Mapping Spectrometer	ASI	352	350-5100 (7-14)
WIS	Wedge Imaging Spectrometer	Hughes St. Barbara Research Center	170	400-2500 (9.6-37.8)

Various studies have addressed relationships between PRI and ε. Examples are summarized in Table 3-7. Some studies have further found PRI to reflect changes in CO_2 assimilation (Gamon *et al.* 1995, Louis *et al.* 2005, Fuentes *et al.* 2006).

However, with respect to ε, Grace *et al.* (2007) noted that despite many studies demonstrating PRI links to ε, the coefficients of determination (r^2) vary significantly (e.g., from 0.38 to 0.94) and remote scale relationships tend to be weaker than those for leaves.

Table 3-7. Research studies suggesting PRI can estimating ε.

Leaf-level	
*Quercus, Phillyrea (*or *Phyllyrea*); significant relationships between PRI and RUE, and between PRI and ΔF/Fm'. But scatter in relations and challenges for remote sensing noted.	Peñuelas *et al.* (1977, 1998)
Chaparral spp.; PRI tracked PSII efficiency and net CO_2 uptake seasonally; PRI of leaves from canopy top indicative of whole canopy.	Stylinski *et al.* (2002)
Eight species; PRI and LUE relationship r^2=0.79, but when simulated for AVIRIS (by calculating using a 10-nm bandwidth) r^2=0.67.	Trotter *et al.* (2002)
Various species: PRI and LUE correlated (r^2=0.58) but for correlation best for species-level relationships (r^2>0.90).	Guo & Trotter (2004)

Prairie site; PRI (and other indices) correlated well to LUE calculated as ratio of carbon uptake by ecosystem and fraction of PAR absorbed by leaves.	Huemmrich *et al.* (2006)
Canopy-level / Remote	
Four boreal species; PRI measured from helicopter linearly correlated with LUE (from eddy covariance data); when data averaged to represent AVIRIS, got weakened relationship for deciduous spp, strengthened for conifers.	Nichol *et al.* (2000)
Aspen forest; MODIS-derived scaled PRI and tower-based LUE relationship, r^2=0.76 or 0.53 for top of atmosphere or surface reflectances, respectively.	Drolet *et al.* (2005)
Scots pine; CO_2 assimilation at the forest canopy level was well correlated with PRI.	Louis *et al.* (2005)
Canopy-level / Remote	
Various spp; PRI from CHRIS Proba images correlated with LUE (calculated as ΔF/Fm') and non-photochemical quenching (NPQ), but PRI strongly affected by soil reflectance, need correction or use of tilted images.	Raddi *et al.* (2005, 2006)
Two tree species; PRI from Earth Observing-1 Hyperion satellite related to LUE as indicated by field measurements of leaf electron transport rate.	Asner *et al.* (2006)
Boreal forest; Classified MODIS pixels into shadow classes to strengthen links between MODIS-PRI and gross LUE.	Drolet *et al.* (2006)
Chaparral; net CO_2 and water flux modeled from AVIRIS-derived reflectance indices including PRI effectively tracked changes in tower fluxes across both drought and fire; pixel scale images from 2 m to 16 m.	Fuentes *et al.* (2006)
Cypress forest; when removed effect of strong light dependence of LUE and selected data during clear sky measurements, PRI almost linearly related to LUE throughout the season.	Rie *et al.* (2006)
Terrestrial ecosystems; PRI from MODIS had exponential relationship with RUE; possible to estimate RUE in real time and therefore actual CO_2 uptake.	Garbulsky *et al.* (2007)

Before it is possible to objectively judge the merits and success of PRI as an indicator or measure of LUE, it is necessary to consider the lack of consistent terminology in studies and reports involving vegetation light usage for photosynthesis.

As discussed in detail by Grace *et al.* (2007), any 'efficiency' should be expressed as a percentage or fraction, such that the numerator and denominator have the same units. The authors note that this convention is respected in physics but not always in biology. As a result, several different formats of efficiency are used. Possible units for ε are mols of carbon dioxide captured per mol photons light absorbed (LUE), or joules captured in chemical bonds during photosynthesis per joule of solar energy absorbed (RUE). Various deviations from these are also used. Agronomists and foresters use biomass as the numerator (without conversion to energy units using heat of combustion). Some authors use solar energy incident on the canopy, not energy absorbed, as denominator. A further confusion arises when solar energy is sometimes expressed as global solar energy (i.e., entire waveband) and at other times as solar energy in the photosynthetically active region PAR (400-700 nm). In photobiology, efficiency of photosynthesis called 'the quantum efficiency', and usually refers to gas exchange of leaves at low light, found from the initial slope of the photosynthesis-light response curve. Finally, PRI has been compared to measures of efficiency derived from chlorophyll fluorescence measurement, usually of the effective PSII efficiency (ΔF/Fm') obtained from light-adapted foliage.

These rather disparate expressions of efficiency confound efforts to draw resilient conclusions about the efficiency of conversion of absorbed radiation to fixed carbon (biomass), particularly when complex variables such as soil or vegetation respiration are introduced into the mix.

3.3.3. Problems and challenges in applying PRI

3.3.3.1. Drought stress situations

Drought development can induce marked alterations in the physiological and morphological (e.g., from wilting) characteristics of foliage which can complicate efforts to link spectral indices such as PRI to photosynthetic or light-use efficiency. For example, Sims *et al*. (2006), in a canopy study of southern California chaparral, found that PRI had inconsistent relationship to LUE (calculated using absorbed PAR). These features were correlated during years with normal rainfall but not in drought years. PRI's inconsistency in drought situations had been noted previously in leaf and canopy studies (Peñuelas *et al*. 1997, Strachan *et al*. 2002, Thenot *et al*. 2002).

Sun *et al*. (2008) examined effects of rapid or gradual induction of drought stress in olive (*Oleo europaea*) leaves, and found that when photosynthetic inhibition from drought occurred within an hour (under rapid drought induction) it was not accompanied by changes in chlorophyll or carotenoid:chlorophyll ratio, and also was not reflected in changes in PRI. However, when drought was allowed to develop more gradually (over longer than 24 hours), producing changes in chlorophyll and carotenoid:chlorophyll ratio, PRI was responsive.

Implications for PRI:LUE relationships may also be drawn from a study of progressive development of drought stress in potted seedlings of paper birch (*Betula papyrifera*) (Richardson *et al*. 2004). Photosynthesis responded to the drought treatment at about 12% to 15% soil moisture content, whereas PRI did not respond until about 9% to 10%, and the chlorophyll fluorescence feature Fv/Fm not until 4% to 5%. The more rapid response of photosynthesis might indicate that LUE changed before PRI.

Research by Suárez *et al*. (2008) involving airborne diurnal campaigns over an orchard field found that PRI was sensitive to water stress. They calculated three vegetation indices (PRI, normalized Transformed Chlorophyll Absorption in Reflectance Index, and NDVI), but only PRI was sensitive to diurnal changes in physiological parameters of water stress, such as canopy temperature minus air temperature, stomatal conductance, and stem water potential. However, the authors found that PRI was also highly affected by canopy structure and background characteristics.

3.3.3.2. Canopy greenness

Sims *et al*. (2006) found inconsistencies in PRI:LUE relationships over long time-scales, e.g., over the course of a season, and postulated that perhaps seasonal responses of PRI are not a direct function of photosynthetic rates. And none of the indices they tested showed consistent relationships with CO_2 flux or LUE over a diurnal time-course, possibly because of confounding effects of sun angle and stand structure on reflectance. They further suggested that in this type of ecosystem (sparse, semi-deciduous shrub), greenness indices (e.g., NDVI at constant solar elevation angle, or a red edge chlorophyll index) may be used to estimate CO_2 exchange at weekly timescales, even if LUE is changing. This would make separate estimates of LUE unnecessary, at least for some vegetation types. Greenness indices would be unlikely to be as good predictors of CO_2 exchange in dense evergreen vegetation, however, relatively few ecosystems are entirely evergreen over large areas or long time spans. In another study, of a Mediterranean shrubland submitted to experimental warming and drought, PRI was less adequate than NDVI in indirectly tracking CO_2 uptake, especially in lower LAI canopies, possibly because photosynthetic fluxes followed canopy seasonal greening (Filella *et al*. 2004).

The dependence of GPP on chlorophyll content is an important consideration that is highlighted by Gitelson (2006). They reported that maize and soybean crops, for example, clearly reveal this

dependence, as both irrigated and rainfed crops had midday GPP that was closely related to total crop chlorophyll content. Their method shows strong potential for remotely tracking GPP and physiological status of crops with contrasting canopy architectures and physiological responses.

3.3.3.3. Chlorophyll and anthocyanin effects

PRI was originally developed by Gamon *et al*. (1992) to estimate rapid changes in the relative levels of xanthophyll cycle pigments that are related to changes in photosynthetic light use efficiency (Gamon *et al*. 1993, 1997; Peñuelas *et al*. 1995a). However, the green region of the spectrum is potentially affected by chlorophyll and anthocyanin pigments as well. This relationship becomes more complicated if pigments other than carotenoids influence PRI. For example, chlorophyll absorption affects the 531 nm band, as well as 551 and 667 nm (Drolet *et al*. 2005).

Sims and Gamon (2002) suggest that interpretation of PRI changes across a range of species likely depends on the time scale of the measurements. Xanthophyll cycle interconversions can occur within minutes, while changes in total carotenoid and chlorophyll contents tend to occur over periods of days to weeks. Consequently, PRI variation over the diurnal cycle might mainly reflect xanthophyll cycle events, while changes over weeks or months may incorporate both xanthophyll cycle changes as well as total pools of carotenoids and chlorophylls.

This could explain why earlier work by Gamon *et al*. (2001) found good correlation between diurnal changes in PRI and xanthophyll cycle epoxidation state for young leaves with high chlorophyll, but weaker relationships when older senescing leaves were included. Nakaji *et al*. (2005) found the sensitivity of PRI to LUE was affected by needle senescence at the end of the season in larch (*Larix kaempferi*), whereas PRI was fairly well-correlated to xanthophyll epoxidation state and LUE in needles earlier in the growing season.

Sims and Gamon (2002) suggest that when sampled across space, PRI may indicate either variation in xanthophyll cycle pigments among plants with different LUE or variation in chlorophyll:carotenoid ratios that have resulted from longer term acclimation to the local environment. They conclude that PRI changes can be a measure of photosynthetic LUE during senescence or stress to the degree that LUE is correlated with carotenoid:chlorophyll ratio.

Anthocyanins can affect various segments of the reflectance spectrum. They have two major absorption peaks in the UV and green regions, typically located in the 270-280 and 510-540 nm regions. They have also been shown to produce a shift in the red edge toward longer wavelengths (Curran *et al*. 1991), but not always (Sims and Gamon 2002).

Anthocyanins have not been considered in traditional equations for measurement of chlorophyll and carotenoids in leaves or extracts (Sims and Gamon 1999). These pigments (typically pink, purple, red) are a diverse group of substances whose roles, while not fully understood, may include ultraviolet-light screening in leaves, scavenging of toxic oxygen radicals, antifungal actions, deterring leaf herbivory, and attracting pollinators and seed dispersers (Sims and Gamon 1999, 2002). They tend to increase in leaves with low photosynthetic rates, either because they are young or are under stress.

Gitelson *et al*. (2001) reported on the anthocyanin spectral features of maple (*Acer platanoides*), cotoneaster (*Cotoneaster alaunica*), dogwood (*Cornus alba*) and pelargonium (*Pelargonium zonale*) leaves with a wide range of pigment content and composition. Comparing absorption spectra of anthocyanin-containing and anthocyanin-free leaves with the same chlorophyll content, absorption spectra of anthocyanin in leaves indicated the main spectral feature of anthocyanin absorption in vivo was a peak around 550 nm.

Drabent *et al*. (1999) reported on the fluorescence behaviour of anthocyanin pigments in *Brassica oleracea* (red cabbage) extracts. They found three fluorescence peaks at 363, 434, and 519 nm. Thus, anthocyanins might affect spectral reflectance results through their absorption and/or fluorescence actions, and they should be taken into consideration in interpreting the results from susceptible indices.

3.3.3.4. Species effects

With respect to interspecific trends, Guo and Trotter's (2004) findings diverged from the work of Gamon's group and suggest that determination of light response functions for PRI in relation to photosynthetic parameters reveals species-specific relationships were stronger than for grouped species (e.g., r^2>90 for species-level PRI / LUE relationships versus r^2=0.58 when grouped). Further, their work showed that PRI was most distinctly correlated with the ratio of carotenoids to chlorophyll content.

Nakaji *et al*. (2007b) elucidated species aspects in their study of monospecific or mixed forests of deciduous conifer and evergreen canopies. In each forest canopy, they calculated seasonal variations in LUE (GPP divided by the difference between incoming and reflected PAR) and found that while PRI was an effective remote estimator of LUE in both deciduous and evergreen forests, sensitivity differed between vegetation types, notably with PRI:LUE relationship weakening in the deciduous conifer (larch) as a result of late-season needle yellowing. An earlier study by Nichol *et al*. (2000) of four boreal forest species found deciduous species exhibited weaker PRI:LUE correlation than did conifers. And Garrity *et al*. (2006) showed that using a combination of scaled PRI and NDVI, daily summed CO_2 fluxes varied with species, with r^2 ranging from 0.69 for birch (*Betula papyrifera*) dominated pixels to 0.45 for those dominated by red pine (*Pinus resinosa*).

3.3.3.5. Complexity of the PRI signal

Gamon *et al*. (1997) supported the use of PRI as an interspecific index of photosynthetic radiation use efficiency for leaves and canopies in full sun (or moderate light intensity, <500 µmol m^{-2} s^{-1}) but not from a wide range of illumination from deep shade to full sun, and not yet for ecosystems-scale work (Inoue *et al*. 2008). Gamon's team found that the 531 nm signal of PRI is actually composed of two spectral components: at low irradiance (e.g., < 100 µmol m^{-2} s^{-1}), the signal is dominated by a 545-nm component which was not closely related to radiation use efficiency, while at progressively higher light levels the 531-nm signal was increasingly dominated by a 526-nm component which was correlated with light use efficiency and with xanthophyll cycle conversions.

3.3.3.6. Spatial and structural aspects

The strength of the PRI correlation to LUE (obtained from eddy covariance flux towers) depends on spatial scale, canopy structural heterogeneity, shadow fraction, sun/sensor geometry, and atmospheric effects.

At small to medium spatial scales (1 to 10 m^2), PRI may be strongly correlated to LUE of well-watered canopies in full sun, across different species and site fertilities; however, at larger spatial scales (100 to 1000 m^2), the relationship may not be as clear (Drolet *et al*. 2005, 2006). For example, several factors appeared to confound the MODIS-sPRI signal at 531 nm, using spatial resolution of a MODIS pixel (1 km^2), despite the relative homogeneity of the boreal deciduous forest studied. And it was suggested by Rahman *et al*. (2003) that, for southern California chaparral and grassland, an optimum pixel size of 6 m or less would permit study of functional properties.

Raddi *et al*. (2005) noted that PRI appeared to be strongly affected by soil reflectance, requiring either correction or use of tilted images. Their work involved ground-based measurements and remote imagery from CHRIS Proba of vegetation types that included crops, herbs, shrubs, deciduous broadleaves, evergreen schlerophylls, and conifers. PRI calculated at leaf level and PRI actually calculated from CHRIS imagery were correlated with a maximum r^2 of 0.57, whereas a preliminary mathematical degradation of the leaf-based PRI to CHRIS band specs indicated an almost perfect 1:1 relationship was possible. In their work with chapparal, Sims *et al*. (2006) also emphasized that, while PRI as a correlate to LUE could potentially be useful in ecosystem evaluation, there would need to be much greater consideration of canopy structure and background effects on stand PRI. Soil and understory reflectance are problems on relatively open sites. Nichol *et al*. (2002) showed that spectral

signals from open boreal forest sites contain significant contributions from lichens, mosses, and other understory vegetation.

Barton and North (2001) found that PRI showed greater variation according to sensor view angle than most vegetation indices. The index is strongly influenced by varying soil background for LAI<3. At large viewing angles (>30°) PRI is also sensitive to leaf angle distributions. Correction for Rayleigh scattering is necessary to relate the index to ground measured PRI. Therefore, application of the index to estimate canopy LUE based on either absorbed or incident light will necessitate independent estimation of canopy LAI differences between dates/locations of in situ measurements and of remote sensing observations.

3.3.3.7. Use of PSII efficiency in PRI:LUE studies

Another factor that can complicate efforts to link PRI and LUE arises from using the effective quantum yield of Photosystem II (i.e., measured under light-adapted conditions) as a surrogate for photosynthetic efficiency. It is well-known that $\Delta F/Fm'$ can diverge from CO_2 uptake, such as in the presence of photorespiration during which electron transport through PSII is diverted to oxygen metabolism instead of sugar synthesis. This is a particular concern among plant species with a tendency toward high rates of photorespiration in the light, notably the C3 species. Since photochemical efficiency is not equivalent to actual photosynthetic LUE, it can be very misleading to consider this feature in evaluating PRI or any other feature that may be related to LUE, despite the view of Cavender-Barea and Bazzaz (2004) that $\Delta F/Fm'$ (which they suggest is the average efficiency with which absorbed radiation is converted to biomass) would be the ideal parameter to estimate ε.

Other factors which can cause PSII efficiency to diverge from CO_2 uptake include the Mehler reaction, and nitrate reduction which, like photorespiration, can compete with carboxylation for reductant generated by photosynthetic electron transport (Peñuelas *et al*. 1997, and references therein). Peñuelas *et al*. (1995b) also noted that PRI and $\Delta F/Fm'$ can exhibit slightly different kinetics upon light transitions, with PRI lagging. They suggested there might be multiple processes with separate time constants affecting reflectance and fluorescence to different degrees. And Guo and Trotter (2006), in their study of thirteen species, found that under elevated CO_2, LUE was considerably enhanced without significantly affecting either $\Delta F/Fm'$ or PRI. They emphasized that PRI is correlated with LUE only insofar as that is coordinated adjustment between PSII photochemical efficiency and the CO_2 fixation rate.

3.3.3.8. Use of absorbed or incident PAR in LUE calculation

Given the wide range of definitions of LUE, it is important to consider potential errors and inconsistencies that arise as a consequence. Sims *et al*. (2006) contains a reminder that the LUE model of (Monteith 1972) states that carbon exchange is a function of the amount of light energy absorbed by vegetation and the efficiency with which that light energy is used to fix carbon. In their study of the chapparal ecosytem, in which they used absorbed PAR for LUE determination, they note that other studies have found correlations between PRI and LUE at the ecosystem scale (Nichol *et al*. 2000, 2002; Rahman *et al*. 2001; Strachan *et al*. 2002), but those studies did not calculate LUE the same way as in Sims' study. Nichol *et al*. used incident PAR, and when Sims recalculated Nichol's data using absorbed PAR there was no relationship. Sims suggests that empirical relationships may be drawn for a given site and set of environmental conditions, but the mechanistic basis for generalization of these relationships across vegetation types and various environmental conditions is still unclear and complicated by diverse physiological and structural factors.

3.3.4. Recommendations

Approaches that may improve the strength of relationships between reflectance and photosynthetic or light-use efficiency are summarized in Table 3-8.

Table 3-8. Summary of approaches for improving reflectance relationships to photosynthetic or light-use efficiency.

Approach	Rationale	Reference
Canopy structural characterization, e.g., through use of LiDAR, directional (tilted, multi-angular) remote measurements rather than nadir.	Minimizes effects on reflectance from understory & soil. Allows discernment of physiological vs. structural effects on BRDF.	Cheng *et al.* (2007), Drolet *et al.* (2006), Hilker *et al.* (2008), Inoue *et al.* (2008)
Assessment of chlorophyll (or other pigment) content.	Reduces likelihood of e.g., low chlorophyll or other pigment content confounding PRI interpretation.	Nakaji *et al.* (2005)
Index improvements.	Better correlation to LUE / photosynthesis.	Rahman *et al.* (2000), Zhao *et al.* (2004), Garrity *et al.* (2006), Mitsunori *et al.* (2006), Nakaji *et al.* (2007a), Inoue *et al.* (2008)
Standardization of LUE definition.	Addresses inconsistencies in findings among studies regarding spectral relationships to LUE.	Sims *et al.* (2006), Grace *et al.* (2007)
Inclusion of ground-based or other supporting measurements.	Provides actual LUE and CO_2 assimilation, species composition, etc.	Garrity *et al.* (2006), Grace *et al.* (2007)

3.3.4.1. Improvement of structural characterization

It is increasingly recognized that canopy-scale work benefits from the use of directional or multi-angular reflectance measurements. For example, Inoue *et al.* (2008 and references therein), in their work with rice, suggest that such measurements provide more accurate or extra information on vegetation canopies, possibly including physiological information on photosynthetic efficiency. Multi-angular measurements allow vegetation reflectance signals to be resolved from the superfluous contributions of soil and understory, and may be especially powerful in open-canopy settings.

Hilker *et al.* (2008) make a good case that multiple angles help to reveal those effects on BRDF that are due to physiological rather than structural factors. They examined PRI correlation with LUE in an evergreen conifer forest, and found that by stratifying PRI observations into categories based on environmental conditions for which the expected physiological variability was low, it was possible to separate bidirectional effects arising purely from physiological status from other effects. Their method produced an impressive improvement in the correlation between PRI and ε (r^2=0.82, vs. 0.38 for unstratified results). Isotropic PRI scattering was highly related to changes in ε, while geometric scattering was associated with canopy-level shading.

Cheng *et al.* (2007), studying the boreal forest, used Light Detection and Ranging (LiDAR) technology to calculate sunlit and shaded canopy fractions as a function of incoming PAR. These automated directional observations allowed them to: 1) investigate diurnal and seasonal changes of PRI under different sky conditions; 2) compare PRI with tower-based micro-meteorological measurements; and 3) separately investigate PRI dynamics for sunlit and shaded partitions of the canopy which differed in response to their light environments. PRI was clearly correlated with the LiDAR-based shadow fraction estimates, and correlation between PRI and LUE was confirmed.

An improved capacity to assess PRI:LUE relationships was presented by Drolet *et al*. (2006) by classifying MODIS pixels according to their respective shadow fraction. Their modelling analyses had suggested that canopy shadow fraction could partially explain problems they have had in observing the MODIS-PRI:$LUE_{(gross)}$ over boreal stands. Using a radiative transfer model to classify the pixels, they were able to analyze relationships inside these shadow classes for boreal forest stands of different ages and origins. Shadow fraction is one factor that affects the ability to observe the relationship from space – others being sun/sensor geometry, atmospheric effects, and canopy structural heterogeneity.

3.3.4.2. Assessment of chlorophyll and other pigments

The influences of chlorophyll and other pigments (carotenoids, anthocyanins) on PRI have been discussed earlier. As discussed above, the sensitivity of PRI to LUE is affected by factors such as needle aging (Nakaji *et al*. 2005) and drought (Sun *et al*. 2008) which alter contents of chlorophyll. Anthocyanin contributions to the PRI spectral regions can also be a complicating factor, especially in young or stress foliage of some species. Measures of such pigments would be helpful to support interpretations of spectral reflectance signals.

3.3.4.3. Index improvements

PRI relationships to ε might be improved by considering alternative formats to the index or by simple scaling or by combining it with other indices. For example, Rahman *et al*. (2001) were able to improve estimation of gross CO_2 fluxes at the landscape scale using AVIRIS-acquired PRI and NDVI, by using their scaled version of PRI, however, the success of this empirically-based approach may be limited by species as shown by Garrity *et al*. (2006).

Nakaji *et al*. (2007a) combined PRI with the Enhanced Vegetation Index (EVI) (a modified NDVI which adjusts for canopy background and atmospheric influences—Liu and Huete 1995), in their study of a mature Japanese larch forest (*Laris kaempferi*), and found the combined index produced an improvement in the accuracy of estimation of CO_2 uptake under both clear sky and cloudy conditions. Their combined index was EVI/(PRI/PRI_{min}), based on a 6-day moving minimum value of PRI (PRI_{min}), and showed a linear relationship with half-hourly values of ε throughout the seasons. However, they note that there are still various issues to resolve. PRI information can also be complemented with that from NDVI (for assessment of plant biomass), and the Water Band Index (WBI=R970/R900) for estimation of plant water conent (Rahman *et al*. 2003).

Redefining the PRI reference band (normally R570) has been shown to improve its performance in some cases. For example, R550 was reported to produce a stronger estimation of photosynthetic efficiency in canopies of rice, which is a drought-prone system (Inoue *et al*. 2008). They used three expressions of radiation use efficiency: net ecosystem exchange of CO2/APAR; gross primary productivity/APAR; and quantum efficiency=initial slope of curve of GPP vs. APAR.

Zhao *et al*. (2004), in their canopy study of wheat, considered several spectral indices for their estimation of biophysical variables such as LAI, leaf chlorophyll concentrations, and dry phytomass under various levels of nitrogen fertilization. They used the wavelength of peak reflectance in the green band, R554, as a new reference band for PRI, and found that the redefined PRI (PRI-re) appeared to be the most sensitive indicator for N availability. Wheat canopies of low N availability were characterized by low 'PRI-re' values, and those with excess N fertilization had medium values.

The results from Inoue's work (above) on rice also suggested that several new spectral indices were more effective than conventional ones such as PRI and NDVI. For example, GPP/APAR was well correlated with certain normalized difference spectral indices, NDSI[using 710,410 nm], and [710, 520 nm] derived from nadir measurements. Quantum efficiency was best correlated with NDSI[450, 1330

nm]. Off-nadir measurements were more closely related to the efficiency parameters than nadir measurements.

Other indices which are able to contribute information relevant to photosynthetic performance include:

- The Structure-Independent Pigment Index, which is indicative of carotenoid:chlorophyll ratio and LUE, and is expressed as SIPI=(R800-R445)/(R800-R680) (Richardson *et al*. 2001, Huemmrich *et al*. 2006);
- The spectral first derivatives at 460, 550, and 615 nm; and the second derivatives at 510 and 620 nm, which are correlated with LUE (Huemmrich *et al*. 2006);
- Differences in reciprocal reflectances using two spectral channels either in the green around 550 nm or in the red edge near 700 nm, and the NIR (beyond 750 nm), which have been found to account for over 90 percent of the variability in midday canopy photosynthesis of irrigated maize (Gitelson *et al*. 2003).

3.3.4.4. Standardize LUE definition

Grace *et al*. (2007) correctly identified the lack of consistency among LUE definitions in the literature as a stumbling block to progress in correlating LUE to PRI or other spectral features. Sims *et al*. (2006) showed how using incident versus absorbed PAR can alter the conclusions of studies. As to what is the best measure of actual LUE, it can be argued that it should depend on the purpose of the work for which the LUE factor is required, and thus a single definition is not desirable. For instance, representing LUE (or ε) as mol CO_2 captured per mol photons incident (or absorbed) light, or on the basis of $\Delta F/Fm'$, would not be ideal if the goal is to quantify carbon sequestration into actual biomass as a long-term carbon sink, as those parameters generally indicate potential rather than actual sequestration into biomass. Or, if the goal is to quantify actual rates of photosynthesis, using PSII efficiency ($\Delta F/Fm'$) as a measure of LUE is likely inappropriate if the products of photochemistry are often diverted to ends other than CO_2 conversion to sugar, e.g., as with C3 species with high rates of photorespiration. So in any evaluation of spectral indices such as PRI for suitability as surrogates to LUE, the rationale for the standard must be clearly stated within the context of the ultimate goal.

3.3.4.5. Need for ground-based measurements

Remote measurement of PRI or other photosynthetically meaningful indices requires a solid foundation of ground-truthing, given that estimation of photosynthetic features is still essentially a semi-empirical exercise. Acquisitions of actual LUE or CO_2 assimiliation from flux towers, and complementary data from airborne sensors important to an integrated program of photosynthetic evaluation (Hilker *et al*. 2007, Drolet *et al*. 2006). Given findings such as those of Garrity *et al*. (2006) and Nichol *et al*. (2000) that relationships between special features and photosynthetic features vary by species, it is also necessary to know the species composition, LAI, etc. within RS imagery pixels.

Grace *et al*. (2007) suggest that development of a system to integrate remote sensing and flux data into an observational system will require seven conditions:

1. Standardization of spectral definition and measurement protocol of PRI.
2. Installation of PRI sensors on flux towers to continuously monitor relationship between PRI and carbon flux.
3. Refinement of atmospheric corrections to remove influence of aerosols on PRI or NDVI acquisition.
4. Parameterization of vegetation structure of canopy.
5. Selection of one or more appropriate global ecosystem models.

6. Development of data transmission to enable communication of remote sensing and flux data.
7. Development of data assimilation methods so models are capable of learning from observations (model training).

4. ANALYSIS OF FLUORESCENCE SPECTRA AND RATIOS

It is now largely accepted that the chlorophyll (Chl) fluorescence (F) spectrum receives contributions from both PSII and PSI photosystems even at physiological temperatures. Yet, the contribution of PSI is mainly at the longer wavelength emission band, F735, while PSII contributes to both Chl F emission bands.

By time-resolved fluorescence spectroscopy, it has been determined that the PSII/PSI F ratio at 735 nm in the steady state condition at room temperature is of the order of 1.5 (Agati *et al.* 2000).

In the leaf, the shorter wavelength Chl F is strongly reduced by reabsorption, so that the Chl F ratio (FR), that is of the order of 5 in isolated PSII particles, can easily reach values around 1 and even below. In these condition, the contribution of PSI at 735 nm compared to the PSII F at 685 nm is quite significant.

4.1. Factors affecting Chl fluorescence ratio

Photochemical quenching (qP), the energy state quenching (qE) and the photoinhibition quenching (qI) all affect Chl F coming from PSII, while PSI F seems to be less sensitive (or insensitive at all) to these process. Therefore, any change occurring on the above parameters should be reflected in a change of the Chl FR.

Furthermore, the third component of the non-photochemical quenching (NPQ), the state transition quenching (qT) induces a redistribution of the excitation energy from PSII to PSI, leading to a decrease and a linked increase of PSII and PSI fluorescence, respectively. State transition quenching should then be inversely related to the Chl FR.

Other important factors which determine the shape of the Chl F spectrum, and then the Chl FR, are the Chl concentration and the leaf optical properties (scattering) and the excitation wavelength.

Increasing Chl concentration and the scattering inside the leaves produces a higher reabsorption of the F685 band. The excitation wavelength effect is also related to the reabsorption process, since most penetrating light will reach deeper leaf layers and the F re-emitted from these will be more reabsorbed with respect to F from the superficial layers.

Furthermore, using UV or blue-light excitation it must be considered that F in the blue-green spectral range from other leaf compounds, such as polyphenols, can be excited. The tail of this fluorescence extending to Chl F region can be not negligible and can affect differently the two Chl F bands, inducing a change in the Chl FR.

Under natural condition, the change in photochemical and non-photochemical quenching as function of different environmental factors will drive changes in the Chl FR, under both normal or stress conditions. The time scale of these changes is expected to be quite large (seconds to days) so that different information can be obtained according to time sampling. For example, during periods in which the Chl content and scattering leaf properties can be considered constant, Chl FR changes are related to the photosynthetic activity. On the contrary, when significant changes in the Chl concentration occur the change in Chl FR will be mainly due to changes in the reabsorption process at the 685 nm peak. By correcting the fluorescence signals for the reabsorption effect, using a suitable correction model, information on the photosynthetic activity can still be obtained.

The effect of single factors, such as temperature and light intensity, and their combination on the Chl FR, should be evaluated in order to predict possible time windows in a daily course in which information on photosynthesis can be found in the Chl FR variation.

4.2. Effect of temperature on the ChlF spectrum

The effect of temperature on the ChlF spectrum was already considered in the past (Agati 1998). In that paper, an inverse linear relationship between both the ChlF maxima, F685 and F730, and leaf temperature (in the 0-25 °C range) was characterized, giving slopes and intercepts for 5 different plant species (broad bean, bean, pea, tomato and ficus). In the FluorMODleaf model, the dependence of F for all the other wavelengths was extrapolated assuming a linear temperature dependence of the whole spectrum. This assumption was verified to be not properly true by analysing available fluorescence spectra as function of leaf temperature (an example of these data was previously published for the bean species; Agati 1998).

We reanalysed all the available data to derive a most accurate dependence of the whole ChlF spectrum from leaf temperature (T). Some of the Chl fluorescence spectra available at different leaf T are reported in Figure 4-1. It can be seen that the fluorescence intensity above all the spectral range increases as leaf T increase, but there is also a change in the spectral shape.

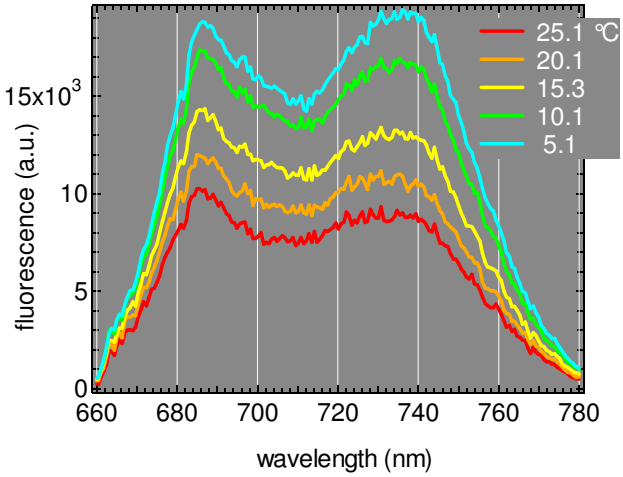

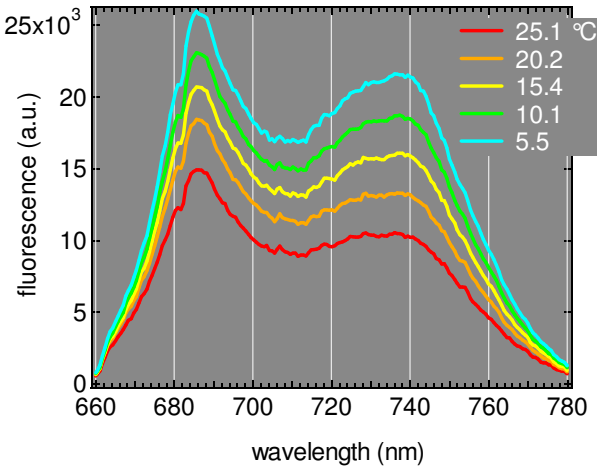

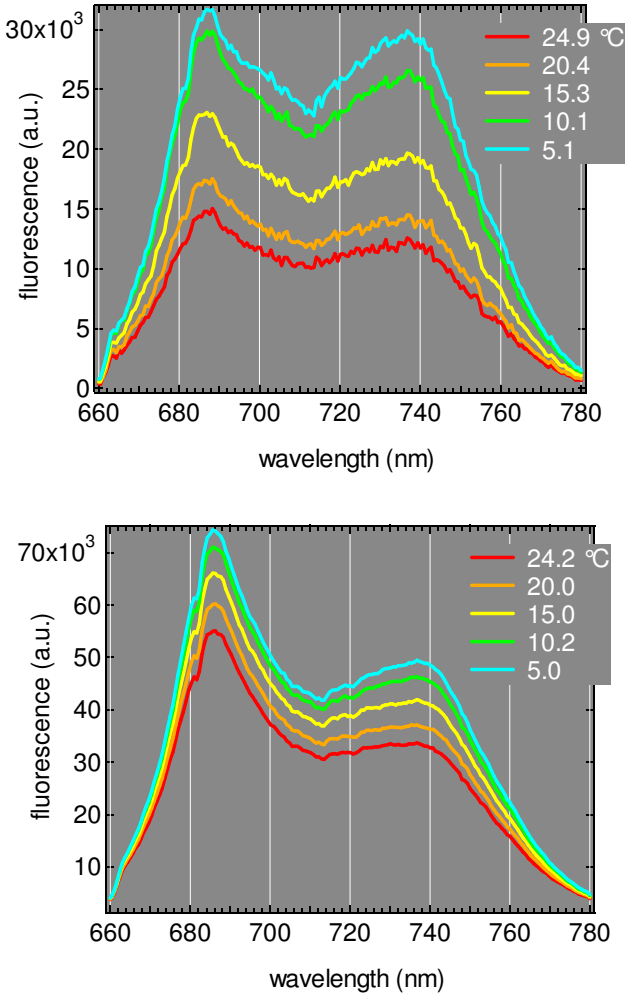

Figure 4-1. Changes in the fluorescence spectra of bean, broad bean, pea and tomato leaves (from top left, clockwise) in response to temperature changes.

Chlorophyll fluorescence was excited at 635 nm by a diode laser (LDA2035-P2, ILEE, Urdorf, Switzerland) focused on a 1 mm^2 spot. One leaf, attached to the plant, was kept in contact with a copper plate coupled with a thermoelectric Peltier module used as temperature control. The laser beam directly irradiated the leaf and the fluorescence was collected by a 1 mm fused silica optical fibre at about 45° with respect to the laser beam. The other end of the fibre was coupled, by two suitable lenses, to the entrance slit of a spectrometer (Jobin Yvon) attached to a 1024-channel intensified diode array detector (EG&G PAR model 1421) and acquired by an optical multi-channel analyser (OMA) system (EG&G PAR OMA III model 1460). The OMA system was calibrated in wavelength in the 620-800 nm spectral region with a neon spectral lamp. The acquired fluorescence spectra were radiometrically corrected for the detector response as a function of wavelength by using a National Institute of Standards and Technology traceable calibrated tungsten lamp.

The temperature effect on the Chl fluorescence spectrum was studied switching on the Peltier system, set at 0 °C, in order to cool rapidly the leaf from room temperature to the copper plate temperature within about 3 min. The leaf was kept under low white light intensity at a photosynthetic photon flux density (PPFD) of 150 $\mu mol \cdot m^{-2} \cdot s^{-1}$. provided by an 8 mm optical fibre bundle of a halogen lamp illuminator (Schott KL1500). The laser beam was attenuated to 30 µW by a neutral density filter to obtain an intensity comparable to that of the white light lamp, so that total PPFD during the

measurement was about 300 μmol·m^{-2}·s^{-1}. Leaf temperature was monitored continuously by a portable infrared thermometer (Land Cyclops Compac 3, Minolta) that integrates on a 35 mm diameter spot at the distance of 1 m.

Results from the study described above are presented in Figure 4-1. . A shift in fluorescence spectra was commonly observed in all four species. In particular, the F685/F740 fluorescence ratio increased with temperature, suggesting a variable role of PSI and PSII fluorescence at different temperatures.

The studies described above refer to controlled experiments in which the leaf T was changed at constant moderate light intensity (about 200-300 μmol·m^{-2}·s^{-1}). Under natural condition, this is not the case since solar irradiance largely changes during the day. Therefore, in order to have an appropriate interpretation of the fluorescence signals measured in the field, by both active and passive (SIF) methods, further studies should be dedicated to evaluate the combined effects of T and light intensity on Chl F.

Yet, no Chl F spectra at leaf T in the 25-45 °C range, that is above the optimal T for photosynthesis seems to be not available. However, some preliminary indications can be obtained from the literature and from results of the recent CEFLES2 campaign.

Dobrowsky *et al.* (2005) reported daily cycles of the steady state fluorescence, Fs, on Vitis vinifera leaves along with photosynthetic parameters (CO2 assimilation, A, and stomatal conductance, g) and photochemical quantum yield as the growth chamber T was changed at a constant light irradiance of 700μmol-1 m-2 s-1. They found that Fs was decreasing early in each day as T was increasing from 23 to about 30 °C and Qp was also increasing. Later on, Fs decreased more rapidly, but also Qp was decreasing (as well as A and g), suggesting the occurrence of significant non-photochemical quenching.

During the CEFLES2 campaign we measured time courses of Chl F spectra on a corn canopy (1 m2), from nadir, using a FLIDAR system with laser excitation at 532 nm. The average canopy temperature was measured at the same time by an infrared thermometer. A large gradient of canopy T from about 15 to 30 °C was found to occur from 9:00 a.m. to around 2:00 p.m. Simultanously the solar irradiance was increasing from 490 to 1500 μmol-1 m-2 s-1. In Figure 4-2. , the Chl FR, calculated as the ratio between the average intensity at the 685 and 740 nm bands, is plotted versus the average corn canopy T measured from about 10:00 to 15:00, local time, on the 15th September 2007.

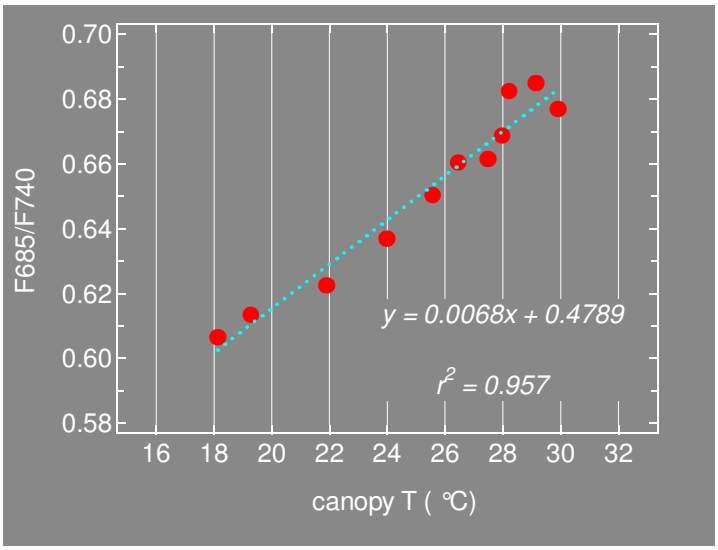

Figure 4-2. Chl FR versus T of a corn canopy monitored from 10:00 to 15:00 local time.

This behaviour is consistent with the observations obtained in the laboratory under constant moderate light intensity on other plant species (see above). Our evidence, as well as those suggested by the Dobrowsky *et al.* (2005) paper, indicates that until about 30 °C, and under a gradual increase of PPFD up to 1500 μmol^{-1} m^{-2} s^{-1}, Chl F is governed by the redox state of plastoquinones (Qp) and energy redistribution between PSII and PSI; the energy state component (qE) of NPQ seems to have a minor role. In fact, since qE operates on PSII only, an increase of qE in relation with the increase of PPFD during the first hours of the day would induce a decrease of PSII F and then of the Chl FR. On the contrary, we observed an opposite trend with day time.

The behaviour of Chl F with T higher than 25-30 °C is less studied, even if this condition can be quite common under high solar irradiance when leaf temperature can increase several degrees Centigrade above air temperature and photosynthesis becomes increasingly inhibited. Photosystem II has been identified as one of the most thermolabile components of the photosynthetic electron transport chain (Srivastava *et al.* 1997), whereas PSI has been demonstrated to be comparatively heat resistant (Havaux *et al.* 1991b; Havaux 1996).

The decrease in Fs at T higher than 35 °C was consistent with a large increase in NPQ, while the decrease from 25 to 35 °C is not accompanied by a corresponding change in both qP and NPQ.

Measurements of F_0 and F_0' suggested that the thylakoid membranes of the oak leaves were not significantly damaged by the heat-stress applied. The Fv/Fm ratio was slightly affected (6%) showing that PSII was rather well protected against thermal damage and/or heat-dependent photoinhibition.

Similar trends with T for NPQ were observed in a tropical rain forest species with values increasing above an optimal temperature around 30 °C. Qp was also observed to increase linearly with rising T from 23 to 43 °C (Leakey *et al.* 2003). On the other hand, in other dipterocarp trees Qp decreased above 35 °C at a PPFD of 180 μmol^{-1} m^{-2} s^{-1} and photoinhibition at high PPFD (1600 μmol^{-1} m^{-2} s^{-1}) was exacerbated by high temperatures (Kitao *et al.* 2000).

All these evidences suggest that a decrease in the Chl FR should be observed above 30-35 °C. Although several experimental data are needed to widely confirm this expectation, it is worth reporting that a decrease in the Chl FR was indeed observed in a continuous daily cycle monitoring of the two Chl F bands under high light and high T conditions in the field (Agati *et al.* 1995).

4.3. Using FR for the deconvolution of PSII fluorescence

A novel algorithm is proposed for the analysis of leaf temperature effects on the chlorophyll fluorescence spectrum, and for the deconvolution of the contribution from PSI and PSII to the overall fluorescence spectrum. Instead of using literature fluorescence spectra of isolated PSII and PSI photosystems to fit the leaf total fluorescence spectrum, a new method was applied to resolve the two spectral contributions. It is based on the measurements of the chlorophyll (Chl) fluorescence (F) spectra during the rising phase of the Kautsky kinetics occurring when dark-adapted leaves are exposed to light.

One important advantage of this method is that it provides the real PSII and PSI spectral contributions of the leaf under investigation, taking directly into account the effect of reabsorption, due to Chl concentration and leaf structure (Lichtenthaler *et al.* 1988), and the PS stoichiometry, depending on the growing light conditions (Pedros *et al.* 2008).

4.3.1. Description of the algorithm

Measured leaf Chl fluorescence as a function of time and wavelength can be expressed as the sum of PSs fluorescence contributions:

$$F(t,\lambda) = h(t) \cdot PSI(\lambda) + g(t) \cdot PSII(\lambda) \qquad \text{(Eq. 4-1)}$$

Where *PSI*(λ) and *PSII*(λ) are the spectral shapes of PSs fluorescence at the leaf level, that is reabsorbed by Chl, and $h(t)$ and $g(t)$ are the intensities of PSs fluorescence at time t.

It is widely accepted that PSI shows little changes in fluorescence as function of the redox state of electron acceptors (Dau 1994). Therefore, during the initial rise of the dark-light fluorescence kinetics PSI contribution can be assumed constant and variation of $F(t, \lambda)$ during the transient is only due to the PSII contribution. With this assumption the fluorescence is

$$F(t,\lambda) = h_c \cdot PSI(\lambda) + g(t) \cdot PSII(\lambda) \qquad \text{(Eq. 4-2)}$$

where h_c is the PSI intensity during the initial rise of the kinetics. With this assumption, *PSII*(λ) can be determined through Principal Component Analysis (PCA) as detailed below.

Measuring the fluorescence time series of the rising phase of the Kautsky kinetics with a number of M spectral channels and N time samples, it is possible to define **F** as a $N \times M$ dimensional fluorescence data matrix where the element $\mathbf{F}_{nm} = F(t_n, \lambda_m)$ is the measured fluorescence at time t_n and at wavelength λ_m. Each measured spectrum can be considered as a point in a M-D space and the N spectra dataset as a N-points cloud in this space. The PCA method, through the analysis of the covariance data matrix obtained from **F,** permits to find a new and particular orthonormal axis system centred in the mean of data-set. We can then write:

$$\mathbf{F} = \mathbf{F}_{\text{mean}} + \mathbf{S} \circ \mathbf{PC} \qquad \text{(Eq. 4-3)}$$

where, indicating the matrix product with the symbol "$\circ$", $\mathbf{F}_{\text{mean}}$ is a $N \times M$ matrix in which each row is the vector $\vec{\mathrm{F}}_{\text{mean}}(\lambda_{1\ldots M})$ of the mean over the time of measured spectra, **PC** is the matrix of the principal components (i.e. the directions of the new axis in the original space) and **S** is the score matrix (i.e. the projection of data on the new axis).

The particularity of the PCA method is that the first principal component, PC_1, the first axes of the new system, is the linear combination of original variables with maximum data variance (i.e. the direction in the original space along which data variance is maximum). The second principal component, PC_2, is the linear combination with maximal residual variance in a orthogonal direction with respect of the PC_1, and so on.

From (3), if most of data variance is described by PC_1 (the portions of data variance described by each principal component are achievable through the method itself) we can approximate:

$$\mathbf{F} \approx \vec{\mathrm{F}}_{\text{mean}}(\lambda_{1\ldots M}) + \vec{\mathrm{S}}_1(t_{1\ldots N}) \circ \overrightarrow{\mathrm{PC}}_1(\lambda_{1\ldots M}) \qquad \text{(Eq. 4-4)}$$

where $\vec{\mathrm{S}}_1(t_{1\ldots N})$ is the first score column vector and $\overrightarrow{\mathrm{PC}}_1(\lambda_{1\ldots M})$ is the first principal component row vector.

From equation (2), that is within the hypothesis that the only variation in the fluorescence spectra during the initial rise of the dark-light fluorescence kinetics is due to a change in $g(t)$, we can obtain the mean fluorescence spectrum $\overline{F(\lambda)}$ as

$$\overline{F(\lambda)} = h_c \cdot PSI(\lambda) + \overline{g(t)} \cdot PSII(\lambda) \qquad \text{(Eq. 4-5)}$$

where $\overline{g(t)}$ is the mean value of $g(t)$ during the transient.

Using the (5), equation (2) can be written as:

$$F(\lambda,t) = \overline{F(\lambda)} + \left(g(t) - \overline{g(t)}\right) \cdot PSII(\lambda) \qquad \text{(Eq. 4-6)}$$

Comparing (6) and (4) results that under this hypothesis $\mathrm{PC}_1(\lambda_{1\ldots M})$ is the best approximation of $PSII(\lambda)$ at the wavelength $\lambda_{1\ldots M}$, thus being the best approximation of its shape. $\vec{\mathrm{S}}_1(t_{1\ldots N})$ represents the variation of $g(t)$ among $\overline{g(t)}$ at the times $t_{1\ldots N}$.

To obtain an estimation of $PSI(\lambda_{1\ldots M})$ through an estimation of the shape of $PSII(\lambda_{1\ldots M})$ but without further hypothesis on the time behaviour of $g(t)$, we consider the evidences that: i) the fluorescence of isolated PSI contributes mainly at about 735 nm (Croce *et al.* 1996); ii) in the leaf, PSI fluorescence at about 685 nm is strongly reabsorbed. Thus, the PSI contribution in the 685 nm band is minimum.

From equation (5) and using $\mathrm{PC}_1(\lambda_{1\ldots M})$ as the best approximation of the shape of $PSII(\lambda_{1\ldots M})$ is possible to write:

$$h_c \cdot PSI(\lambda_{1\ldots M}) = \vec{\mathrm{F}}_{\mathrm{mean}}(\lambda_{1\ldots M}) - k \cdot \mathrm{PC}_1(\lambda_{1\ldots M}) \qquad \text{(Eq. 4-7)}$$

where the value of the coefficient k is unknown.

The *PSI* spectral shape can be obtained finding the value of k so that the contribution of $h_c \cdot PSI(\lambda_{1\ldots M})$ at 685 nm is minimum and with the physical constraint that it is greater or equal to zero for each wavelength.

With this method it is therefore possible to achieve not only the shape but also the intensity of $PSI(\lambda_{1\ldots M})$ during the initial rise of the dark-light fluorescence kinetics.

For a generic measured fluorescence spectrum $\mathrm{F}(\lambda_{1\ldots M})$, with the hypothesis that the shapes of PSs are the same of the retrieved ones, we can write:

$$\mathrm{F}(\lambda_{1\ldots M}) = h \cdot PSI(\lambda_{1\ldots M}) + g \cdot PSII(\lambda_{1\ldots M}) \qquad \text{(Eq. 4-8)}$$

and retrieve the values of the h and g coefficients by applying a least squares fitting (LSF).

4.3.2. Results of the analysis

4.3.2.1. Application to a simulated data set

The algorithm for the spectral resolution of PSI and PSII fluorescence components was at first tested on a simulated data set. PSI F spectrum was generated using a Gaussian curve centred at 730 nm (FWHM = 45 nm), while the PSII F spectrum was the convolution of two Gaussian curves peaked at 685 (FWHM = 35 nm) and 735 nm (FWHM=56 nm), with a 685/735 peak ratio of 0.75. Figure 4-3a shows the two simulated spectra normalized to their area. We then used a temporal variation for PSI and PSII intensity as reported in Figure 4-3. b, that is, an initial constant PSI F while PSII F increased to a maximum followed by a decrease of PSII F and a linear increase of PSI F. This simulation represents a situation similar to what is expected to occur during the Chl fluorescence kinetics induced when a dark adapted leaf is exposed to light. In Figure 4-3c the simulated fluorescence spectra generated by the combination of the PSI and PSII spectral shapes of Figure 4-3a during the initial 120 temporal steps are reported. A noise component to have a SNR of 40 was added to the spectra.

The comparison of the retrieved PSI and PSII F spectra with the simulated ones is shown in Figure 4-3d. We found that the PC_1 described more than 97% of data variance. By applying LSF to the complete simulated data-set using The retrieved PSI and PSII spectral shapes we assessed the h(t) and g(t) PSs intensity contributions,

- The goodness of fitting can be evaluated by the example reported in Figure 4-3. e, calculated for time sample 200. Finally, in Figure 4-3. f we show the comparison between the temporal evolution of retrieved and simulated PSI and PSII contributions,
- The algorithm was also tested on data with reduced SNR, as low as 10, still obtained satisfactory results (data not shown).

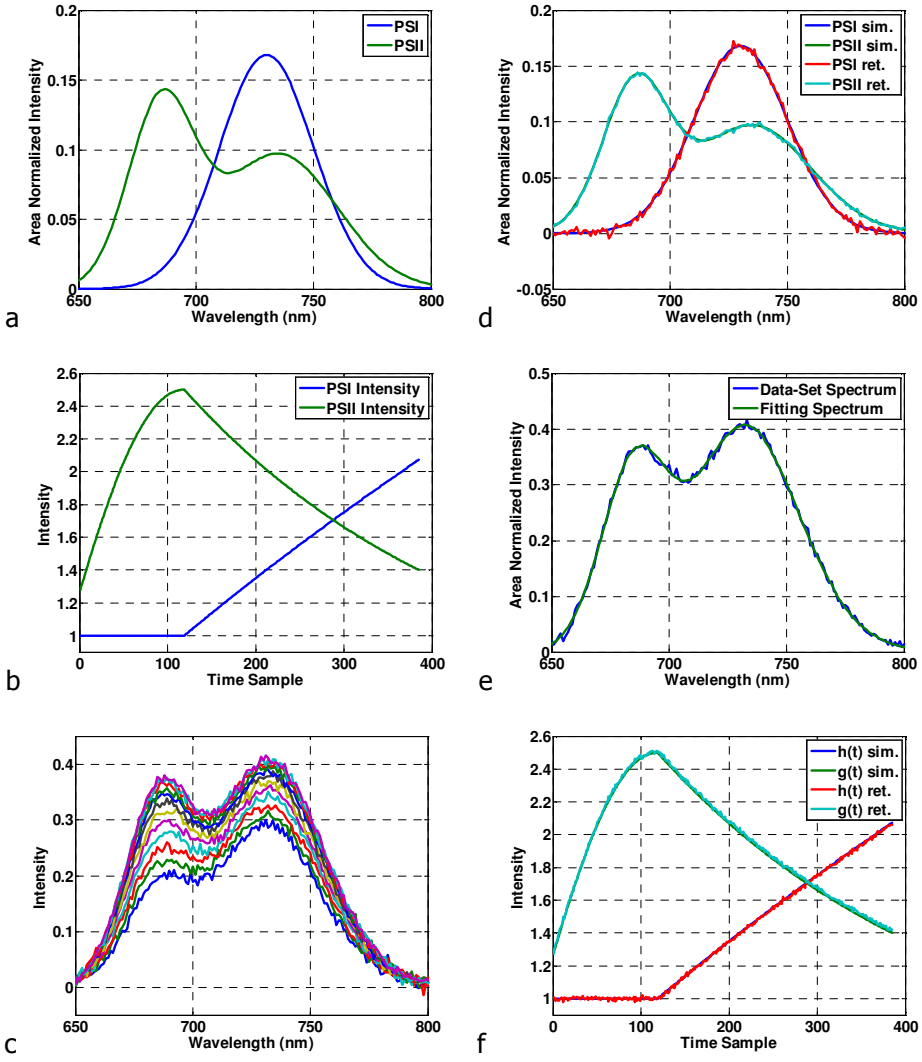

Figure 4-3. Simulated spectral data. a) PSI and PSII fluorescence spectra as single Gaussian and convolution of two Gaussian, respectively; b) temporal evolution of PSII and PSI intensity; c) generated spectra as combination of spectra in a) during the initial 100 temporal steps; d) comparison between retrieved and simulated PSI and PSII spectra; e) least square fitting of spectrum at time; f) comparison of retrieved and simulated intensity variation for PSI and PSII fluorescence.

4.3.2.2. Application to measured fluorescence spectra

Fluorescence spectra were collected from the adaxial side of a *Ficus benjamina* L. leaf, while the abaxial side was kept in contact with a copper plate coupled with a thermoelectric Peltier module used as temperature control. Leaf temperature was continuously monitored through a thermocouple kept in contact with the upper leaf surface.

Chl fluorescence was excited by a 180 W Xenon optical fibre lamp (LINOS Photonics, Goettingen, Germany) through a short pass filter (6200 SP 35-5404, Ealing Electro Optics) to remove radiation above 620 nm. A PPFD of 40 μmol m^{-2} s^{-1} (measured by a QUANTUM sensor, LI-COR Inc. Lincoln, NE, USA) was used to record a whole Kautsky kinetics. The intensity was increased to 2000 μmol m^{-2} s^{-1} to induce a photoinhibitory stress.

The fluorescence signal was collected by a 1 mm optical fibre at a 5 cm distance from the leaf, after filtered by a long pass RG 630 Schott filter to remove residual excitation light, and detected by an ARC SpectraPro 2300i spectrometer (300 mm of focal length) coupled to a PI-MAX (Princeton Instrument) intensified, gateable CCD (Thomson 7895, 512x512 pixels, 24x24-microns effective pitch). The spectrometer was fitted with a 150 grooves/mm grating providing a spectral coverage of 260 nm between 560 and 820 nm, with a 2 nm spectral resolution. A narrow band peak at 580 nm, outside the Chl F band, collected through a second optical fibre as a filtered (580 nm interference filter FWHM=10 nm) fraction of the incident beam, was used to continuously monitor the excitation light.

Sampling frequency was set at 56 Hz during detection of the Kautsky kinetics and reduced to 2 Hz for the monitoring of slower fluorescence changes induced by different conditions of light intensity and temperature.

Application of the retrieval method to the F spectra recorded during the initial rise of the Kautsky kinetics provided the PSI and PSII F spectra reported in Figure 4-4a. The retrieval method has been applied to spectra normalized to the instantaneous excitation light intensity. The shapes of PSs have been normalized to PSI intensity during the initial rise of the kinetics. The PC_1 described more than 95% of data variance, while each of the other components, PC_2 to PC_M, described less than 0.3% of data variance. This result confirms that there is only one significant independent source of data variance and that this is a good approximation of the PSII F spectrum.

Using the retrieved PSI and PSII to fit all the fluorescence spectra we obtained the temporal behaviour of PSI and PSII contributions, as shown in Figure 4-4b and Figure 4-4c for the initial part and the whole induced F kinetics, respectively. It can be seen in Figure 4-4b that the PSI components remains constant during the first 1-1.5 s, confirming the goodness of the initial hypothesis done to develop the algorithm.

The PSII F change is very similar to that of a leaf Kautsky kinetics recorded by integrating the whole F signal. This is in accordance with the well known process of reduction and subsequent re-oxidation of pastoquinones in the PSII photosystem. A much smaller change was observed for PSI F, probably due to energy redistribution between the two PSs.

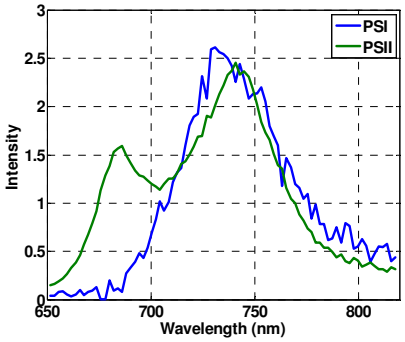

a

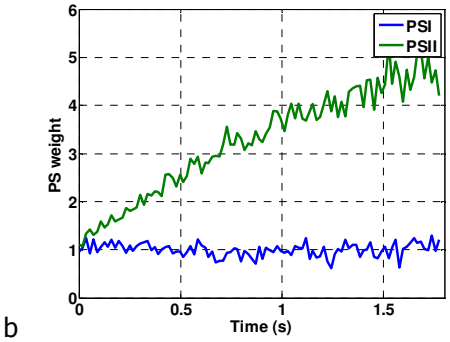

b

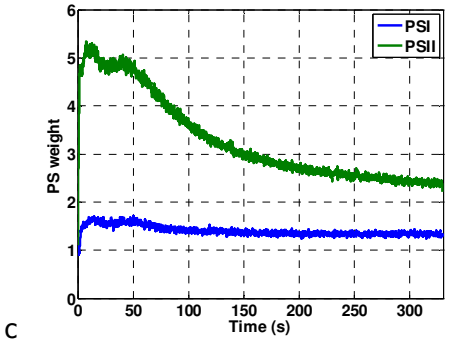

c

Figure 4-4. a) Retrieved PSI and PSII fluorescence spectra, PSII area is normalized to the PSI one. Retrieved PSI and PSII F during the initial rise (b) and the whole (c) F induction of a *F. benjamina* leaf.

The LSF was then applied to leaf F fluorescence spectra recorded under high light intensity or at different leaf temperature, conditions that are expected both to induce distinct variations of PSII and PSI F.

Resulting retrieved PSI and PSII F contributions are presented in Figure 4-5.

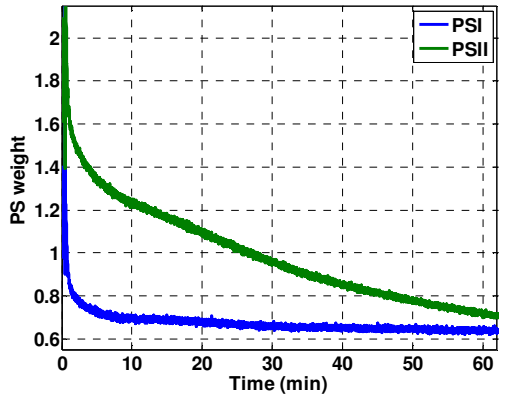

a

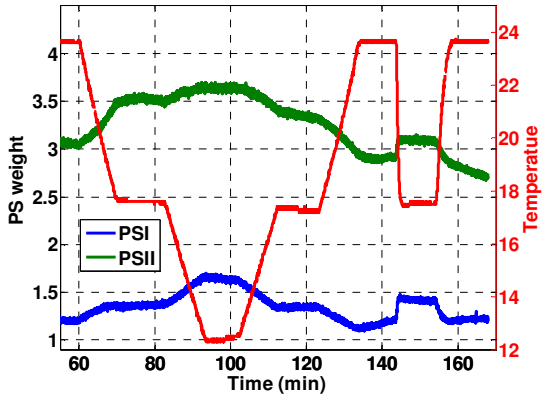

b

Figure 4-5. PSI and PSII fluorescence contribution changes induced by high-light (2000 µmol m^{-2} s^{-1}) intensity irradiation (a) and leaf temperature variation (b) of a *F. benjamina* leaf.

When the irradiation light was increased from 40 to 2000 µmol m^{-2} s^{-1} a rapid transient of F was observed for both PSs contributions. Then, the PSII F continued to decrease markedly while PSI contribution remained almost constant. This evidence is consistent with a photoinhibitory effect aimed to protect the photosynthetic apparatus from excess light energy (Powles, 1984). The dissipating mechanisms of photoinhibition are in competition with the radiative relaxation of Chl. Consequently, photoinhibition induces a reduction in the Chl fluorescence. The higher resistance of PSI to strong

light stress with respect to PSII (Havaux *et al.* 1991a) explains the observed decrease of PSII F. On the other hand, measurements at 77 K showed that the fluorescence quenching at 690 nm caused by photoinhibition also occurs at 735, but to a lower extent (Somersalo *et al.* 1989).

Decreasing leaf temperature induced a F increase for both PSs, however the increasing slope was different for PSII and PSI and changed depending on the temperature range. This diverse effect is due to the fact that PSII F is affected by both photochemical and non-photochemical quenching which are temperature-dependent, while PSI F can change just because of an energy transfer from PSII to PSI due to state transition. The found behavior of PSII and PSI F with leaf T confirms results of previous studies in which only the two short-wavelength and long-wavelength Chl F bands were analyzed (Agati *et al.* 2000).

4.3.3. Deconvolution of the PSII signal by two bands detection

Being

$$F(\lambda_1) = h \cdot PSI(\lambda_1) + g \cdot PSII(\lambda_1)$$
$$F(\lambda_2) = h \cdot PSI(\lambda_2) + g \cdot PSII(\lambda_2) \qquad \text{(Eq. 4-9)}$$

It is still possible to retrieve the PSs contributions, h and g, by using fluorescence data on only two bands and the PSs normalized spectral shapes.

If we consider the 687 and 760 nm wavelengths, corresponding to the O_2B and O_2A atmospheric oxygen absorption bands, respectively, and using the PSII and PSI spectral shape retrieved from data of the initial rising of Kautsky kinetics we have that PSI(687) / PSI(760)=0.26 and that PSII(687) / PSII(760)=1.15.

We applied a least squares fitting (LSF) procedure to the temporal change of F687 and F760 of Figure 4-6a due to light adaptation and leaf T variations and compared the resulting PSI and PSII contributions to those previously obtained by the fitting on the whole F spectra. It can be seen in Figure 4-6b that the two set of data are completely overlapped.

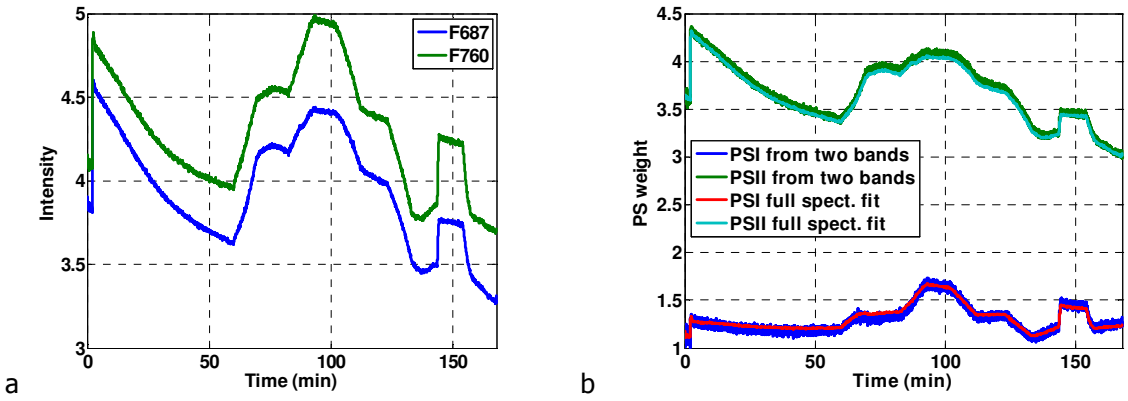

Figure 4-6. a) Measured fluorescence values at 687 and 760 nm on the adaxial side of a *F. benjamina* leaf under light adaptation and leaf T variations. b) Comparison of PSI and PSII F contributions retrieved from two spectral band data and those retrieved from the whole F spectrum.

4.3.4. Potential application to SIF

The present analysis applied to the two SIF bands can be used to monitor the photosynthetic activity at the leaf level, once the relative PSI/PSII fluorescence contribution under unstressed conditions, and

under sun-like excitation conditions (white broad spectral excitation light), of the species investigated is known.

However, due to the marked effect of Chl reabsorption on the short wavelength band fluorescence, it is limited to situations with high Chl content (> 300 mg/m^2), when the reabsorption saturates. Yet, it can be used during periods when Chl content is unlikely to change significantly, for example within diurnal cycles. Alternatively, the dependence of F on the Chl content should be separated by using a suitable spectral method to correct for reabsorption. To do this, particularly useful is the resolution of the PSII and PSI components as showed below.

In Figure 4-5. we report the results of the above LSF analysis for four different *F. benjamina* leaves, for which the total reflectance spectra were also measured (Figure 4-5.). The PSI retrieved spectra are quite similar (Figure 4-5. b) while small but significant differences are found for the PSII spectra (Figure 4-5. a). From reflectance data the Chl content can be deduced, for example using the index suggested by Gitelson and Merzlyak (Gitelson *et al.* 2004):

$$(\mathrm{Chl})\mathrm{RI}_{\mathrm{green}} = \frac{R_{750\div800}}{R_{520\div585}} - 1$$

$$\mathrm{Chl}\ (mg/m^2) = \frac{(\mathrm{Chl})\mathrm{RI}_{\mathrm{green}} + 0.7718}{0.0229} \qquad \text{(Eq. 4-10)}$$

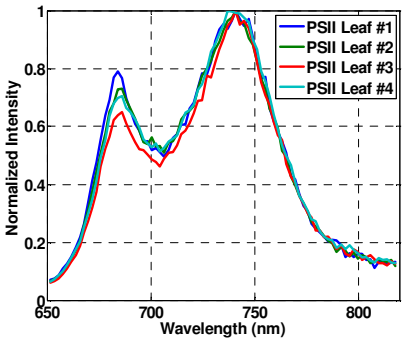

a

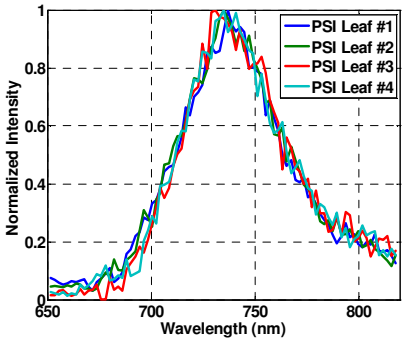

b

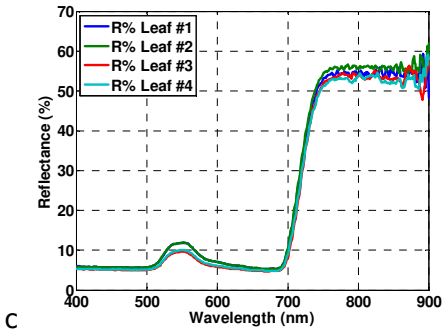

Figure 4-7. PSII (a) and PSI (b) normalized F spectra retrieved from measured data on four different *F. benjamina* leaves with different reflectance spectra (c).

The red/far red fluorescence ratio of PSII is well correlated with the Chl content, much better than the fluorescence ratio (FR) directly derived from the whole Chl F spectrum Figure 4-8. This is probably due to the large contribution of PSI to the long-wavelength F band.

Although only preliminary data are at present available, our results indicate that isolation of the PSII F spectrum and its comparison with that from isolated PSII particles (Franck *et al.* 2002) can be useful to quantify the F reabsorption inside the leaves and find a spectral correction curve for this effect. The spectrum of the reciprocal of reflectance, R, seems to be a good candidate as a correction function for remote sensing measurements, even if confirmation on a large set of data and the scaling up to the canopy level, where multiple reabsorption processes occur, must be carried out.

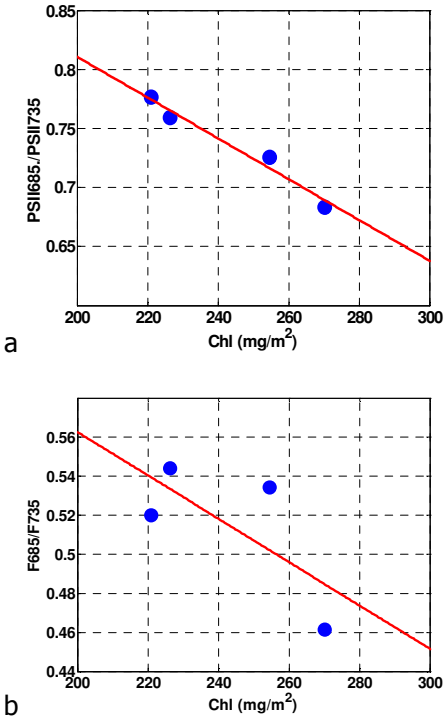

Figure 4-8. Relationship between F685/F735 fluorescence ratio from the PSII spectrum (a) or from the whole leaf spectrum (b) and the Chl content derived from reflectance.

The proposed method, through the measurement of the time resolved fluorescence spectra of the initial rising of Kautsky kinetics, allows the retrieval of the leaf PSs spectral shape and their relative fluorescence contribution.

- No preliminary assumptions of reabsorption/scattering needed,
- The assumptions made are anyway checkable *a posteriori,*
- The method has been tested for different leaves and in different condition of light exposure and temperature,
- The method shows a good sensitivity in the evaluation of the PSs spectral shape,
- Good perspectives for a two-wavelength detection (operation from space).

The knowledge of the PSs spectral contribution is fundamental for the accurate interpretation of the vegetation fluorescence signals (PSI contribution is significant and has to be taken into account).

The retrieval of the PSs spectral contribution permits to find a relationship between the reabsorption effects and other remotely measurable optical properties as reflectance. This can be used to obtain a more direct link between fluorescence and photosynthetic activity.

4.4. A novel algorithm for the representation of leaf temperature effects on Chl F spectra

It is known that reducing leaf T results in the inhibition of plastoquinone reoxidation because of a decreased fluidity of the thylakoid membrane (Havaux *et al.* 1993), leading to an increase of the PSII F signal. This is in agreement with the positive correlation observed between Qp and leaf T (Brüggemann *et al.* 1995; Agati *et al.* 2000; Dobrowski *et al.* 2005). On the other hand PSI F seems to be insensitive to the redox state of plastoquinones (Krause *et al.* 1991) and then the effect of the T change on it must have a different origin. It is likely that the increase of PSI F with decreasing T is due to a state transition (spillover) determining a redistribution of excitation energy from PSII to PSI (Agati *et al.* 2000). This can occur by migration of the weakly bound PSII light-harvesting complex (LHCII) to PSI. Furthermore, it seems that the regulation of antenna functions in plants grown at lower temperatures are not qualitatively different from those induced by high light stress (Ballottari *et al.* 2007), consistent with the idea of a common response to elevated PSll excitation pressure (Gray *et al.* 1996).

Within the hypothesis that the T effect on Chl F consists in the alteration of plastoquinone redox states and related spillover from PSII to PSI, we can follow the formulation used in the bipartite model by Butler & Kitajima (Butler 1978) to find the relationship between the F contributions of the two photosystems. Accordingly, if α and β are the factions of the absorbed photons initially delivered to PSI and PSII, respectively, so that $\alpha+\beta = 1$, the fluorescence of PSII (F_{PSII}) and PSI (F_{PSI}) can be written as:

$$F_{PSII} = \beta I_a \left[A_{II} + \frac{1 - A_{II}}{1 - \psi_{TII}\psi_{tII}} \right] \psi_{FII} \qquad \text{(Eq. 4-11)}$$

$$F_{PSI} = \left[\alpha + \beta \varphi_{T(II \rightarrow I)} \right] I_a \psi_{FI} \qquad \text{(Eq. 4-12)}$$

where I_a is the absorbed quantum flux; A_{II} is the fraction of open reaction centers; ψF, ψT, ψt are the quantum yields for fluorescence, energy trapping and transfer back to the antenna, respectively, and

$$\varphi_{T(II \rightarrow I)} = \psi_{T(II \rightarrow I)} \left[A_{II} + \frac{1 - A_{II}}{1 - \psi_{TII}\psi_{tII}} \right] \qquad \text{(Eq. 4-13)}$$

is the yield of energy transfer from PSII to PSI.

By combining the above equations, we expect to find a linear relationship between F_{PSI} and F_{PSII}:

$$F_{PSI} = \alpha I_a \psi_{FI} + \psi_{T(II \rightarrow I)} \frac{\psi_{FI}}{\psi_{FII}} F_{PSII} \qquad \text{(Eq. 4-14)}$$

Indeed, using the results of the above spectral fitting analysis we could plot the PSI F component versus the PSII one and verify the present of a linear regression between them, in the temperature range between 25 and 8 °C Figure 4-9.

We can conclude that the effect of T on Chl F, below optimal T values for photosynthesis, is reasonably well represented by the bipartite model of the photochemical apparatus which considers the energy distribution between the two photosystems. However, it can not be ruled out that the much more rigorous tripartite model which includes a detailed interaction of Chl LH complex with the two photosystems (Butler 1978), might give more accurate results.

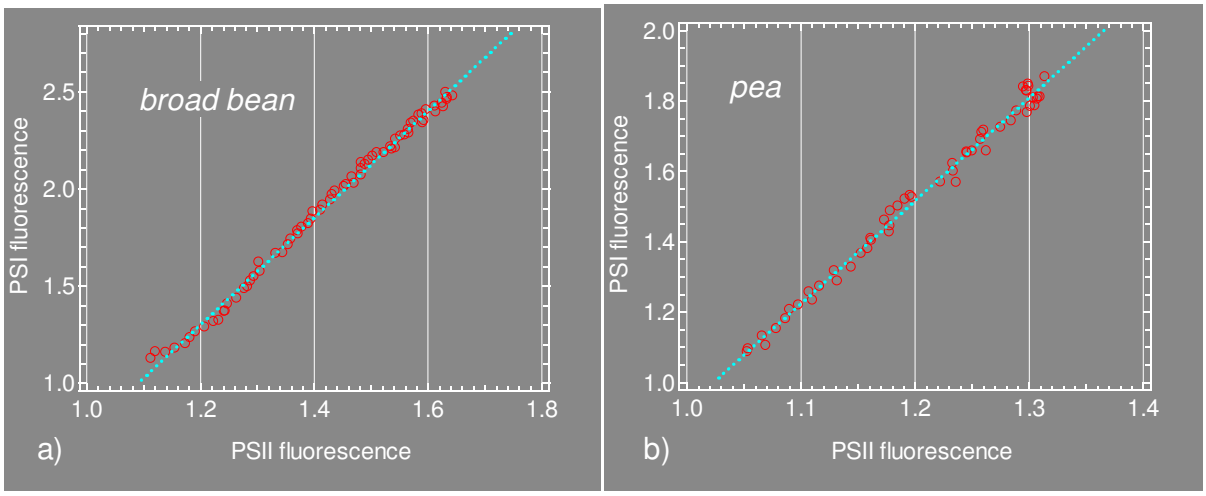

Figure 4-9. Spectral fitting component of F_{PSI} as function of F_{PSII} for different leaf T.

4.5. Appendix: some remarks on FluorMODleaf

In the FluorMODleaf model developed as part of the ESA project ESTEC Contract No. 16365/02/NL/FF - Final Report Development of a Vegetation Fluorescence Canopy Model (Miller *et al.* 2005), the contribution of PSI to the Chl F spectrum at physiological temperatures has been considered to be significant. Accordingly, the shape of the ChlF spectrum was based on the combination of emission spectra of isolated PSI and PSII Chl-protein complexes (Croce *et al.* 1996, 2000; Franck *et al.* 2002).

The stoichiometry of PSII and PSI reaction centres was an input of the model and set to 1.1 for shade leaves and 2 for sun leaves, according to Chow *et al.* 1988. However, this data refers to the ratio of PSII/PSI reaction centres without considering the corresponding antennas. The same authors reported that shade plants with lower Chla/Chlb ratios have more LHC-II and concomitantly less core Chl a-proteins of PSII, while sun plants have smaller antenna of PSII. What is important for the ChlF signal is the absorbed energy that goes into fluorescence, then we should consider the ratio between the absorbance efficiency of PSII and PSI. In this the antenna size is fundamental.

Data from Leong & Anderson (1984), which report the distribution of Chl among all the various Chl-protein complexes as function of growing light intensity, seem to be more appropriate. They considered the ratio between the Chl associated with PSII (sum of core and LHCP) and the Chl associated with PSI. This ratio increased from 2.1 at 840 $\mu Em^{-2}s^{-1}$ to 3 at 10 $\mu Em^{-2}s^{-1}$. It is also interesting to note that the ratio between LHCP and the core reaction centre complex of PSII varied from 3.5 at high light to 8.6 at low light. Then, there is a large rearrangement in the Chl-protein complexes of PSII as the growing light intensity is changed. Melis (1984) reported that sun-adapted

species had PSII/PSI ratio in the range 1.3-1.9, while shade-adapted species had higher PSII/PSI ratio in the range 2.2-4. Leong & Anderson (1984) also reported that since "most of the Chl b present in the thylakoid membranes is associated with LHC-II, it is possible from the Chl a/b ratio to roughly predict the abundance of Chl associated with PSII or PSI. A high Chl a/b ratio would mean less LHC-II and thus lower PSII Chl content and higher PSI Chl content and viceversa".

The Chl a/b ratio is generally higher in sun-exposed leaves with respect to shade leaves; therefore, a negative relationship between PSII/PSI ratio and growing light intensity is expected.

The parameter Sto should correspond to the PSII/PSI ratio, and then should be in the range 1-2. Accordingly, it seems that the legend in the report "Development of aVegetation Fluorescence Canopy model, ESTEC contract No 16365/02/NL/FF is not appropriate, since it refers to a PSII/PSI range between 5 and 12. Instead, it probably refers to the Sto values multiplied by the factor 5 that accounts for the difference in quantum yield between PSII and PSI.

The issue concerning PSII/PSI contributions to the Chl F spectrum has been recently revised by Pedrós *et al*. (2008), in which both the ratio of PSII/PSI reaction centres (Sto) and the two photosystem antennas, SII and SI, have been used as weighting factors in the combination of the photosystem emission spectra. They presented the resulting emission spectra of leaves under low light and high light conditions using Sto, SII and SI of 1.8, 250 and 230 Chl/unit (Melis, 1989), respectively, for high light leaves and 1.47, 377 and 220 Chl/unit (Lokstein *et al*., 2002), respectively, for low light leaves. Both spectra have a similar shape with a peak ratio of about 4, due to the fact that a higher PSII/PSI ratio is balanced by a smaller PSII antenna size.

Alternatively, the relative contribution of the two photosystems can be obtained by measuring the Chl fluorescence induction kinetics at the 685 and 740 nm fluorescence bands and by plotting the two signals during the fast initial rising one against the other (Agati *et al*., 2000). It resulted that the relative contribution of PSI to the F740 band was about 30-36% at the steady state. Interestingly, using this normalizing factor in the combination of PSII and PSI emission spectra, we found a convoluted fluorescence leaf spectrum quite similar to that presented by Pedrós *et al*. (2008).

These proposed fluorescence spectra represent a good reference for modelling re-absorption effects inside a leaf.

5. MODELLING FLUORESCENCE AT CANOPY SCALE: MODEL DESCRIPTION

5.1. The FluorMod model

The representation of the functional link between chlorophyll fluorescence and photosynthesis, and the propagation of the fluorescence signal through the canopy has been the subject of a previous study funded by the European Space Agency (Development of a Vegetation Fluorescence Canopy Model, ESTEC Contract No. 16365/02/NL/FF). In the FluorMod model developed as part of the study (Zarco-Tejada *et al.* 2006), solar-induced fluorescence is modelled at the leaf as a function of fluorescence yield and energy partitioning between photosystems (as well as chlorophyll content, in order to account for re-absorption effects). The fluorescence signal generated by the FluorMODleaf sub-model is then propagated to the canopy scale by the FluorSAIL sub-model. The assumption in the FluorMod model of un-stressfull conditions (Rosema *et al.* 1998), however, made the model of little applicability under real conditions.

The SCOPE (Soil-Canopy Observation, Photosynthesis and Energy balance) model produced as part of the current study is a direct development of the FluorMod/FluorSAIL model that will be therefore first briefly described. A more detailed description of the model can be found in the final report of the ESA FluorMod project (ESTEC Contract No. 16365/02/NL/FF).

5.1.1.1. FluorMODleaf

The FluorMODleaf model represents an extension of the PROSPECT model (Jacquemoud *et al.* 1996) for the representation of leaf fluorescence as well as reflectance and transmittance. As in the PROSPECT model, the leaf is represented as one or several absorbing plates with rough surfaces giving rise to isotropic diffusion. Leaf reflectance and transmittance are represented as a function of four input parameters, related to leaf structure and biochemistry: a leaf structure parameter (N, number of compact layers specifying the average number of air/cell walls interfaces within the mesophyll), the chlorophyll a+b concentration (C_{ab}), the equivalent water thickness of the leaf (C_w) and leaf dry matter content (C_m, equivalent to SLA, specific leaf area).

An elegant and powerful approach was developed in the FluorMODleaf model for the representation of leaf fluorescence, first of an elementary layer, and then of a pile of N layers.

Fluxes are considered as a network in the model (see Figure 5-1). The thickness of the plate D is initially set to unity, resulting in a system of linear equations in i_0, i_1, i_2, i_3, i_4 and i_5 which is easily solved for leaf transmittance ($T = i_3$) and reflectance ($R = i_5$). In order to calculate the fluorescence fluxes, it is necessary to know the excitation fluxes at any position within the plate. The integration of the resulting equations is not amenable to an analytical solution, but can be obtained numerically for any given set of parameters and stored in a look-up-table.

The source function ϕ which gives rise to the fluorescence photons inside the leaf has been generally studied at the leaf scale and related to the PSI and PSII fluorescence emission spectra; it is a function of the partitioning of absorbed energy between the two photosystems, the fluorescence spectrum of PSI and PSII and the corresponding fluorescence yield. Only the fluorescence yield of PSII is generally assumed to be modulated by environmental factors. A constant partitioning among photosystems is assumed in the FluorMODleaf model, although the spillover could be itself a function of PSII state and environmental conditions (see Chapter 4.5).

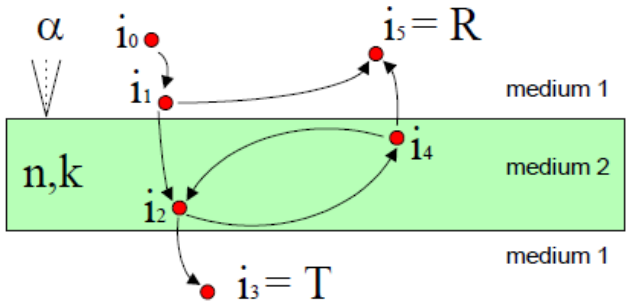

(a)

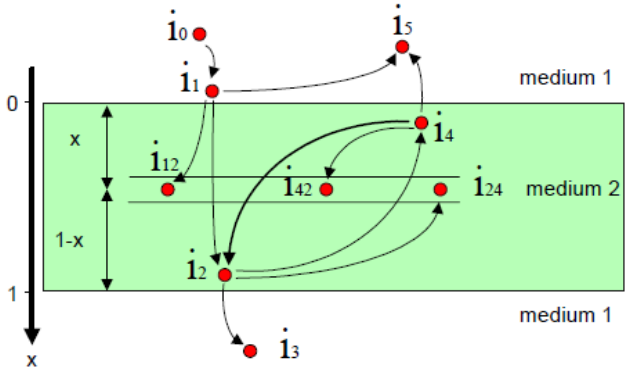

(b)

Figure 5-1 - Schematic representation of the FluorMODleaf approach for the radiative transfer of the fluorescence signal. (a) Flux network produced by a semi-transparent plate with rough surfaces for the computation of leaf reflectance (R) and transmittance (T). (b) The flux network showing the excitation fluxes at position x for the computation of leaf fluorescence.

5.1.1.2. FluorSAIL

A new canopy fluorescence model has been developed as part of the FluorMod model in order to include the dependence of fluorescence at different levels in the canopy upon the light environment experienced by the leaf. In this case, one has to consider that the solar flux intercepted by leaves depends strongly on their orientation with respect to the sun, and that for the diffuse upward and downward incident fluxes the spectral character of the light (the so-called light quality) changes with depth inside the canopy layer. The latter effect can be simulated very well with a numerically robust and speed-optimized recent version of the canopy reflectance model called 4SAIL, and therefore this model has been selected as a basis for the development of the model *FluorSAIL*, which simulates hyperspectral canopy fluorescence observations at both the top-of-canopy (TOC) and the top-of-atmosphere (TOA) level. However the representation of the response of fluorescence upon absorbed light at the leaf level is based in the FluorMod model upon the Rosema (Rosema *et al.* 1998) model, which is admittedly only intended for un-stressed conditions as seldom encountered in the field.

Moreover, the model in its original form did not represent radiative transfer in the thermal infrared, with a potential error in the computation of leaf temperature and a potential effect on photosynthesis and fluoresence, in particular in closed canopies (grassland, agricultural crops, …) not well coupled to the atmosphere (Jarvis *et al.* 1986).

The model, finally, did not include a representation of canopy gas exchange, making it unsuitable for the analysis of the impact of fluorescence remote sensing on the estimation of vegetation gross primary production (GPP).

The SCOPE model developed as part of the project therefore departs from the FluorMOD model under three respects:

1. it includes a detailed representation of radiative transfer in the thermal infrared and of leaf temperature. This will also make it possible to simulate canopy temperature, as detectable by the proposed satellite according to agreed specifications;
2. it comprises a state-of-the-art representation of canopy gas exchange and GPP;
3. it accounts for the functional link between photosynthetic processes and chlorophyll fluorescence, according either to the van der Tol-Verhoef-Rosema model or to the Magnani model (see Chapter 3).

5.2. Incorporation of thermal infrared radiation into the SCOPE model

In a homogenous leaf canopy, sunlit and shaded leaves receive various amounts of incident radiation, depending on the leaf's orientation, its vertical position, and the wavelength of the radiation. Because of this, leaves may get different temperatures depending on these factors, and the probability of sunshine (gap fraction). In this contribution, these effects are analysed in order to establish a basis for a computer model that includes leaf and soil thermal radiances

5.2.1.1. Including thermal fluxes

So far, the diffuse fluxes have been based on optical inputs (non-thermal) only. It is possible however to extend the analytical solution with thermal emission from the foliage and the soil, even in the case of differentiation between sunlit and shaded components (Verhoef *et al.*, 2007), but one may expect that in reality sunlit leaves will all have different temperatures, depending on their orientation with respect to the sun, and their depth in the canopy layer, so in this case a numerical solution should be preferred. For this, the energy balance equation is solved on the level of individual leaves, for 13×36 leaf orientations (leaf slope and azimuth), and 60 vertical positions in the canopy layer. The energy balance includes all absorbed radiation from 0.4 to 50 microns, sensible heat, latent heat (evapotranspiration), and thermal emission. The thermal emission term closes the energy balance equation, and in turn determines the leaf's temperature.

The incident radiation on leaves should not only include the optical radiation and thermal radiation from the sky, but also all thermal radiation generated internally by leaves and by the soil. In order to compute the internally generated fluxes by thermal emission from leaves and the soil, it is initially assumed that the temperature of the leaves and the soil are equal to the air temperature. Next, the external radiation sources are added, and the energy balance is solved. This gives new temperatures of the leaves and the soil, whereby also sunlit and shaded components are differentiated.

The numerical solution of the fluxes without considering optical fluxes proceeeds as follows:

We start with the differential equations

$$\frac{\mathrm{d}}{L\mathrm{d}x}F_1 = mF_1 - m(1-r_\infty)H_v$$
$$\frac{\mathrm{d}}{L\mathrm{d}x}F_2 = -mF_2 + m(1-r_\infty)H_v \qquad \text{(Eq. 5-1)}$$

For the fluxes at the soil level one can write

$$E^+(-1) = r_s E^-(-1) + (1 - r_s) H_s \qquad \text{(Eq. 5-2)}$$

where τ_{ss} is the direct transmittance of the canopy layer, r_s is the soil's reflectance and H_s is the blackbody emittance of the soil.

Eqs. (5-1) and (5-2) can be used as the basis for a numerical solution of the fluxes in the case of heterogeneous foliage temperatures. An advantage of working with transformed fluxes is that these can be directly expressed in those of the layer directly above or below the current one. For a finite difference numerical solution we then obtain the recursive equations

$$F_1(x + \Delta x) = (1 - mL\Delta x) F_1(x) + m(1 - r_\infty) H_v(x) L\Delta x$$
$$F_2(x) = (1 - mL\Delta x) F_2(x + \Delta x) + m(1 - r_\infty) H_v(x) L\Delta x \qquad \text{(Eq. 5-3)}$$

If the first transformed flux is given at the canopy top, it can next be computed recursively down to the soil level. Starting the second transformed flux at the soil level, this eventually leads to this flux at the top-of-canopy (TOC) level. However, the second transformed flux at the soil level is not known initially, so it has to be obtained from the boundary equation, Eq. (5-2).

Since for the fluxes at soil level one can write

$$F_1(-1) = E^-(-1) - r_\infty E^+(-1)$$
$$F_2(-1) = -r_\infty E^-(-1) + E^+(-1)$$

one obtains

$$r_\infty F_1(-1) + F_2(-1) = (1 - r_\infty{}^2) E^+(-1)$$
$$F_1(-1) + r_\infty F_2(-1) = (1 - r_\infty{}^2) E^-(-1) \qquad \text{(Eq. 5-4)}$$

Eq. (2) can be rewritten as

$$(1 - r_\infty{}^2) E^+(-1) = r_s (1 - r_\infty{}^2) E^-(-1) + (1 - r_\infty{}^2)(1 - r_s) H_s \ ,$$

and substitution of Eqs. (4) then gives

$$r_\infty F_1(-1) + F_2(-1) = r_s [F_1(-1) + r_\infty F_2(-1)] + (1 - r_\infty{}^2)(1 - r_s) H_s(-1) \text{ , or}$$

$$(1 - r_s r_\infty) F_2(-1) = (r_s - r_\infty) F_1(-1) + (1 - r_\infty{}^2)(1 - r_s) H_s$$

This finally gives a direct relation between the transformed fluxes at the soil level, which reads

$$F_2(-1) = \frac{(r_s - r_\infty)}{(1 - r_s r_\infty)} F_1(-1) + \frac{(1 - r_\infty{}^2)}{(1 - r_s r_\infty)} (1 - r_s) H_s \qquad \text{(Eq. 5-5)}$$

This relation can be used to link the downward and upward sequences of difference equations, and finally both transformed fluxes at the TOC level will be available.

The initial guess of $F_1(0)$ is made under the assumption that there is no downward incident flux at the top of the canopy. Since in the thermal infrared r_∞ is also small, we simply assume that $F_1(0)$ initially is zero.

After the downward and upward sequences have been completed, also the second transformed flux at TOC level, $F_2(0)$, is known. At this moment one can correct the initial guess of $F_1(0)$, since it was based on the assumption of an upward flux of zero. For this, use is made of the equation

$$F_1(0) + r_\infty F_2(0) = (1 - r_\infty{}^2) E^-(0) = 0 \ ,$$

which is rewritten as $F_1(0) = -r_\infty F_2(0)$.

In practice, a single iteration is usually sufficient to arrive at the correct fluxes at both boundaries. Figure 5-2 shows an example obtained from a simulation for a canopy LAI of 3 and a soil which is hotter than the foliage. The foliage emittance was supposed to decrease exponentially in downward direction.

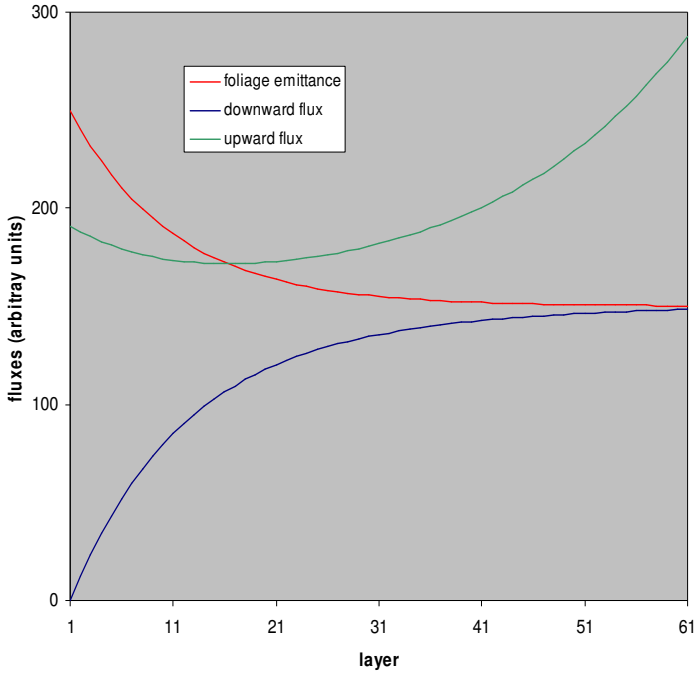

Figure 5-2 - Simulated TIR upward and downward fluxes in a 60-layer canopy with varying foliage temperature. Solar flux was neglected here.

5.2.1.2. Coupling with the atmosphere

For calculation of the radiation balance at the level of single leaves, the direct solar flux and the upward and downward fluxes incident on leaves have to be known at a spectral resolution high enough to take properly into account the atmospheric absorption bands. These can be obtained from the atmospheric model MODTRAN.

Two MODTRAN runs, for surface albedos of 50% and 100%, are sufficient to estimate the spherical albedo and the diffuse and direct solar fluxes incident at the top of the canopy. These MODTRAN runs should be done for a low sensor altitude (1 m above the surface is recommended) under nadir viewing angle in order to keep the atmospheric transmittance as high as possible. All relevant quantities can be determined as follows:

$$\rho_{dd} = \frac{\mathrm{GRFL}_{100} - 2 \times \mathrm{GRFL}_{50}}{\mathrm{GRFL}_{100} - \mathrm{GRFL}_{50} - \mathrm{SFEM}_{50}}$$

$$\tau_{oo} = \mathrm{TRAN}$$

$$L_s = 2 \times \mathrm{SFEM}_{50} / \tau_{oo}$$

$$O + T = (1 - \rho_{dd})(\mathrm{GRFL}_{100} - 2 \times \mathrm{SFEM}_{50}) / \tau_{oo}$$

$$E_{\mathrm{sun}} = \pi \times \mathrm{GSUN}_{100} / \tau_{oo}$$

Here, the ρ and τ quantities refer to the atmosphere, not to the canopy layer. In the above equations, the following MODTRAN outputs are used:

TRAN = direct transmittance from target to sensor

SFEM = radiance contribution due to surface emission

GSUN = ground-reflected radiance due to direct solar radiation

GRFL = total ground-reflected radiance contribution

The subscripts indicate the associate percentages of surface albedo.

Note, that the sky irradiance onto the surface is a derived quantity, which also depends on the surface albedo in the surroundings. It can be estimated by

$$E_{\mathrm{sky}} = \pi \left[\frac{O + T}{1 - a\rho_{dd}} + L_s \right] - E_{\mathrm{sun}} \ ,$$

where

$$O = (\tau_{ss} + \tau_{sd}) E_s(\mathrm{t}) / \pi$$
$$T = L_a(\mathrm{b}) - (1 - \rho_{dd}) L_s$$

Figure 5-3 shows E_{sun} and E_{sky} (in $\mathrm{Wm^{-2}\mu m^{-1}}$) and the spherical albedo ρ_{dd} obtained from MODTRAN4 runs for 50% and 100% albedo. The E_{sky} is the one for a surface albedo of zero. From these results it can be concluded that already at 2.5 µm the diffuse sky irradiance starts to rise due to thermal emission, and at 10 µm it is the dominant source of incident radiation. In spectral regions of low atmospheric absorption (high transmittance) the sky radiance is less than in absorption bands. This is caused by the correspondingly lower atmospheric emissivity and the fact that higher and colder layers of the atmosphere contribute to the radiance at surface level.

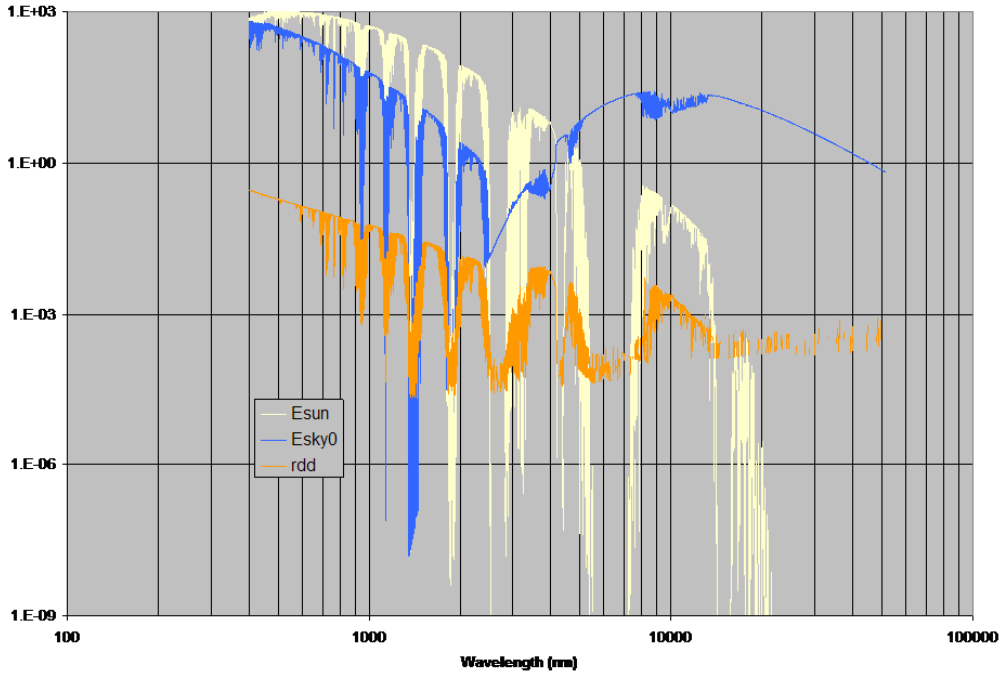

Figure 5-3 - Direct and diffuse irradiances (for zero albedo) and the spherical albedo on logarithmic scales. Plotted wavelength range is 0.4 – 50 µm.

The sky irradiance in general is given by

$$E_{\text{sky}} = \frac{(\tau_{sd} + \tau_{ss} a \rho_{dd}) E_s(\text{t}) + \pi L_a(\text{b}) + (1-a)\rho_{dd} \pi L_s}{1 - a\rho_{dd}} \quad ,$$

and for zero albedo this gives

$$E_{\text{sky}}(0) = \tau_{sd} E_s(\text{t}) + \pi L_a(\text{b}) + \rho_{dd} \pi L_s$$

From these equations it follows that

$$E_{\text{sky}} = \frac{E_{\text{sky}}(0) + a\rho_{dd}(E_{\text{sun}} - \pi L_s)}{1 - a\rho_{dd}}$$

5.2.1.3. Net radiation on leaves

With the given solar and sky irradiance spectra it is possible to calculate the spectral radiation fields inside the canopy. The energy balance for single leaves is calculated on the basis of the net radiation integrated over the whole spectrum from visible to thermal (0.4 – 50 µm. The net spectral radiation on a leaf is equal to the absorption minus its total emission from the two sides, or, for leaves in the shade

$$R_n(x) = [E^-(x) + E^+(x) - 2H_{vd}(x)](1 - \rho - \tau)$$

For leaves in the sun with a given orientation relative to the sun we get

$$R_n(x, \theta_\ell, \varphi_\ell) = [|f_s| E_{\text{sun}} + E^-(x) + E^+(x) - 2H_{vs}(x, \theta_\ell, \varphi_\ell)](1 - \rho - \tau)$$

Here, $$f_s = \frac{\cos\delta_s}{\cos\theta_s} = \frac{\cos\theta_s\cos\theta_\ell + \sin\theta_s\sin\theta_\ell\cos\varphi_\ell}{\cos\theta_s}$$

The numerator of the above expression is the projection of the leaf onto a plane perpendicular to the sunrays. Its absolute value is maximum if the leaf's normal points to the sun or in the opposite direction. The division by the cosine of the solar zenith angle is applied because the solar irradiance is defined for a horizontal plane. The leaf's emittances (emitted fluxes) are defined for leaves in the shade and in the sun. For leaves in the shade the emittance depends only on the vertical position, Leaves in the sun will all have different temperatures and emittances, depending on their orientation and depth.

The spectrally integrated net fluxes are used in the energy balance on single leaf level. This results into new hemispherical thermal fluxes on elementary layer level by applying a weighted averaging, taking into account the leaf angle distribution and the probability of sunshine.

This gives

$$H_v(x) = P_s(x)\sum_{\substack{13\theta_\ell \\ 36\varphi_\ell}} f(\theta_\ell)H_{vs}(x,\theta_\ell,\varphi_\ell)/36 + [1-P_s(x)]H_{vd}(x)$$

The new thermal fluxes per layer so obtained are inserted into Eq. 5-3 again and this results into a new energy balance on the level of single leaves. This process should be re-iterated until stability has been reached.

After the establishment of overall numerical stability, the following quantities are known for leaves in the sun and in the shade:

- Leaf temperature
- Relative fluorescence
- Photosynthesis

5.2.1.4. Top-of-canopy radiances

From leaf temperature, fluorescence, and the direct and diffuse fluxes at all levels in the canopy, one can calculate the top-of-canopy spectral radiances all over the spectrum. This is obtained from the spectral radiance of single leaves and integrating these over canopy depth, and leaf orientation. One can also express this directly into incident fluxes, and use scattering and extinction coefficients defined for single leaves.

For individual leaves, the SAIL scattering and extinction coefficients in the direction of viewing can be summarised as follows:

$$\cos\delta_s = \cos\theta_\ell\cos\theta_s + \sin\theta_\ell\sin\theta_s\cos\varphi_\ell$$
$$\cos\delta_o = \cos\theta_\ell\cos\theta_o + \sin\theta_\ell\sin\theta_o\cos(\varphi_\ell - \psi)$$

ψ = relative azimuth sun-view

$$f_s = \frac{\cos\delta_s}{\cos\theta_s} \quad ; \quad f_o = \frac{\cos\delta_o}{\cos\theta_o}$$

$$
\begin{aligned}
K &= |f_o| \\
v &= |f_o|\frac{\rho+\tau}{2} + f_o\frac{\rho-\tau}{2}\cos\theta_\ell \\
v' &= |f_o|\frac{\rho+\tau}{2} - f_o\frac{\rho-\tau}{2}\cos\theta_\ell \\
w &= |f_s f_o|\frac{\rho+\tau}{2} + f_s f_o\frac{\rho-\tau}{2}
\end{aligned}
\qquad \text{(Eq. 5-6)}
$$

TOC radiance contribution from a leaf (times π) in the direction of viewing:

$$\pi L_\ell = wE_s(0)P_{so}(x) + [vE^-(x) + v'E^+(x) + K\varepsilon_v H_v(x,\theta_\ell,\varphi_\ell)]P_o(x)$$

The above equation should be averaged (weighted) over all leaf orientations and split into fractions in the sun and in the shade, so one gets

$$\pi L_{\ell d} = \sum_{\substack{13\theta_\ell \\ 36\varphi_\ell \\ 60x}} \{[vE^-(x) + v'E^+(x)]P_o(x)[1-P_s(x)] + K\varepsilon_v H_{vd}(x)[P_o(x) - P_{so}(x)]\} f(\theta_\ell)/36 \times \frac{\mathrm{LAI}}{60}$$

This assumes there are 36 leaf azimuth angles and 60 layers. The above equation can be decomposed in quantities that depend either on the leaf orientation or on the level. The weighted averaging over the leaf inclination and azimuth could be done first, and next the mean values (these are the analytical SAIL coefficients) could be used in the summation over level. For leaves in the sun one obtains

$$\pi L_{\ell s} = \sum_{\substack{13\theta_\ell \\ 36\varphi_\ell \\ 60x}} \left\{ \begin{array}{l} [wE_s(0) + K(\theta_\ell,\varphi_\ell)\varepsilon_v H_{vs}(x,\theta_\ell,\varphi_\ell)]P_{so}(x) \\ +[vE^-(x) + v'E^+(x)]P_o(x)P_s(x) \end{array} \right\} f(\theta_\ell)/36 \times \frac{\mathrm{LAI}}{60}$$

Here again the averaging over *w* could be computed beforehand. Only *K* must be differentiated according to leaf orientation, since the leaves' thermal emittances vary with leaf orientation as well.

The bidirectional gap fraction here is given by

$$P_{so}(x) = \exp[(K+k)x + \sqrt{Kk}\,\frac{\ell}{\alpha}(1 - \mathrm{e}^{x\frac{\alpha}{\ell}})]$$

where ℓ is the ratio of leaf width to canopy height, and

$$\alpha = \sqrt{\tan^2\theta_s + \tan^2\theta_o - 2\tan\theta_s\tan\theta_o\cos\psi}$$

Finally, the contributions from the soil background (sunlit and shaded) should be added. They are given by

$$
\begin{aligned}
\pi L_{sd} &= [r_s E^-(-1) + \varepsilon_s H_{sd}][P_o(-1) - P_{so}(-1)] \\
\pi L_{ss} &= \{r_s[E^-(-1) + E_s(0)] + \varepsilon_s H_{ss}\}P_{so}(-1)
\end{aligned}
$$

The sum is given by

$$\pi L_s = [r_s E^-(-1) + \varepsilon_s H_{sd}]P_o(-1) + [r_s E_s(0) + \varepsilon_s(H_{ss} - H_{sd})]P_{so}(-1)$$

Final result:

$$\pi L_o(0) = \left[\begin{array}{l} v\sum_{60x} E^-(x)P_o(x) + v'\sum_{60x} E^+(x)P_o(x) + K\varepsilon_v \sum_{60x} H_{vd}(x)[P_o(x) - P_{so}(x)] \\ + wE_s(0)\sum_{60x} P_{so}(x) + \varepsilon_v \sum_{\substack{13\theta_\ell \\ 36\varphi_\ell \\ 60x}} K(\theta_\ell,\varphi_\ell)H_{vs}(x,\theta_\ell,\varphi_\ell)f(\theta_\ell)P_{so}(x)/36 \end{array}\right] \frac{LAI}{60} \qquad \text{(Eq. 5-7)}$$

$$+[r_s E^-(-1) + \varepsilon_s H_{sd}]P_o(-1) + [r_s E_s(0) + \varepsilon_s(H_{ss} - H_{sd})]P_{so}(-1)$$

Here, the analytical SAIL coefficients are applied in front of the summations whenever possible. In 5-. 7) the terms containing the SAIL coefficients *v*, *v'* and *w* together form the directional reflectance contribution from the canopy layer. Incorporating also the contributions due to soil reflectance, one could use SAIL to calculate these contributions analytically, which is much faster. In this case one could write

$$\pi L_o(0) = r_{so}E_{\text{sun}} + r_{do}E_{\text{sky}} + \left[\begin{array}{l} + K\varepsilon_v \sum_{60x} H_{vd}(x)[P_o(x) - P_{so}(x)] \\ + \varepsilon_v \sum_{\substack{13\theta_\ell \\ 36\varphi_\ell \\ 60x}} K(\theta_\ell,\varphi_\ell)H_{vs}(x,\theta_\ell,\varphi_\ell)f(\theta_\ell)P_{so}(x)/36 \end{array}\right] \frac{LAI}{60}$$

$$+\varepsilon_s H_{sd}P_o(-1) + \varepsilon_s(H_{ss} - H_{sd})P_{so}(-1)$$

5.3. Incorporation of a realistic representation of canopy gas exchange and fluorescence

In order to represent conveniently canopy gross primary production and its relationship with light absorption and canopy fluorescence, a detailed representation of photosynthetic processes and leaf gas exchange has been introduced into the SCOPE model. The same multi-layer structure adoptedfor the representation of shortwave and thermal energy transfer is also used for the representation of gas exchange, differentiating sunlit and shaded leaves within each layer (Figure 5-4). The radiative transfer and gas exchange scheme (MLFL, multi-layer Farquhar-Leuning module) can be run in stand-alone mode (e.g. for validation against field data or calibration) or in combination with the fluorescence module. Inclusion of the fluorescence module considerably increases computation times.

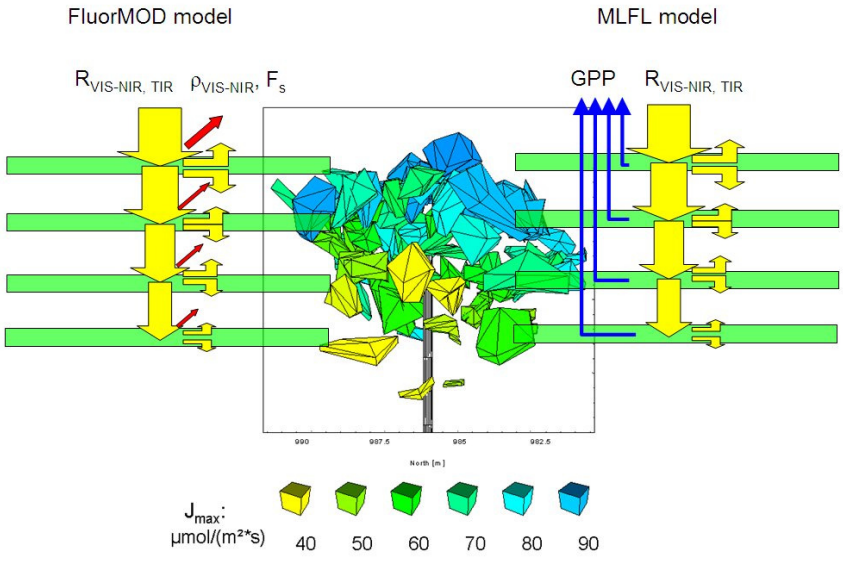

Figure 5-4 Combination of the FluorMOD model of leaf and canopy fluorescence and hyperspectral reflectance (on the left) with the selected multi-layer Farquhar-Leuning (MLFL) model of canopy gas exchange (on the right). The two models share the same representation of canopy structure and exchange information as described in the text. The reflectance and transmittance (yellow arrows), fluorescence (red arrows) and gas exchange (in blue) are represented for sunlit and shaded leaves in each layer of the canopy. The vertical variability of functional characteristics through the canopy (here depicted electron transport rate Jmax, for a real broadleaf tree) is duly considered in the model.

A simplifying assumption is introduced in the model (Figure 5-5), whereby fluorescence and photosynthesis are locally (i.e. for an individual leaf) interdependent, but light absorption and photosynthesis are assumed to be independent of the small fluorescence radiance from other layers in the canopy. This is deemed to be a reasonable assumption, given the low fluorescence yield generally observed (3-5%) and the spectral distribution of the emitted energy, largely outside the photosynthetically active range.

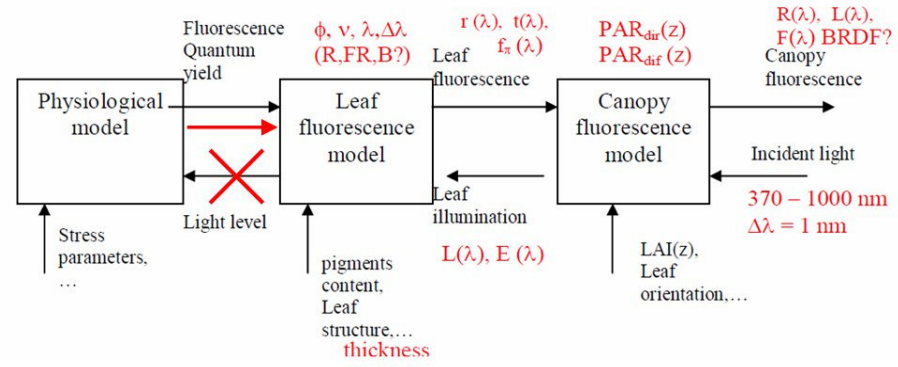

Figure 5-5. Representation of the FluorMOD model, as developed in a previous ESA project, and of the conceptual changes brought about for its integration with the dynamic MLFL model of canopy photosynthesis: the introduction of additional effects of photosynthesis on fluorescence yield and PSII-PSI stoichiometry (red arrow) and the neglectance of the secon-order effects of re-emitted red light on photosynthetic processes.

5.3.1. The Farquhar model of photosynthesis

Leaf photosynthetic parameters are integrated over sunlit and shaded foliage and adjusted as a function of absorbed photosynthetically active radiation (*PPFD*), leaf temperature and CO_2 concentration at carboxylation sites (C_c).

After the mechanistic representation proposed by Farquhar *et al.* (Farquhar *et al.* 1980), which is now assumed as a standard, modeling the effects of CO_2 intercellular concentration and temperature on plant assimilation in C_3 species is a task that can be addressed with a good degree of confidence.

In the Farquhar's model, (1982) plant assimilation is assumed to be limited by either the rate of ribulose 1-5 biphosphate (Rubp) regeneration through the photosynthetic carbon reduction cycle, i.e. by light availability and electron transport rate, or by the capacity of the enzyme Rubp carboxylase-oxygenase (Rubisco). According to these constraints, leaf net photosynthesis A can be expressed as:

$$A = V_c - 0.5 \cdot V_o - R_d = V_c \cdot \left(1 - \frac{0.5 \cdot O}{\tau \cdot C_c}\right) - R_d \qquad \text{(Eq. 5-8)}$$

where V_c and V_o are rates of carboxylation and oxygenation of Rubisco, R_d is leaf dark respiration, τ is a specificity factor for Rubisco and O and C_c are the partial pressures of O_2 and CO_2 in equilibrium with their dissolved concentrations at the site of oxygenation and carboxylation.

The rate of carboxylation is assumed to be limited alternatively by two co-occurring processes:

$$V_c = \min\left\{W_c, W_j\right\} \qquad \text{(Eq. 5-9)}$$

where W_c is the rate of carboxylation limited solely by the amount, activation state and kinetic properties of Rubisco and obeys Michaelis-Menten kinetics with two competing substrates, O_2 and CO_2:

$$W_c = \frac{V_{c\,max} \cdot C_c}{C_c + K_c \cdot \left(1 + \frac{O}{K_o}\right)} \qquad \text{(Eq. 5-10)}$$

Here V_{cmax} is maximum carboxylation rate and K_c and K_o are Michaelis-Menten constants for carboxylation and oxygenation, respectively.

The rate of carboxylation limited solely by the rate of Rubisco regeneration in the Calvin cycle (W_j) is a function of the rate of electron transport J:

$$W_j = \frac{J \cdot C_c}{4 \cdot \left(C_c + O/\tau\right)} \qquad \text{(Eq. 5-11)}$$

A more detailed presentation of the Farquhar photosynthesis model can be found in Chapter 3.2.1.

The response of electron transport rate (J) to absorbed irradiance is represented by a non-quadratic hyperbola (Farquhar *et al.* 1984).

Unique relationships can be used to estimate the dependence of Farquhar's photosynthetic parameters (electron transport rate, Rubisco activity, dark respiration rate) on nitrogen content per unit leaf area in a large number of species (Wullschleger 1993; Leuning 1997), resulting in particular in a strict linear proportionality between photosynthetic potentials associatedwith light and dark processes (J_{max} and V_{cmax}, respectively).

In a first version of the model no vertical changes in photosynthetic parameters across the canopy were assumed (see Table 5-1). In the final version of the model (SCOPE-D+ and SCOPE-I), a vertical exponential profile of leaf nitrogen over the canopy is assumed, parallel to the reduction in diffuse *PPFD*, and both dark respiration and maximum carboxylation rate are assumed to be proportional to leaf nitrogen across the canopy (Sands 1995).

5.3.2. Response of photosynthetic processes to temperature

In the latest versions of the SCOPE model (see Table 5-1) the response of photosynthetic rates upon leaf temperature is represented in detail. The representation of the instantaneous response is based on the detailed model proposed by Bernacchi *et al.* (2001; Bernacchi *et al.* 2003); a different response to temperature of maximum carboxylation rates and maximum electron transport rates is predicted by the model (see Figure 5-6), with important implications for the response to temperature of leaf fluorescence.

The acclimation of photosynthetic processes to seasonal temperatures is also represented using the empirical model proposed by Kattge and Knorr (Kattge *et al.* 2007), making it possible to account for different optimum temperatures among sites and species..

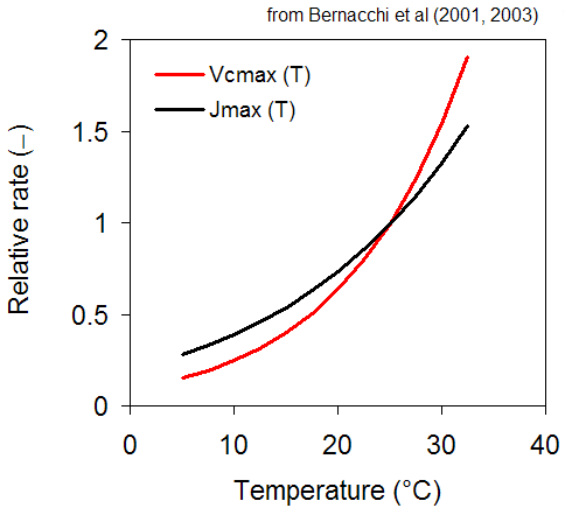

Figure 5-6. Results of a re-analysis of literature data for the overall variability and mutual relationship between the two parameters of the Leuning stomatal model (a1 and Do). The dataset comprises 54 values corresponding to 32 species,

5.3.3. Foliage respiration

The respiration of foliage is computed on a hourly basis as a function of instantaneous temperature, tissue biomass and nitrogen content, as suggested by Ryan (1991). The empirical model presented by Lloyd and Taylor (1994) is used to represent the dependence of tissue respiration upon temperature, instead of the more common Q_{10} approach, to account for the often observed shift in Q_{10} with temperature (Breymeyer *et al.* 1996).

Given the focus of the model on gross primary production (the only component of vegetation C balance directly related to fluorescence and reflectance), neither sapwood or fine root nor soil respiration are currently represented in the model.

5.3.4. Stomatal conductance and transpiration

A full description of the response of leaf gas exchange to environmental factors requires an understanding of the parallel response of stomata, which determines the concentration of CO_2 in the leaf intercellular spaces and sets transpiration rates.

In a first version of the SCOPE model (SCOPE-D, applied e.g. in the LHOAT sensitivity analysis, see below) the gas exchange response to the environment has been based on the optimality approach first proposed by Cowan (1977): the hypothesis is made that transpiration, which comes with stomatal opening, represents a cost for the plant, and that stomata are regulated in such a way as to balance such a cost with the advantage of increased photosynthesis. Such a goal-seeking approach has indeed successfully predicted leaf gas exchange under present environmental conditions (Berninger *et al.* 1996; Hari *et al.* 2000), although Thomas *et al.* (Thomas *et al.* 1999) warned that stomatal optimization was only partial in a number of tropical species. It should be noted, moreover, that existing analytical solutions to the problem of gas exchange optimisation are based on the assumption of a linear response of assimilation to intercellular CO_2 concentration, which runs contrary both to detailed photosynthetic models and to a large body of experimental evidence. Such an assumption could lead to considerable errors when applied to the prediction of plant response to climate change. Friend (Friend 1991), on the other hand, resorted to numerical means to couple a model of optimal stomatal behaviour to the Farquhar model of photosynthesis, so predicting in a convenient way the saturating response of assimilation to elevated CO_2, as well as the maintenance of the ratio of

intercellular to ambient CO_2 concentrations under a wide range of C_a and environmental conditions that is the basis of the semi-empirical models described below. One would therefore expect these empirical models to imply a quasi-optimal stomatal response, and the two approaches used in the SCOPE model to yield identical results.

The semi-empirical models proposed by Ball *et al*. (Ball *et al*. 1987) and Leuning (1995) are currently most commonly applied for the representation of stomatal dynamics. The two models differ only in their representation of the effects of air humidity, but both assume that the stomatal response to CO2 is mediated by photosynthetic rates, in agreement with experimental evidence (Wong *et al*. 1979). A comparison of the Ball-Berry and Leuning models for their suitability to incorporate a soil water stress function in their formulation and for their performance in modeling forest ecosystem fluxes is provided by Van-Wijk *et al*. (van Wijk *et al*. 2000).

In the latest versions of the SCOPE model (SCOPE-D+ and SCOPE-I), the dependence of stomatal conductance upon assimilation and air vapour pressure deficit is captured by the Leuning (1995) model, which predicts that the linear relationship between stomatal conductance and photosynthesis is modulated by air vapour pressure deficit:

$$g_s^c = \mathrm{a}_1 \cdot \frac{A}{c_a - \Gamma} \cdot \frac{D_0}{D + D_0} \qquad \text{(Eq. 5-12)}$$

where Γ is the CO_2 compensation point and a_1 and D_0 are empirical coefficients.

Leaf transpiration can be therefore expressed as:

$$E \approx 1.6 \cdot \mathrm{a}_1 \cdot \frac{A}{P \cdot \left(c_a - \Gamma\right)} \cdot \frac{D_0 \cdot D}{D + D_0} \qquad \text{(Eq. 5-13)}$$

A simple linear dependence of stomatal conductance upon soil water potential is assumed. A simple pedotransfer function is applied for the representation of the dependence of soil water potential upon soil water content, based on measured soil texture and bulk density (Campbell1985).

A re-analysis of available literature provided a realistic range of values for the two stomatal parameters a1 and Do and of their mutual relationship, as well as specific values to be applied at the three test sites (Figure 5-7).

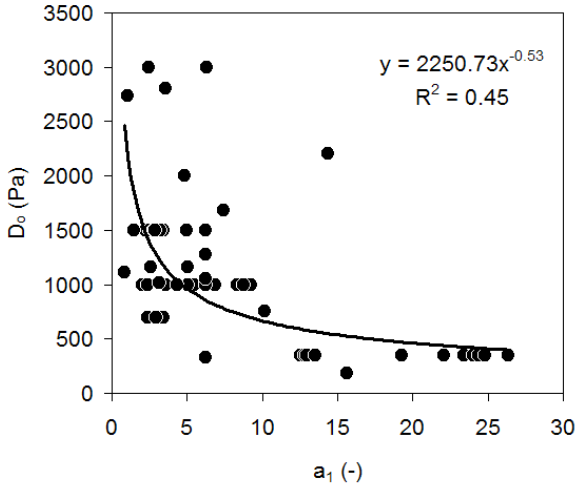

Figure 5-7. Results of a re-analysis of literature data for the overall variability and mutual relationship between the two parameters of the Leuning stomatal model (a1 and Do). The dataset comprises 54 values corresponding to 32 species, including those represented at the three test sites.

5.3.5. Representation of leaf-level fluorescence

Two alternative leaf-level models of solar-induced fluorescence and its relationship with photosynthetic processes have been implemented in the model, since available experimental information at the leaf level does not appear sufficient to discriminate between the two models with a sufficient degree of confidence. The two leaf-level models have been described in detail elsewhere. The version of the SCOPE model implementing the van der Tol - Verhoef - Rosema model (van der Tol *et al.* 2008) will be henceforth referred to as SCOPE-D (for Dutch), whilst the version implementing the Magnani leaf-level model will be referred to as SCOPE-I (for Italian).

In addition, two different versions of the SCOPE-D model have been applied, which differ in the representation of photosynthetic processes and their response to environmental factors. The latest version of the SCOPE-D model, implementing the best available information on leaf-level and canopy processes, will be referred to as SCOPE-D+

A summary of key version characteristics and differences is presented in Table 5-1 below.

Table 5-1. Summary of the main differences among the versions of the SCOPE model applied in the project

	SCOPE-D	SCOPE-D+	SCOPE-I
Temperature effects on photosynthesis	Not considered	Bernacchi *et al.* 2001, 2003	Bernacchi *et al.* 2001, 2003
Photosynthetic acclimation to temperature	Not considered	Kattge and Knorr 2007	Kattge and Knorr 2007
Stomatal conductance	Cowan 1977	Leuning 1995	Leuning 1995
Vertical profiles in photosynthetic potential	Not considered	Exponential (Sands 1995)	Exponential (Sands 1995)
Leaf-level fluorescence	Van der Tol-Verhoef-Rosema model	Van der Tol-Verhoef-Rosema model	Magnani model

5.3.6. Ancillary changes

A new parameterization of the aerodynamic conductances was introduced in order to avoid some problems of convergence in the cases of stable atmospheric conditions (in case of non convergence, wrong results were generated). This problem was recurrent in SCOPE (as usual in other turbulent transfer - energy balance model and SVAT models). Some preliminary tests showed that the problem was in the computation of the aerodynamic resistances. Few bugs were first corrected (i.e. bad transcription of the theoretical expressions of the aerodynamic resistances in the script) and new parameterizations of the aerodynamic conductances were then implemented within the model in order to account for stable and very stable aerodynamic conditions (we used here the classical stability functions given in Brutsaert (1982)). Further, a minimum value of 0.15m.s^{-1} for the friction velocity had to be considered. This threshold value was manually tuned in order to reduce the last recurrent problems of convergence.

A second series of improvements concerned the description of the physical processes in the soil. First, a new parameterization of the thermal soil inertia was introduced, because the original formulation provided unrealistic values in the case of dry soil conditions. The new formulation, proposed by van de Griend and O'Neil (1986), is currently used on the experimental crane site at Avignon. It was expressed as:

$$\Gamma = \quad 3516 \cdot \theta_{0-5} + 841 \qquad \text{(Eq. 5-14)}$$

where Γ is the thermal inertia and $\theta_{0\text{-}5}$ the water content in the five first centimetres of soil ($m^3.m^{-3}$). Moreover, in SCOPE, the soil surface resistance to vapour transfer was assumed to be constant. Such an assumption appeared to be unrealistic for studying long temporal series, especially if frequent variations of the soil moisture occurred. It would also cause wrong determination of the searched parameters, and in particular λ. This parameter is related to plant transpiration and its estimation from evapotranspiration measurements required realistic calculations of soil surface evaporation (which depends on soil surface resistance). We decided to use the equation proposed by Olioso (1992) which was fitted on simulations for a similar soil type performed with a detailed soil water transfer model (based on Richard's equations accounting for coupled heat and water transfer and for vapour transfers in the soil top layers):

$$r_{ss} = 1.439.10^5 \left(\theta_{sat} - \theta_{0-5}\right) \qquad \text{(Eq. 5-15)}$$

where r_{ss} was the soil surface resistance ($s.m^{-1}$) and θ_{sat} was the soil water content at saturation ($m^3.m^{-3}$).

The two above modifications required to input the soil surface moisture as a different variable as the moisture of the rest of the soil (soil moisture was considered as a whole before).

5.4. Integration of solar-induced fluorescence over the canopy

Fluorescence from single leaves can be calculated if the incident fluxes over the PAR region (400 – 700 nm) are known. In addition, two excitation-fluorescence matrices (EF-matrices) must be given to represent fluorescence from both sides of the leaf. It is also assumed that a leaf level photosynthesis-fluorescence model gives the relative amount of fluorescence depending on PAR light level, temperature and the energy balance (a Farquhar-Cowan-Rosema type of model, Van der Tol *et al.*, 2007, submitted to AFM).

Absorbed PAR light can be calculated by integrating incident radiation over the PAR wavelength range as follows:

$$E_{\text{apsun}} = \int_{400}^{700} E_{\text{sun}}(\lambda)[1-\rho(\lambda)-t(\lambda)]\,\mathrm{d}\lambda$$

$$E_{\text{apsh}}(x) = \int_{400}^{700} [E^{-}(x,\lambda)+E^{+}(x,\lambda)][1-\rho(\lambda)-t(\lambda)]\,\mathrm{d}\lambda$$

The second expression can be used directly to obtain the absorbed PAR radiation by leaves in the shade. For leaves in the sun, also their orientation must be taken into account, and one so obtains:

$$E_{\text{apsu}}(x,\theta_\ell,\varphi_\ell) = |f_s| E_{\text{apsun}} + E_{\text{apsh}}(x)$$

Application of the photosynthesis-fluorescence model gives fluorescence amplification factors $g_{su}(x,\theta_\ell,\varphi_\ell)$ and $g_{sh}(x)$ for leaves in the sun and in the shade, respectively, that should be treated as correction factors applied to the EF-matrices, which determine the spectral distribution of the fluorescent flux. The EF-matrices are symbolised as $\Phi(\lambda_e,\lambda_f)$ and $\Phi'(\lambda_e,\lambda_f)$ for backward and forward fluorescence, respectively.

For the fluorescent radiance response to incident light for leaves in the sun with a particular orientation one can write

$$\pi L_{\ell su}^{f}(x,\lambda_f,\theta_\ell,\varphi_\ell) = g_{su}(x,\theta_\ell,\varphi_\ell)\int_{400}^{750}\begin{bmatrix} w_f(\lambda_e,\lambda_f,\theta_\ell,\varphi_\ell)E_{\text{sun}}(\lambda_e) \\ +v_f(\lambda_e,\lambda_f,\theta_\ell,\varphi_\ell)E^{-}(x,\lambda_e) \\ +v'_f(\lambda_e,\lambda_f,\theta_\ell,\varphi_\ell)E^{+}(x,\lambda_e)\end{bmatrix}\mathrm{d}\lambda_e \qquad \text{(Eq. 5-16)}$$

Here it was assumed that the range of excitation wavelengths is from 400 to 750 nm. The coefficients are defined by analogy with Eqs. (11) and are given by

$$v_f(\lambda_e,\lambda_f,\theta_\ell,\varphi_\ell) = |f_o|\frac{\Phi(\lambda_e,\lambda_f)+\Phi'(\lambda_e,\lambda_f)}{2} + f_o\frac{\Phi(\lambda_e,\lambda_f)-\Phi'(\lambda_e,\lambda_f)}{2}\cos\theta_\ell$$

$$v'_f(\lambda_e,\lambda_f,\theta_\ell,\varphi_\ell) = |f_o|\frac{\Phi(\lambda_e,\lambda_f)+\Phi'(\lambda_e,\lambda_f)}{2} - f_o\frac{\Phi(\lambda_e,\lambda_f)-\Phi'(\lambda_e,\lambda_f)}{2}\cos\theta_\ell$$

$$w_f(\lambda_e,\lambda_f,\theta_\ell,\varphi_\ell) = |f_s f_o|\frac{\Phi(\lambda_e,\lambda_f)+\Phi'(\lambda_e,\lambda_f)}{2} + f_s f_o\frac{\Phi(\lambda_e,\lambda_f)-\Phi'(\lambda_e,\lambda_f)}{2}$$

For leaves in the shade the fluorescent radiance can be described by

$$\pi L_{\ell sh}^{f}(x,\lambda_f) = g_{sh}(x)\int_{400}^{750}[v_f(\lambda_e,\lambda_f)E^{-}(x,\lambda_e)+v'_f(\lambda_e,\lambda_f)E^{+}(x,\lambda_e)]\mathrm{d}\lambda_e, \qquad \text{(Eq. 5-17)}$$

where both fluorescent scattering coefficients are supposed to have been obtained by weighted averaging over all leaf orientations, i.e.

$$v_f(\lambda_e,\lambda_f) = \frac{1}{36}\sum_{13\,\theta_\ell} f(\theta_\ell)\sum_{36\,\varphi_\ell} v_f(\lambda_e,\lambda_f,\theta_\ell,\varphi_\ell)$$

$$v'_f(\lambda_e,\lambda_f) = \frac{1}{36}\sum_{13\,\theta_\ell} f(\theta_\ell)\sum_{36\,\varphi_\ell} v'_f(\lambda_e,\lambda_f,\theta_\ell,\varphi_\ell)$$

The total top-of-canopy fluorescent radiance is now obtained by a summation over all layers and orientations, taking into account the probabilities of viewing sunlit and shaded components.

This gives

$$\pi L_f^{\text{TOC}} = \frac{\text{LAI}}{60}\sum_{60\,x}\left[\frac{P_{so}(x)}{36}\sum_{13\,\theta_\ell} f(\theta_\ell)\sum_{36\,\varphi_\ell}\pi L_{\ell su}^{f}(x,\lambda_f,\theta_\ell,\varphi_\ell)+[P_o(x)-P_{so}(x)]\pi L_{\ell sh}^{f}(x,\lambda_f)\right]$$

6. MODELLING FLUORESCENCE AT CANOPY SCALE: SIMULATION RESULTS

In order to explore conveniently the expected fluorescence radiance from plant canopies and its response to photosynthesis and environmental factors, a range of simulations have been carried out as part of the project. Reference has been made to three different sites, each representative of a different vegetation type, for which estimates of vegetation gross primary production were available, as derived from eddy-covariance measurements.

The seasonal dynamics of canopy fluorescence radiance and gross primary production have been modelled at each site for one reference year, using different versions of the SCOPE model for a comparison.

Moreover, a detailed model sensitivity analysis based on the LHOAT procedure has been carried out using one version of the model (SCOPE-D). A simpler sensitivity analysis has been carried out using the SCOPE-D+ and SCOPE-I versions of the model.

The results of a detailed calibration of the SCOPE-D model on one of the available datasets are also presented, which provided useful preliminary information for the LHOAT sensitivity analysis, as well as for the further refinement of the model into the later SCOPE-D+ and SCOPE-I versions.

Differences between model versions have already been described (see Chapter 5.3 and Table 6-1 therein). The use of different versions of the SCOPE model are due to the present lack of a definitive knowledge about the best representation of leaf-level fluorescence (van der Tol – Verhoef – Rosema model, as implemented in SCOPE-D and SCOPE-D+, or Magnani model as implemented in SCOPE-I) and to the continuous refinement in the representation of gas exchange processes over the course of the project. The latest versions of the SCOPE model are thought to implement the best available representation of ecophysiological processes at leaf and canopy scale.

A summary of the model version applied in each modelling exercise can be found in the following table.

Table 6-1. Differences between model versions

Modelling exercise	Model version
Preliminary model calibration	SCOPE-D
LHOAT sensitivity analysis	SCOPE-D
Simple sensitivity analysis	SCOPE-D+ SCOPE-I
Simulation for three vegetation functional types	SCOPE-D+ SCOPE-I

6.1. Description of test sites

In order to explore its predictions over a wide range of conditions, the SCOPE canopy model described above has been applied at three experimental sites, representative of the three main vegetation types in Europe:

- a maritime pine (*Pinus pinaster* Ait.) forest canopy in San Rossore, Italy, representative of evergreen coniferous forests;

- a mixed forest in Nonantola, Italy, dominated by pedunculate oak (*Quercus robur* L.) and ash (*Fraxinus* spp.) and representative of deciduous broeadleaf forests;
- a winter wheat (*Triticum aestivum* L.) crop in Avignon, France, representative of C_3 agricultural crops.

Additional details on the three sites are provided in Table 6-2.

Table 6-2. Description of site and canopy characteristics at the three test sites. Age refers at plant age at the time of measurements. Reference is made to classes in the LPJ dynamic vegetation model (Stitch *et al.* 2003; Jung *et al.* 2008) for the identification of plant functional types

		San Rossore	Nonantola	Avignon
Latitude		43°43' N	44°41' N	43°55' N
Longitude		10°20' E	11°02' E	4°53' E
Main (ancillary) species		*Pinus pinaster* Ait. (*Pinus pinea* L.)	*Quercus robur* L. *Fraxinus* spp.	*Triticum aestivum* L.
Age (years)		47	10	annual
Plant functional type		Temperate needle-leaved evergreen	Temperate broad-leaved summergreen	Cropland (C_3)
Mean annual temperature (°C)		14.8	13.7	16.0
Annual precipitation (mm yr^{-1})		932	750	700 (+ 20 mm irrigation)
Soil texture (%)	sand Silt	95 4	6 36	15 51

At each site, canopy C, water and sensible heat fluxes are being measured by the eddy-covariance technique (Aubinet *et al.* 2000), together with key meteorological and environmental parameters required for SCOPE simulations (Table 6-3).

Detailed data are also available at each site about the seasonal development of key plant variables (leaf area index, leaf chlorophyll content and photosynthetic potential, V_{cmax}) needed for a proper parameterisation of the model.

Canopy GPP and TOC fluorescence have been simulated for an entire vegetative period at each site, so exploring a wide interval of environmental conditions. Target years with a complete dataset of environmental, eddy-covariance and ancillary records were selected, so as to avoid the confounding effects of gap-filling. In particular, canopy function at the San Rossore site was simulated over the course of 2003, a particularly hot and dry year throughout Europe (Ciais *et al.* 2005). Canopy processes were simulated for the year 2002 in Nonantola and 2006 in Avignon.

Experimental data of TOC fluorescence are currently being acquired as part of companion ESA projects, but the processed dataset is not yet available for a proper validation of the SCOPE model. No fluorescence data were therefore available at any of the test sites considered in the analysis. However, the model was calibrated against available gross primary production (GPP) data derived from eddy covariance measurements, so as to ensure the greatest possible degree of reality given our understanding of leaf-level processes.

Canopy GPP was derived from measured net C ecosystem fluxes using the procedure described by Reichstein *et al.* (Reichstein *et al.* 2005).

Table 6-3. Description of environmental and plant variables used as an input to the SCOPE model, and corresponding units. Also specified is the temporal resolution of individual input datasets. A constant site-specific value of maximum carboxylation rate and leaf chlorophyll content can be used if daily values are not available.

Files with 1-column, representing the data at time 't' (1/2 hourly)			
Name of file	**Description**	**Unit**	**Required**
CO2	Carbon dioxide concentration at height z	µmol m^{-3}	yes
ea	Air vapour pressure at height z	hPa	yes
p	Air pressure	hPa	yes
Rin	Incoming shortwave radiation (0.3-2.5 µm)	W m^{-2}	yes
Rli	Incoming longwave radiation (2.5-50 µm)	W m^{-2}	yes
SMC	Soil moisture content, volume fraction	-	yes
t	Decimal Julian day of the year	-	yes
Ta	Air temperature at height z	°C	yes
u	Wind speed at height z	m s^{-1}	yes
year	Year (Julian calendar)	-	yes
Tabular files, containing 1 column with julian day, second column with corresponding data (daily)			
Name of file	**Description**	**Unit**	**Required**
z	Measurement height of meteorological parameters	M	yes
Table_hc	Canopy height	M	yes
Table_LAI	One-sided leaf area index	m^2 m^{-2}	yes
Vcmo	Maximum carboxylation rate	µmol m^{-2} s^{-1}	no
Chl	Chlorophyll content	mg m^{-2}	no

6.2. Seasonal dynamics of GPP and SIF

A formal sensitivity analysis of the SCOPE model was performed using the LHOAT method which made it possible to analyze at the same time the global sensitivity of output variables over the whole space of input parameters and more local sensitivity by looking at specific zone in the parameter space. The method provided a clear framework for the ranking of the more influential parameters.

Additional information on the sensitivity of the model was also obtained by means of simple simulations along the crop cycle following several input parameters scenarios based on simulations by the ISBA-A-gs model and measurements.

Before implementing the sensitivity analysis, in order to test the model and to have information on the variation of some of the most important input parameters, a calibration of SCOPE was performed on the wheat dataset in Avignon. This was an important step for the understanding of the model and the setting of the sensitivity analysis.

The work presented here was done using the latest version of the SCOPE model developed at ITC by Christiaan van der Tol (SCOPE-D). This version was made available mid-September 2008 in its present version, which did not provide enough time for performing all the required analysis, nor the possibility to have a deep interpretation of the results.

The implementation of a LHOAT sensitivity analysis on the SCOPE versions developed at UNIBO (termed SCOPE-D+ and SCOPE-I) was also foreseen, but this version was not delivered in time and only a simple sensitivity analysis was carried out as presented below.

Due to the limited available time, the analyses were performed on the sole wheat dataset in Avignon.

6.2.1. SCOPE-D calibration

Before implementing the sensitivity analysis, in order to test the model and to have information on the variation of some of the most important input parameters an intensive calibration of the SCOPE-D version was performed over the wheat dataset in Avignon. For our purpose, only two parameters were retrieved, the maximal carboxylation capacity (*Vcmo*) and the marginal cost of assimilation (λ)

In this exercise, the calibration was performed by comparing simulated evapotranspiration and CO_2 fluxes to the measurements. The calibration process was performed for 70 individual days over the wheat crop cycle allowing catching the time evolution of the parameters.

6.2.1.1. Implementation of the calibration method

Driving variables required as input of SCOPE related to half hourly climate forcing and were derived from the micrometeorological dataset (Incident solar and longwave radiations, Air temperature, Specific air humidity, Wind speed, Atmospheric CO_2 concentration, Atmospheric pressure).

The calibration of the SCOPE model was performed using the automatic optimization "fminsearch" procedure, proposed in the MATLAB optimization toolbox. It is a multidimensional unconstrained non linear minimization procedure, based on the Simplex algorithm (Nelder & Mead, 1965). For our purpose, only two parameters were retained in the calibration procedure: the maximal carboxylation capacity (*Vcmo*) and the marginal cost of assimilation (λ). These two parameters were chosen because

I. from bibliographic knowledge, they were supposed to have a large influence on photosynthesis and transpiration processes (this was confirmed by the first tests of sensitivity analysis performed on SCOPE),

II. the possibility to prescribe these parameters from other source of information was limited (it might be possible to do it for *Vcmo* from leaf nitrogen content, but this relied on few experimental results and more experimental evidence was still required; it was almost impossible to set values for λ since its behaviour toward possible determinants was not yet well understood),

III. a larger number of parameters to retrieve would have requested a very large computer time (at present the calibration for the two parameters and one day of simulation required around two hours). In this exercise, the calibration was performed by comparing simulated evapotranspiration and CO_2 fluxes to the measurements presented above.

The calibration process was performed independently for 70 different days over the wheat crop cycle for which a significant number of measured data of both evapotranspiration and CO_2 flux were available. This allowed catching the time evolution of the searched parameters. The calibration was not performed in winter because the retrieval process was impaired by the low parameter sensitivity due to the low level of the fluxes and by the low atmospheric instability that may generate ill-convergence in the turbulent transfer calculations. For similar reason night data were discarded.

The cost function to be minimised was the mean of the two relative root mean square errors calculated between the model and the observed variables with:

$$F(\theta) = \frac{1}{2}\cdot\left(\frac{\frac{1}{N_A}\cdot\sqrt{\sum_{t=1}^{N_A}\left(A_{C\,\mathrm{mod}}(\theta,t)-A_{C\,obs}(t)\right)^2}}{\overline{A_{C\,obs}}} + \frac{\frac{1}{N_{LE}}\cdot\sqrt{\sum_{t=1}^{N_{LE}}\left(LE_{\mathrm{mod}}(\theta,t)-LE_{obs}(t)\right)^2}}{\overline{LE_{obs}}}\right)$$

(Eq.6-1)

where $F(\theta)$ is the cost-function evaluated for a candidate set of input parameters $\theta = \{Vcmo, \lambda\}$, A_{Cobs} and LE_{obs} respectively the observed net ecosystem exchange of CO_2 and the evapotranspiration flux, A_{Cmod} and LE_{mod} are respectively the modelled net ecosystem exchange of CO_2 and the modelled evapotranspiration flux, and N_A and N_{LE} the numbers of available daily observations A_{obs} and LE_{obs}, respectively. The two right terms in the cost function were normalized using the mean of the observations in order to give them a similar weight in the calculation.

Table 6-4. List of the main SCOPE input parameters. Two parameters were retrieved during the calibration process (Vcmo and λ).

Name	Description	Units	Status/origin	Range/value
Vcmo	**Maximum carboxylation capacity**	$\mu molCO_2.m^{-2}.s^{-1}$	**calibrated**	**results in Figure 6-2**
C_{ab}	Leaf chlorophyll content	$\mu g.cm^{-2}$	prescribed	**60**
LAI	**Leaf area index**	$m^2.m^{-2}$	**measured**	**Figure A- 3**
λ	**Marginal cost of assimilation**	-	**calibrated**	**Figure 6-3**
Jmo	**Maximum electron transport rate**	$\mu molCO_2.m^{-2}.s^{-1}$	**calculated**	**2.65 * *Vcmo***
θ	**Soil moisture content (root zone)**	$m^3.m^{-3}$	**measured**	**results in Figure A- 3**
θ0-5	**Surface soil moisture content (0-5 cm)**	$m^3.m^{-3}$	**measured**	
θ_{sat}	Soil moisture content at saturation (soil)	$m^3.m^{-3}$	prescribed	0.48
gcmin	Minimum stomatal conductance (biochemical)	$m.s^{-1}$	prescribed	$1e^{-6}$
Rdopt	Dark respiration rate at 25°C (biochemical)	$\mu molCO_2.m^{-2}.s^{-1}$	prescribed	0.5
C_{dm}	Leaf dry matter content	$g.cm^{-2}$	prescribed	0.012
C_w	Leaf water equivalent thickness	cm	prescribed	0.009
N	Leaf structure parameter	-	prescribed	1.4

6.2.2. Description of the LHOAT sensitivity analysis method

The objective of the sensitivity analysis is to evaluate the potential of the SIF to track the main surface processes, in comparison to the others spectral domains. Toward this objective, we have decided to analyse the impacts of the first order parameters which are classically known to be involved in the biochemical processes. Moreover, the possibility to implement sensitivity analysis depends on the available computing time and on the assurance that models won't generate errors (convergence) during the process of simulation. SCOPE being highly non-linear and computationally expensive and always in a development phase, a simple sensitivity analysis approach has been implemented within the SCOPE model. This approach, called LH-OAT, has been developed at the University of Tucson in Arizona (Ann van Griensven and Tom Meixner, 2005). It is an evolution of the classical OAT approach (Morris 1991). The advantage of the LH-OAT method is that it combines

- the robustness of the "Latin-Hypercube" (LH) sampling, which ensures that the full range of all parameters has been sampled;
- with the precision of an "One-factor-at-a-time" OAT method, assuring that the changes in the output in each model run can be unambiguously attributed to the input parameter changed in such a simulation;
- in addition this combination leads to an efficient sensitivity analysis method because of the few model runs required (Francos *et al.*, 2001; van Griensven *et al.*, 2002).

Latin-Hypercube Simulations (LH): The concept of the LH simulation (McKay, 1988) is based on the Monte-Carlo simulation but uses a stratified sampling approach that allows efficient estimation of the output statistics. Upper and lower limits for each parameter are established based on the users experience with a given model and from the literature. The LH subdivides the distribution (range) of each parameter into several N segments, each with a probability of occurrence equal to 1/N. Random values for each parameter were generated such that each of the N segments is sampled once.

One-factor-At-a-Time (OAT) Method: The LH samples are then used as initial points for the OAT procedure. The OAT method as proposed by Morris (1991) is an example of an integration of local and global sensitivity analysis methods (also called multi local). As in local methods, each run has only one parameter changed, so the changes in the output in each model run can be unambiguously attributed to the input parameter changed.

The method operates by loops. Each loop starts with a Latin Hypercube point (Figure 6-1). Around each Latin Hypercube point *j*, a partial effect $S_{i,j}$ for each parameter e_i is calculated as (in percentage):

$$S_{i,j} = \left| \frac{100 * \left(\frac{M(e_1,...,e_i*(1+f_i),...,e_P) - M(e_1,...,e_i,...,e_P)}{\left[M(e_1,...,e_i*(1+f_i),...,e_P) + M(e_1,...,e_i,...,e_P) \right]/2} \right)}{f_i} \right| \qquad \textbf{(Eq 6-2)}$$

where *M(.)* refers to the model functions, f_i is the fraction by which the parameter e_i is changed (a predefined constant) and *j* refers to a LH point. In equation 4, the parameter was increased with the fraction f_i, but it can also be decreased since the sign of the change is defined randomly. Therefore a loop requires P+1 runs and the whole approach requires a total of $N^P*(P+1)$ runs. If few parameters are considered, it is efficient.

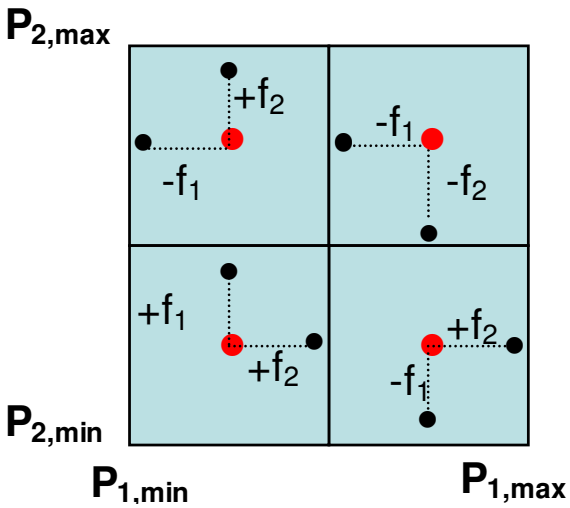

Figure 6-1. Illustration of the LH-OAT sampling, considering both two parameters (P1, P2) and two segments for the subdivision of the parameter uncertainty range. Each coloured point represents an OAT point for which a simulation run must be performed, and f1 and f2 represents the positive/negative variation associated to P1 and P2, respectively.

A final effect is calculated by averaging these partial effects of each loop for the all N^P points of the Latin Hypercube.

$$\overline{S_i} = \sum_{j=1}^{N \wedge P} S_{i,j} \Big/ N^P \qquad \textbf{(Eq 6-3)}$$

These final effects can be ranked with the largest effect being given rank 1 and the smallest effect being given a rank equal to the total number of parameters analysed. During a sensitivity analysis for a particular dataset some parameters may have no effect on model predictions or performance. In this case they are all given a rank equal to the number of parameters.

6.2.3. Implementation of the LHOAT method on SCOPE-D

The LH-OAT algorithm has been applied on SCOPE for various daily periods in order to analyse the range of the output variations as a function of the range of input variations for various environmental conditions (all other inputs are not varied). Four daily periods have been selected according to the availability of ground observations (Table 6-3).

For each of these periods, the model sensitivity has been studied in a two step procedure. First, the set of the SCOPE simulations performed has been analysed on various output variables in order to check the coherence of the last SCOPE version. Second, the partial effects provided have been computed using the LH-OAT algorithm (see Eq. 6-2 and Eq. 6-3) for the following variables: the fluorescence bands at 760 nm {*F760*} and 680nm {*F680*}, the carbon assimilation by photosynthesis {*A*}. Parameters which are involved in the computations of these processes have been isolated (Table 6-4). The major of those have been taken into account in the sensitivity analysis experiment as free parameters: the maximum carboxylation capacity (*Vcmo*), the leaf chlorophyll content (C_{ab}), the leaf area index (*LAI*) and the marginal cost of assimilation (*Lam* or λ). For each of them, large uncertainty ranges have been prescribed and 3 levels of subdivision of these ranges have been retained for the Latin Hypercube sampling of the LH-OAT algorithm. This implies that a set of 405 simulations has been performed for each studied cases, representing a whole night of simulation for an efficient computer. All the other input parameters have been prescribed to a fixed value, listed in Table 6-4; excepting the maximum electron transport rate (*Jmo*) for which two particular cases have been studied. On one hand, a link between this parameter and the maximum carboxylation capacity has

been established (*Jmo = 2.65 Vcmo*). This link is the same as the one used in the SCOPE-D+ and SCOPE-I versions. On the other hand, a constant value has been prescribed. In this study, the impact of the *Jmo* parameterization on the model response has been evaluated by comparing the model sensitivity for the DoY 118 using the one or the other *Jmo* formulation.

Table 6-5. List of the day of year for which the sensitivity analysis experiment has been performed

Day of year	Date	Description
32	01/02/2006	Winter day, very low vegetation, clear sky
71	12/03/2006	Beginning of spring, growing phase, clear sky
118	28/04/2006	Spring, LAI reaches its maximum, clear sky
140	20/05/2006	End of spring, senescent phase, presence of clouds

Table 6-6. List of the main SCOPE input parameters. 4 free parameters (Vcmo, Cab, LAI and Lam) have been sampled from large uncertainty ranges following the Latin Hypercube rules of the LH-OAT algorithm. Concerning Jmo, two alternatives have been investigated from either a relation between itself and Vcmo or either a fixed value All the others parameters have been prescribed to a fixed-typical value.

Name	Description	Units	Status	Range/value
Vcmo	Maximum carboxylation capacity	$\mu molCO_2.m^{-2}.s^{-1}$	free	10 - 160
C_{ab}	Leaf chlorophyll content	$\mu g.cm^{-2}$	free	10 – 100
LAI	Leaf area index	$m^2.m^{-2}$	free	1.0 – 5.0
Lam or λ	Marginal cost of assimilation	-	free	800 - 2000
Jmo	Maximum electron transport rate	$\mu molCO_2.m^{-2}.s^{-1}$	free	2.65.Vcmo
			fixed	120
θ	Soil moisture content (soil)	$m^3.m^{-3}$	prescribed	0.30
θ_{sat}	Soil moisture content at saturation (soil)	$m^3.m^{-3}$	prescribed	0.48
Gcmin	Minimum stomatal conductance (biochemical)	$m.s^{-1}$	prescribed	$1e^{-6}$
Rdopt	Dark respiration rate at 25°C (biochemical)	$\mu molCO_2.m^{-2}.s^{-1}$	prescribed	0.5
C_{dm}	Leaf dry matter content	$g.cm^{-2}$	prescribed	0.012
C_w	Leaf water equivalent thickness	cm	prescribed	0.009
N	Leaf structure parameter	-	prescribed	1.4

6.2.4. Simplified sensitivity analysis using SCOPE-D+ and SCOPE-I

A thorough sensitivity analysis, as described in the preceding paragraphs, could not be carried out for the latest versions of the SCOPE model, developed and tested in the last phases of the project, due to time constraints.

A simple sensitivity analysis was carried out, however, using a limited number of simulations.

The sensitivity of predicted gross primary production (GPP) and fluorescence radiance to key parameters and input variables was explored:

- maximum carboxylation rate (Vcmo) and maximum electron transport rate (Jmo), assumed as linearly related as described above;
- canopy leaf area index (LAI), affecting the total amount of light intercepted by the canopy;
- soil water content (SWC), determining the degree of stomatal limitations. Given the structure of the model, changing SWC is equivalent to a change in one of the parameters in the stomatal model (a_1 or the response to soil water or vapour pressure deficit, in the Leuning model, or the efficiency parameter λ in the Cowan model).

Based on a thorough analysis of the literature a realistic range of each parameter was defined (Vcmo = 20-180 μmol m^{-2} s^{-1}; LAI = 1-5 m^2 m^{-2}; SWC = 0.15-0.35 m^3 m^{-3}), and model simulations carried out for each of the resulting combination of parameters.

The partial effect of a step change in each parameter was computed as described above (Eq. 6-2) and the final effect over the full range of variation derived as from Eq. 6-3.

Simulations were carried out for a winter wheat (*Triticum aestivum*) crop, using meteorological data corresponding to one of the field campaigns of the ESA CEFLES-2 project in La Masquere, Bordeaux (FR), so as to make it possible to integrate the results with the resulting experimental results at canopy and landscape scale. In particular, data for 18 April, 2007 were used in the modelling exercise.

6.3. Results: LHOAT sensitivity analysis using SCOPE-D

6.3.1. SCOPE-D calibration

Figure 6-2 and Figure 6-3 present the evolution of *Vcmo* and λ as retrieved each day by the calibration procedure.

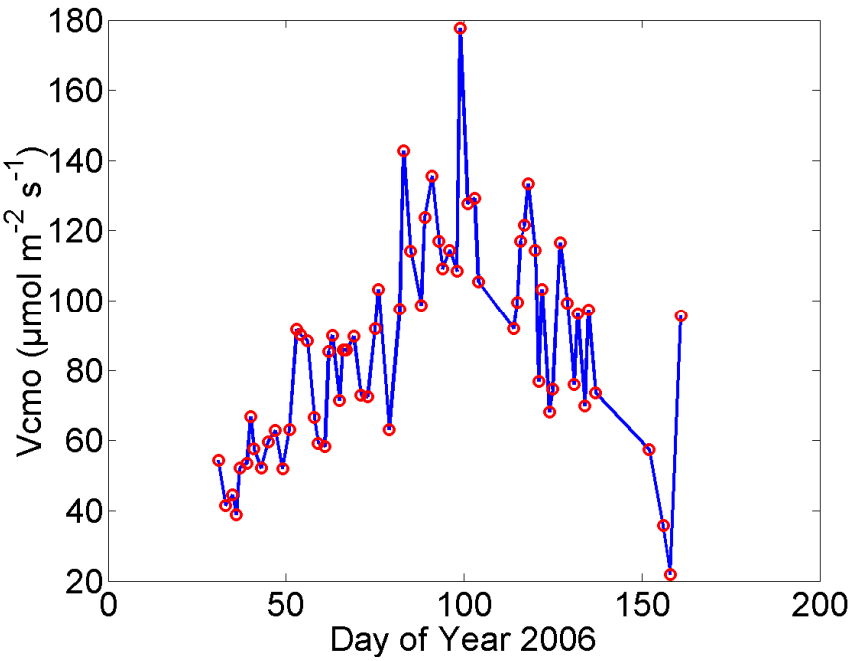

Figure 6-2. Time evolution of retrieved value of *Vcmo* over the wheat crop dataset in Avignon

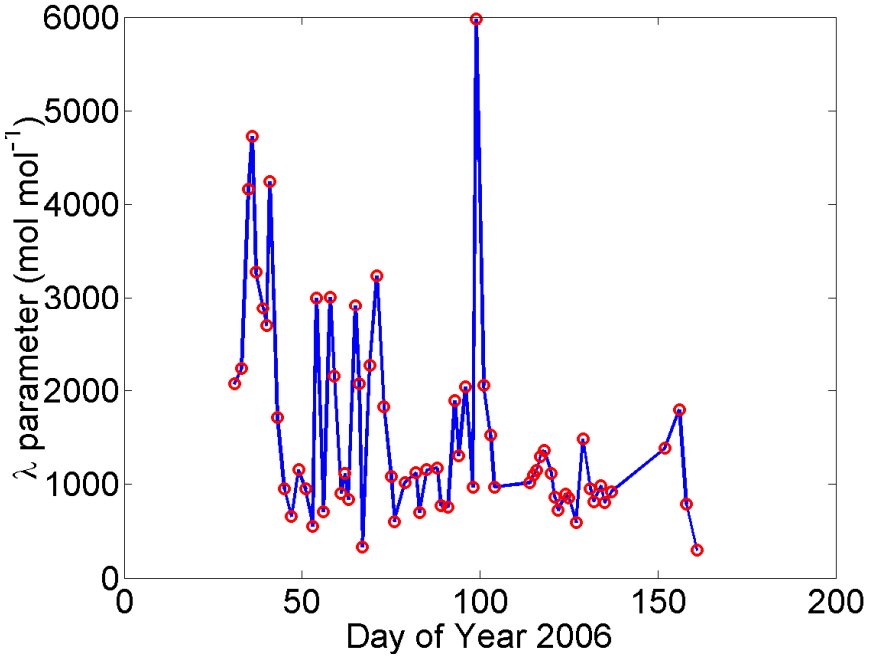

Figure 6-3. Time evolution of retrieved value of λ over the wheat crop dataset in Avignon.

Retrieved values of the maximum carboxylation capacity *Vcmo* were in the range of widely accepted values (Leuning *et al*. 1995, Leuning 2002, Medlyn *et al*. 2002, Xu and Baldocchi 2003, Bunce 2000...). It increased from winter (~40 µmol.m^{-2}.s^{-1}) to spring (~120 µmol.m^{-2}.s^{-1}), then decreased to summer (~40 µmol.m^{-2}.s^{-1}). This trend was not in agreement with the results obtained on wheat by Grossman-Clarke *et al*. (1999) with high values of *Vcmo* in winter (and no increase). The calculated *Vcmo* from the leaf nitrogen content also presented high values in winter before decreasing as nitrogen content decreased. Conversely, the trend in retrieved *Vcmo* was in agreement with the data presented by Xu and Baldocchi (2003) for an oak species. In our case, this trend seemed to be well correlated to LAI evolution or to canopy photosynthesis. A good linear relation can be derived between *Vcmo* and LAI (Figure 6-4). However, it was important to note that in the present Dutch version of the SCOPE model, no variation of *Vcmo* as a function of temperature was introduced. Several studies have shown that the influence of temperature was large (see Leuning 2002, Medlyn *et al*. 2002...) and a possible influence of low temperature in winter may have to be considered here. Figure 6-4 shows that a good correlation existed between the daily maximum temperature and *Vcmo* for wintertime (before DOY 95). Several studies have also shown that *Vcmo* decreases with soil drying and decrease in leaf nitrogen content (Xu and Baldocchi 2003, Grossman-Clarke *et al*. 1999, Wilson *et al*. 2000) both processes occurring in our dataset in spring.

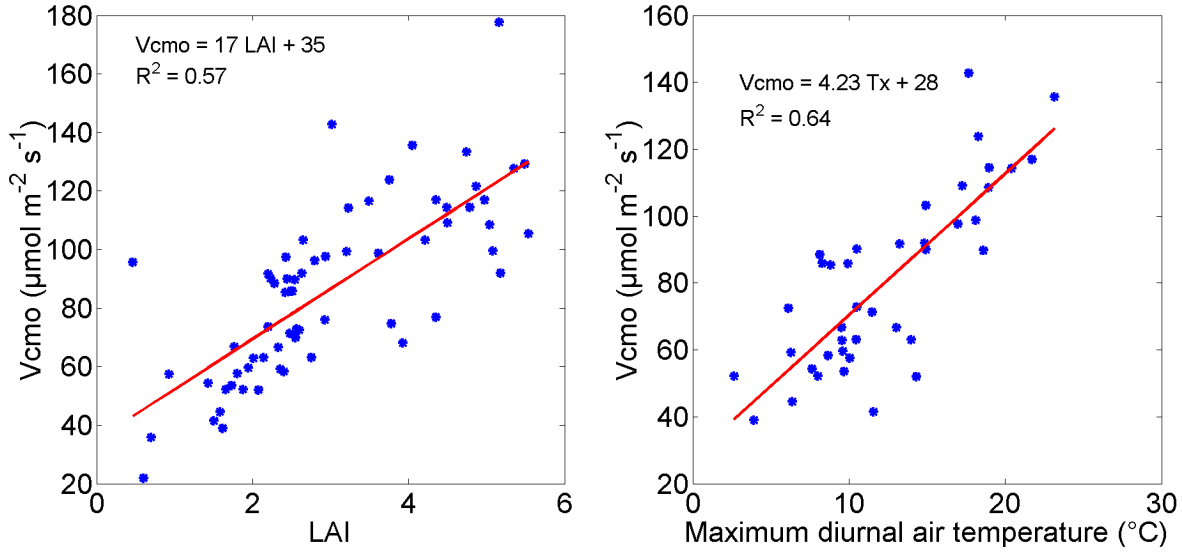

Figure 6-4. Relations between *Vcmo* and LAI (over the whole period) and maximum diurnal temperature (Tx) in winter.

Calibrated values of the marginal cost of assimilation λ were also in the expected range, even for the very high value close to 6000 (van der Tol *et al*. 2007, Lloyd and Farquhar 1994, Schymanski *et al*. 2008, Hall and Schulze 1980, Arneth *et al*. 2002, Thomas *et al*. 1999a and b). The global evolution of λ showed a general decrease during the year from around 3000 to 900 reaching a common value for herbaceous crops (with a high dispersion around the general trend). This evolution may be in agreement with the theoretical proposal by Cowan (1977) that λ should decline under water limiting conditions. The studies by Hall and Schulze (1980), Arneth *et al*. (2002), Thomas *et al*. (1999b) confirmed this decline experimentally. However, if such decline may be seen in Figure 6-5 where λ was plotted as a function of soil moisture, a maybe more obvious decline appeared when λ was plotted against net radiation. Decline of λ at low radiation was evocated by Hall and Schulze (1980) and discussed from experimental data by Thomas *et al*. (1999b).

It should be noted also that the calibration process may be difficult in conditions with low available energy because the sensitivity to the retrieved parameter can drop. Parameter values obtained in such conditions have to be considered with more cautions. This was particularly the case for DoY 99 with very high values both for *Vcmo* (~180 µmol.m^{-2}.s^{-1}) and λ (~6000). The calibration processes may also be difficult when the canopy was not fully covering the ground since *–i)* the calibration variables (measure latent heat flux and CO_2 flux) were less sensitive to the parameters, which affected only the vegetation flux, and *–ii)* the soil parts of the calibration variables (soil evaporation and CO_2 efflux) may be not described accurately enough.

However, SCOPE calibration results were very positive in the sense that calibrated parameters have a behaviour in agreement with previous knowledge. It is a significant indication for evaluating the quality of the model (for energy, water and CO_2.transferts).

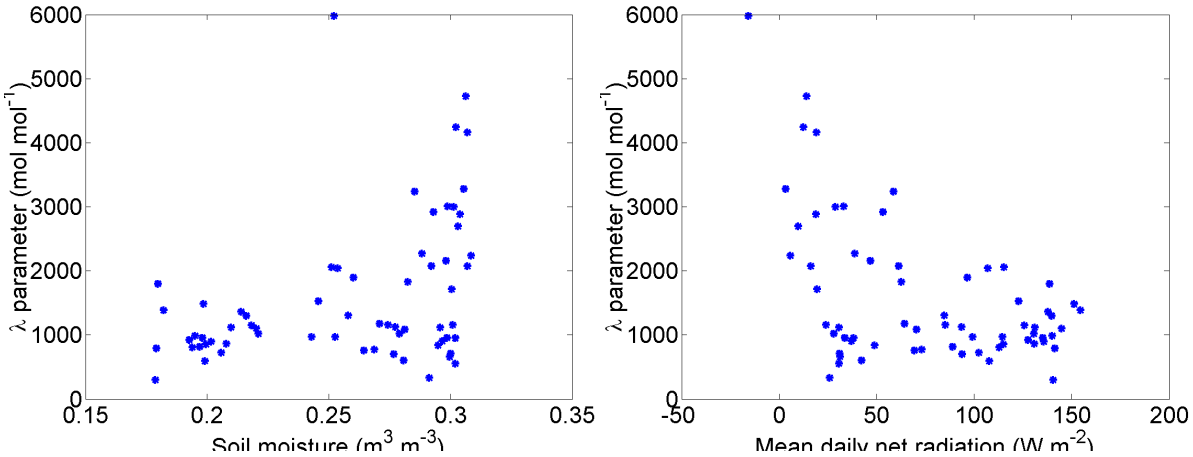

Figure 6-5. Retrieved *λ* plotted against soil moisture (left) and mean daily net radiation (right).

6.3.2. SCOPE-D sensitivity (DOY 118), considering a link between J_{mo} and V_{cmo}

Figure 6-6 presents the set of the 405 SCOPE simulations in terms of energy and mass fluxes. It is composed by 4 subplots showing the net radiation Rn, the carbon assimilation by photosynthesis A, the sensible heat flux H and the latent heat flux LE. Results show that the simulation set provides moderate variations of the net radiation. These variations are mainly due to the variations of the chlorophyll content (not shown here). This last is an input parameter of the Prospect model which is used in SCOPE to compute the leaf optical properties. By consequence, this parameter is also involved in the computation of the surface albedo which is directly used to estimate the net radiation. In an opposite way, high variations in the modelled turbulent fluxes are observed. This implies that the parameter ranges allow the simulations of low or high assimilation and evapotranspiration rates, as those observed for instance in the cases of a stomatal closure or in a well developed canopy without water stress, respectively. The sensible heat shows also very high variations, but in an opposite way of LE in order to balance the energy budget.

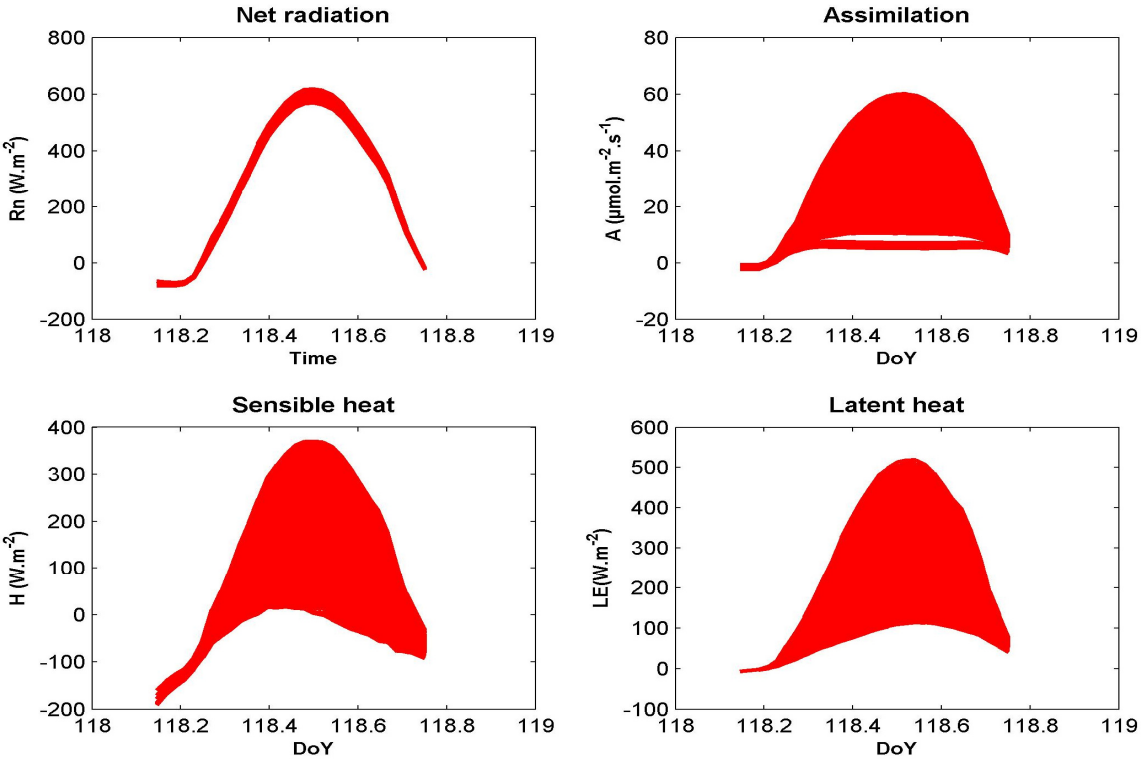

Figure 6-6. Time course of the energy and mass fluxes simulated with SCOPE in the framework of the sensitivity analysis experiment (405 simulations, parameter range listed in Table 6-4, DOY 118 and considering that Jmo is linked to Vcmo): net radiation (top, left), carbon assimilation (top right), sensible heat (bottom left) and latent heat (bottom, right)

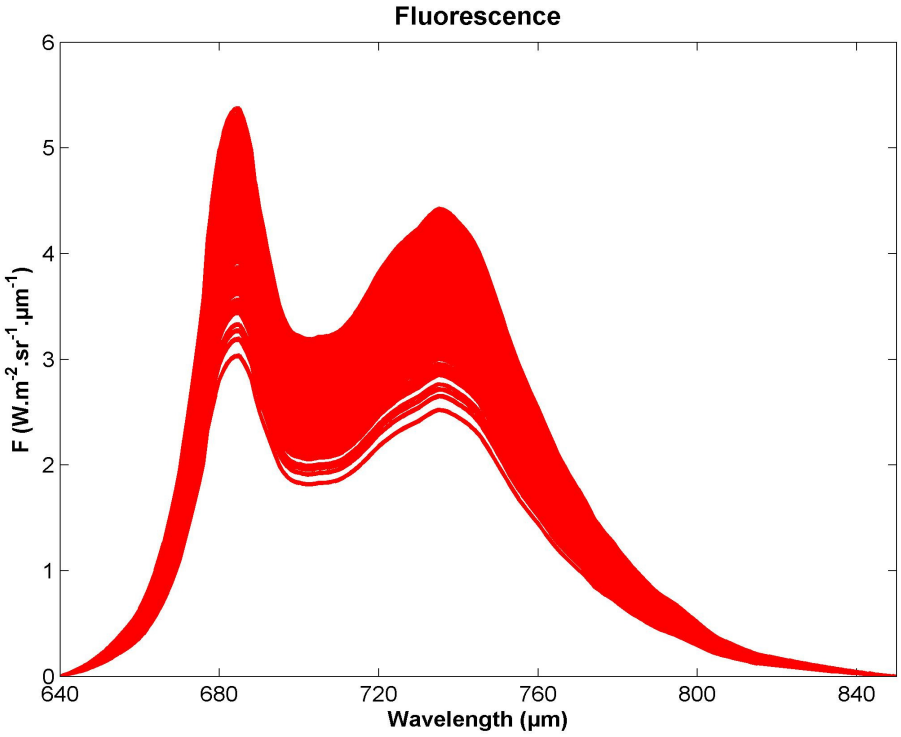

Figure 6-7. Fluorescence spectrums simulated with SCOPE at 10:30 am in the framework of the sensitivity analysis experiment (405 simulations, parameter range listed in Table 2, DOY 118 and considering that Jmo is linked to Vcmo).

Figure 6-7 shows the same simulation set as Figure 6-6 but in terms of fluorescence spectrums in the spectral range 640-840 nm at 10:30 am. As observed for the mass fluxes, large variations in the fluorescence spectrums are modelled. However, it has been observed that the variations of the free parameters induce low changes in the spectral shape of the fluorescence. This is a direct consequence of an actual inconsistency in the current SCOPE-D model in that it allows changing C_{ab} but that the fluorescence matrices (top and bottom side of the leaf) are constant. So, when the C_{ab} is changed the reflectance and the transmittance of single leaves are changed accordingly, but fluorescence from the leaves remains the same.

Figure 6-8 to Figure 6-10 show the impacts of the free parameters sampling on the simulations of the O2-A (760nm) fluorescence band (Figure 6-8), the O2-B (680nm) fluorescence band (Figure 6-9), and the band ratio (Figure 6-10). All the presented results correspond to the signal observed at 10:30 am in the morning (close to the possible satellite overpass). Results indicate that the maximum carboxylation capacity has not a clear impact on the simulations in each fluorescence bands, since no trend between fluorescence and *Vcmo* is observed (see top left subplots). It is explained by the link introduced now between *Vcmo* and *Jmo*, for which there is some compensations of the effect. Inversely, the fluorescence bands becomes positively correlated with the chlorophyll content, revealing that if the leaf chlorophyll content increases, a higher canopy fluorescence emission is modelled (see top right subplots). The colour legend used makes it possible to show that the LAI is the other key parameter to assess fluorescence. As for the chlorophyll content, a positive correlation is found between both fluorescence bands and LAI, indicating that an increase of fluorescence emission is modelled in response to an increase of the canopy density.

Furthermore, in our modelling experiment, it seems that LAI induces more variations in fluorescence than C_{ab}:

for a given value of C_{ab}, the maximum differences in *F780* due to LAI range between 0.4 and 0.6 $W.m^{-2}.sr^{-1}.\mu m^{-1}$,

while for a given value of LAI, the maximum differences due to C_{ab} range between 0.2 and 0.4 $W.m^{-2}.sr^{-1}.\mu m^{-1}$.

A similar response is observed for the O2-B band at 680nm.

Moreover, the ratio between the two fluorescence bands shows only slight variations (in the 0.509-0.515 range). This confirms that the spectral shape of the fluorescence emission is only slightly modified by the input parameter sampling. For it, negative correlations between the fluorescence ratio with C_{ab} and LAI are observed.

It was also interesting to plot the relation between the modelled fluorescence bands and the product of C_{ab} by LAI (C_{ab} x LAI) which represent the integrated content of chlorophyll over the canopy; this last being easier to track by remote sensing than C_{ab}. As expected, positive correlations are observed between each of the fluorescence bands and the C_{ab} xLAI product, with a saturation effect occurring for the highest values.

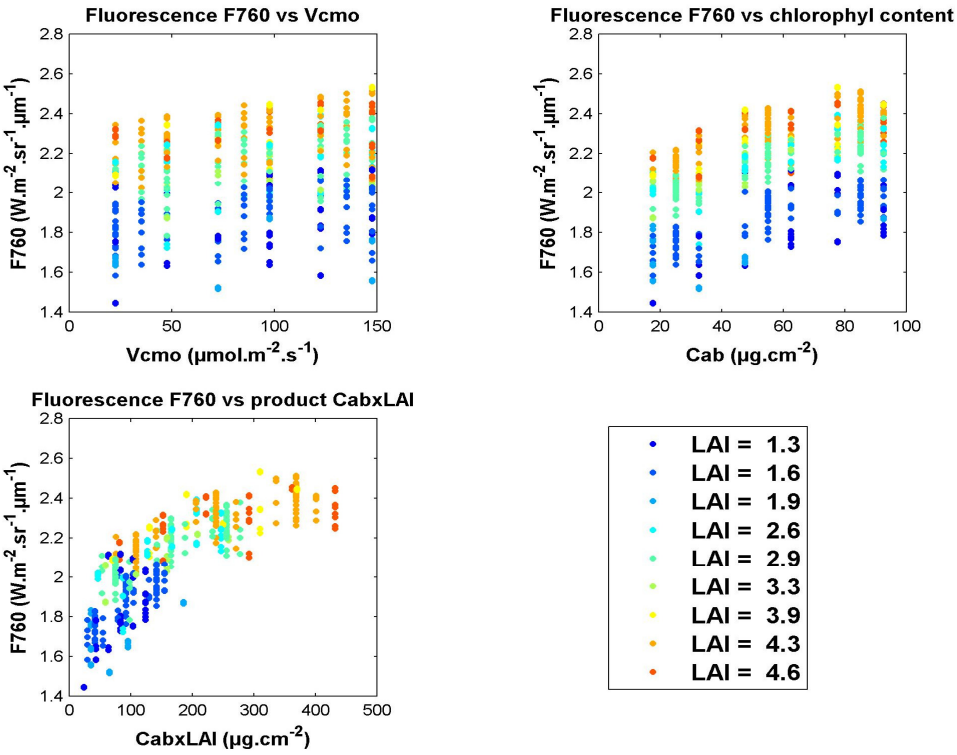

Figure 6-8. Relation between the fluorescence band at 760nm (O2-A) at 10:30 am, with the maximum carboxylation capacity (Vcmo top, left), the chlorophyll content (Cab top, right) and the product between Cab and LAI (bottom, left). Each coloured circle is one of the 405 simulations performed for DoY 118 considering that Jmo is linked to Vcmo. The colour legend is attributed by ranking on LAI.

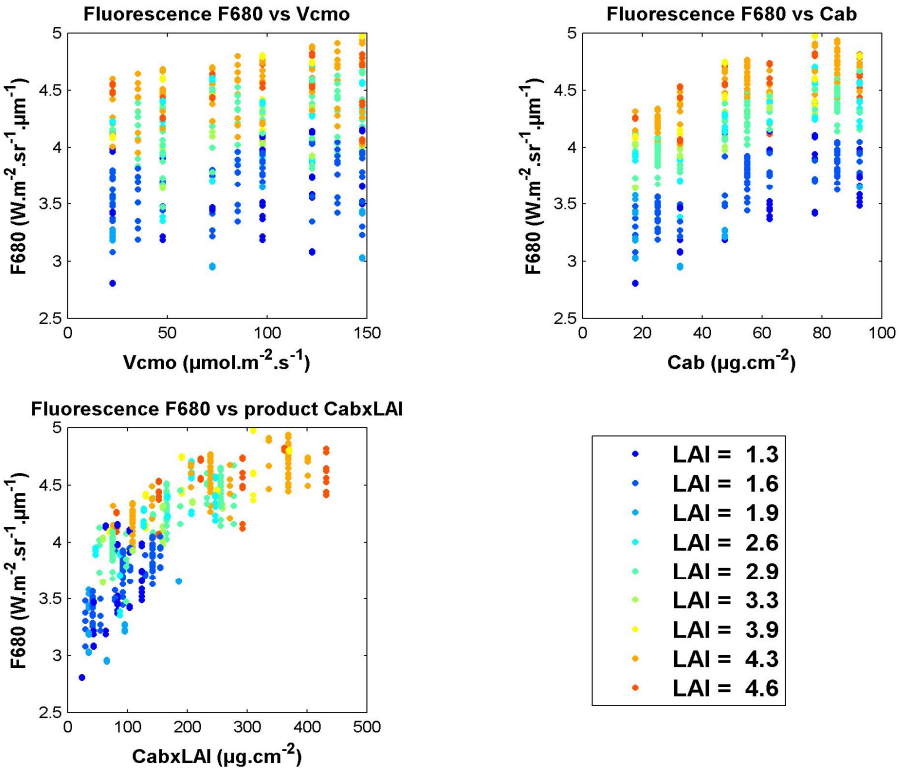

Figure 6-9. Same as in Figure 8, but for the fluorescence signal at 680nm (O2-B) at 10:30 am.

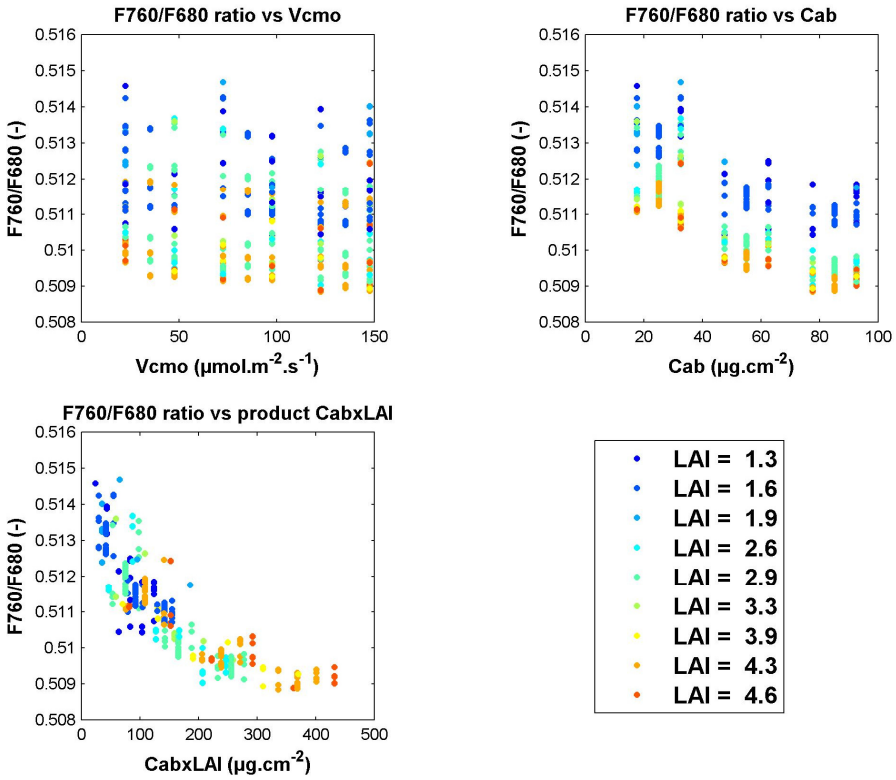

Figure 6-10. Same as for Figure 8, but for the F760/F680 ratio at 10:30 am.

Figure 6-11 to Figure 6-12 show the impacts of the free parameters on photosynthesis and evapotranspiration. The positive correlations obtained between the modelled variables and *Vcmo* and LAI, show that they are key parameters to control the photosynthesis and the water flow through the leaf. Results also show that the *Lam* parameter, which allows the control of the stomatal closure, has only a small impact on the modelled evapotranspiration, and that C_{ab} has no important impact on both assimilation and evapotranspiration.

In order to analyse the link between fluorescence and photosynthesis in a more operational context, Figure 6-13 presents scatterplots between the fluorescence band at 760nm and the photosynthesis, both modelled at 10:30 am. A different colour legend has been given according to the values taken by the free parameters. Results confirm that the LAI plays an important role on the modelling of the both variables, and that *Vcmo* and C_{ab} controls photosynthesis and fluorescence, respectively. No clear relation between photosynthesis and fluorescence can be established.

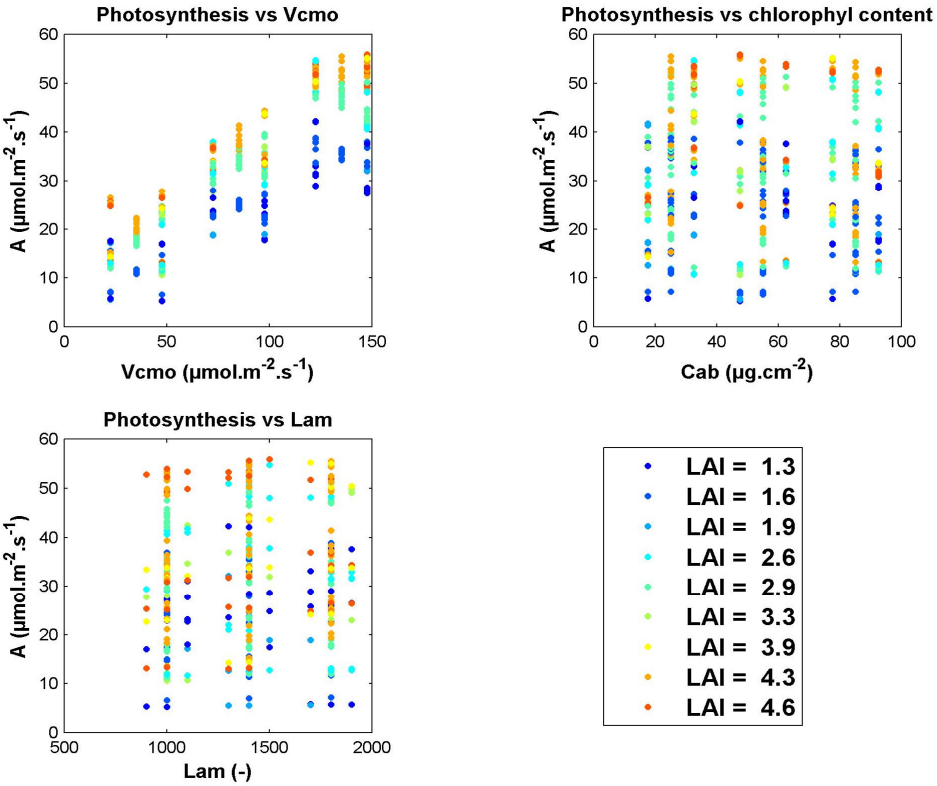

Figure 6-11. Same as Figure 8, but for the photosynthesis at 10:30 am, with the maximum carboxylation capacity (Vcmo, top, left), the chlorophyll content (Cab top, right) and the Lam parameter (bottom, left).

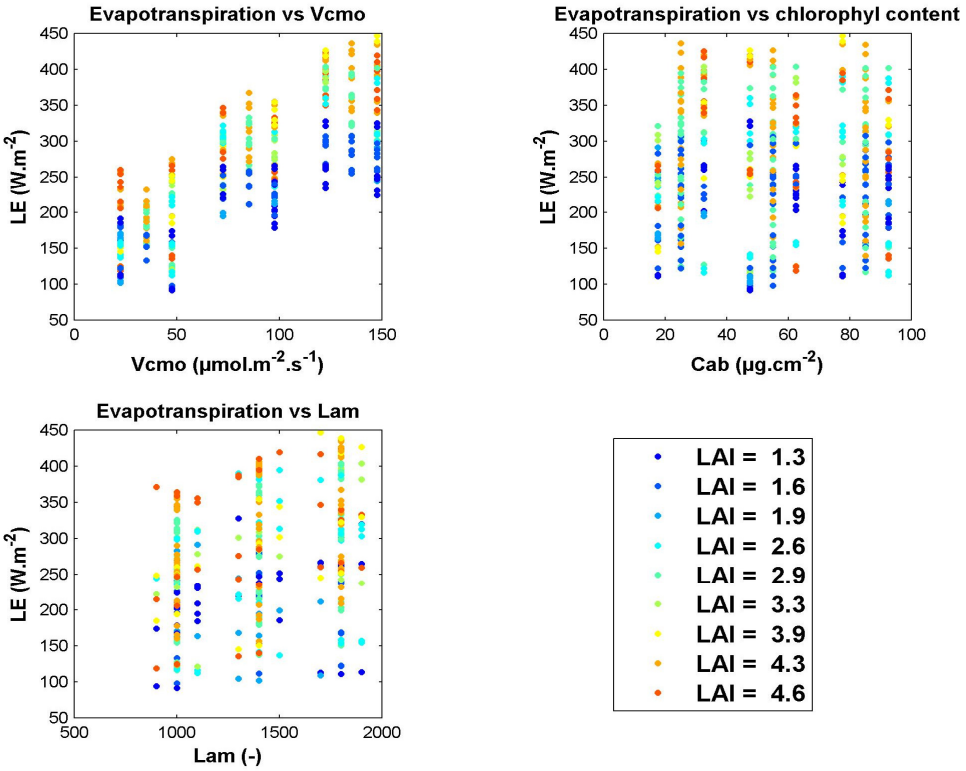

Figure 6-12. Idem as Figure 11 but for the evapotranspiration at 10:30 am.

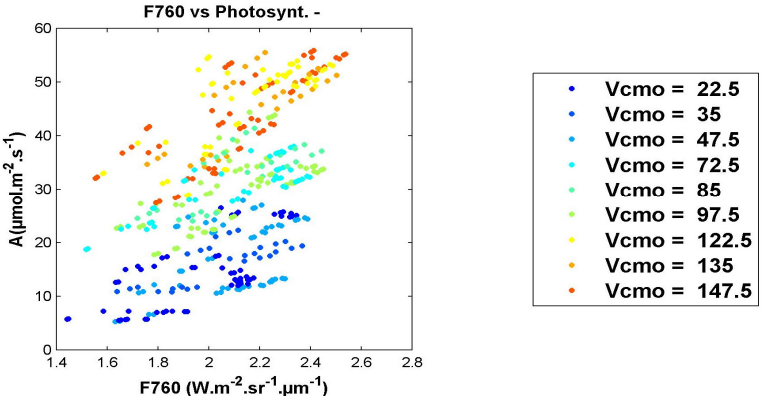
F760 vs Photosynt. -
A(µmol.m-2.s-1)
F760 (W.m-2.sr-1.µm-1)
Vcmo = 22.5
Vcmo = 35
Vcmo = 47.5
Vcmo = 72.5
Vcmo = 85
Vcmo = 97.5
Vcmo = 122.5
Vcmo = 135
Vcmo = 147.5

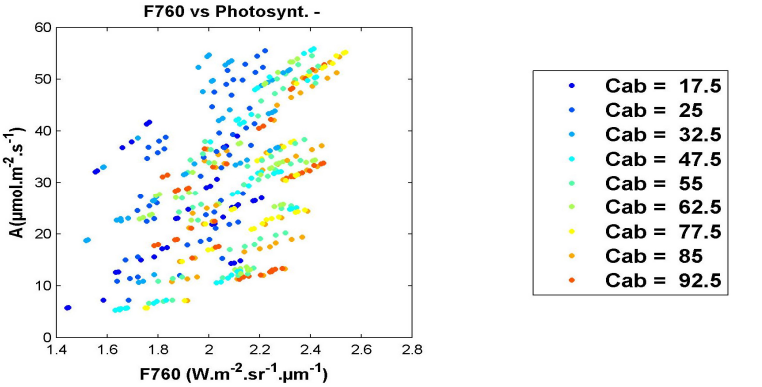
F760 vs Photosynt. -
A(µmol.m-2.s-1)
F760 (W.m-2.sr-1.µm-1)
Cab = 17.5
Cab = 25
Cab = 32.5
Cab = 47.5
Cab = 55
Cab = 62.5
Cab = 77.5
Cab = 85
Cab = 92.5

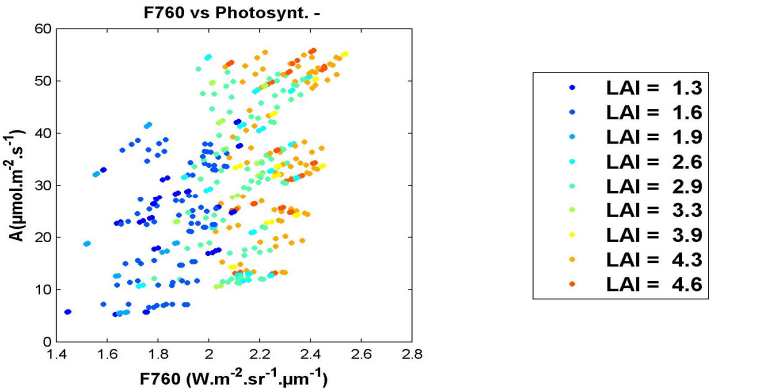
F760 vs Photosynt. -
A(µmol.m-2.s-1)
F760 (W.m-2.sr-1.µm-1)
LAI = 1.3
LAI = 1.6
LAI = 1.9
LAI = 2.6
LAI = 2.9
LAI = 3.3
LAI = 3.9
LAI = 4.3
LAI = 4.6

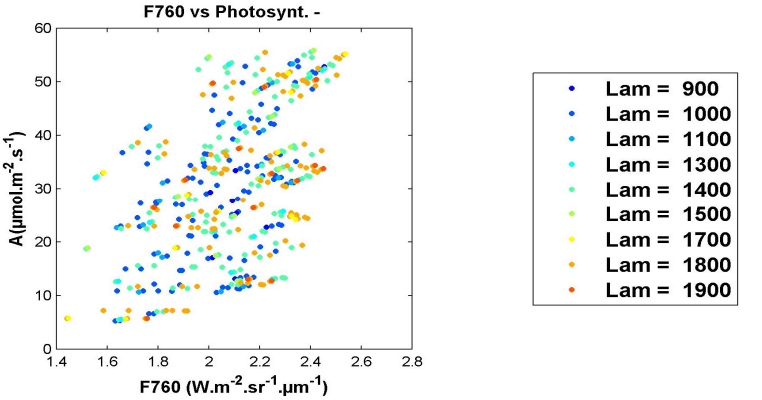
F760 vs Photosynt. -
A(µmol.m-2.s-1)
F760 (W.m-2.sr-1.µm-1)
Lam = 900
Lam = 1000
Lam = 1100
Lam = 1300
Lam = 1400
Lam = 1500
Lam = 1700
Lam = 1800
Lam = 1900

Figure 6-13. Scatterplots between the fluorescence band at 760nm and the photosynthesis at 10:30 am, according to a ranking on the value of the free parameter: a) Vcmo, b) Cab, c) LAI and d) Lam (or λ).

Figure 6-14 to Figure 6-15 present the LH-OAT sensitivity analysis. The sensitivity analyses have been carried out for two individual modelled variables; the fluorescence band O2-A at 780nm and the carbon assimilation by photosynthesis. We show that the model response to the input parameters is different for each of the output variables. As expected, we find that the key parameters to control the carbon assimilation by photosynthesis are the maximum carboxylation capacity *Vcmo* and the leaf area index. Such a result is explained by the facts that *Vcmo* controls the energy rate which is used by photosynthesis and that the LAI controls the foliage density. Concerning, the fluorescence band at 780nm, two main results have been obtained.

First, it is clear that the key parameters controlling the fluorescence emission are the chlorophyll content and the leaf area index (*Vcmo* has a noticeable impact but low).

Second, the partial effect of LAI is higher than the partial effect of C_{ab} (Note here that the partial effect of LAI might be slightly underestimated since, when compared to reality, variation range of LAI, set to 1-5, is 'smaller' than the variation range of C_{ab} which encompass a wider range of situations (10-100 µg cm^{-2})).

It is also important to note that a higher model response is observed for the lowest values of the input parameters. This underlines the non-linearity in the processes simulated by SCOPE.

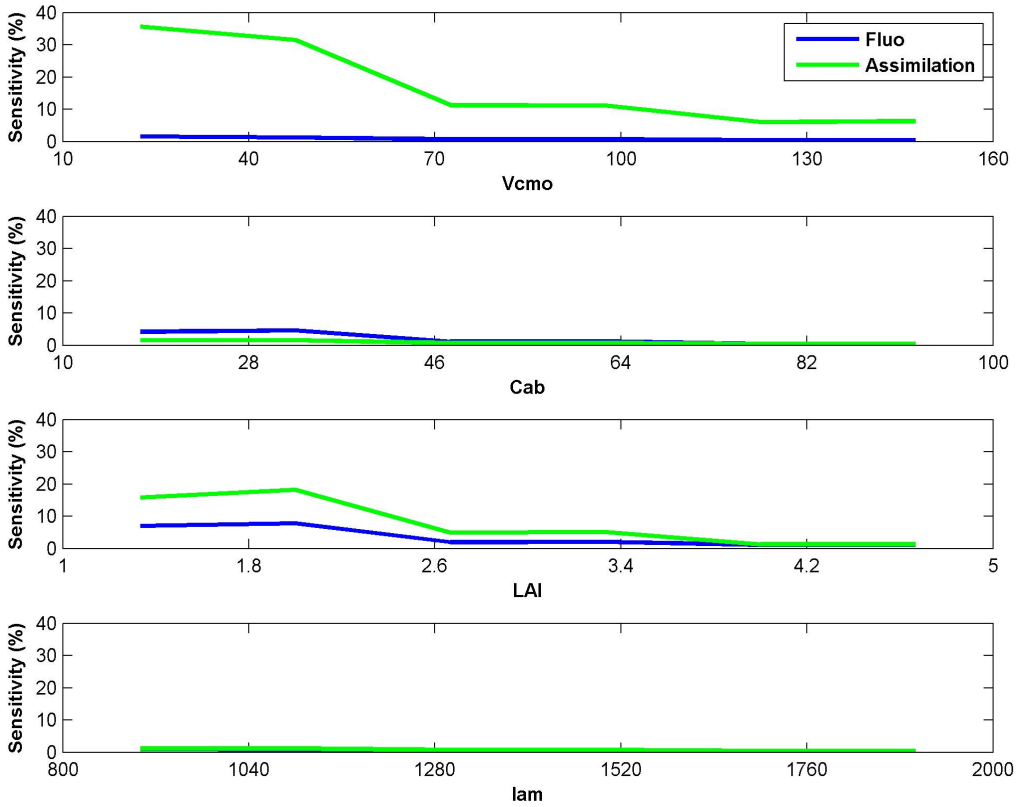

Figure 6-14Partial effect of the input parameters on the fluorescence signal at 760nm and on the photosynthesis, both simulated at 10:30 am (LH-OAT algorithm, DoY 118, considering the relation between *Jmo* and *Vcmo*).

Figure 6-15 presents the dynamics of the mean partial effects for each of the output variables. As fluorescence emission and photosynthesis are diurnal processes, these dynamics have been investigated over the diurnal cycle on DoY 118. Results often show a positive correlation between the model sensitivity and the diurnal cycle of the incident solar radiation showing that sensitivities decrease when moving apart of solar noon (DoE 118.5). However, sensitivity of fluorescence signal remains high at 10:30 am (around 118.44 on the X-axis, black vertical line). Those Figures are also a good mean to rank the effect of each parameter on the modelled outputs. Main results show that the ranking of the main parameters does not change during the day even if the shapes of the diurnal courses of their sensitivities are different. A more careful attention will be required in the future to analyse the differences in shape of the diurnal courses (e.g. between LAI and C_{ab} for fluorescence) and the reason of the slight diurnal asymmetry in fluorescence sensitivity.

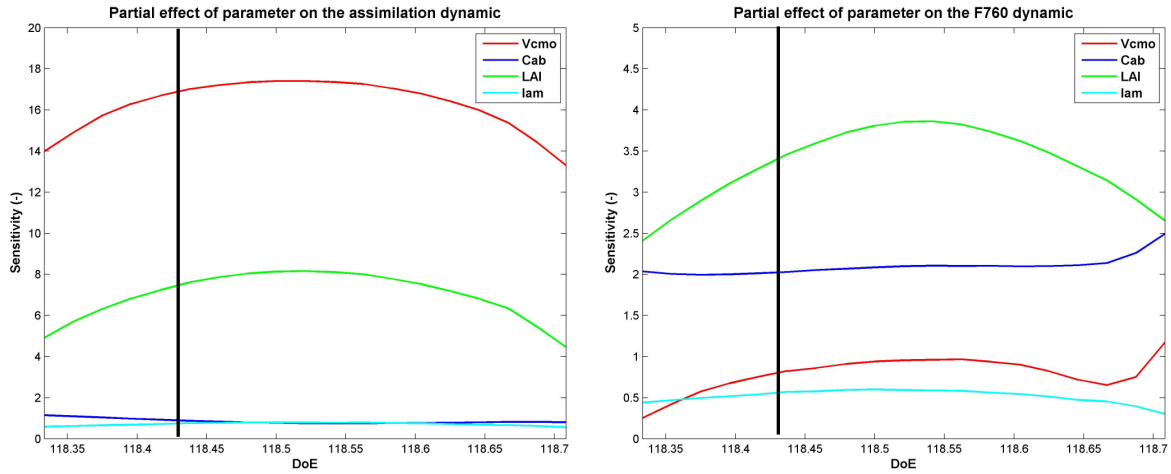

Figure 6-15. Left: Diurnal dynamic of the mean partial effects on the photosynthesis (LH-OAT algorithm, DoY 118 and considering Jmo linked to Vcmo). Right: Diurnal dynamic of the mean partial effects on the fluorescence signal at 760 nm (LH-OAT algorithm, DoY 118 and considering Jmo linked to Vcmo).

The black vertical lines indicate 10:30 am.

6.3.3. SCOPE-D sensitivity (DOY 118), using a constant J_{mo}

For DoY 118, a sensitivity analysis was also performed considering a constant value for *Jmo*. This last has provided interesting results (Figure 6-16 to Figure 6-18), especially on the role of the maximum carboxylation capacity. Conversely to previous results, the influence of *Vcmo* on fluorescence was then very large (its sensitivity was almost 20 times higher!). Its influence on photosynthesis decreased by a factor 2 but remained high. The sensitivity of fluorescence and photosynthesis to the three other parameters did not change. The changing impact of *Vcmo* must be related to changes in the repartition of the limitation factor affecting the calculation of photosynthesis. It also clearly affects the relationship between fluorescence and photosynthesis. There are many experimental evidences that *Jmo* and *Vcmo* values are not independant in real life (Xu and Baldocchi 2003, Leuning 2002, Wilson *et al*. 2000, Medlyn *et al*. 2002...), so that the results presented here with a constant value of *Jmo* may be unrealistic. However, the relation between *Vcmo* and *Jmo* may vary depending on the species and the season. The difference between the two simulated cases is an indication that variations in *Vcmo / Jmo* ratio might affect the sensitivity of fluorescence and photosynthesis to *Vcmo*, as well as the potential relationship between fluorescence and photosynthesis. It will be interesting in the next future to perform new sensitivity analysis for various *Vcmo / Jmo* ratios (in the range of values already reported in the literature).

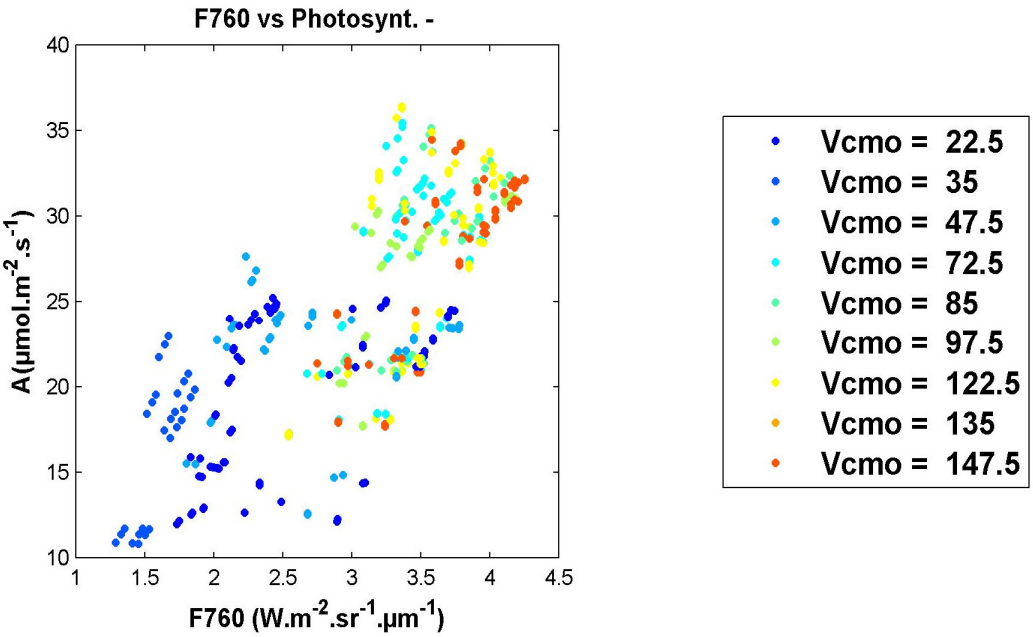

Figure 6-16. Relation between the fluorescence band at 760nm and the photosynthesis at 10:30 am, according to a ranking on the Vcmo values (405 simulations performed, studied cases DoY 118, Jmo equals to 120 µmol.m-2.s-1).

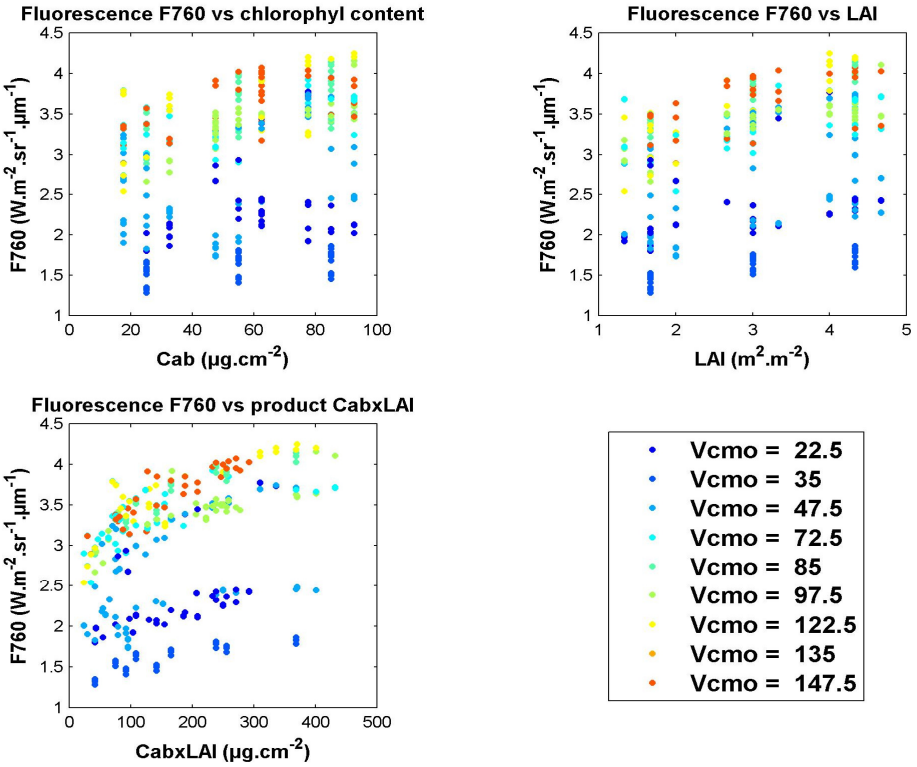

Figure 6-17. Relation between the fluorescence band at 760nm (O2-A) at 10:30 am, with the maximum carboxylation capacity (top, left), the chlorophyll content (top, right) and the product between C_{ab} and LAI (bottom, left). Each coloured circle is one of the 405 simulations performed for the studied case DoY 118 with a constant *Jmo* = 120 µmol.m^{-2}.s^{-1}. The colour legend is performed by ranking on LAI.

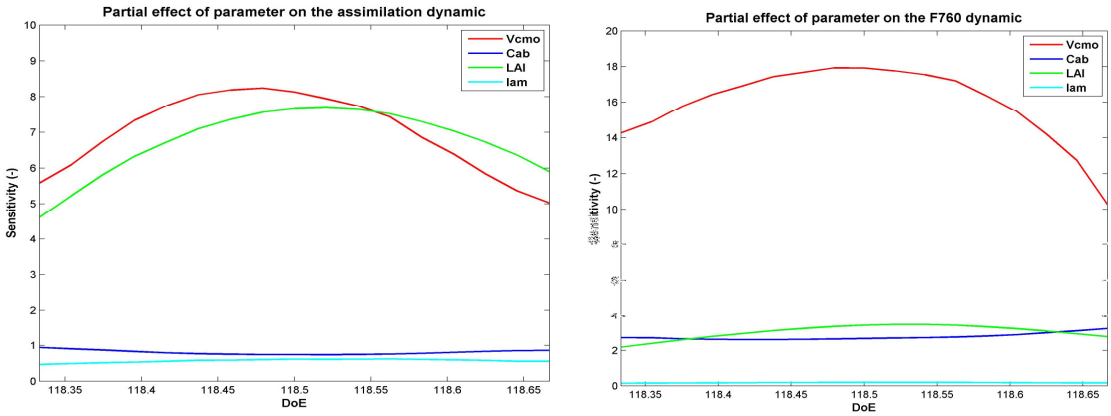

Figure 6-18. Left: Diurnal dynamic of the mean partial effects on the photosynthesis (LH-OAT algorithm, studied case DoY 118 and *Jmo* equals to 120 µmol.m^{-2}.s^{-1}). Right: Diurnal dynamic of the mean partial effects on the fluorescence bands at 760 nm (LH-OAT algorithm, studied case DoY 118 and *Jmo* equals to 120 µmol.m^{-2}.s^{-1}).

6.3.4. SCOPE-D sensitivity (DOY 71 and 140), link between J_{mo} and V_{cmo}

Figures 6-19 to 6-20 show results of the sensitivity analysis obtained for the studied cases on DoY 71 and DoY 140, both with a link between *Jmo* and *Vcmo*. For both cases, the results are very similar to the results obtained for DoY 118, implying at least for these cases that the climatic conditions are not influential in our sensitivity analysis experiment. This point would have to be investigated further in the future.

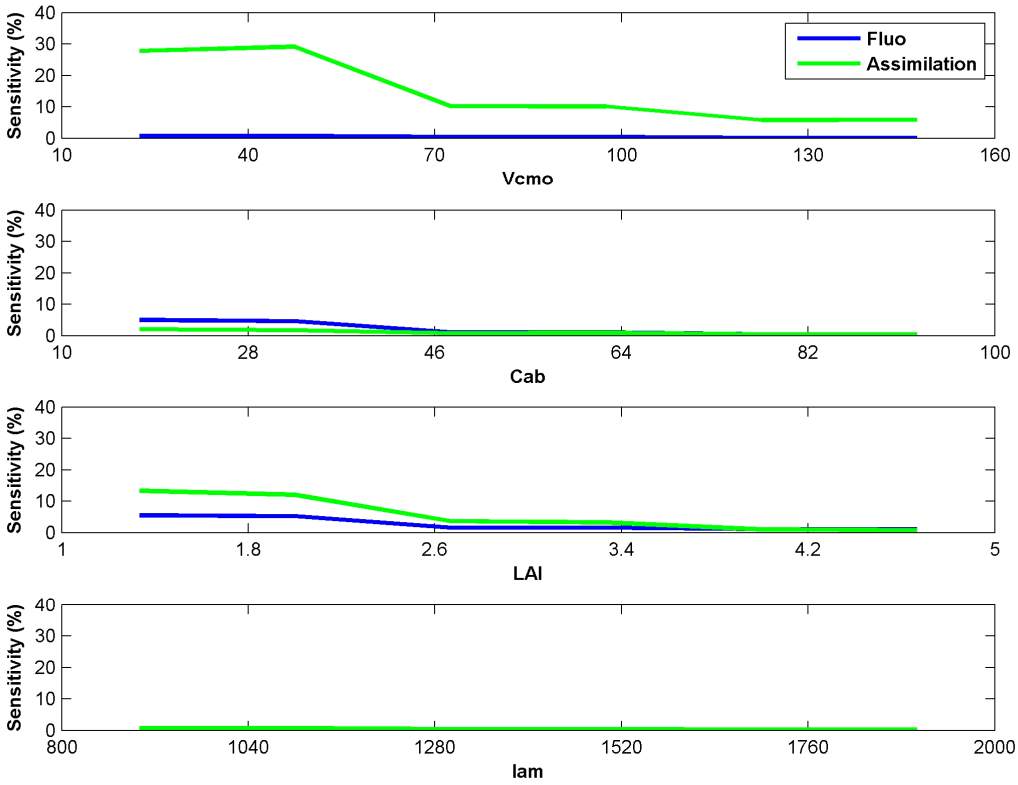

Figure 6-19.Partial effect of the input parameters on the fluorescence signal at 760nm and on the photosynthesis, both simulated at 10:30 am (LH-OAT algorithm, DoY 71, considering the relation between Jmo and Vcmo).

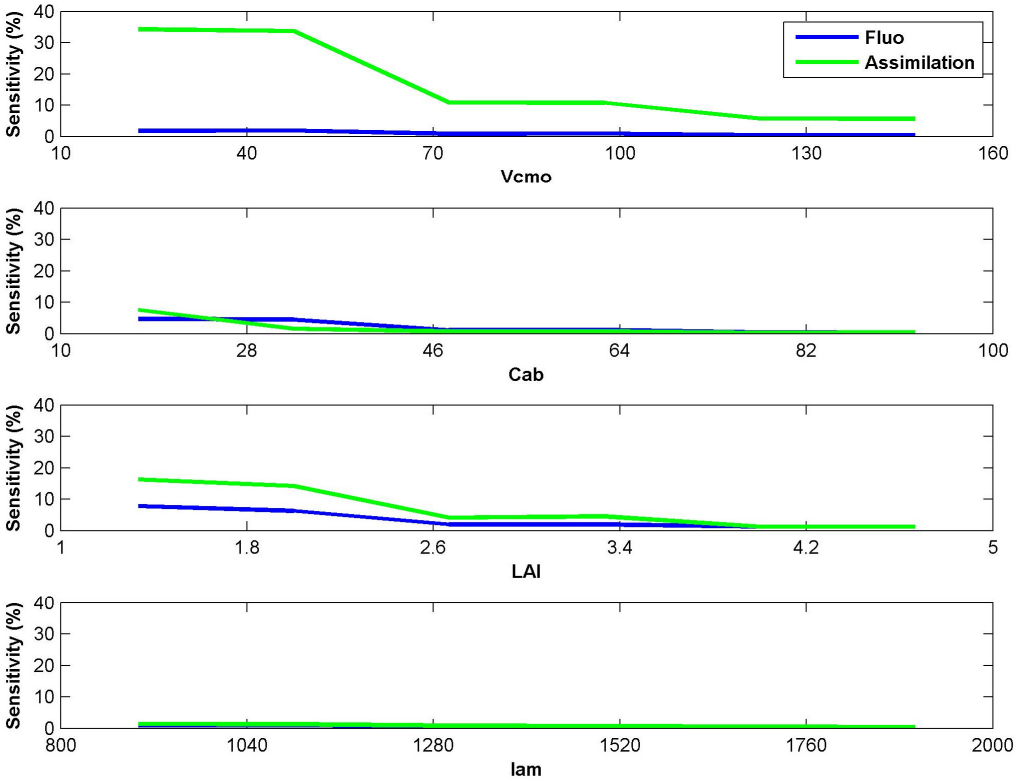

Figure 6-20. Partial effect of the input parameters on the fluorescence signal at 760nm and on the photosynthesis, both simulated at 10:30 am (LH-OAT algorithm, DoY 140, considering the relation between Jmo and Vcmo).

6.3.5. SCOPE-D sensitivity analysis: preliminary considerations

The sensitivity analysis performed on the SCOPE model, together with the calibration exercise, allow to conclude that the last developments of the SCOPE-D version provides now coherent results, as well in terms of modelled surface fluxes, as in terms of modelled fluorescence spectrum. Retrieved parameters in the calibration study were in good agreement with bibliographic knowledge. Responses of the model to the perturbation introduced in the main input parameters during the sensitivity analysis were also providing logical and 'expected' results.

6.3.5.1. Fluorescence

- Positive correlations between the fluorescence signals and the chlorophyll content were obtained;
- A positive correlation was also obtained with LAI;
- Very good relations were obtained with the integrated chlorophyll content (despite saturation occurring at high level);
- The sensitivity analysis also underlined the key role of the chlorophyll content in the computation of the fluorescence emission at the canopy scale;
- The sensitivity analysis provided a clear ranking of the influential parameters on the fluorescence signal (when *Vcmo = 2.6 Jcmo*):

  1 – LAI **>>** 2 - C_{ab} **>>** 3 – *Vcmo* > 4 - *Lam* (or λ).

- This ranking was not fundamentally affected by the time of acquisition of the fluorescence data (however higher sensitivities are obtained near solar noon for some parameters);
- The ranking of the influential parameters may be modified if the relationship between *Vcmo* and *Jmo* was modified (actually in the presented cases only the sensitivity to *Vcmo* was changed). At the same time, the relationship between photosynthesis and fluorescence may be changed. This point will have to be investigated further in particular if the relation between *Vcmo* and *Jmo* is very different from one species to another or from one season to another;
- Sensitivities of the fluorescence signal were always higher at lower values of the parameters (illustrating saturation effect when parameters increase);
- Our results supported the idea that changes in the environmental conditions are not strongly affecting the results of the sensitivity analysis.

6.3.5.2. Assimilation and evapotranspiration

- As expected, *Vcmo* was the most influential parameter on canopy photosynthesis;
- It was also the most influential parameter on canopy transpiration which was more surprising, since a more significant impact of *lam* could be expected as a first guess (at light of new publications on the Cowan model it is possible that the range chosen as input of the sensitivity analysis for *lam* was not large enough...);
- Assimilation and evapotranspiration were also very sensitive to LAI (which was expected);
- The modification of the relation between *Vcmo* and *Jmo* may affect significantly the sensitivity of photosynthesis to *Vcmo*.

The calibration exercise also provided interesting information giving confidence in the behaviour of the model. Retrieved parameters were in the expected ranges from bibliography sources and their evolutions were in agreement with several other studies.

6.4. Results: simple sensitivity analysis using SCOPE-D+ and SCOPE-I

Results from the SCOPE-I version of the canopy model are presented in Figure 6-21 to Figure 6-23. In contrast with what already observed for the SCOPE-D version of the model, predicted canopy fluorescence radiance appears to be highly sensitive to changes in maximum carboxylation rates (see Figure 6-22), in line with what already observed at the leaf scale. The sensitivity of fluorescence to Vcmo appears to mirro the response of GPP to this parameter, so that a rather tight correlation is observed between F760 and GPP across a wide but realistic range of photosynthetic potentials.

The same appears to be true for the response to changes in LAI, although the effects on both dependent variables appear to be more limited because of the saturating response of light absorption to LAI.

The response to soil water content and stomatal limitations, on the contrary, appears to be more complex. Both variables are little sensitive to soil water over a vast range of the realistic range, largely as a result of the highly curvilinear nature of the relationship between SWC and soil water potential, to which stomata are directly related. Only at a soil water content below 0.2 m^3 m^{-3} does fluorescence (and GPP) decline sharply. Below this level of SWC, however, the sensitivity of the two variables to a sharp increase in stomatal limitations appears to differ markedly, with a stronger effect on GPP than on F_{760}, so that the tight linear relationship generally observed between them is lost (Figure 6-22). This appears to limit the applicability of such an empirical relationship under extreme drought conditions, when GPP could be overestimated by as much as 10 µmol m^{-2} s^{-1} when estimated from corresponding values of canopy fluorescence radiance.

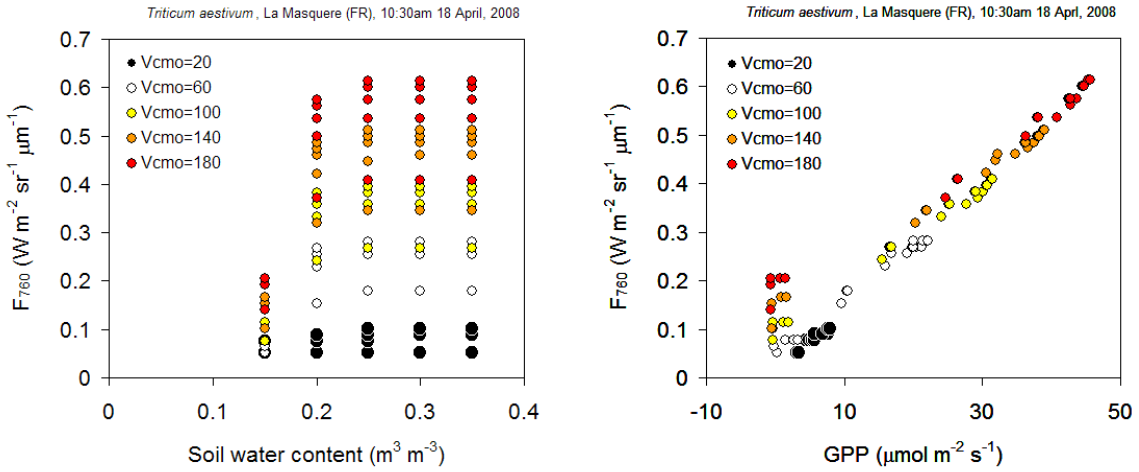

Figure 6-21. Left: simulated response of fluorescence in the O2-A band (F760) to changes in the three selected parameters, using the SCOPE-I version of the model. Results are arranged by levels of soil water content (SWC) and maximum carboxylation rate (Vcmo). Right: corresponding relationship between F760 and canopy GPP. Results correspond to a simulated overpass at 10:30am.

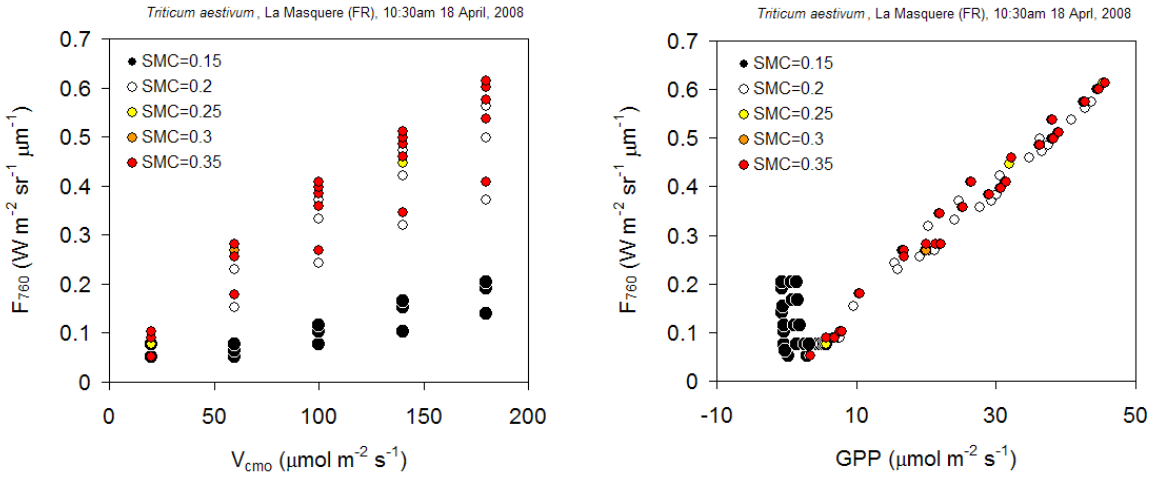

Figure 6-22. Same as for Figure 6-21, but highlighting the effect of maxmum carboxylation rate.

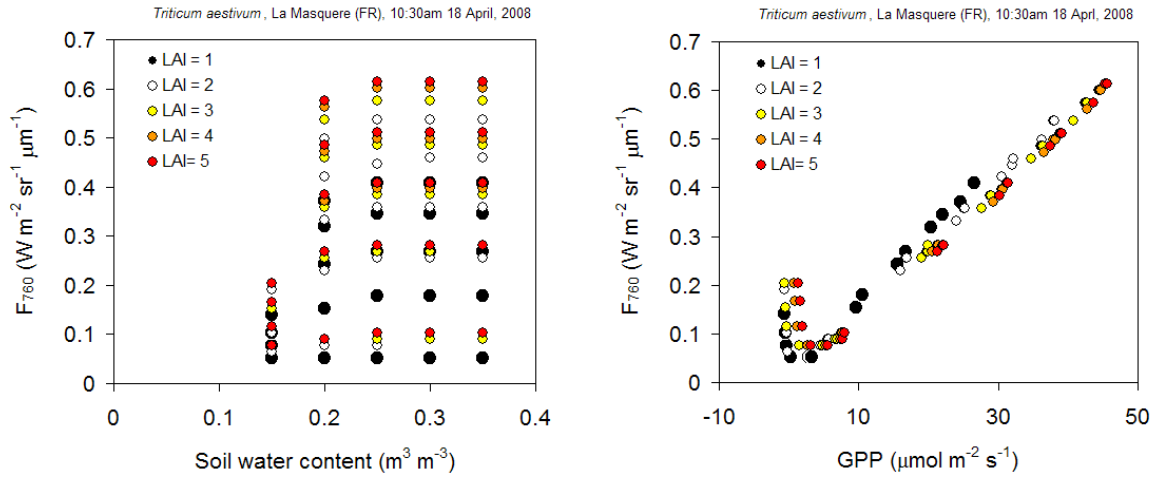

Figure 6-23. Left: simulated response of fluorescence in the O_2-A band (F_{760}) to changes in the three selected parameters, using the SCOPE-I version of the model. Results are arranged by levels of soil water content (SWC) and leaf area index (LAI). Right: corresponding relationship between F_{760} and canopy GPP. Results correspond to a simulated overpass at 10:30am.

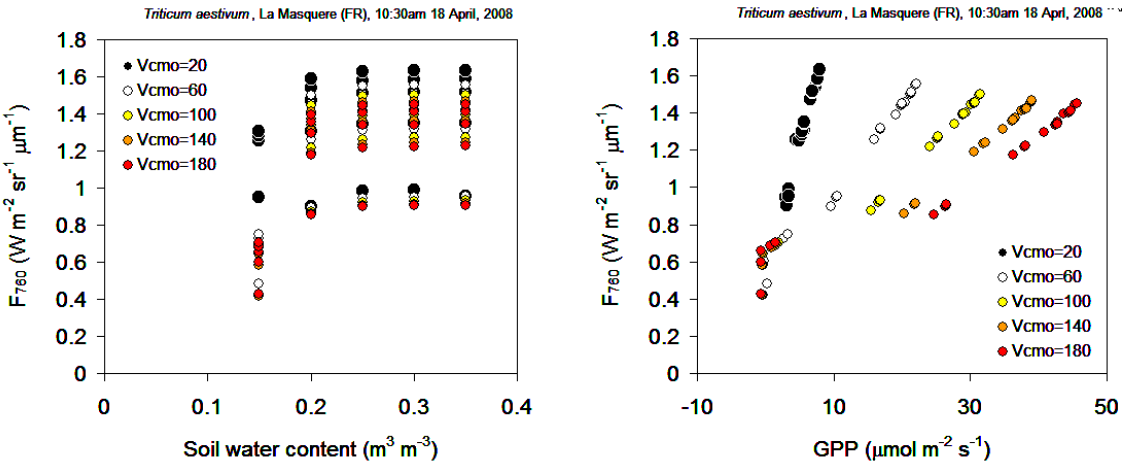

Figure 6-24. Left: simulated response of fluorescence in the O2-A band (F760) to changes in the three selected parameters, using the SCOPE-D+ version of the model. Results are arranged by levels of soil water content (SWC) and maximum carboxylation rate (Vcmo). Right: corresponding relationship between F760 and canopy GPP. Results correspond to a simulated overpass at 10:30am.

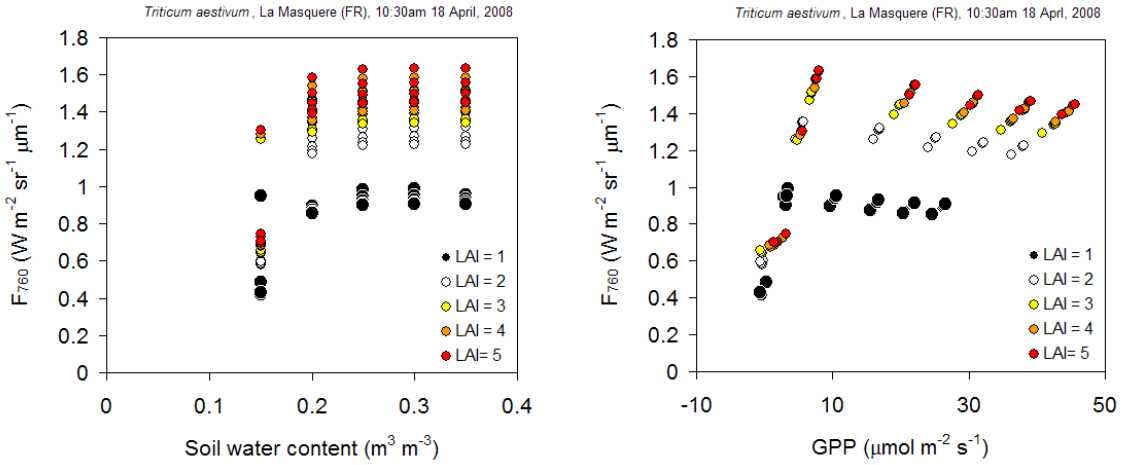

Figure 6-25. Same as for Figure 6-24, but highlighting the effect of maxmum carboxylation rate.

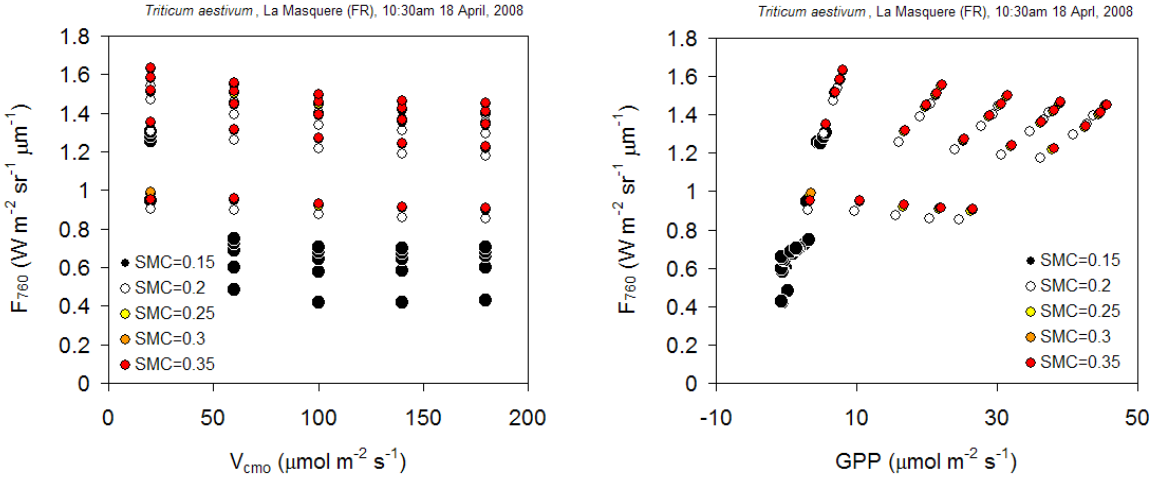

Figure 6-26. Left: simulated response of fluorescence in the O_2-A band (F_{760}) to changes in the three selected parameters, using the SCOPE-D+ version of the model. Results are arranged by levels of soil water content (SWC) and leaf area index (LAI). Right: corresponding relationship between F_{760} and canopy GPP. Results correspond to a simulated overpass at 10:30am.

The overall sensitivity of gross primary production and fluorescence radiance to the three parameters, according to the two versions of the SCOPE model, is summarized in Table 6-5. It should be stressed that the two versions differ only in their leaf-level representation of the functional link between PSII fluorescence and photosynthesis, based on the van der Tol-Verhoef-Rosema model and on the Magnani model, respectively. Simulated sensitivity of GPP is therefore the same for both models.

Gross primary production appears to be highly sensitive to changes in photosynthetic potentials (V_{cmo} and J_{mo} being assumed as linearly related, consistent with experimental evidence) over the entire range of variation (data not shown). The sensitivity to changes in LAI in the range explored appears to be more limited, as a result of the saturating effect on light absorption. As for sensitivity to soil water content, the high sensitivity observed is largely the result of the leverage exerted by extremely low values of SWC, resulting in extreme stomatal limitations and an almost complete reduction of gas exchange.

Considering the simulated sensitivity of fluorescence radiance, the SCOPE-I version of the model suggests a similar ranking of effects, although with a lower sensitivity to LAI and, to an even greater extent, to soil water content. The sensitivity appears to mirror what observed for GPP, as expected from the quasi-linear relationship between the two variables (Figure 6-21 to Figure 6-23).

A completely different picture emerges from simulations using the SCOPE-D+ version of the model (Figure 6-24 toFigure 6-26), which are consistent with what already observed in the LHOAT sensitivity analysis using SCOPE-D.

As already observed for SCOPE-I, fluorescence radiance appears to be strongly affected by soil water content and stomatal limitations, in parallel with gross primary production. For any given level of photosynthetic potential (V_{cmo}) a linear relationship is observed between F760 and GPP, that is maintained also under conditions of extreme drought (in contrast with what predicted by SCOPE-I). The slope of the relationship, however, appears to be strongly modulated by photosynthetic potentials, in contrast with the consistent relationship predicted by the SCOPE-I version of the model. As already noted for the SCOPE-D model (see above, LHOAT analysis), predicted canopy fluorescence is little affected by maximum photosynthetic rates (and therefore site fertility), in sharp contrast with the strong sensitivity of GPP (see Table 6-6).

The different effects of V_{cmo} predicted by SCOPE-I and SCOPE-D+ appear to be the result of the different representation of the link between photosynthesis and fluorescence at the leaf level, since the two versions share all other features. And a different effect of maximum carboxylation rates was indeed observed at the leaf scale (see Chapter 3.2.5), that is consistent with predictions at canopy scale.

In conclusion, intinsic differences in the two leaf-level models and in their representation of the relationship between electron transport and fluorescence directly translate in contrasting predictions at canopy scale, highlighting the need for a thorough test of the two alternative models of solar-induced fluorescence.

Table 6-7. - Final effect $\overline{S_i}$ (%; see Eq. 3) of changes in carboxylation potential (Vcmo), leaf area index (LAI) and soil moisture content (SMC) on vegetation gross primary production (GPP) and fluorescence radiance in the O2-A band (F760), as predicted by the SCOPE-I and the SCOPE-D+ versions of the model using a simplified analysis procedure

	GPP	F760	
		SCOPE-I	SCOPE-D+
V_{cmo}	73.1	76.2	7.85
LAI	32.8	22.1	24.9
SMC	144.1	81.1	54.0

6.5. Results: comparison of alternative canopy fluorescence models

6.5.1. Seasonal dynamics of GPP and fluorescence radiance

Although a thorough validation was beyond the objectives of the project, a preliminary comparison of modelled values of canopy gross primary production with measured values is presented, in order to add confidence in the general validity of the results also for simulated fluorescence.

The seasonal dynamics of gross primary production appear to be well captured by the most advanced version of the canopy gas exchange model, parameterized with field values of environmental variables and plant parameters (Figure 6-27.). Differences among sites in absolute values of GPP also appear to be well represented (note the different scaling on the y-axis in the three graphs), with higher peak values in the agricultural crop, followed by the broadleaf forest and by the the coniferous canopy. Apart from the overall seasonal pattern, also the response to sudden changes in environmental conditions appears to be well captured: not only overcast days (notably in the Avignon dataset) but also periods of increasing drought and sudden rewetting in the San Rossore dataset over the summer. The hot and dry summer of 2003 is known to have strongly reduced the sequestration of C in European forests, and in particular in the pine forest in San Rossore (Ciais *et al.* 2005).

The model, however, appears to underestimate peak values of GPP in the agricultural crop, and was not able to resolve some of the sudden changes in gas exchange in the broadleaf forest.

Summary statistics of model goodness-of-fit for the three sites are reported in Table 6-6, where reference is made to the entire dataset of half-hourly data rather than to daily totals. A large part of the error appears to be un-systematic, as demonstrated by the comparison of the systematic and un-systematic components of MSE. It is apparent from the slope of the correlation between modelled and measured data (parameter *b*), however, that the model tends to underestimate on average gross primary production, in particular towards the upper end of the spectrum.

Contrary to what often observed, model goodness-of-fit appears to be as good for half-hourly data as for daily totals.

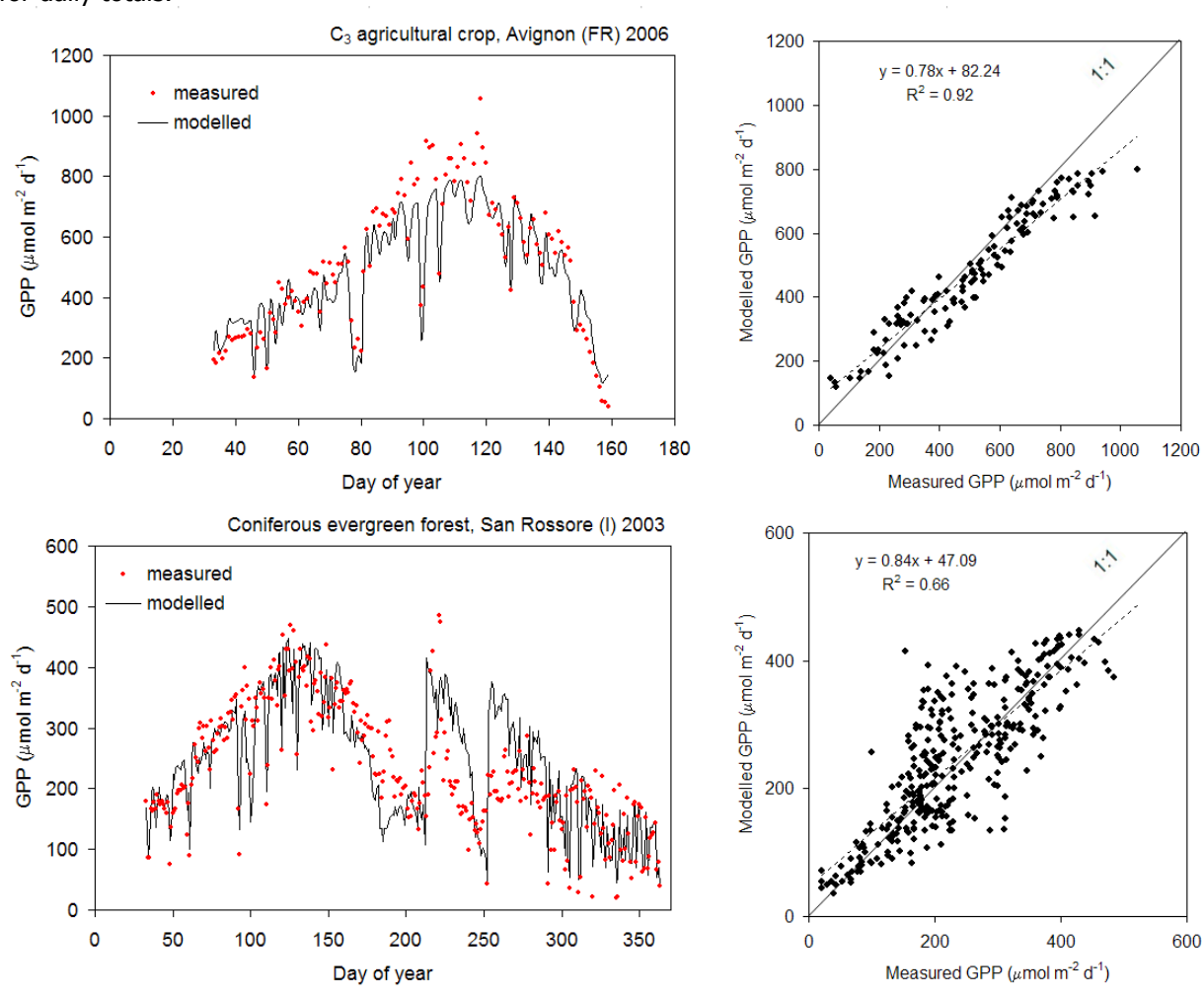

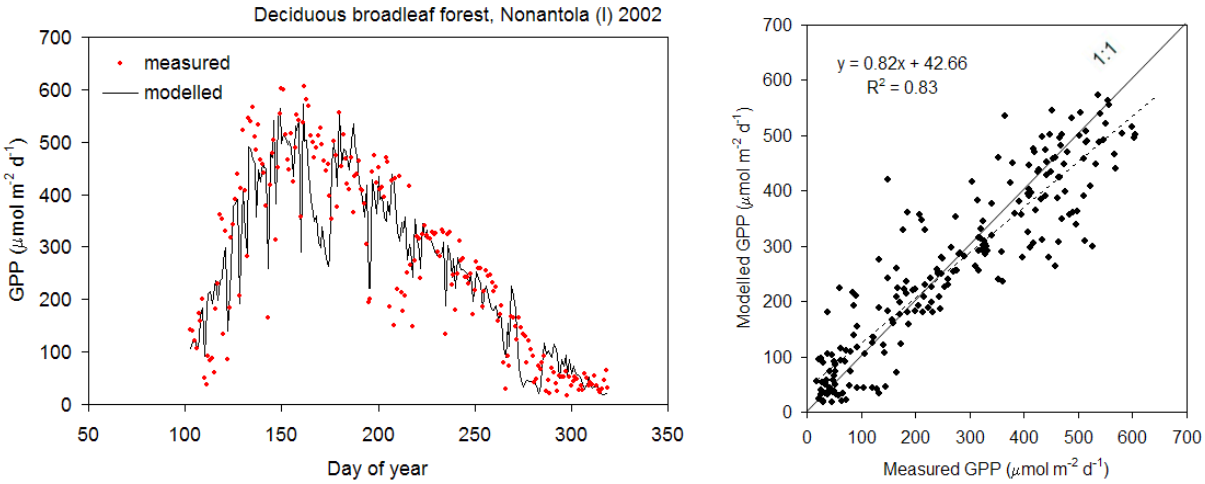

Figure 6-27. Seasonal dynamics of vegetation gross primary production (GPP) as predicted by the SCOPE-I (and SCOPE-D+) model for different vegetation types at the three test sites, as compared with experimental estimates derived from eddy covariance measurements. Note the different range of GPP predicted for different vegetation types. Reference is made to daily totals for presentation purposes; summary statistics for half-hourly values are reported in a companion table.

Table 6-8. - Comparison of modelled vs measured seasonal dynamics of half-hourly values of GPP at the three test sites. The intercept (a) and slope (b) of the linear correlation are reported, together with root mean square errors (RMSE), Pearson coefficients (R^2) and systematic (MSE_s) and un-systematic (MSE_u) components of mean

	Nonantola Broadleaf deciduous forest	San Rossore Coniferous evergreen forest	Avignon C3 agricultural crop
a	1.53	2.57	0.45
b	0.71	0.83	0.90
RMSE	0.198	0.099	0.449
R^2	0.65	0.66	0.94
MSE_s	0.020	0.419	0.008
MSE_u	0.031	0.407	0.246

Coming to consider the simulated seasonal pattern of canopy fluorescence radiance, the two versions of the SCOPE model provide markedly different results, as a consequence of the differences alreadyobserved at the leaf level.

The seasonal course of TOC fluorescence radiance at the three sites, as simulated by the SCOPE-I model is presented in Figure 6-27, together with a comparison with results from the SCOPE-D+ version of the model. Canopy fluorescence at 10:30am is predicted to vary widely over the season as well as over short periods. It should be noted, however, that the observed short-term variability (i.e. from one day to the next) is largely attributable to varying sky conditions, resulting in different levels of incoming radiation, and would be lost by satellite measurements over clear days.

Both the long- and the short-term variability appear to mirror the parallel pattern of GPP (see next chapter), both in response to long term patterns in canopy structure and biochemistry and as a result

of environmental limitations (see for example the response to soil drying and re-wetting at the San Rossore site).

A comparison of model predictions by the two versions of the model demonstrates important differences both in absolute values (up to 1.8 W m^{-2} sr^{-1} μm^{-1} in the SCOPE-D+ version, as opposed to 0.7 W m^{-2} sr^{-1} μm^{-1} for SCOPE-I) and in the response to internal and external factors, as demonstrated by the curvilinear and scattered nature of the relationship. Whilst the first discrepancy can be largely attributed to the parameterisation of the leaf-level model (with parameters largely drawn from the literature for laboratory conditions and not adjusted to field conditions), the second is essentially the result of the different structure and assumptions of the two models, with reference in particular to the response of fluorescence and photochemistry to non-photochemical quenching and heat dissipation.

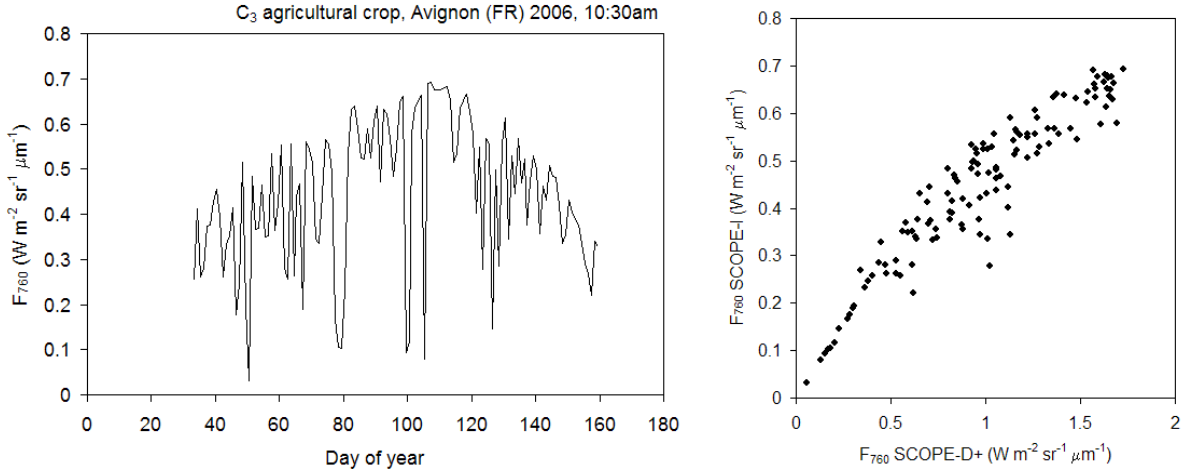

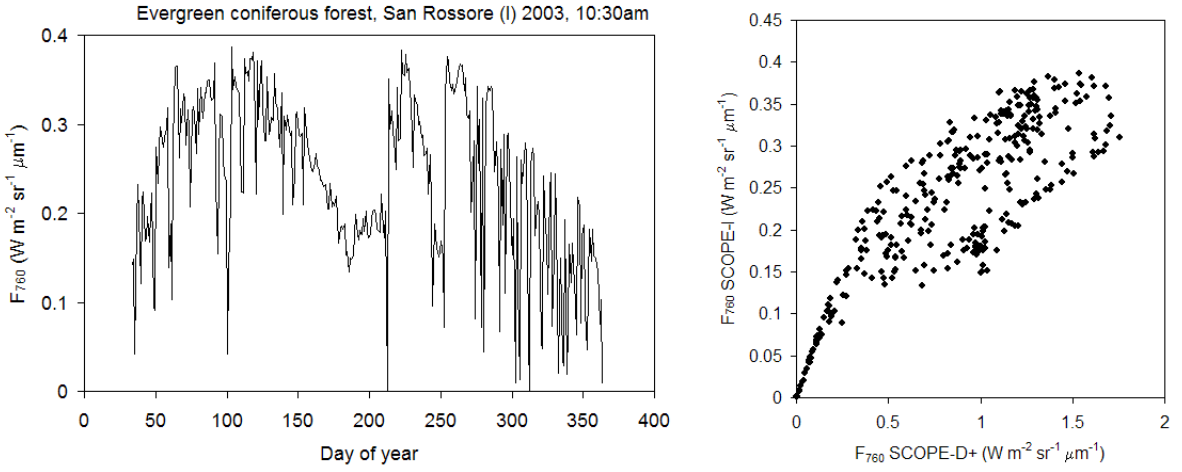

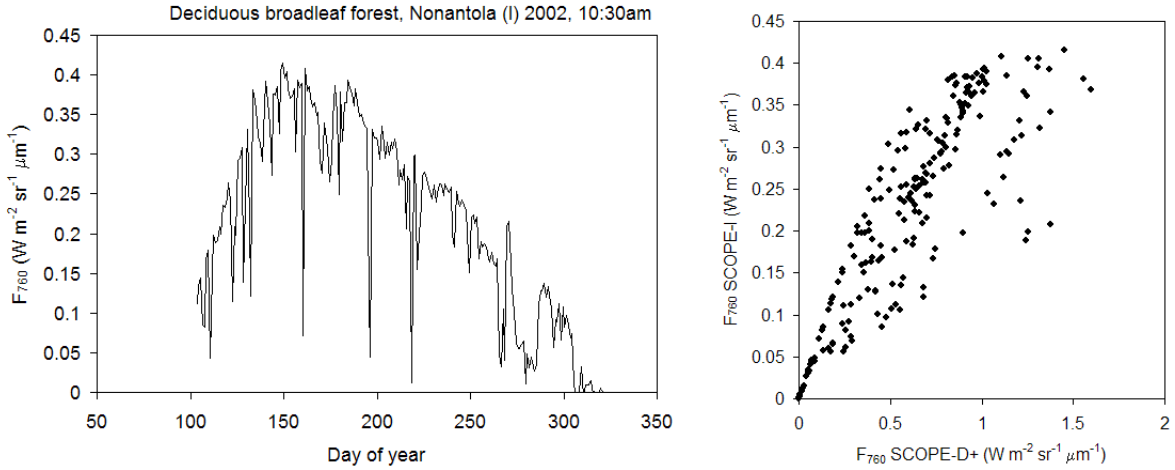

Figure 6-28 - Seasonal dynamics of vegetation TOC fluorescence radiance at 760 nm (F_{760}, corresponding to the O_2-A band) as predicted by the SCOPE-I model for different vegetation types at the three test sites. Values corresponding to the expected time of overpass (10:30am) are presented. Right: predictions by the SCOPE-I model (based on the Magnani leaf-level fluorescence model) are compared with predictions by the SCOPE-D+ model (identical but for the representation of leaf-level fluorescence, based on the can der Tol-Verhoef-Rosema model).

6.5.2. Overall relationship between GPP and canopy fluorescence

Scaling-up to the canopy scale by the SCOPE model, the relationship between TOC fluorescence radiance and gross primary production has been explored for three different vegetation types: a winter wheat crop in Avignon, a maritime pine evergreen forest in San Rossore and a mixed broadleaf deciduous forest in Nonantola.

SCOPE results of half-hourly GPP and fluorescence based on the two leaf-level models are presented in Figure 6-29. . A selection of model results, corresponding to the expected time of satellite overpass (10.30 am) is presented in Figure 6-30. .

A positive association is predicted by both models, mainly as a result of the parallel effect of incoming radiation and canopy LAI (leaf area index) and fAPAR (fraction of absorbed photosynthetically active radiation). A much wider scatter in the relationship is predicted based on the Tol model, however, so confirming what already observed at the leaf level. Large differences are also observed between the three datasets, either because of different environmental conditions or out of structural and physiological differences between the three canopies.

A much tighter relationship is predicted, on the contrary, by SCOPE when implementing the Magnani leaf-level model, in good agreement with field measurements at canopy and landscape scale as part of the ESA CEFLES-2 project. A certain degree of histeresis is however observed over the year, in particular in the wheat crop in Avignon, presumably because of the seasonal pattern in environmental conditions. Differences between sites also appear to be reduced.

The different behavior of the two versions of the SCOPE model seems to be largely attributable to the different effects of leaf photosynthetic potentials, as already noted at the leaf level. This is clearly demonstrated by are-analysis of results for the deciduous forest in Nonantola (Figure 6-29), where marked seasonal changes in the parameter V_{cmax} were imposed based on detailed field measurements at the site (Grassi *et al.* 2005).

A rather different relationship between GPP and canopy fluorescence is predicted using the SCOPE-D+ model (implementing the van der Tol-Verhoef-Rosema leaf-level model) for periods of high- or low photosynthetic potentials, whilst a rather tight common relationship is predicted by the SCOPE-I version, based on the Magnani leaf-level model.

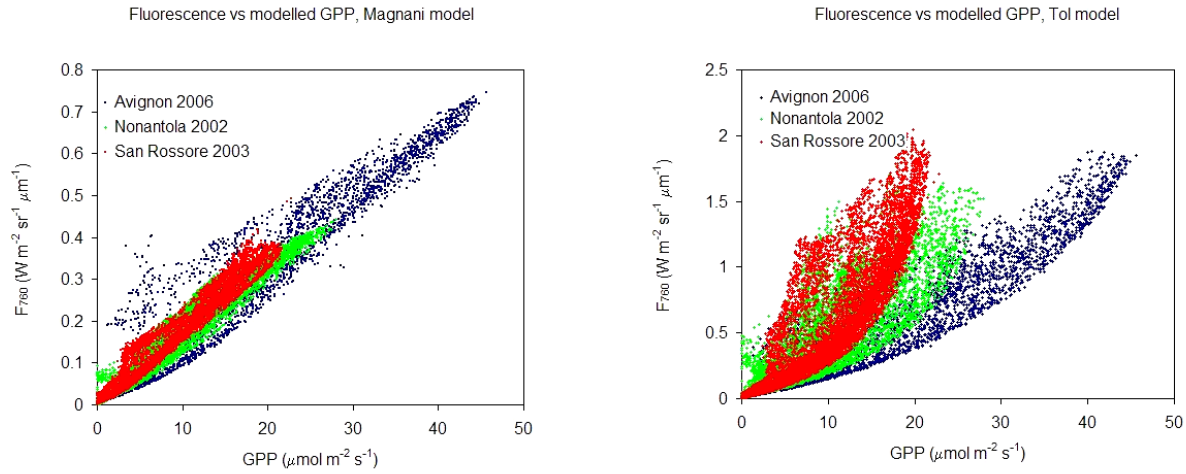

Figure 6-29. Simulated values of canopy gross primary production (GPP) and TOC fluorescence radiance at 760 nm (F_{760}) over the course of the year at the three test sites (winter wheat, Avignon; mixed deciduous forest, Nonantola; coniferous forest, San Rossore) according to the SCOPE model. Results are presented based both on the SCOPE-I (left) and on the SCOPE-D+ version of the model (right).

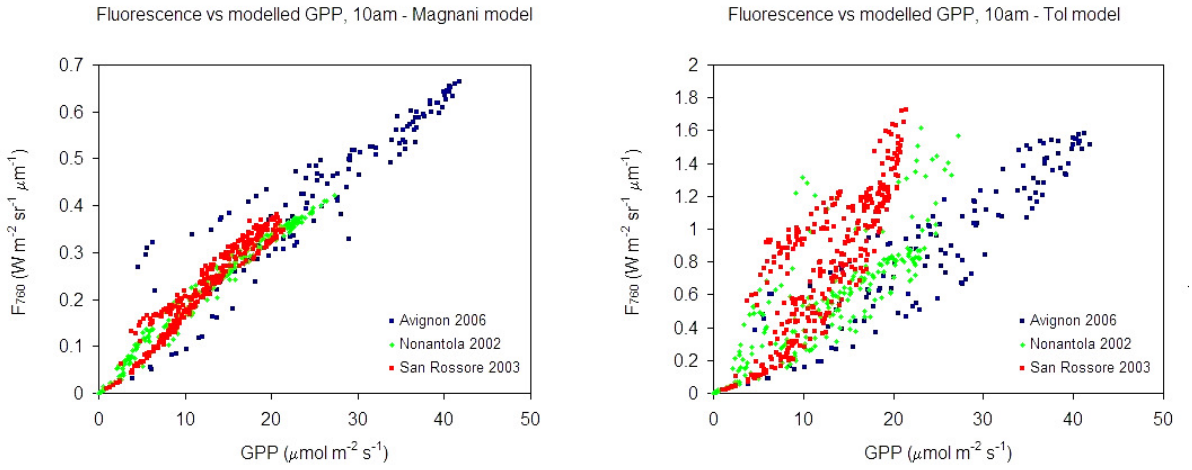

Figure 6-30. Simulated values of canopy gross primary production (GPP) and TOC fluorescence radiance at 760 nm (F_{760}) at 10 am (expected satellite overpass time) over the course of the year at the three test sites (winter wheat, Avignon; mixed deciduous forest, Nonantola; coniferous forest, San Rossore) according to the SCOPE model. Results are presented based both on the SCOPE-I (left) and on the SCOPE-D+ version of the model (right).

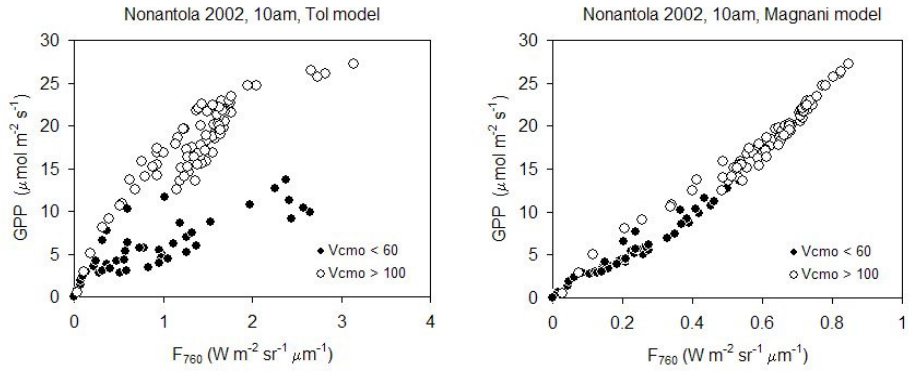

Figure 6-31. Demonstration of the the effects of leaf photosynthetic potentials (V_{cmo}, maximum carboxylation rates, and J_{mo}, maximum electron transport rate, assumed proportional to V_{cmo}) on the relationship between canopy gross primary production (GPP) and TOC fluorescence radiance at 760 nm (F_{760}) over the course of the year at the deciduous forest site in Nonantola according to the SCOPE model. Only days with high (> 100 μmol m^{-2} s^{-1}) and low (< 60 μmol m^{-2} s^{-1}) values of maximum carboxylation potential are presented for clarity. Results are presented based both on the SCOPE-I (left) and on the SCOPE-D+ version of the model (right).

7. Dynamic simulation of fluorescence signals together with other remote sensing signals.

7.1. Introduction

The possibility of simulating realistic remote sensing variables relies on the simulation of canopy radiative transfers in association with the evolution of the canopy cover and of the canopy processes such as energy balance (basis for the simulation of thermal infrared signals) and photosynthesis (basis for the simulation of fluorescence signals). It is a required step before having the possibility to implement procedure for assimilating remote sensing data.

The SCOPE model was used for simulating spectral reflectances (BRDF), thermal brightness temperature and SIF. In order to simulate the remote sensing data along the crop season, the SCOPE model has to be fed by the time evolution of soil moisture and vegetation variables, such as LAI, which are not simulated by the model (SCOPE does not include soil water transfer and vegetation growth descriptions: leaf area index, soil moisture…). These variables maybe obtained from field measurements (interpolated at the required time step, as shown in Chapter 6 of this report over forest and wheat datasets) or from the simulations of a dynamic vegetation soil-vegetation-atmosphere transfer model. In the latter case, we have here coupled the SCOPE model to the ISBA-A-gs model. Both models were calibrated over the wheat dataset and several simulation scenarios were proposed. The calibration of SCOPE-D has been presented earlier in this report (Chapter 6.2). ISBA-Ags was also calibrated over the Avignon sorghum dataset in order to provide information on C4 plants; however as some of the SCOPE parameterizations were unsure for C4 plants at the time of the work, the ISBA-A-gs-SCOPE coupling was not implemented during this study.

The SCOPE model was developed for the combined simulation of reflected solar radiation, emitted thermal radiation and solar induced fluorescence signals. It is based on a combination of several models describing radiative, turbulent and mass transfers inside of the canopy. Most relevant parts here were derived from the SAIL radiative transfer model (Verhoef 1998, Verhoef et al. 1997), from the biochemical model by Farquhar et al. (1980) to simulate photosynthesis, the stomatal regulation description by Cowan (1977), and a new fluorescence parameterisation (van der Tol et al. 2007a). Several versions of the SCOPE model were developed and used in the frame of this FLEX-DVM project (see Chapter 5 of this report). In this section, we only used the initial SCOPE-D version (with minor changes as described in the '5.3.6 Ancillary changes'paragraph) since the other versions (SCOPE-D+ and SCOPE-I) were not yet available or too much instable at the time of the work.

The ISBA-A-gs model was chosen in this study as a demonstrator of a DVM model. It was developed at Météo-France for being used as a surface parameterisation in atmospheric model dedicated to study the interaction between climate and land surface processes by accounting for vegetation retroaction with the atmospheric system in terms of energy exchanges, CO2 exchanges and plant growth. The model is described in details in the following text.

After coupling and calibrating both models, combined simulations were performed for the wheat dataset in order to provide dynamic datasets of solar induced fluorescence, in comparison to réflectances and surface temperature, over the crop cycle. A specific protocol was implemented in order to provide also information on the potential of fluorescence signal in discriminating vegetation canopies with different growth conditions keeping in mind the objective of using remote signals for data assimilation purpose. Thus, simulations were performed for three cases:

1. using directly LAI and soil moisture measurements for feeding SCOPE (calibrated over the dataset and not coupled to ISBA-A-gs)
2. using as SCOPE inputs the LAI and the soil moisture simulated by ISBA-A-gs calibrated over the wheat dataset (termed as 'local' calibration)
3. using as SCOPE inputs the LAI and the soil moisture simulated by ISBA-A-gs using the parameters presented by Gibelin et al. (2006) for use at the global scale (termed as 'global' calibration)

The comparison between scenarios 2 and 3 should inform us on the potential of the fluorescence signals for improving simulations by a global carbon model by recalibrating plant or soil parameters from remote sensing data on a specific site (where model parameters or soil conditions may diverge from global value).

7.2. Description of selected Dynamic Vegetation Model: *the ISBA-A-gs model*

7.2.1. Energy and water processes (from the ISBA model)

The ISBA land surface scheme has been developed by Météo-France and described by Noilhan and Planton (1989). The relevance of the scheme has been shown with regard to vegetated and bare surfaces (Mahfouf and Noilhan, 1991; Noilhan and Mahfouf, 1996). It is based on the equations of the force-restore method, initially applied by Bhumralkar (1975) to compute ground-surface temperature in an atmospheric general circulation model. Deardorff (1977, 1978) developed a similar parameterization to compute the ground-surface moisture content of bare soils and vegetated surfaces. As a consequence, ISBA predicts the time variations of five main variables: surface temperature (T_S), volumetric water content at the soil surface (w_G; $m^3.m^{-3}$), mean soil temperature (T_2), the mean volumetric water content in the root-zone (w_2; $m^3.m^{-3}$), and the water content of an interception reservoir (W_r). The surface soil moisture (w_G) is the volumetric moisture content of the surface soil layer (0-5 cm). This layer thickness is commonly used with ISBA. The model is driven by measurements of the following atmospheric forcing variables, generally on a 30-minute basis: incoming radiation, rainfall, atmospheric pressure, air temperature, air humidity and wind speed at a reference level. In the ISBA version, two vegetation characteristics LAI and crop height (h_C) are ascribed on a daily basis. The five main variables: T_S, T_2, w_G, w_2 and W_r, are initialized at the beginning of the simulation period. The main equations of the model are summarized below.

The simple water budget for w_G and w_2 derived from the force-restore method can be written as:

$$\frac{\partial w_G}{\partial t} = \frac{C_1}{\rho_w d_1}\left(P_G - E_G\right) - \frac{C_2}{\tau_1}\left(w_G - w_2\right), \qquad 0 \le w_G \le w_{sat} \qquad \text{(Eq. 7-1)}$$

)

$$\frac{\partial w_2}{\partial t} = \frac{1}{\rho_w d_2}\left(P_G - E_G - E_{TR}\right) - \frac{C_3}{\tau_1}\max\left(0, \left(w_2 - w_{FC}\right)\right), \qquad 0 \le w_2 \le w_{SAT} \qquad \text{(Eq. 7-2)}$$

The first term on the right of (1) represents the influence of surface atmospheric fluxes (outputs due to soil evaporation (E_G) and inputs due to rainfall (P_G)). The second term in (1) characterizes the diffusivity of water in the soil which tends to restore surface soil moisture w_G to the bulk value (w_2), and τ_1 is a restore constant of one day. The dimensionless coefficients C_1 and C_2 are highly dependent on soil moisture (w_G and w_2) and soil texture. They can be calibrated from measurements or

estimated using parameterizations derived from numerical experiments (Noilhan and Planton, 1989). The water budget for the mean volumetric water content (w_2) in (2) is similar to that in (1) and it is computed as a function of P_G, E_G, transpiration rate (E_{TR}), and gravitational drainage, parameterized by the dimensionless coefficient C_3. The value we used for C_1 was obtained by Mahfouf and Noilhan (1991) from model calibration (C_1/d_1 = 300). The values of the two other soil parameters C_2 and C_3 in (1) and (2) are derived from the soil texture.

The soil water reservoir R_2 (mm) can be directly related to the mean soil moisture w_2 (m^3/m^3) and to root depth d_2 (m):

$$R_2 = \mathbf{1000} \cdot (w_2 \cdot d_2) \qquad \text{(Eq. 7-3)}$$

Water vapor flux (E) is the sum of soil evaporation (E_G) and of vegetation transpiration (E_{TR}), which are given by:

$$E_G = \frac{(1-veg)\,\rho_a}{ra}\,(h_u \cdot q_{sat}(T_s) - q_a) \qquad \text{(Eq. 7-4)}$$

$$E_{TR} = \frac{veg \cdot \rho_a}{ra + Rs}\,(q_{sat}(T_s) - q_a) \qquad \text{(Eq. 7-5)}$$

where veg is the fraction of vegetation cover; ρ_a and q_a are the air density and specific humidity at atmospheric level z_a; $q_{sat}(T_S)$ is the saturated specific humidity at surface temperature T_S; r_a is the aerodynamic resistance; and h_u is the relative humidity at the ground surface. R_S is the surface resistance which corresponds to an integration of leaf stomatal conductance g_s in the vegetation (in ISBA, it depends on photosynthetically active radiation, water availability in the root-zone, air vapor pressure deficit, and surface temperature). The evaporation of water on the leaves (interception reservoir) is also accounted but not shown here.

The vapor flux E is linked to the energy fluxes (net radiation, Rn, ground heat flux, G, sensible heat flux, H) by the standard energy balance equation

$$L\,.\,E = Rn - G - H \qquad \text{(Eq. 7-6)}$$

L being the latent heat of vaporization. G is computed using the force restore method in relation to surface temperature (T_S), mean soil temperature (T_2) and heat capacity of soil and plants. Rn is calculated from surface albedo, emissivity and temperature, and incident radiations.

In (4), relative humidity (h_u) is related to surface soil moisture (w_G) as follows:

$$h_u = \frac{\mathbf{1}}{\mathbf{2}}\left[\mathbf{1} - \cos\left(\frac{w_G}{w_{FC}}\pi\right)\right] \qquad si\ w_G \le w_{FC}$$
$$h_u = \mathbf{1} \qquad si\ w_G > w_{FC} \qquad \text{(Eq. 7-7)}$$

7.2.2. Photosynthesis and stomatal conductance (A-gs model)

The description of photosynthesis and stomatal conductance is based on the Jacobs' leaf model (or A-gs model, Jacobs 1994, Jacobs et al. 1996). It is a semi-empirical physiological model of the leaf photosynthesis rate and net assimilation of CO_2 (An), and of the leaf conductance g_s. The A-gs approach can be considered as more physical than the original description used in ISBA because both physiological responses to external parameters and nonlinear interactions between the various factors are handled, based on rather general relationships. For example, g_s is calculated according to An, consistently with observations showing the strong correlation between water use and CO_2 assimilation (Cowan, 1982). The net assimilation computed by the coupled physiology-SVAT model ISBA-A-gs can be used to estimate LAI through simple parameterizations according to the prescribed climate and CO_2 concentration. This approach seems more pragmatic than coupling a SVAT scheme with very complex

crop or ecosystem models for use in atmospheric models (Ji, 1995). Alternatively, ISBA-A-gs may work with a prescribed value of LAI, like the standard version of ISBA.

The A-g_s approach employed to describe the leaf-scale physiological processes in ISBA-A-g_s (Calvet *et al.*, 1998a) is the model proposed by Jacobs et al. (1996). The photosynthesis rate Am in light-saturating conditions is expressed as:

$$A_m = A_{m,\max}\left[1-\exp\left\{\frac{-g_m^*(C_i-\Gamma)}{A_{m,\max}}\right\}\right] \qquad \text{(Eq. 7-8)}$$

The g_m* parameter (the unstressed mesophyll conductance) is corrected for leaf temperature using a Q_{10}-type function, together with the maximum photosynthesis $A_{m,max}$ and the compensation point Γ. Typical values of $A_{m,max}$ and Γ at a temperature of 25 °C, for C_3 and C_4 plants, are given in Table 7-1.To avoid lengthy iterations, the internal CO_2 concentration C_i is obtained by combining the air CO_2 concentration C_s and Γ through the following closure equation

$$C_i = f\,C_s + (1-f)\,\Gamma \qquad \text{(Eq. 7-9)}$$

Table 7-1. Standard values of the parameters of the A-gs model photosynthesis module, according to the plant type (C3 or C4) (reproduced from Jacobs (1994) in Calvet et al. 1998a)

Parameter (X)	X(@25)	Q_{10}	T_1, °C	T_2, °C
C_3				
ε_0, mg J^{-1}	0.017			
Γ, ppm	45	1.5		
g_m^*, mm s^{-1}	see Table 2	2.0	5	36
$A_{m,\max}$, mg m^{-2} s^{-1}	2.2	2.0	8	38
C_4				
ε_0, mg J^{-1}	0.014			
Γ, ppm	2.8	1.5		
g_m^*, mm s^{-1}	see Table 2	2.0	13	36
$A_{m,\max}$, mg m^{-2} s^{-1}	1.7	2.0	13	38

[a] ε_0 is the maximum quantum use efficiency, Γ the compensation point, g_m^* the mesophyll conductance, and $A_{m,\max}$ the maximum net assimilation of the leaf. The Q_{10}, T_1 and T_2 values modulate the sensitivity of each parameter to temperature through either $X(T_s) = X(@25) \times Q_{10}^{(Ts\,-\,25)/10}$ for Γ or $X(T_s) = X(@25) \times Q_{10}^{(Ts\,-\,25)/10}/\{[1+\exp\{0.3(T_1-T_s)\}]\,[1+\exp\{0.3(T_s-T_2)\}]\}$ for g_m^* and $A_{m,\max}$, where $X(T_s)$ and $X(@25)$ are the values of the parameters corresponding to the leaf temperatures T_s and 25°C, respectively.

The coupling factor f is sensitive to air humidity, expressed through Ds the leaf-to-air saturation deficit, and depends on the cuticular conductance g_c and on g_m* , f_o*, and D_{max}* by

$$f = f_0^*\left(1-D_s/D_{\max}^*\right)+\left(g_c/\left[g_c+g_m^*\right]\right)\left(D_s/D_{\max}^*\right) \qquad \text{(Eq. 7-10)}$$

where f_o* is the value of f for D_s = 0 g kg^{-1} in unstressed conditions. D_{max}* is the maximum leaf-to-air saturation deficit (representing the sensitivity of stomatal aperture to air humidity). D_{max}* is calculated from the value of g_m* (herbaceous species: Calvet 2000, woody species: Calvet et al. 2004). For herbaceous species the maximum ratio between the intercellular and the atmospheric CO_2 concentration is set to a constant value (Calvet, 2000), while it is variable and derived from g_m* for woody species.

The net assimilation *An* is limited by a light deficit according to a saturation equation applied to the photosynthetically active radiation I_a:

$$A_n = (A_m + R_d)[1 - \exp\{-\varepsilon I_a/(A_m + R_d)\}] - R_d \quad \text{(Eq. 7-11)}$$

where leaf respiration is given by $R_d = A_m/9$, and the light conversion efficiency by $\varepsilon = \varepsilon_0 (C_i - \Gamma)/(C_i + 2\Gamma)$, ε_0 being the maximum quantum use efficiency. Finally, the stomatal conductance is

$$g_s = g_c + 1.6\left(A_n - A_{\min}\frac{D_s}{D_{\max}^*}\left(\frac{A_n+R_d}{A_m+R_d}\right) + R_d\left(1 - \frac{A_n+R_d}{A_m+R_d}\right)\right)\Big/(C_s - C_i) \quad \text{(Eq. 7-12)}$$

where A_{min} represents the residual photosynthesis rate (at full light intensity) associated with cuticular transfers when the stomata are closed because of a high saturation deficit:

$$A_{\min} = g_m^* \times g_c (C_s - \Gamma)/(g_m^* + g_c) \quad \text{(Eq. 7-13)}$$

From the above equations, the water use efficiency (i.e. the ratio of A_n to leaf transpiration) can be expressed simply, in the case of a nil value of g_c:

$$W_{UE} = \frac{C_s - \Gamma}{1.6\rho_a}\left[\frac{f_0^*}{D_{\max}^*} + \frac{1 - f_0^*}{D_s}\right] \quad \text{(Eq. 7-14)}$$

where ρ_a is air density. The W_{UE} variable presents a potential minimum value W_{UEn} corresponding to idealistic high values of D_s:

$$W_{UEn} = \frac{C_s - \Gamma}{1.6\rho_a}\left[\frac{f_0^*}{D_{\max}^*}\right] \quad \text{(Eq. 7-15)}$$

In the case of a nil value of both g_c and D_s, the gross photosynthesis rate at high light intensities is

$$A_m = A_{m,\max}\left[1 - \exp\left\{\frac{-g_m^* f_0^* (C_s - \Gamma)}{A_{m,\max}}\right\}\right] \quad \text{(Eq. 7-16)}$$

Leaf assimilation and stomatal conductance are scaled to the canopy level by using a 3 canopy layers radiative transfer model and a Gauss integration procedure. Canopy assimilation A_{nI} and canopy conductance g_{sI} (inverse of the surface resistance R_S) are then given by

$$A_{nI} = \mathrm{LAI} \times \sum_{i=1}^{3} W_i A_n(z_i) \quad \text{(Eq. 7-17)}$$

$$g_{sI} = \mathrm{LAI} \times \sum_{i=1}^{3} W_i g_s(z_i) \quad \text{(Eq. 7-18)}$$

where *zi* and *Wi* are the Gauss levels and weights, respectively.

The impact of soil moisture on stomatal regulation and photosynthesis is accounted in the model. Two different types of drought responses are distinguished for both herbaceous vegetation (Calvet, 2000) and forests (Calvet et al., 2004), depending on the evolution of water use efficiency (W_{UE}) under moderate stress: W_{UE} increases in the early stages of soil water stress in the case of the drought-avoiding response (also called "defensive" strategy), whereas W_{UE} decreases or remains stable in the case of the drought-tolerant response ("offensive" strategy). The main concerned parameters are the classical bounds for extractable water (wilting point and field capacity) and a critical level of extractable soil water (θ_c) defining the early stages of soil water stress.

7.2.3. Growth and mortality in ISBA-A-gs

The most obvious way to predict LAI is to use the canopy net assimilation A_{nI} (kg CO_2 $m^{-2}.s^{-1}$): growth may be described as the accumulation of carbon obtained from the atmospheric CO_2 assimilation, and senescence as the result of a deficit of photosynthesis (due to external factors). In the present version of the model (Gibelin et al. 2006), the leaf biomass B (kg.m^{-2}) is obtained from a differential equation:

$$\mathrm{d}B = \frac{M_\mathrm{c}}{P_\mathrm{c} M_{\mathrm{CO}_2}} \times A_\mathrm{nI}\mathrm{d}t - B\mathrm{d}(t/\tau) \qquad \text{(Eq. 7-19)}$$

In the growth increment term of Eq. 7-19, P_C is the proportion of carbon in the dry plant biomass, M_C and M_{CO2} are the molecular weights of carbon and CO_2 (12 and 44 g.mol^{-1}), respectively. Typical values of P_C can be found in Scholes and Walker (1993, Table 10.1). Here, a constant value of 40% is assumed. The mortality increment term of Eq. 7-19 represents an exponential extinction of B characterized by a time dependent effective life expectancy $\tau(t)$

$$\tau(t) = \tau_\mathrm{M} \frac{A_\mathrm{nfm}(t)}{A_{\mathrm{n,\,max}}} \qquad \text{(Eq. 7-20)}$$

where τ_M is the maximum effective life expectancy, $A_{nfm}(t)$ the maximum leaf net assimilation reached on the day before time t and $A_{n,max}$ the optimum leaf net assimilation. The value of A_{nfm} corresponds to the highest average leaf net assimilation computed on the considered day. Here, the mortality due to unfavourable meteorological factors is estimated daily, according to the ratio between the maximum leaf net assimilation A_{nfm} (computed on the day before) and the optimum leaf net assimilation $A_{n,max}$ (Eq. 7-20): following Eq. 7-19, the biomass B is multiplied (each day) by the factor $exp(-1/\tau)$, where τ (expressed in units of days) is the effective life expectancy on the considered day. The optimum leaf net assimilation $A_{n,max}$ is a constant. It corresponds to the leaf net assimilation given by the Jacobs' model with optimal input values D_s = 0 g.kg^{-1}, I_a = 500 W.m^{-2}, T_S = 25°C for C3 plants and T_S = 35°C for C4 plants. The effective maximum life expectancy of the leaves τ_M represents the period after which 37% of the initial biomass would remain (e-folding), in optimal conditions (i.e. if the maximum leaf net assimilation A_{nfm} would equal $A_{n,max}$ at least once every day).

A simple allocation scheme is used (Gibelin et al. 2006, appendix B), so that two biomass reservoirs are considered: the leaf biomass (B) and the structural biomass (B_s), forming the total nonwoody aboveground biomass (B_T):

$$B_T = B + B_s \qquad \text{(Eq. 7-21)}$$

The structural biomass loses carbon through respiration:

$$R_{Bs} = \eta_R B_S Q_{10}^{(T-25)/10} dt, \qquad \text{(Eq. 7-22)}$$

where T is surface temperature (in degree C), η_R a respiration coefficient of 1% of B_s per day, and Q_{10} = 2.

As in Mougin et al. (1995), Ji (1995), the value of LAI was obtained from B by assuming that for a given vegetation canopy, the ratio between B and LAI is a constant α. Therefore, LAI is given by

$$LAI = \frac{B}{\alpha} \qquad \text{(Eq. 7-23)}$$

The computed value of LAI is related to the integrated net assimilation through the growth model represented by Eqs. 7-19 to 7-23. In Calvet et al. (1998a), only two parameters, the α ratio and τ have to be determined for each canopy type. Also note that an initial prescribed value of LAI is required. The value of the ratio may be set to a specific value in given plant-pedo-climatic conditions (Calvet et al. 1998a), for example as a results of model calibration. However, B/LAI may also be computed from the plant or the leaf nitrogen content (Calvet and Soussana 2001, Gibelin et al. 2006). The nitrogen distribution in the plant biomass depends on growing conditions and has a strong influence on the plant nitrogen concentration (N). Calvet and Soussana (2001) made use of the plant N decline model to relate N to biomass and to estimate the ratio α from the total biomass and the nitrogen content of a so-called 'active biomass'. The plant N decline model is a well-established agronomical law relating the plant nitrogen in non-limiting N-supply conditions to the accumulated above-ground dry matter (Greenwood et al., 1990; Greenwood et al., 1991; Justes et al., 1994; Lemaire and Gastal, 1997). The resulting application of the concept to ISBA-A-gs has been simplified by Gibelin et al. (2006) in order to provide a simple relation between α and the leaf nitrogen content N_l (%):

$$\alpha = \frac{B}{LAI} = \frac{1}{SLA} = \frac{1}{eN_l + f} \qquad \text{(Eq. 7-24)}$$

In the previous equation, α defined as the ratio of leaf biomass to LAI turns to be the inverse of the Specific Leaf Area (SLA). The plasticity parameters e (in m^2 kg^{-1} $\%^{-1}$) and f (in m^2 kg^{-1}) are calibrated parameters (for example for each biome). In the present version of the model, the leaf nitrogen content has to be given as input. While e and f are considered here as genetic parameters of the plant and do not depend on growing or climatic conditions, N_l depends on external factors (e.g., agricultural practice of N fertilisation) and may be calibrated.

7.2.4. List of ISBA-Ags inputs and typical prescribed parameter values

Input parameters for the ISBA-Ags dynamic soil-vegetation-atmosphere transfer model are sorted in different categories:

Soil characteristics:

wilting point,	w_{WP}	(m^3m^{-3})
field capacity,	w_{FC}	(m^3m^{-3})
soil texture	% clay and % sand	

These parameters depend on the soil at the site of application of the model.

Vegetation and soil composite characteristics:

Surface albedo	a	
Surface emissivity	ε	
Soil column or root zone maximum depth	d_2	(m)

These parameters depend on the vegetation type and the soil at the site of application. They may have to be changed in time because of the evolution of the vegetation, for example from remote sensing or climatology maps (Champeaux et al. 2005).

Vegetation characteristics

Photosynthetic and stomatal conductance parameters

Unstressed mesophyll conductance at 25°C	g_m*	(mm s^{-1})
Maximum leaf-to-air saturation deficit	D_{max}*	(g kg^{-1})
Maximum value of the leaf [CO2] ratio	f_o*	
Cuticular conductance	g_c	(mm s^{-1})
Critical extractable soil moisture	θ_c	(m^3m^{-3})
Strategy of response to water stress	S	
Photosynthesis type	C3 or C4	

Plant growth and mortality parameters

Potential leaf life expectancy	τ_M	(day)
Minimum leaf area index	LAImin	(m^2 m^{-2})
Nitrogen plasticity parameter (slope)	(m^2 kg^{-1} $\%^{-1}$)	
Nitrogen plasticity parameter (intercept)	(m^2 kg^{-1})	
Leaf nitrogen concentration	N_l	(%)

These parameters depend on the vegetation type. However, while a large work was done for giving generic values to the parameters (see the paper list in the sorted bibliography below), they may depend on the interaction between the canopy processes and the environment in terms of climate, soil type and management practices (fertilisation, irrigation…). Thus, when the model has to be applied to a specific site some of these parameters may have to be tuned. The experience on tuning ISBA-A-gs parameters leads mainly to tune parameters related to mesophyll conductance (g_m*), life expectancy (τ_M), minimum leaf area index (LAImin) and leaf nitrogen concentration (N_l). The tuning is usually done by comparing ISBA-A-gs outputs to measured soil moisture, LAI and Biomass (e.g. Inoue and Olioso 2006 on an earlier version of ISBA-A-gs).

Parameters for the Plant Functional Type (PFT)

The PFT used for ISBA-A-gs at global scale have been defined in Gibelin et al. (2006). The values of plant parameters and plant-soil composite parameters at global scale are given in Table 7-2**.** Parameters values were obtained from a compilation of the studies by Gibelin (2007), Gibelin et al. (2006), Mafhouf et al. (1995) and Calvet et al. (2007).

ISBA-A-gs driving variables

Driving variables required as input of ISBA-A-gs relate to climate forcing:

- Incident solar and longwave radiations
- Air temperature and specific air humidity
- Wind speed
- Precipitation amount and Irrigation amount
- Atmospheric CO_2 concentration
- Atmospheric pressure

Table 7-2. Parameter values for the various PFT presented in Gibelin et al. (2006). Parameters values were given from the study by Gibelin (2007), Gibelin et al. (2006), Mafhouf et al. (1995) and Calvet et al. (2007). For the strategy of response to water stress in column '*S*', 'a' means drought-avoiding and 't' drought-tolerant strategy.

	A	ε	d_2	g_m*	D_{max}*	f_o*	g_c	θ_c	τ_M	LAImin	e	f	N_l	S
	-	-	(m)	(mm s^{-1})	(g kg^{-1})	-	(mm s^{-1})	($m^3 m^{-3}$)	(day)	(m^2 m^{-2})	(m^2 kg^{-1} $\%^{-1}$)	(m^2 kg^{-1})	(%)	
Deciduous broadleaf trees	0.12	0.970	2.00	3	109	0.51	0.15	0.3	230	0.3	4.83	2.53	2	t
Evergreen broadleaf trees	0.12	0.970	3.00	2	124	0.57	0.15	0.3	365	1	4.83	2.53	2.5	a
Needleleaf trees	0.10	0.970	2.00	2	124	0.57	0.00	0.3	365	1	4.85	-0.24	2.8	a
C3 crops	0.20	0.970	0.95	1	50	0.95	0.25	0.3	150	0.3	3.79	9.84	1.3	a
C4 crops	0.20	0.970	0.95	9	33	0.60	0.15	0.3	150	0.3	7.68	-4.33	1.9	t
Irrigated crops	0.20	0.970	0.95	9	33	0.60	0.15	0.3	150	0.3	7.68	-4.33	1.9	t
C3 natural herbaceous	0.20	0.970	0.95	1	50	0.95	0.25	0.3	150	0.3	5.56	6.73	1.3	t
C4 natural herbaceous	0.20	0.970	0.95	6	52	0.60	0.15	0.3	150	0.3	7.68	-4.33	1.3	t
Irrigated herbaceous	0.20	0.970	0.95	1	50	0.95	0.25	0.3	150	0.3	5.56	6.73	1.3	t

7.2.5. Sorted ISBA ISBA-A-gs bibliography

- *Description of the ISBA model*

  Noilhan, J. and Planton, S. (1989). A simple parameterization of land surface processes for meteorological models. *Monthly Weather Review*, 117, 536–549.

  Mahfouf, J.-F., and J. Noilhan (1991), Comparative study of various formulations of evaporation from bare soil using in situ data, *Journal of Applied. Meteorology., 30*, 1354-1365

  Noilhan, J., Mahfouf, J.-F., (1996). The ISBA land surface parameterisation scheme. *Global Planetary Changes*, 13, 145-159.

  Mahfouf, J.-F., Noilhan, J., (1996), Inclusion of gravitational drainage in a land surface scheme based on the force restore method, *J. Appl. Meteorol.*, 35(6), 987-992.

- *Description and in situ validation of the original version of the ISBA-Ags SVAT model*

  Calvet, J.-C., J. Noilhan, J.-L. Roujean, P. Bessemoulin, M. Cabelguenne, A. Olioso and J.-P. Wigneron (1998a), An interactive vegetation SVAT model tested against date from six contrasting sites, *Agric. For. Meteorol.*, 92, 73–95.

- *Improvement of the response to the soil moisture stress*

  Calvet, J.-C. (2000), Investigating soil and atmospheric plant water stress using physiological and micrometeorological data, *Agric. For. Meteorol.*, 103, 229– 247.

  Calvet, J.-C., V. Rivalland, C. Picon-Cochard and J.-M. Guehl (2004), Modelling forest transpiration and CO_2 fluxes - Response to soil moisture stress*, Agric. For. Meteorol.*, 124, 143–156.

- *Account for nitrogen impact on leaf growth*

  Calvet, J.-C., and J.-F. Soussana (2001), Modelling CO2-enrichment effects using an interactive vegetation SVAT scheme, *Agric. For. Meteorol.*, 108, 129– 152.

- *Global scale application of the ISBA-A-gs model*

  Gibelin A.L., J.-C. Calvet, J. L. Roujean, L. Jarlan and S.O. Los (2006), Ability of the land surface model ISBA-A-gs to simulate leaf area index at the global scale: Comparison with satellites products*, Journal of Geophysical Research*, Vol 111, D18102, doi:10.1029/2005JD006691

- *Analysis of climate change scenarios with ISBA-A-gs*

  Gibelin A.L., J.-C. Calvet, J. L. Roujean, L. Jarlan and S.O. Los (2006), Ability of the land surface model ISBA-A-gs to simulate leaf area index at the global scale: Comparison with satellites products, Journal of Geophysical Research, Vol 111, D18102, doi:10.1029/2005JD006691

- *Use of ISBA and ISBA-Ags in assimilation studies*

  Calvet, J.-C., J. Noilhan and P. Bessemoulin, (1998b). Retrieving the root-zone soil moisture from surface

  soil moisture or temperature estimates: a feasibility study based on field measurements. *J. Appl. Meteor.*, Vol. 37, No. 4, pp. 371-386.

  Calvet, J.-C., and J. Noilhan, (2000). From near-surface to root-zone soil moisture using year-round

  data. *J. Hydromet.*, Vol. 1, No. 5, pp. 393-411.

  Inoue, Y., Olioso, A., (2004). Estimating the Dynamics of CO2 Flux in Agro-Ecosystems based on Synergy of Remote Sensing and Process Modeling - A Methodological Study. *In Global Environmental Change in the Ocean and on Land*, Eds., Masae Shiyomi, Hodaka Kawahata, Hiroshi Koizumi, Atsushi Tsuda and Yoshio Awaya, pp. 375-390. TERRAPUB, Tokyo, 2004.

Inoue, Y., Olioso A., (2006). Estimating the dynamics of ecosystem CO2 flux and biomass production in agricultural fields on the basis of synergy between process models and remotely sensed signatures.

Journal of Geophysical Research., Vol. 111, No. D24, D24S91, doi: 10.1029/2006JD007469

Mahfouf, J.-F., (1991). Analysis of soil moisture from near-surface parameters: a feasibility study. *J. Appl. Meteor.*, Vol. 30, No. 11, pp. 1534-1547.

Olioso, A., Inoue, Y., Ortega-Farias, S., Demarty, J., Wigneron, J.-P.,Braud, I., Jacob, F., Lecharpentier, P., Ottlé, C., Calvet, J.-C., Brisson, N., (2005). Future directions for advanced evapotranspiration modeling: assimilation of remote sensing data into crop simulation models and SVAT models.

Irrigation and Drainage Systems, 19, 377-412.

Munoz-Sabater J. M., L. Jarlan, J.-C. Calvet, F. Bouyssel and P. de Rosnay, (2007). From near-surface to root-zone soil moisture using different assimilation techniques, *Journal of Hydrometeorology*, 8, 194-206.

Wigneron, J.-P., Chanzy, A., Calvet, J.-C., Olioso, A., Kerr, Y., (2002). Modeling approaches to assimilating L-band passive microwave observations over land surfaces. *Journal of Geophysical Research*, 107(D14), 10.1029/2001JD000958.

Wigneron, J.-P., Calvet, J.-C., Olioso, A., Chanzy, A., Bertuzzi, P., (1999). Estimating the root-zone soil moisture from the combined use of time series of surface soil moisture and SVAT modeling.

Physics and Chemistry of the Earth, Part B, 24(7), 837-843.

Wigneron, J.-P., Olioso, A., Calvet, J.-C., et Bertuzzi, P., (1999). Estimating root-zone soil moisture from surface soil moisture data and soil-vegetation-atmosphere transfer modeling. *Water Resources Research*, 35 (12), 3735-3745.

7.3. Coupling SCOPE and ISBA-A-gs

The actual coupling between SCOPE and ISBA-A-gs is presented in . One central point in the combination of both models concerns the coupling variables which are simulated by ISBA-A-gs and then used as input for SCOPE at each required time step: leaf area index, surface soil moisture and root zone soil moisture. Another key coupling point concerns the nitrogen apparatus of the leaves: leaf nitrogen content (N_l) is used as an input parameter in ISBA-A-gs for computing the specific leaf area and then the leaf area index from simulated biomass. It may also be used for computing two very important SCOPE parameters, C_{ab} the leaf chlorophyll content (input for radiative transfer simulations in the solar domain and which has a large influence on SIF signals) and *Vcmo* the maximum carboxylation capacity which is a main parameter for computing leaf photosynthesis.

Vcmo and C_{ab} have been related to leaf nitrogen content in many studies (Xu and Baldocchi 2003, Wilson et al. 2000, Leuning et al. 1998, Houlès et al. 2007, Grossman-Clarcke et al. 1999, Johnson et al. 1987...). In Johnson et al. (1987) a relationship between *Vcmo* and the leaf nitrogen content N_l is given for wheat as:

$$Vcmo = 20 * Vcmo\_ref * N_l \quad (7\text{-}25)$$

with $Vcmo\_ref = 150$ µmol.m^{-2}.s^{-1}.

In Houlès et al. (2007) relations between leaf nitrogen content and chlorophyll content (C_{ab} in µg cm^{-2}) have been obtained at several phenological stages. A median relation (beginning of May) is :

$$C_{ab} = 50 * N_l - 50 \quad (7\text{-}26)$$

C_{ab} calculations were also performed from nitrogen information using the relationships developed by Weiss et al. (2001) relating the chlorophyll content to the nitrogen index N_u defined by the plant N decline model. The plant N decline model is a well-established agronomical law relating the plant nitrogen in non-limiting N-supply conditions to the accumulated above-ground dry matter (Greenwood et al., 1990; Greenwood et al., 1991; Justes et al., 1994; Lemaire and Gastal, 1997).

$$C_{ab} = 15.78\ N_u^2 + 52.89\ N_u + 24 \qquad (7\text{-}27)$$

with C_{ab} never exceeding 93 µg cm^{-2}.

The coupling between ISBA-A-gs and SCOPE is only one way, SCOPE being used as an operator for the simulation of remote sensing signal. Thus, SCOPE may be activated independently of ISBA-A-gs each time remote sensing signal simulations are required (e.g. only for clear sky conditions). SCOPE is well suited for that use since it does not include water transfers in the soil and vegetation growth which impairs the possibility to use it over time rage larger than a few consecutive days. Similar types of coupling developed for implementing assimilation of remote sensing data into vegetation processes models were presented by Weiss et al. (2001) or Olioso et al. (2005).

In order to save time when the demonstration of reflectance and thermal infrared data only were required, we implemented the direct coupling of ISBA-A-gs to simpler radiative transfer models following the same scheme as in as an alternative to the ISBA-A-gs - SCOPE coupling (several hundred times slower). We used a standard mono-layer version of SAIL including the PROSPECT leaf optical property model for simulating reflectances (Weiss et al. 2001) and the SAIL-Thermique version for simulating thermal infrared brightness temperature (Olioso 1995, et al. 2007).

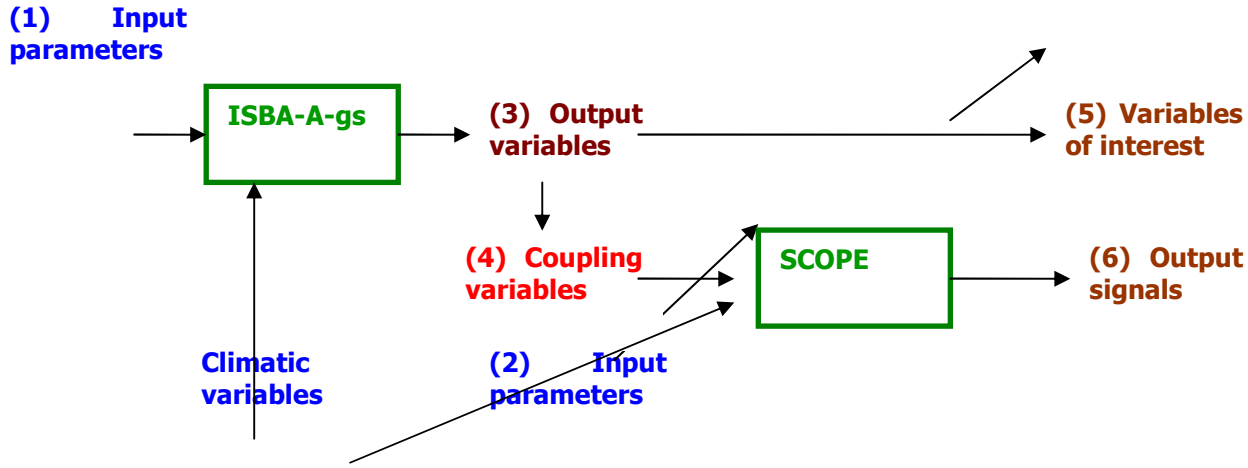

Figure 7-1. Coupling scheme between ISBA-A-gs and SCOPE

(1) Input parameters for ISBA-A-gs	Examples: wilting point, field capacity, leaf nitrogen content, mesophyll conductance, albedo...
(2) Input parameters for SCOPE	Examples: leaf inclination distribution (input parameters for SAIL), soil optical properties, input parameters for PROSPECT, marginal cost of assimilation (λ).....
(3) ISBA-A-gs output variables	Examples: LAI, surface soil moisture, soil moisture in the root zone, biomass, energy balance fluxes, aerodynamic surface temperature...
(4) Coupling parameters and variables	LAI, surface and root zone soil moisture Nitrogen content (ISBA-A-gs input parameter) used for computing specific leaf area, leaf chlorophyll content content and *Vcmo* (the maximum carboxylation capacity).
(5) Variables of interest	Examples: photosynthesis, biomass, evapotranspiration....
(6) Output signals	directional spectral reflectances directional thermal infrared radiances directional SIF

7.4. Implementation and calibration of ISBA-A-gs on Avignon dataset (local and global simulation sets)

ISBA-A-gs was calibrated over the Avignon test site for the two crop types that were considered in this study. The calibration process was a simple eye-fitting method since no high accuracy requirements were given for this study.

Driving variables required as input of ISBA-A-gs relate to climate forcing and were derived from the micrometeorological data:

- Incident solar and longwave radiations — direct measurements of Rg and Ra
- Air temperature — direct measurements of Ta
- Specific air humidity — derived from relative humidity RH measurements using standard thermodynamic relationships
- Wind speed — direct measurements
- Precipitation amount — direct measurements
- Irrigation amount — estimated from irrigation schedule
- Atmospheric CO2 concentration — direct measurements
- Atmospheric pressure — direct measurements

Input parameters for the ISBA-Ags dynamic soil-vegetation-atmosphere transfer model used in the study were either derived from the study by Gibelin et al. (2006), Gibelin (2007), from the Avignon site database, or by calibrating the model. The model was calibrated by considering the seasonal course of LAI as a major driving variable, and the evolution of soil moisture as a secondary variable. Five main parameters were tuned: the maximum mesophyll conductance (g_m*), the maximum leaf life expectancy (τ_M), the leaf nitrogen content (N_l), the field capacity and the wilting point (w_{WP} and w_{FC}; these two last parameters were just used for setting soil moisture limits from the measurements). The values derived for each parameter and for the two crop cycles are given in Table 7-3 and the graphs with the calibration results expressed as a function of Day of the Year (DOY) in Figure 7-2 to Figure 7-5. The calibration results are also compared to parameter values and model simulations obtained from parameters used at the global scale by Gibelin et al. (2006). These parameters and simulations were termed as 'global' in reference to their use at the global scale in Gibelin et al. (2006). Conversely, parameters and simulations obtained after calibration were termed as 'local'. Table 7-3 display parameters both before calibration (C3 crop PFT, 'global set') and after on-site calibration (Wheat (local set)). Figure 7-2 and Figure 7-3 display LAI and soil moisture simulations for the two sets of parameters (local and global).

Simulations using both sets of parameters show the impact of the calibration processes. Impact was larger for the wheat simulations which presented significant differences in terms of parameters and LAI. The reason of such differences will have to be investigated further. In the case of sorghum the differences were very low despite the differences in parameter values (g_m* and τ_M mainly). However, the g_m* value of 6 is in very good agreement with the meta-analysis performed by Calvet (2000) for C4 crops. Soil moisture simulations were not perfectly fitting the measurements for both crops. This fitting was not improved further as soil moisture in the root zone was not a determinant input for the remote sensing signal simulation study.

Table 7-3. Values of ISBA-A-gs input parameters used for simulating wheat (C3) and sorghum (C4) processes. In the case of wheat local (using parameters calibrated at the local site) and global (C3 crop PFT using the original parameters, e.g. from Gibelin et al. (2006)) were presented.

Parameter	Symbol	Unit	Wheat (local set)	Sorghum	Source of information	C3 crop PFT (Global set)
Wilting point	w_{WP}	(m^3m^{-3})	0.2	0.2	Calibrated	0.2
Field capacity	w_{FC}	(m^3m^{-3})	0.3	0.3	Calibrated	0.3
Clay fraction		(%)	33.5	33.5	Site information	33.5
Sand fraction		(%)	15.6	15.6	Site information	15.6
Surface albedo	a		0.2	0.2	Mahfouf et al (1996) confirmed by measurements on site	0.2
Surface emissivity	ε		0.97	0.97	Mahfouf et al (1996) confirmed by measurements on site	0.97
Soil column	d_2	(m)	1	1	Site information	0.95
Unstressed mesophyll conductance at 25°C	g_m*	($mm\ s^{-1}$)	6	5	Calibrated	1
Maximum leaf-to-air saturation deficit	D_{max}*	($g\ kg^{-1}$)	50	33	Gibelin et al. (2006)	50
Maximum value of the leaf [CO_2] ratio	f_o*		0.95	0.60	Gibelin et al. (2006)	0.95
Cuticular conductance	g_c	($mm\ s^{-1}$)	0.25	0.15	Gibelin et al. (2006)	0.25
Critical extractable soil moisture	θ_c	(m^3m^{-3})	0.3	0.3	Gibelin et al. (2006)	0.3
Strategy of response to water stress	S		avoiding	tolerant	Gibelin (2007)	avoiding
Potential leaf life expectancy	τ_M	(day)	180	100	Calibrated	150
Minimum leaf area index	LAImin	($m^2\ m^{-2}$)	0.05	0.05	Calibrated	0.3
Nitrogen plasticity parameter (slope)	e	($m^2\ kg^{-1}\ \%^{-1}$)	3.79	7.68	Gibelin et al. (2006)	3.79
Nitrogen plasticity parameter (intercept)	f	($m^2\ kg^{-1}$)	9.84	-4.33	Gibelin et al. (2006)	9.84
Leaf nitrogen concentration	N_l	(%)	3	2.1	Calibrated	1.3

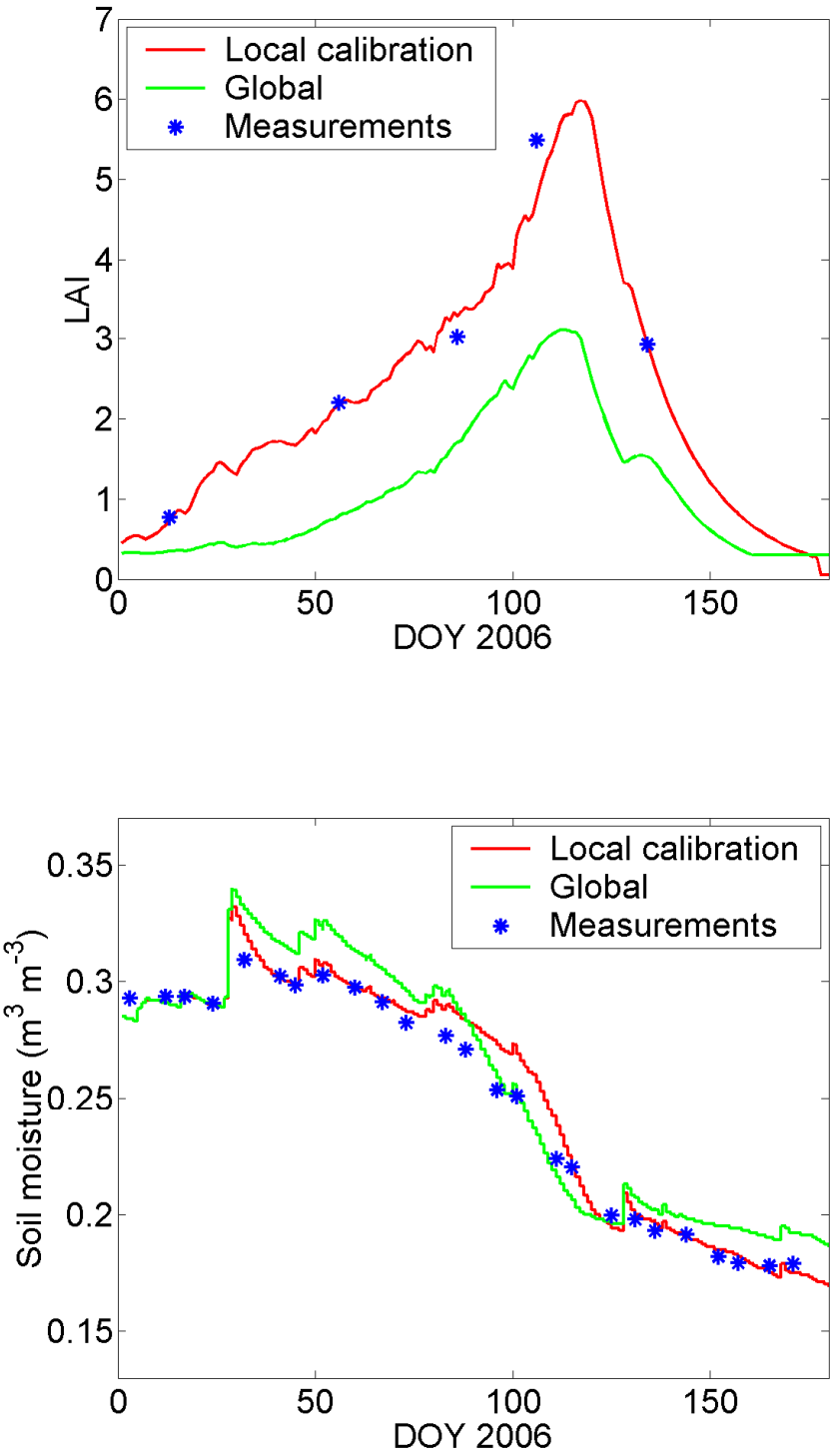

Figure 7-2. Evolution of LAI and soil moisture simulated by ISBA-A-gs with the global set of parameters (C3 crop PFT) and the local calibration for wheat in Avignon. Measurements that were used for the calibration are also presented. DOY is the Day Of the Year.

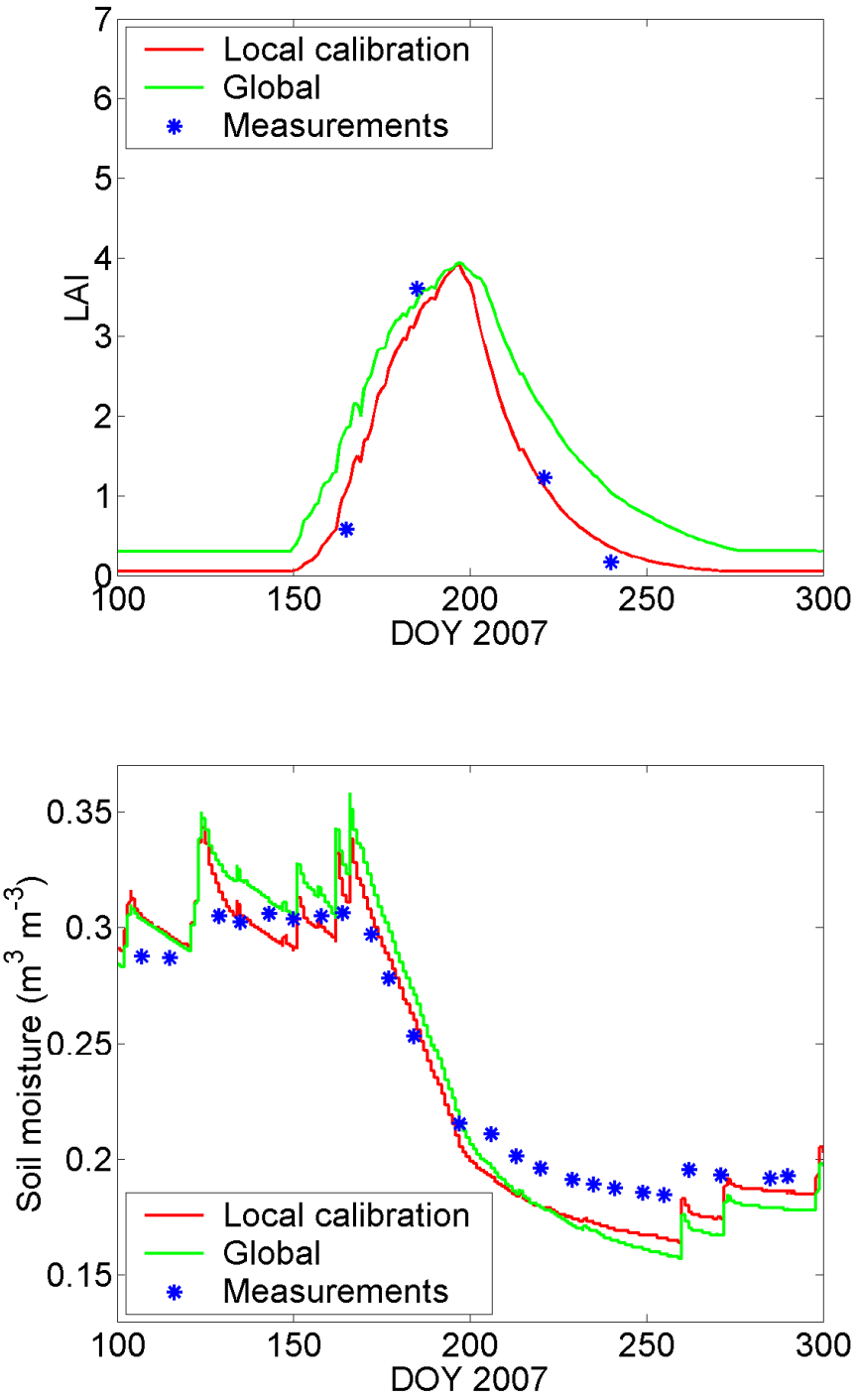

Figure 7-3. Evolution of LAI and soil moisture simulated by ISBA-A-gs with the global set of parameters (C4 crop PFT from Table 7-2) and the local calibration for sorghum in Avignon. Measurements that were used for the calibration are also presented. DOY is the Day Of the Year.

Figure 7-4 to Figure 7-6present the simulations of gas exchanges by ISBA-A-gs as a function of the Day of Year (DOY) for the whole sorghum and wheat season, as well as for specific three days sequences in January-February, March, April and May. *LE* is the latent heat flux and *Ac* the CO_2 flux. The black lines are the half-hourly simulations and the green lines the daily average. The figures show that flux values were globally correlated to LAI with a strong decrease at the end of the vegetation cycle. Latent heat flux also displayed peaks which were linked to rain events. CO_2 flux presents positive values outside of the vegetation season which were linked to CO_2 efflux from the soil (soil respiration). Its variations are linked to surface temperature variations which were considered as the main driving variable for soil respiration.

7.5. Implementation and calibration of SCOPE on Avignon dataset

The implementation and the calibration of SCOPE-D over the Avignon wheat dataset has been presented above in Chapter 6.2.

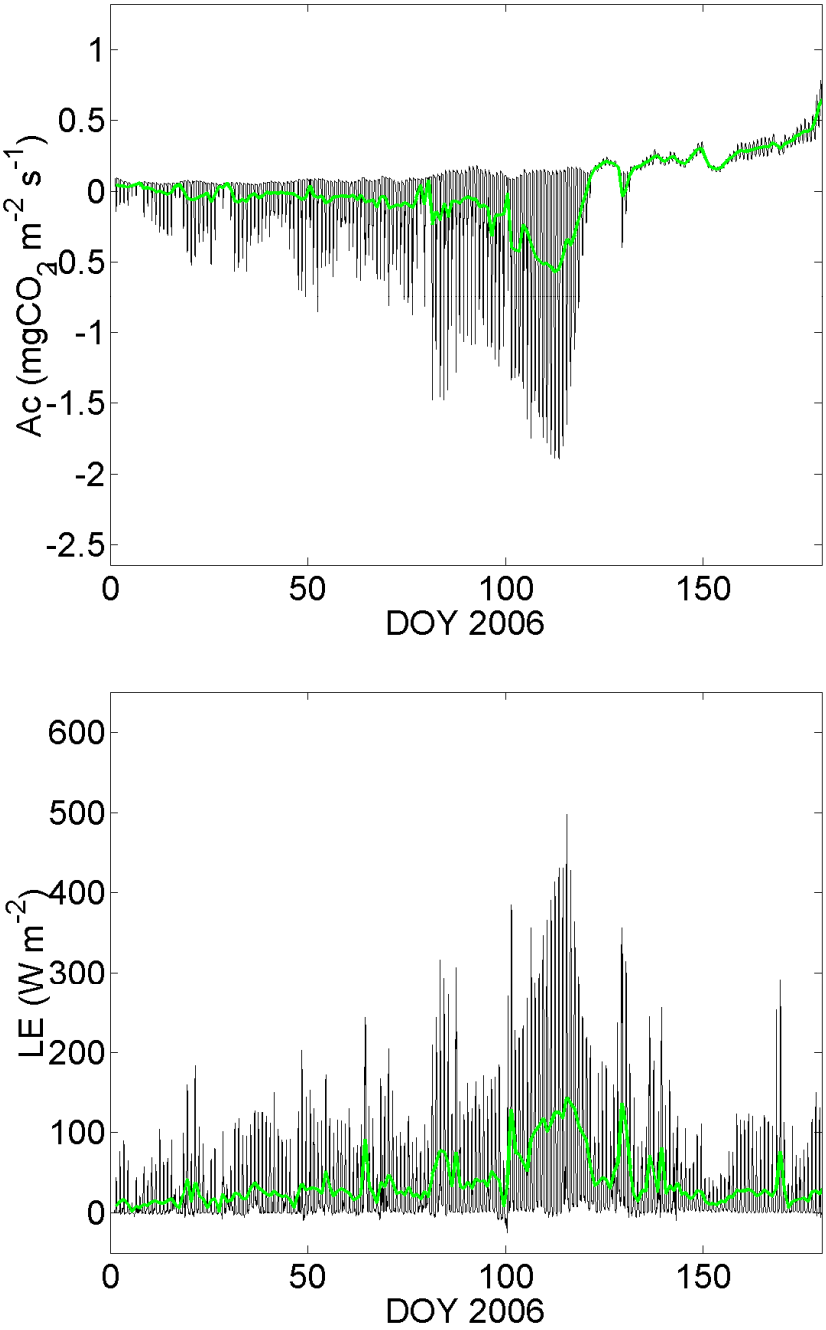

Figure 7-4. Evolution of CO2 (*Ac*) and latent heat (*LE*) flux simulated by ISBA-A-gs with the local set of parameters for wheat in Avignon. DOY is the Day Of the Year. The black lines are the half-hourly simulations and the green lines the daily average.

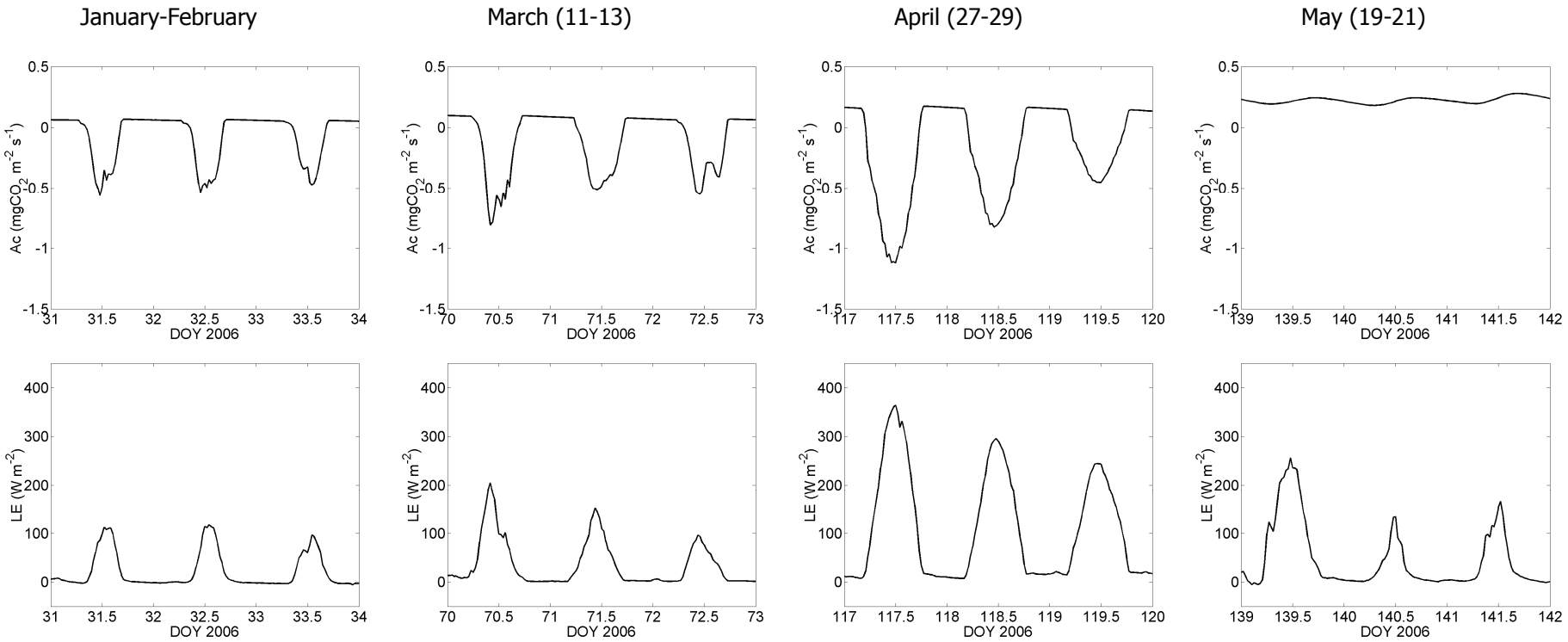

Figure 7-5. CO2 (*Ac*) and latent heat (*LE*) flux simulated by ISBA-A-gs with the local set of parameters for wheat in Avignon for specific period of time along the crop season. DOY is the Day Of the Year.

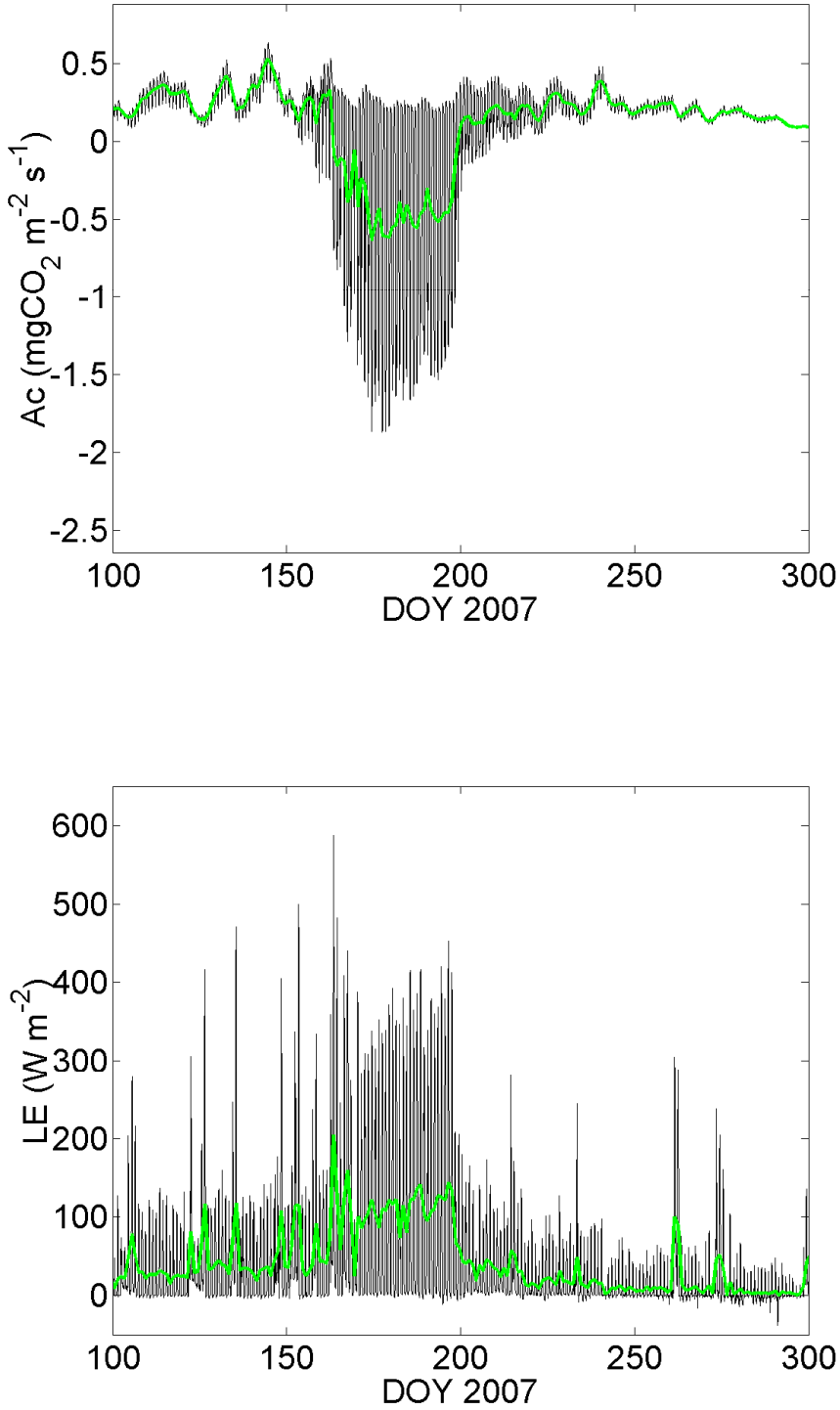

Figure 7-6. Evolution of CO2 (*Ac*) and latent heat (*LE*) flux simulated by ISBA-A-gs with the local set of parameters for wheat in Avignon. DOY is the Day Of the Year. The black lines are the half-hourly simulations and the green lines the daily average.

7.6. Simulation of remote sensing data time profiles from the coupled ISBA-A-gs – SCOPE model

Simulations of remote sensing data were performed using SCOPE-D, SAIL and SAIL-Thermique plugged on the output of ISBA-A-gs at 10 am and at nadir:

- green (550 nm), red (640nm) and near infrared reflectances (810 nm) (SCOPE, SAIL);
- thermal infrared brightness temperature (SCOPE, SAIL-Thermique);
- solar induced fluorescence (SCOPE).

Parameters values used in the coupling are given in Table 7-3 for the wheat dataset in three cases:

- 'global ISBA' based on the input parameter set used for global studies (Gibelin et al. 2006);
- 'local ISBA' based on the 'local' calibration performed for the study (described just above);
- 'observations' based on the measured data in Avignon (see section 7.5).

		ISBA global	ISBA local	Observation
Vcmo	$\mu molCO_2.m^{-2}.s^{-1}$	39 (derived from N_l)	90 (derived from N_l)	Figure A- 4
C_{ab}	$\mu g.cm^{-2}$	80 (derived from N_l)	90 (derived from N_l)	Figure A- 4
LAI	$m^2.m^{-2}$	simulated LAI, Figure 7-2	simulated LAI, Figure 7-2	Figure A- 4
Lam (or λ)	-	1000	1000	1000
Jmo	$\mu molCO_2.m^{-2}.s^{-1}$	2.65 x Vcmo	2.65 x Vcmo	2.65 x Vcmo
θ		simulated w_2 Figure 7-2	simulated w_2 Figure 7-2	Figure A- 3
$\theta_{0\text{-}5f}$	$m^3.m^{-3}$	simulated w_G	simulated w_G	measured

Table 7-4. List of the main SCOPE and SAIL input parameters used in the three simulated cases. Other parameters and the signification of each parameter are given in Figure 7-3. w_2 and w_G are the simulated root zone and surface soil moisture as simulated by ISBA-A-gs.

Simulation of fluorescence signal at 680 and 760 nm are shown in Figure 7-7**.** Simulations of thermal infrared brightness temperature, reflectances and NDVI are presented in Figure 7-8 to Figure 7-11for comparison**.** The three remote sensing domains present differences between the simulated scenarios in agreement with the differences in the evolution of LAI and soil moisture (Figure 7-2)**.**

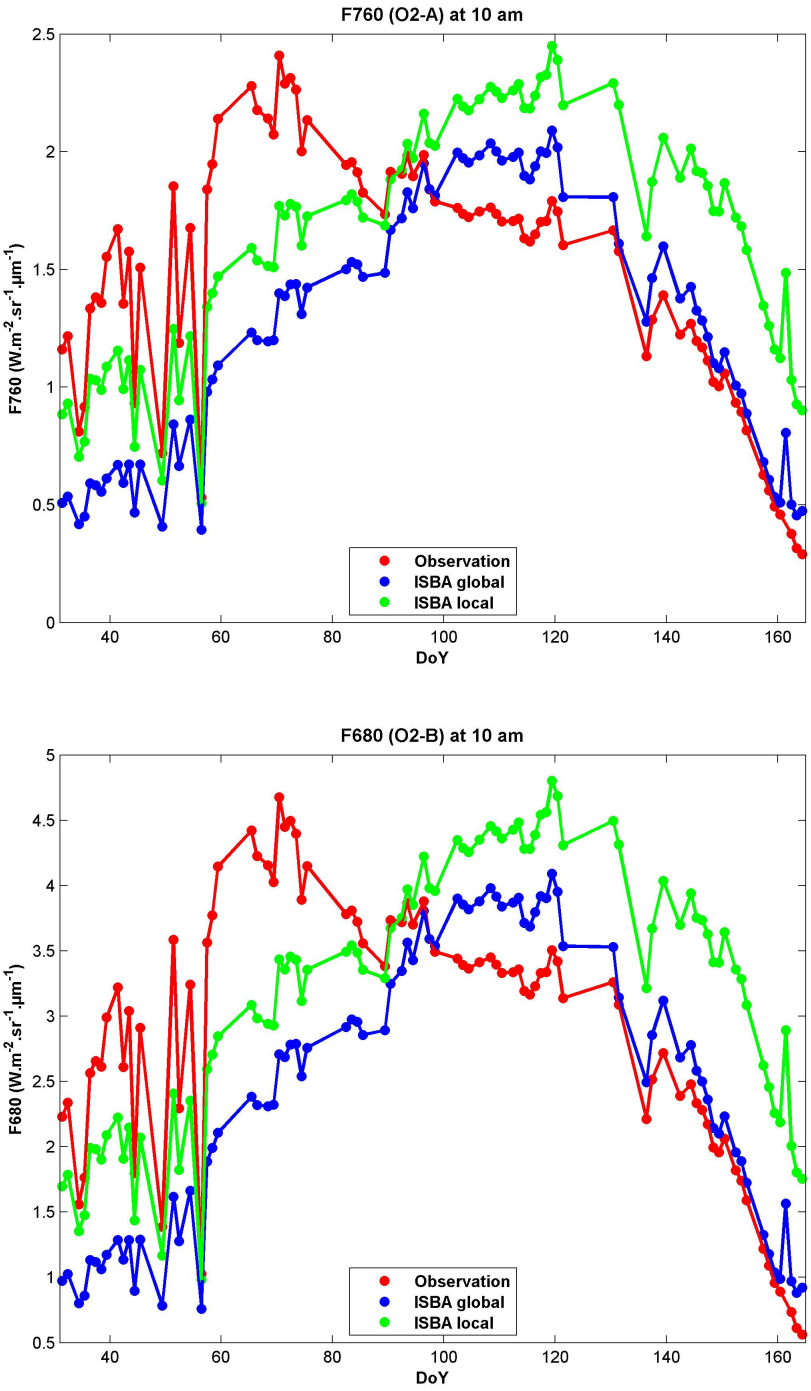

Figure 7-7. Simulation of fluorescence at 760 and 680 nm for the three scenarios in Figure 7-4.

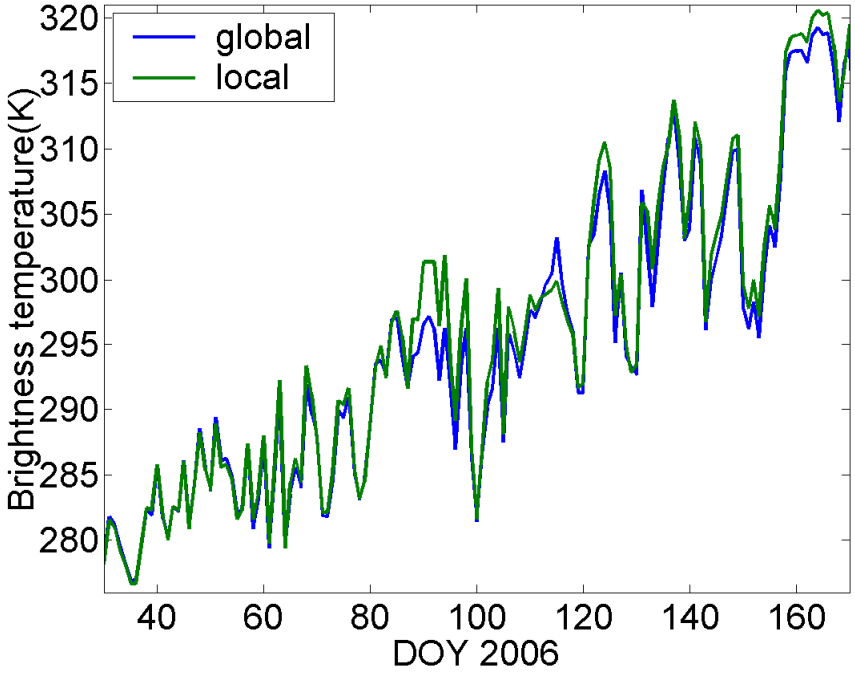

Figure 7-8. Simulation of thermal infrared brightness temperature for the two ISBA-A-gs simulations.

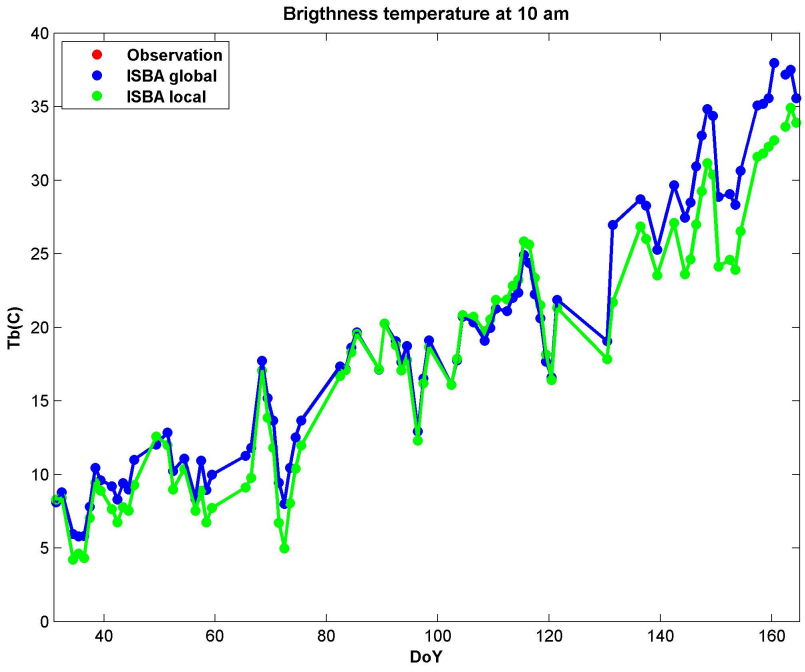

Figure 7-9. Simulation of thermal infrared brightness temperature at nadir with SCOPE from the two ISBA-A-gs scenarios 'local' and 'global'.

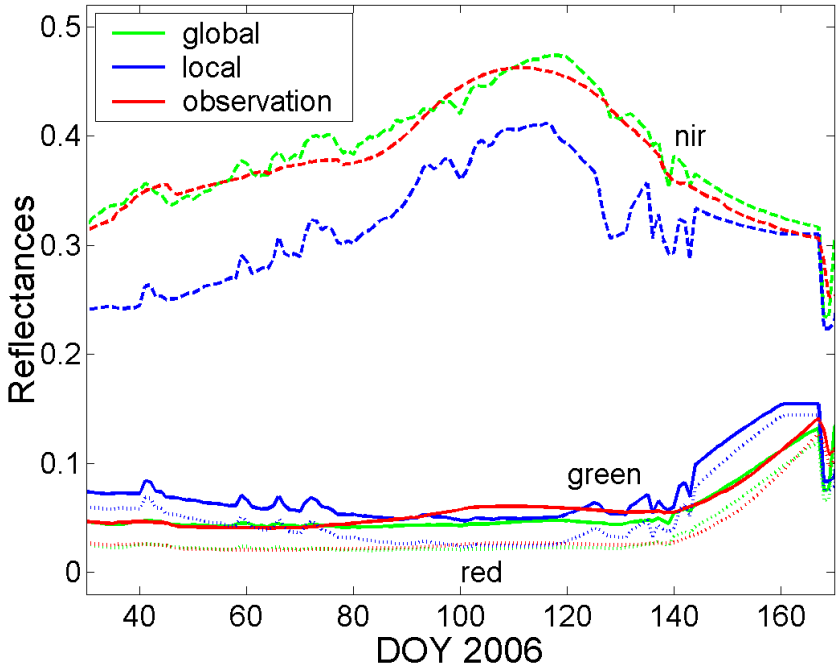

Figure 7-10. Simulation of reflectances in green (550 nm, full lines), red (640nm, dotted lines) and near infrared reflectances (810 nm) for the three scenarios in Figure 7-4.

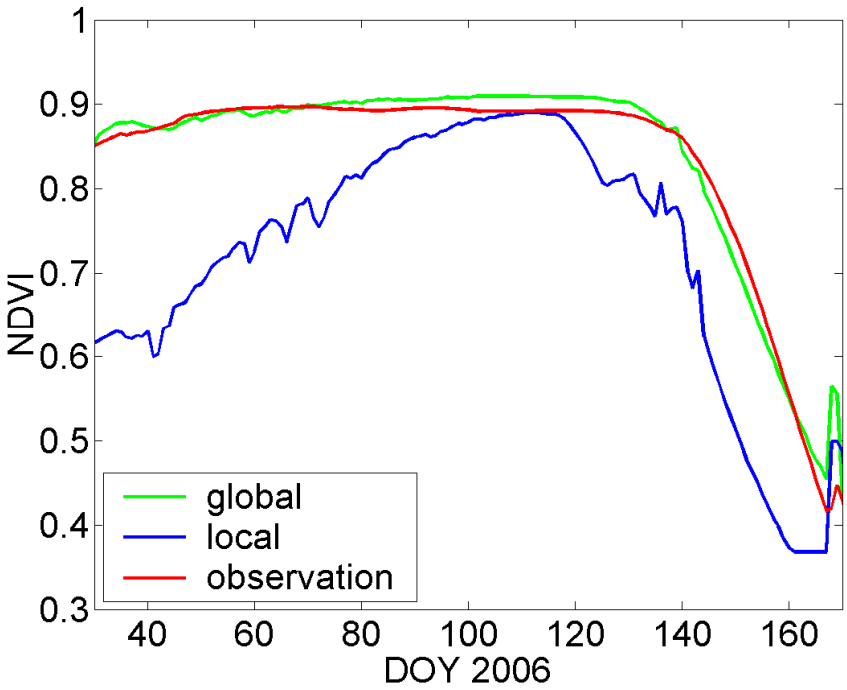

Figure 7-11. Simulation of NDVI for the three scenarios in Figure 7-4.

Concerning fluorescence emission:

- for the 'local' and the 'global' scenarios the seasonal evolutions of signals were mainly linked to the evolution of LAI (signal increasing with LAI);
- differences between 'local' and 'global' scenarios were mainly linked to the differences in LAI (with a small contribution of the differences in V*cmo*, C_{ab} being close in the two scenarios);
- scenario 'observation' presented a different time structure with higher values at the beginning of the simulated period and lower values at the end, with a strong decrease between DOY 70 and 90;
- the differences were linked to the time evolution of V*cmo* and C_{ab} which had high values at the beginning of the period (V*cmo* was very high, up to 170 µmol.m^{-2}.s^{-1}) while they were constant in the two other scenarios
- signal oscillations at the beginning of the simulated period are linked to variations in solar irradiance

For brightness temperature and reflectances:

- general evolution of reflectances and NDVI were mainly related to LAI; oscillations were linked to variations in surface soil moisture)
- differences in reflectances were mainly linked to differences in LAI ('local' and 'observation' scenarios have almost similar LAI); they are mostly visible in the near infrared channel
- general evolution and fluctuations of temperature were mainly linked to the evolutions of incident radiation and air temperature
- simulations of brightness temperatures by the two models were different; actually, SCOPE simulations did not accounted fully of the evolution of soil moisture impact on canopy processes since the parameter λ was kept constant; thus, for SCOPE simulations, temperature differences were mainly linked to differences in LAI;
- in the case of ISBA-A-gs, differences in surface temperature were more complex to interpret since they were linked to a combination of the effect of LAI (increasing transpiration / evaporation), level of soil moisture in the root zone and in surface, and level of mesophyll conductance in ISBA-A-gs (which was very different between 'local' and 'global')

When comparing the various signals, it was possible to notice that

- only near infrared reflectances and fluorescence were providing systematic differences between the 'global' and the 'local' scenarios (which greatly differed in terms of canopy evolution);
- conversely to reflectances, fluorescence signal were very sensitive to physiological processes of photosynthesis (*Vcmo*) which could make it possible to discriminate two canopies with a similar cover but a different photosynthetic activity (comparison between 'local' and 'observation' scenarios).

8. CONCLUSIONS AND RECOMMENDATIONS

Based on the results of the project it is possible to draw a set of recommendations for the design and operation of a future satellite mission aimed at the remote sensing of chlorophyll fluorescence and the estimation of vegetation photosynthetic processes and primary production. It is also possible to suggest further research needs, in terms both of new experimental studies and of further model developments, that would be needed in order to improve our understanding of the functional relationship between chlorophyll solar-induced fluorescence and photosynthesis, and our ability to represent and exploit it.

8.1. Recommendations for a future satellite mission

Based on the results of the project, the following recommendations can be made for the design and operation of a future satellite mission:

- measurements should be made in both O2 bands, for either (i) the retrieval of fluorescence contribution from PSII alone or (ii) the use of the full information on photosynthetic processes provided by the full fluorescence spectrum (see below);
- the parallel measurement of both fluorescence and VIS-NIR reflectance should be recommended, for the assessment of canopy chlorophyll content (from measurements in the red-edge region) and of PRI (Photochemical Reflectance Index; Gamon *et al.* 1997a; Drolet *et al.* 2008) from measurements in the 530-570 nm region. The latter, in particular, could provide additional information on photosynthetic processes for the joint assessment of instantaneous processes and steady-state potentials (see DL 3.2 Algorithms for the inclusion of fluorescence and leaf optical properties in functional models at leaf level);
- less important appears the measurement of canopy temperature, despite the effects of temperature on energy partitioning among PSI and PSII and on photosynthetic processes;
- measurements should be taken preferentially around midday or in the early afternoon, since according to available model simulations the sensitivity of canopy fluorescence to photosynthetic parameters appears to be highest around this time (see Figure 8-1).

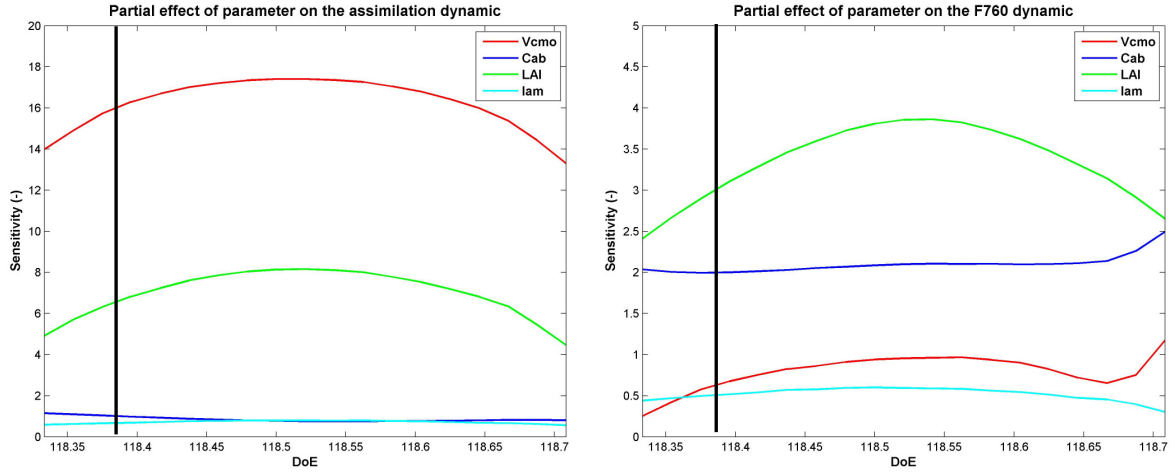

Figure 8-1 - Recommendations of optimal overpass time, based on the results of the sensitivity analysis. Left: Diurnal dynamic of the mean partial effects on the photosynthesis (LH-OAT algorithm, DoY 118 and considering Jmo linked to Vcmo). Right: Diurnal dynamic of the mean partial effects on the fluorescence signal at 760 nm (LH-OAT algorithm, DoY 118 and considering Jmo linked to Vcmo).

8.2. Recommendations for further research

The project has also highlighted the need for further research (in terms both of new experimental studies and of further model developments) that would be recommended in order to improve our understanding of the functional relationship between chlorophyll solar-induced fluorescence and photosynthesis, and our ability to represent and exploit it.

8.2.1. Further research needs

- New laboratory studies are needed, to be carried out under controlled conditions, in order to test the two alternative leaf-level models (van der Tol *et al.* 2008; Magnani *et al.* 2009) developed as part of the project. The two models make it possible to predict the link between chlorophyll fluorescence and photosynthesis in response to a range of environmental and internal conditions, and their predictive ability can be therefore carefully tested at the leaf level;
- A network of long-term measurement sites should be developed, where canopy fluorescence is measured continuously over the course of the year in parallel with eddy-covariance measurements of canopy gas exchange. This would provide a robust set of measurements for the test of the SCOPE model at the canopy level;
- Design a limited number of field campaigns over selected vegetation types, where the measurement of all the parameters required by the models could be combined with fluorescence and photosynthesis measurements over a range of scales (from leaf to airborne).

8.2.2. New model developments

Further developments of the SCOPE model can be recommended, in order to increase its predictive ability and application potential. Suggested developments are described below.

- Include variable fluorescence matrix, effects of variable chlorophyll content and energy partitioning between photosystems. A comparison of SCOPE model predictions with field measurements from the CEFLES-2 campaigns has highlighted unrealistic values of the ratio between O2-A and O2-B fluorescence, suggesting an underlying error in the simulation of fluorescence spectra. The SCOPE fluorescence ratio at canopy level is partly determined by canopy structure (leaf angle distribution) in connection with sun-viewing geometry, but mainly by the excitation-fluorescence (E-F) matrix, which in turn depends strongly on leaf chlorophyll content and energy partioning. In the present version of the SCOPE model, the E-F matrix is fixed so that fluorescence spectra could consistently deviate from field measurements. variable E-F matrix is available in the Fluspect model (Verhoef, pers. comm.; see Figure 7-2), already applied in other studiesrelated to the FLEX candidate mission, and could be introduced in future versions of the SCOPE model;
- In order to be able to parameterize the model for the representation of E-F matrices and fluorescence spectra, the model of energy partitioning between PSI and PSII proposed by G. Agati as part of the project should be further developed and tested against measurements under controled conditions. Other effects on fluorescence spectra, associated with chlorophyll content, leaf angle distribution and solar geometry, on the contrary, could be easily parameterized for a realistic model application;
- As an alternative to the representation of fluorescence spectra, the method developed as part of the project for the isolation of PSII contribution to leaf fluorescence could be expanded into a procedure applicable at canopy scale. The method uses measurements of O2-A and O2-B fluorescence for the reconstruction of the contribution from PSI and PSII at the two wavelengths. Only PSII fluorescence is directly associated with photosynthetic processes and is represented in the leaf-level models of photosynthesis-fluorescence interactions.

- The effects of PSII photoinhibition should be included in the representation of the relationship between photosynthesis and fluorescence. Field measurements from CEFLES-2 campaigns have highlighted the potential confounding role of photoinhibition (i.e. a decrease in maximum photochemical PSII yield under dark-adapted condition). Preliminary simulations with the SCOPE model have demonstrated the strong effect of PSII photoinhibition on absolute fluorescence values;
- Further develop the detailed model of electron transport and photosynthesis proposed as part of the project into an operational canopy-scale model, for the joint simulation of fluorescence and the Photochemical Reflectance Index. Such a development has been strongly recommended by MAG members, as it would make it possible to simulate the full range of interactions between photosynthetic processes and TOC radiance. Albeit computationally intensive, such an approach is well within the reach of available computers;
- Relax the assumption of canopy homogeneity, currently made in the SCOPE model, in order to expand the model to represent open canopies and the contribution of the understorey to the overall fluorescence signal, highlighted by CEFLES-2 measurements as a potentially important issue.

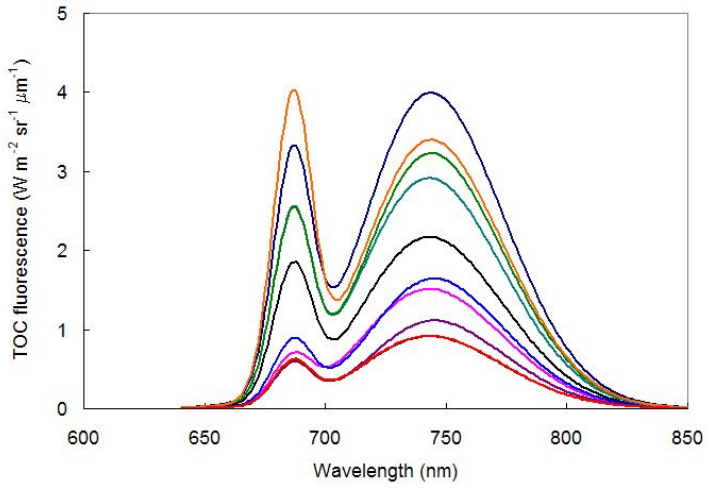

Figure 8-2 - Simulated variability in TOC fluorescence spectra, as predicted by the Fluspect model together with FluorSAIL3.0. The SCOPE fluorescence ratio at canopy level is partly determined by canopy structure (leaf angle distribution) in connection with sun-viewing geometry, but mainly by the excitation-fluorescence (E-F) matrix. In the present version of the SCOPE model, the E-F matrix is fixed so that fluorescence spectra could consistently deviate from field measurements. This matrix in turn depends strongly on leaf chlorophyll content and energy partioning. This can be modelled with the simple leaf model Fluspect, which uses doubling to calculate leaf optical properties; although the Fluspect model makes simple assumptions about absolute fluorescence values, it could be combined in the future with the SCOPE model.

8.2.3. Further model applications

Apart from new developments of the model, a number of technical changes and applications can be recommended.

- Port the SCOPE model from MatLab into a more computationally effective language (Fortran, C, …). Albeit useful in the model development phase, the MatLab language currently used for SCOPE is not computationally efficient and should be replaced by another language more suitable for computationally-intensive applications;
- Expand model simulations to a larger number of vegetation types (e.g. C4 species, tropical forests,…) and conditions, so as to confirm the generality of the results;
- Develop a procedure for full model inversion and the estimation of canopy parameters from observed fluorescence. Because of the non-uniqueness of the relationship between fluorescence and photosynthesis, however, this will presumably require the inclusion of both SIF and PRI into a joint modelling scheme (see DL 3.2 Algorithms for the inclusion of fluorescence and leaf optical properties in functional models at leaf level).

Implement the improved SCOPE model in combination with dynamic vegetation models in order to make it possible the simulation of realistic time course of fluorescence signals, together with other remote sensing signals. Such combined model is a prerequisite for the design of data assimilation procedure. Dynamic vegetation models to consider should include standard surface parameterisations used in GCM or DVM, as well as models designed for specific ecosystems (forest, crops...) in order to analyse thedevelopment of methodologies at different spatial scales.

If data assimilation show to be a promising way of using fluorescence data, the possibility of deriving mathematical tools for a better implementation of assimilation procedure will have to be investigated (e.g. derivation of a adjoint models) as well as the full integration of models from canopy processes to signals at the satelite level.

9. REFERENCES

Adams III WW, Demmig-Adams B (2004) Chlorophyll fluorescence as a tool to monitor plant response to the environment. In: Chlorophyll a Fluorescence. A Signature of Photosynthesis (eds Papageorgiou GC, Govindjee), pp. 583-604. Springer, Dordrecht.

Agati G (1998) Response of the in vivo chlorophyll fluorescence spectrum to environmental factors and laser excitation wavelength. Pure & Applied Optics 7 797-807.

Agati G, Cerovic ZG, Moya I (2000) The effect of decreasing temperature up to chilling values on the in vivo F685/F735 chlorophyll fluorescence ratio in Phaseolus vulgaris and Pisum sativum: the role of the Photosystem I contribution to the 735 nm fluorescence band. Photochemistry & Photobiology 72 75-84.

Agati G, Mazzinghi P, Fusi F, Ambrosini I (1995) The F685/F730 chlorophyll fluorescence ratio as a tool in plant physiology: response to physiological and environmental factors. Journal of Plant Physiology 145 228-238.

Agati G, Mazzinghi P, Lipucci di Paola M, Fusi F, Cecchi G (1996) The F685/F730 chlorophyll fluorescence ratio as indicator of chilling stress in plants. Journal of Plant Physiology 148 384-390.

Amerongen H, Dekker JP (2003) Light-harvesting in photosystem II. In: Light-Harvesting Antennas in Photosynthesis (eds Green BR, Parson WW), pp. 219-251. Kluwer Academic, Dordrecht.

Ananyev G, Kolber ZS, Klimov D, et al (2005) Remote sensing of heterogeneity in photosynthetic efficiency, electron transport and dissipation of excess light in Populus deltoides stands under ambient and elevated CO2 concentrations, and in a tropical forest canopy, using a new laser-induced fluorescence transient device. Global Change Biology 11 1195-1206.

antimycin, dibucaine and cation exchanger, A23187. Australian Journal of Plant Physiology 22 239-247.

Arora, V., (2002), Modeling vegetation as a dynamic component in soil–vegetation–atmosphere transfer schemes and hydrological models. Rev. Geophys. 40 (2), Art. No. 1006.

Asner GP, Martin RE, Carlson KM, Rascher U, Vitousek PM (2006) Vegetation-climate interactions among native and invasive species in Hawaiian rainforest. Ecosystems 9 1106-1117.

Asner, G.P., K.M. Carlson and R.E. Martin, Substrate age and precipitation effects on Hawaiian forest canopies from spaceborne imaging spectroscopy, Remote Sensing of Environment 98 (2005), pp. 457–467

Aubinet M, Grelle A, Ibrom A, et al (2000) Estimates of the annual net carbon and water exchange of forests: the Euroflux methodology. Advances in Ecological Research 30 113-175.

Bachelet, D., Neilson, R.P., Hickler, T., Drapek, R.J., Lenihan, J.M., Sykes, M.T., Smith, B., Sitch, S., Thonicke, K., (2003), Simulating past and future dynamics of natural ecosystems in the United States. Global Biogeochem. Cycles 17 (2), 1045, doi:10.1029/2001GB001508.

Baldocchi D, Falge E, Gu L, et al (2001) FLUXNET: A new tool to study the temporal and spatial variability of ecosystem-scale carbon dioxide, water vapor, and energy flux densities. Bulletin of the American Meteorological Society 82 2415-2434.

Ball JT, Woodrow IE, Berry JA (1987) A model predicting stomatal conductance and its contribution to the control of photosynthesis under different environmental conditions. In: Progress in Photosynthesis Research (ed Biggens J), pp. 221-224. Martinus Nijhoff, The Netherlands.

Ballottari M, Dall'Osto L, Morosinotto T, Bassi R (2007) Contrasting behavior of higher plant photosystem I and II antenna systems during acclimation. Journal of Biological Chemistry 282 8947-8958.

Baraldi R, Canaccini F, Cortes S, et al (2008) Role of xanthophyll cycle-mediated photoprotection in Arbutus unedo plants exposed to water stress during the Mediterranean summer. Photosynthetica 46 378-386.

Barber J, Malkin S, Telfer A (1989) The origin of chlorophyll fluorescence in vivo and its quenching by the photosystem II reaction centre. Philosophical Transactions of the Royal Society of London, Series B 323 227-239.

Baret, F., Guyot, G., Major, D., (1988). Coupled fluorescence and reflectnace measurements to improve crop productivity evaluation. In Applications of Chlorophyll Fluorescence, Lichtenthaler H.K. (ed.). Kluwer Academic Publishers. Pages 319-324.

Barton CVM, North PRJ (2001) Remote sensing of canopy light use efficiency using the photochemical reflectance index model and sensitivity analysis. Remote Sensing of Environment 78 264-273.

Bayle F, Wigneron JP, Kerr YH, Waldteufel P, Anterrieu E, Orlhac JC, Chanzy A, Marloie O, Bernardini M, Sobjaerg S, Calvet JC, Goutoule JM, Skou N, 2002. Two-dimensional synthetic aperture images over a land surface scene. IEEE Transactions on Geoscience and Remote Sensing, 40 (3), 710-714.

Bernacchi CJ, Pimentel C, Long SP (2003) In vivo temperature response functions of parameters required to model RuBP-limited photosynthesis. Plant Cell and Environment 26 1419-1430.

Bernacchi CJ, Portis AR, Nakano H, von Caemmerer S, Long SP (2002) Temperature response of mesophyll conductance. Implications for the determination of Rubisco enzyme kinetics and for limitations to photosynthesis in vivo. Plant Physiology 130 1992-1998.

Bernacchi CJ, Singsaas EL, Pimentel C, Portis AR, Long SP (2001) Improved temperature response functions for models of Rubisco-limited photosynthesis. Plant Cell and Environment 24 253-259.

Bernhardt K, Trissl HW (1999) Theories for kinetics and yields of fluorescence and photochemistry: how, if at all, can different models of antenna organisation be distinguished experimentally? Biochimica et Biophysica Acta 1409 125-142.

Berninger F, Mäkelä A, Hari P (1996) Optimal control of gas exchange during drought: empirical evidence. Annals of Botany 77 469-476.

Bhumralkar, C. M. (1975), Numerical experiments on the computation of ground surface temperature in an atmospheric general circulation model, J. Appl. Meteorol., 14, 1246-1258.

Bhumralkar, C.M., 1975. Numerical experiments on the computation of ground surface temperature in an atmospheric general circulation model. J. Appl. Meteorol., 14, 1246-1258.

Bilger W, Bjorkman O, Thayer SS (1989a) Light induced spectral absorbance changes in relation to photosynthesis and the epoxidation state of xanthophyll cycle components in cotton leaves. Plant Physiology 91 542-551.

Bilger W, Bjorkman O, Thayer SS (1989b) Light induced spectral absorbance changes in relation to photosynthesis and the epoxidation state of xanthophyll cycle components in cotton leaves. Plant Physiology 91 542-551.

Bonan, G.B., Levis, S., Sitch, S., Vertenstein, M., Oleson, K.W., (2003), A dynamic global vegetation model for use with climate models: concepts and description of simulated vegetation dynamics. Global Change Biol. 9, 1543–1566.

Botta, A., N. Viovy, P. Ciais, and P. Friedlingstein (2000), A global prognostic scheme of leaf onset using satellite data, Global Change Biol., 6, 709– 726.

Bouman B.A.M. (1992). Linking physical remote sensing models with crop growth simulation models, applied for sugar beet. International Journal of Remote Sensing 13: 2565-2581.

Breymeyer, A. I., Hall, D. O., Melillo, J. M., and Ågren, G. I. (Eds.) (1996) Global Change: Effects on Coniferous Forests and Grasslands. J. Wiley, Chichester, 459 p.

Brisson N., Gary C., Justes E. et al. (2003). An overview of the crop model STICS. European Journal of Agronomy 18: 309-332.

Brüggemann W, Koroleva OY (1995) Chilling sensitivity of violaxanthin de-epoxidation inhibits the development of energy-dependent chlorophyll fluorescence quenching in vivo. Plant Physiology and Biochemistry 33 251-259.

Brugnoli E, Bjorkman O (1992) Chloroplast movement in leaves: influence on chlorophyll fluorescence and measurements of light-induced absorbance changes related to DpH and zeaxanthin formation. Photosynthesis Research 32 23-35.

Brutsaert, W., 1982. Evaporation into the atmosphere. Reidel Publishing Company.

Bunce, J.A., 2000. Acclimation of photosynthesis to temperature in eight cool and warm climate herbaceous C3 species: Temperature dependence of parameters of a biochemical photosynthesis model. Photosynthesis Research, 63, 59–67.

Butler WL (1978) Energy distribution in the photochemical apparatus of photosynthesis. Annual Review of Plant Physiology 29 345-378.

Calvet J.-C., J. Noilhan, and P. Bessmoulin (1998b), Retrieving the Root-Zone Soil moisture from Surface Soil moisture or temperature Estimates: A Feasibility Study Based on Field Measurements, J. Appl. Meteor., 37, 371-386.

Calvet, J.-C. (2000), Investigating soil and atmospheric plant water stress using physiological and micrometeorological data, Agric. For. Meteorol., 103, 229– 247.

Calvet, J.-C., 2000. Investigating soil and atmospheric plant water stress using physiological and micrometeorological data. Agricultural and Forest Meteorology, 103, 229– 247.

Calvet, J.-C., and J.-F. Soussana (2001), Modelling CO2-enrichment effects using an interactive vegetation SVAT scheme, Agric. For. Meteorol., 108, 129– 152.

Calvet, J.-C., Gibelin, A.-L., Roujean, J.-L., Martin, E., Le Moigne, P., Douville, H., Noilhan, J., (2007). Past and future scenarios of the effect of carbon dioxide on plant growth and transpiration for three vegetation types of south-western France. Atmos. Chem. Phys. Discuss. 7, 4761–4779.

Calvet, J.-C., Gibelin, A.-L., Roujean, J.-L., Martin, E., Le Moigne, P., Douville, H., Noilhan, J., 2007. Past and future scenarios of the effect of carbon dioxide on plant growth and transpiration for three vegetation types of south-western France. Atmos. Chem. Phys. Discuss., 7, 4761–4779.

Calvet, J.-C., J. Noilhan, J.-L. Roujean, P. Bessemoulin, M. Cabelguenne, A. Olioso and J.-P. Wigneron (1998a), An interactive vegetation SVAT model tested against date from six contrasting sites, Agric. For. Meteorol., 92, 73–95.

Calvet, J.-C., V. Rivalland, C. Picon-Cochard and J.-M. Guehl (2004), Modelling forest transpiration and CO2 fluxes - Response to soil moisture stress, Agric. For. Meteorol., 124, 143–156.

Camillo P. (1991). Using one- and two-layer models for evaporation estimation with remotely sensed data. In Land Surface Evaporation. Measurement and Parameterization, pp. 183–197, Springer-Verlag, New York, USA.

Campbell GS (1985) Soil Physics with BASIC. Transport Models for Soil-Plant Systems. Elsevier, Amsterdam, 150 p.

Carlson T., Perry E. & Schmugge T. (1990). Remote estimation of soil moisture availability and fractional vegetation cover for agricultural fields. Agricultural and Forest Meteorology 52: 45–69.

Carter GA (1998) Reflectance wavebands and indices for remote estimation of photosynthesis and stomatal conductance in pine canopies. Remote Sensing of Environment 63 61-72.

Carter GA, Freedman A, Kebabian PL, Scott HE (2004) Use of a prototype instrument to detect short-term changes in solar-excited leaf fluorescence. International Journal of Remote Sensing 25 1779-1784.

Cavender-Barea J, Bazzaz FA (2004) From leaves to ecosystems: using chlorophyll fluorescence to assess photosynthesis and plant function in ecological studies. pp. 737-755 In: Papageorgiou GC, Govindjee (eds.) Chlorophyll a Fluorescence: A Signature of Photosynthesis. Dordrect: Springer.

Cayrol, P., L. Kergoat, S. Moulin, G. Dedieu, A. Chehbouni, (2000), Calibrating a coupled SVAT-Vegetation growth model with remotely sensed reflectance and surface temperature – A case study for the HAPEX-Sahel grassland Sites, Journal of Applied Meteorology, 39, 2452-2472

Cerovic ZG, Goulas Y, Gorbunov M, Briantais J-M, Camenen L, Moya I (1996) Fluorosensing of water stress in plants. Diurnal changes of the mean lifetime an yield of chlorophyll fluorescence, measured simultaneously and at distance with a t-LIDAR and a modified PAM-fluorimeter, in maize, sugar beet and Kalanchoë. Remote Sensing of Environment 58 311-321.

Champeaux JL, Masson V, Chauvin R, 2005. ECOCLIMAP: a global database of land surface parameters at 1 km resolution. Meteorological Applications, 12, 29-32.

Cheng Y, Hilker T, Middleton EM, Coops NC, Black TA, Krishnan P (2007) Tower based measurements of bio-indicators over the growing season at a mature Douglas-fir coniferous forest. Eos Trans. Agu. 88(52), Fall Meeting Supp.

Ciais, P., et al. (2005), European-wide reduction in primary productivity caused by the heat and drought in 2003, Nature, 437, 529 – 533, doi:10.1038/nature03972.

Clevers J.G.P.W. & van Leeuwen H.J.C. (1996). Combined use of optical and microwave remote sensing data for crop growth monitoring. Remote Sensing of Environment, 56, 42-51.

Clevers, J.G.P.W., O.W. Vonder, R.E.E. Jongschaap, J.F. Desprats, C. King, L. Prevot, and N. Bruguier, (2002), Monitoring wheat growth by calibrating a crop growth model using optical satellite data, Agronomie, 22, 687-694.

Collatz GJ, Ribas-Carbo M, Berry JA (1992) Coupled photosynthesis-stomatal conductance model for leaves of C4 plants. Australian Journal of Plant Physiology 19 519-538.

Cornic G, Briantais J-M (1991) Partitioning of photosynthetic electron flow between CO2 and O2 reduction in a C3 leaf (Phaseolus vulgaris L.) at different CO2 concentrations and during drought stress. Planta 183 178-184.

Cowan IR (1977) Stomatal behaviour and environment. Advances in Botanical Research 4 117-227.

Cowan, I.R., (1982). Regulation of water use in relation to carbon gain in higher plants. In: Lange, O.L., Nobel, P.S., Osmond, C.B., Ziegler, H. (Eds.), Encyclopedia of Plant Physiologie, New Series. Physiological Plant Ecology II, vol. 12B. Springer, Berlin, pp. 589-615.

Cowan, I.R., 1977. Stomatal behaviour and environment. Adv. Bot. Res., 4, 117-228.

Cramer W, Kicklighter DW, Bondeau A, et al (1999) Comparing global models of terrestrial net primary productivity (NPP): overview and key results. Global Change Biology 5 1-15.

Cramer, W., Bondeau, A., Woodward, F.I., Prentice, I.C., Betts, R.A., Brovkin, V., Cox, P.M., Fisher, V., Foley, J., Friend, A.D., Kucharik, C., Lomas, M.R., Ramankutty, N., Sitch, S., Smith, B., White, A., Young-Molling, C., (2001). Global response of terrestrial ecosystem structure and function to CO2 and climate change: results from six dynamic global vegetation models., Global Change Biol., 7, 347–373.

Cramer, W., D.W. Kicklighter, A. Bondeau, B. Moore , G. Churkina, B. Nemry, A. Ruimy, A.L. Schloss and the participants of the Potsdam NPP model intercomparison (1999) Comparing global models of terrestrial net primary productivity (NPP): overview and key results. Global Change Biology, 5 (suppl. 1), 1-15

Croce R, Zucchelli G, Garlaschi FM, Bassi R, Jennings RC (1996) Excited state equilibration in the Photosystem I-Light-Harvesting I Complex: P700 is almost isoenergetic with its antenna. Biochemistry 35 8572-8579.

Curran PJ, Dungan JL, Macler BA, Plummer SE (1991) The effect of a red leaf pigment on the relationship between red edge and chlorophyll concentration. Remote Sensing of Environment 35 69-76.

Dau H (1994) Molecular mechanisms and quantitative models of variable photosystem II fluorescence. Photochemistry & Photobiology 60 1-23.

Deardorff, J.W., (1977). A parameterization of the ground surface moisture content for use in atmospheric prediction models. J. Appl. Meteor., 16, 1182–1185.

Deardorff, J.W., (1978). Efficient prediction of ground temperature and moisture with inclusion of a layer of vegetation. J. Geophys. Res., 83, 1889–1903.

Delécolle R., Maas S.J., Guérif M. & Baret F. (1992). Remote sensing and crop production models: present trends. ISPRS Journal of Photogrammetry and Remote Sensing 47, 145–161.

Delire, C., Foley, J.A., (1999). Evaluating the performance of a land surface/ecosystem model with biophysical measurements from contrasting environments. J. Geophys. Res. (Atmos.) 104 (D14), 16,895–16,909.

Delire, C., Foley, J.A., Thompson, S., (2003). Evaluating the carbon cycle of a coupled atmosphere-biosphere model. Global Biogeochem. Cycles 17 (1), doi:10.1029/2002GB001870.

Delire, C., Foley, J.A., Thompson, S., (2004). Long-term variability in a coupled atmosphere–biosphere model. J. Clim., 20, 3947–3959.

Demarty J., F. Chevallier, A.D. Friend, N. Viovy, S. Piao & P. Ciais (2007), Assimilation of global MODIS leaf area index retrievals within a terrestrial biosphere model, Geophysical Research Letters, 34, L15402, doi:10.1029/2007GL030014

Demmig-Adams B, Adams WW (2000) Harvesting sunlight safely. Nature 403 371-374.

D'Haese D, Vandermeiren K, Caubergs RJ, Guisez Y, De Temmerman L, Horemans N (2004) Non-photochemical quenching kinetics during the dark to light transition in relation to the formation of antheraxanthin and zeaxanthin. Journal of Theoretical Biology 227 175-186.

Dobrowski SZ, Pushnik JC, Zarco-Tejada PJ, Ustin SL (2005) Simple reflectance indices track heat and water stress-induced changes in steady-state chlorophyll fluorescence at the canopy scale. Remote Sensing of Environment 97 403-414.

doi:10.1016/j.agrformet.2008.05.013

Drabent R, B. Pliszka, and T. Olszewska (1999) Fluorescence properties of plant anthocyanin pigments. I. Fluorescence of anthocyanins in Brassica oleracea L. extracts. J. Photochem. Photobiol. B: Biology 50 53-58.

Drolet GG, Huemmrich KF, Hall FG, Middleton EM, Black TA, Barr AG, Margolis HA (2005) A MODIS-derived photochemical reflectance index to detect inter-annual variations in the photosynthetic light-use efficiency of a boreal deciduous forest. Remote Sensing of Environment 98 212-224.

Drolet GG, Huemmrich KF, Middleton EM, Hall FG, Margolis HA (2006) Pixel shadow fraction effects on the relationship between gross light-use efficiency of boreal forests and the MODIS Photochemical Reflectance Index. Eos Trans. AGU, 87(36), Jt. Assem. Suppl.

Drolet GG, Middleton EM, Huemmrich KF, et al (2008) Regional mapping of gross light-use efficiency using MODIS spectral indices. Remote Sensing of Environment 112 3064-3078.

Drolet, G.G., K.F. Huemmrich, F.G. Hall, E.M. Middleton, T.A. Black and A.G. Barr et al., (2005). A MODIS-derived Photochemical Reflectance Index to detect inter-annual variations in the photosynthetic light-use efficiency of a boreal deciduous forest, Remote Sensing of Environment 98, pp. 212–224

Droogers P., Bastiaanssen W. (2002). Irrigation performance using hydrological and remote sensing modeling. Journal of Irrigation and Drainage Engineering 128: 11-18.

Ducoudré N. I., K. Laval and A. Perrier (1993), SECHIBA: a new set of parameterizations of the hydrologic exchanges at the land-atmosphere interface within the LMD atmospheric general circulation model, J. Climate, 6, 248-273

Dufrêne E, Davi H, François C, Le Maire G, Le Dantec V, Granier A (2005) Modelling carbon and water cycles in a beech forest. Part I: Model description and uncertainty analysis on modelled NEE. Ecological Modelling, 185, 407–436.

El Maayar, M., Price, D.T., Black, T.A., Humphreys, E.R., Jork, E.M., (2002), Sensitivity tests of the Integrated Biosphere Simulator to soil and vegetation characteristics in a Pacific Coastal Coniferous Forest. Atmos. Ocean 40 (3), 313–332.

El Maayar, M., Price, D.T., Delire, C., Foley, J.A., Back, A.T., Bessemoulin, P., (2001), Validation of the Integrated Biosphere Simulator over Canadian deciduous and coniferous boreal forest stands. J. Geophys. Res. 106 (D13), 14,339–14,355.

Entekhabi D., H. Nakamura, and E.G. Njoku (1994), Solving the Inverse Problem for Soil Moisture and Temperature Profiles by Sequential Assimilation of Multifrequency Remotely Sensed Observations, IEEE Transactions on Geoscience and Remote Sensing, 32 (2), 438-448.

Eskling M, Arvidsson PO, Akerlund HE (1997) The xanthophyll cycle, its regulation and components. Physiologia Plantarum 100 806-816.

Evain S, Flexas J, Moya I (2004) A new instrument for passive remote sensing. 2. Measurement of leaf and canopy reflectance changes at 531 nm and their relationship with photosynthesis and chlorophyll fluorescence. Remote Sensing of Environment 91 175-185.

Evain S, Flexas J, Moya I (2004). A new instrument for passive remote sensing: 2. Measurement of leaf and canopy reflectance changes at 531 nm and their relationship with photosynthesis and chlorophyll fluorescence. Remote Sensing of Environment 91, 175-185.

Evain S, Ounis A, Baret F, Goulas Y, Louis J, Cerovic ZG, Moya I (2002) Passive vegetation fluorosensing using atmospheric oxygen absorption bands. In: Proceedings of the First International Symposium on Recent Advances on Remote Sensing. Torrent, Spain 16-20 September 2002 (ed Sobrino JA), pp. 509-513.

Farquhar G.D., S. von Caemmerer and J.A. Berry, 1980. A biochemical model of photosynthetic CO2 assimilation in leaves of C3 species. Planta, 149, 78-90.

Farquhar GD, von Caemmerer S (1982) Modelling of photosynthetic response to environmental conditions. In: Encyclopedia of Plant Physiology. New Series. Vol. 12B. Physiological Plant Ecology II (eds Lange OL, Nobel PS, Osmond CB, Ziegler H), pp. 549-587. Springer Verlag, Berlin.

Farquhar GD, von Caemmerer S, Berry JA (1980) A biochemical model of photosynthetic CO2 assimilation in leaves of C3 species. Planta 149 78-90.

Farquhar GD, Wong SC (1984) An empirical model of stomatal conductance. Australian Journal of Plant Physiology 11 191-210.

Filella I, PeZuelas J, Llorens L, Estiarte M (2004) Reflectance assessment of seasonal and annual changes in biomass and CO2 uptake of a Mediterranean shrubland submitted to experimental warming and drought. Remote Sensing of Environment 90 308-318.

Flexas J, Briantais J-M, Cerovic ZG, Medrano H, Moya I (2000) Steady-state and maximum chlorophyll fluorescence responses to water stress in grapevine leaves: a new remote sensing system. Remote Sensing of Environment 73 283-297.

Flexas J, Escalona JM, Evain S, et al (2002) Steady-state chlorophyll fluorescence (Fs) measurements as a tool to follow variations of net CO2 assimilation and stomatal conductance during water-stress in C-3 plants. Physiologia Plantarum 114 231-240.

Flexas, J., J.M. Escalona, S. Evain, J. Gulías, I. Moya, C.B. Osmond, and H. Medrano (2000). Steady-state chlorophyll fluorescence (Fs) measurements as a tool to follow variations of net CO2 assimilation and stomatal conductance during water-stress in C3 plants. Physiologia Plantarum, 114, 231–240.

Foley, J.A., Levis, S., Costa, M.H., Cramer, W., Pollard, D., (2000), Incorporating dynamic vegetation cover within global climate models. Ecol. Appl. 10 (6), 1620–1632.

Foley, J.A., Levis, S.I.C., Prentice, I.C.D., Pollard, D., Thompson, S.L., (1998). Coupling dynamic models of climate and vegetation. Global Change Biol. 4, 561–579.

Foley, J.A., Prentice, I.C., Ramankutty, N., Levis, S., Pollard, D. Sitch, S., Haxeltine, A., (1996). An integrated biosphere model of land surface processes, terrestrial carbon balance, and vegetation dynamics. Global Biogeochem. Cycles 10 (4), 603–628.

Franck F, Juneau P, Popovic R (2002) Resolution of the Photosystem I and Photosystem II contributions to chlorophyll fluorescence of intact leaves at room temperature. Biochimica et Biophysica Acta 1556 239-246.

Freedman A, Cavender-Bares J, Kebakian PL, Bhaskar R, Scott H, Bazzaz FA (2002) Remote sensing of solar-excited plant fluorescence as a measure of photosynthetic rate. Photosynthetica 40 127-132.

Friend AD (1991) Use of a model of photosynthesis and leaf microenvironment to predict optimal stomatal conductance and leaf nitrogen partitioning. Plant Cell and Environment 14 895-905.

Friend, A.D., A. K. Stevens, R. G. Knox & M. G. R. Cannell, (1997). A process-based terrestrial biosphere model of ecosystem dynamics (Hybrid v3.0). Ecol. Model. 95, 249–287.

Fuentes DA, Gamon JA, Cheng Y, Claudio HC, Qui H-L, Mao Z, Sims DA, Rahman AF, Oechel W, Luo H (2006) Mapping carbon and water vapor fluxes in a chaparral ecosystem using vegetation indices derived from AVIRIS. Remote Sensing of Environment 103 312-323.

Fuentes DA, Gamon JA, Cheng Y, et al (2006) Mapping carbon and water vapor fluxes in a chaparral ecosystem using vegetation indices derived from AVIRIS. Remote Sensing of Environment 103 312-323.

Fuentes, D.A. , J.A. Gamon, Y. Cheng, H.C. Claudio, H.L. Qiu and Z. Mao et al., (2006), Mapping carbon and water vapour fluxes in a chaparral ecosystem using vegetation indices derived from AVIRIS, Remote Sensing of Environment 103, 312–323.

Gamon JA, Field CB, Bilger W, Bjorkman O, Fredeen AL, Penuelas J (1990) Remote sensing of the xanthophyll cycle and chlorophyll fluorescence in sunflower leaves and canopies. Oecologia 85 1-7.

Gamon JA, Field CB, Fredeen AL, Thayer S (2001) Assessing photosynthetic downregulation in sunflower stands with an optically-based model. Photosynthesis Research 67 113-125.

Gamon JA, Filella I, PeZuelas J (1993) The dynamic 531-nm) reflectance signal: a survey of 20 angiosperm species. In: HY Yamamoto, Smith CM (eds.), Photosynthetic Responses to the Environment. Rockville, MD: American Socieity of Plant Physiologists. pp. 172-177.

Gamon JA, Penuelas J, Field CB (1992a) A narrow wave band spectral index that tracks diurnal changes in photosynthetic efficiency. Remote Sensing of Environment 41 35-44.

Gamon JA, Peñuelas J, Field CB (1992b) A narrow wave band spectral index that tracks diurnal changes in photosynthetic efficiency. Remote Sensing of Environment 41 35-44.

Gamon JA, PeZuelas J, Field CB (1992) A narrow-waveband spectral index that tracks diurnal changes in photosynthetic efficiency. Remote Sensing of Environment 41 35-44.

Gamon JA, Qiu H-L (1999) Ecological applications of remote sensing at multiple scales. pp. 805-845 In: Pugnaire FI and Valladares F (eds.) Handbook of Functional Plant Ecology. New York: Marcel Dekker.

Gamon JA, Roberts DA, Green RO (1995) Evaluation of the photochemical reflectance index in AVIRIS imagery. In: Green RO (ed.) Proceedings of the Fifth Annual JPL Airborne Earth Science Workshop, Pasadena, 23-26 January 1995, JPL Publication 95-1: 55-58.

Gamon JA, Serrano L, Surfus JS (1997a) The photochemical reflectance index: an optical indicator of photosynthetic radiation use efficiency across species, functional types, and nutrient levels. Oecologia 112 492-501.

Gamon JA, Serrano L, Surfus JS (1997b) The photochemical reflectance index: an optical indicator of photosynthetic radiation use efficiency across species, functional types, and nutrient levels. Oecologia 112 492-501.

Gamon JA, Surfus JS (1999a) Assessing leaf pigment content and activity with a reflectometer. New Phytologist 143 105-117.

Gamon JA, Surfus JS (1999b) Assessing leaf pigment content and activity with a reflectometer. New Phytologist 143 105-117.

Gamon JA, Surfus JS (1999c) Assessing leaf pigment content and activity with a reflectometer. New Phytologist 143 105-117.

Gamon, J.A., Serrano, L. and Surfus, J.S (1997) The photochemical reflectance index: an optical indicator of the photosynthetic radiation use efficiency across species, functional types, and nutrient levels. Oceologia 112 492-501.

Garbulsky MF, Peñuelas J, Papale D, Filella I (2008) Remote estimation of carbon dioxide uptake by a Mediterranean forest. Global Change Biology 14 2860-2867.

Garbulsky MF, PeZuelas J, Papale D, Filella I (2007) Remote estimation of carbon dioxide uptake of terrestrial ecosystems. Available from Nature Precedings <http://hdl.handle.net/10101/npre.2007.977.2> (2007)

Garratt, J.R., 1992. The Atmospheric Boundary Layer. Cambridge University Press, Cambridge, United Kingdom.

Garrity SR, Vierling LA, Turnipseed A, Vogel CS, Martins DK, Shepson PB (2006) A comparison between spectrally derived vegetation indices and CO2 fluxes measured over a hardwood forest. Eos Trans. AGU, 87(52), Fall Meet. Suppl.

Genty B, Briantais J-M, Baker NR (1989a) The relationship between quantum yield of photosynthetic electron transport and quenching of chlorophyll fluorescence. Biochimica et Biophysica Acta 990 87-92.

Genty B, Briantais J-M, Baker NR (1989b) The relationship between quantum yield of photosynthetic electron transport and quenching of chlorophyll fluorescence. Biochimica et Biophysica Acta 990 87-92.

Gerten, D., Schaphoff, S., Haberlandt, U., Lucht, W., Sitch, S., (2004), Terrestrial vegetation and water balance-hydrological evaluation of a dynamic global vegetation model. J. Hydrol., 286, 249–270.

Gibelin A.L., 2007. Cycle du carbone dans un modèle de surface continentale: modélisation, validation et mise en œuvre à l'échelle globale. Thèse de doctorat, Université de Toulouse III – Paul Sabatier.200 pages.

Gibelin A.L., J.-C. Calvet, J. L. Roujean, L. Jarlan and S.O. Los (2006), Ability of the land surface model ISBA-A-gs to simulate leaf area index at the global scale: Comparison with satellites products, Journal of Geophysical Research, 111, D18102, doi:10.1029/2005JD006691

Gibelin A.L., J.-C. Calvet, J. L. Roujean, L. Jarlan and S.O. Los (2006), Ability of the land surface model ISBA-A-gs to simulate leaf area index at the global scale: Comparison with satellites products. Journal of Geophysical Research, 111, D18102, doi:10.1029/2005JD006691

Gibelin, A.L., J.C. Calvet, N. Viovy (2008). Modelling energy and CO2 fluxes with an interactive vegetation land surface model-Evaluation at high and middle latitudes. Agricultural and Forest Meteorology, in press; available on line:

Gilmore AM, Mohanty N, Yamamoto HY (1994) Epoxidation of zeaxanthin and antheraxanthin reverses non-photochemical quenching of photosystem II chlorophyll a fluorescence in the presence of trans-thylakoid D-pH. FEBS Letters 350 271-274.

Gilmore AM, Shinkarev VP, Hazlett TL, Govindjee (1998a) Quantitative analysis of the effects of intra-thylakoid pH and xanthophyll cycle pigments on Chlorophyll a fluorescence lifetime distributions and intensity in thylakoids. Biochemistry 37 13582-13593.

Gilmore AM, Shinkarev VP, Hazlett TL, Govindjee (1998b) Quantitative analysis of the effects of intra-thylakoid pH and xanthophyll cycle pigments on Chlorophyll a fluorescence lifetime distributions and intensity in thylakoids. Biochemistry 37 13582-13593.

Gilmore AM, Yamamoto HY (1992) Dark induction of zeaxanthin-dependent nonphotochemical fluorescence quenching mediated by ATP. Proceedings of the National Academy of Sciences of the USA 89 1899-1903.

Gitelson A, Merzylak MN (2004) Non-destructive assessment of chlorophyll, carotenoid and anthocyanin content in higher plant leaves: Principles and algorithms. In: Remote Sensing for Agriculture and the Environment (eds Stamatiadis S, Lynch JM, Scheppers JS), pp. 78-94. Peripheral Editions, Larissa, Greece.

Gitelson AA (2006) Remote estimation of gross primary production in crops: problems and solutions. Eos Trans, AGU, 87(36), Jt. Assem. Suppl.

Gitelson AA, Merzlyak MN, Chivkunova OB (2001) Optical properties and nondestructive estimation of anthocyanin content in plant leaves. Photochemistry and Photobiology 74 38-45.

Gitelson AA, Verma SB, Vina A, Rundquist DC, Keydan G, Leavitt B, Arkebauer TJ, Burba GG, Suyker AE (2003) Novel technique for remote estimation of CO2 flux in maize. Geophysical Researh Letters 30 1486, doi:10.1029/2002GL016543.

Goetz, S. J., S. D. Prince, J. Small, and A. C. R. Gleason, (2000). Interannual variability of global terrestrial primary production: Results of a model driven with satellite observations, J. Geophys. Res., 105, 20,077–20,091.

Goodale CL, Apps MJ, Birdsey RA, et al (2002) Forest carbon sinks in the Northern Hemisphere. Ecological Applications 12 891-899.

Gordon, W.S., Famiglietti, J.S., Fowler, N.L., Kittel, T.G.F., Hibbard, K.A., (2004). Validation of simulated runoff from six terrestrial ecosystem models: results from VEMAP. Ecol. Appl. 14 (2), 527–545.

Govindjee (1995) Sixty-three years since Kautsky: chlorophyll a fluorescence. Australian Journal of Plant Physiology 22 131-160.

Grace J, Nichol C, Disney M, Lewis P, Quaife T, Bowyer P (2007) Can we measure terrestrial photosynthesis from space directly, using spectral reflectance and fluorescence? Global Change Biology 13 1484-1497.

Grassi G, Vicinelli E, Ponti F, Cantoni L, Magnani F (2005) Seasonal and interannual variability of photosynthetic capacity in relation to leaf nitrogen in a deciduos forest plantation in northern Italy. Tree Physiology 25 349-360.

Gray GR, Savitch LV, Ivanov AC, Huner NPA (1996) Photosystem II excitation pressure and development of resistance to photoinhibition. 2. Adjustment of photosynthetic capacity in winter wheat and winter rye. Plant Physiology 110 61-71.

Greenwood, D.J., Gastal, F., Lemaire, G., Draycott, A., Millard, P., Neeteson, J.J., (1991). Growth rate and %N of field grown crops: theory and experiments. Ann. Bot. 67, 181–190.

Greenwood, D.J., Lemaire, G., Gosse, G., Cruz, P., Draycott, A., Neeteson, J.J., (1990). Decline in percentage N of C3 and C4 crops with increasing plant mass. Ann. Bot. 66, 425–436.

Greenwood, D.J., Lemaire, G., Gosse, G., Cruz, P., Draycott, A., Neeteson, J.J., 1990. Decline in percentage N of C3 and C4 crops with increasing plant mass. Ann. Bot. 66, 425–436.

Grossman-Clarke S., Kimball B.A., Hunsaker D.J., Long S.P., Garcia R.L., Kartschall Th, Wall G.W., Printer P.J., Jr Wechsung F., LaMorte R.L., 1999. Effects of elevated atmospheric CO2 on canopy transpiration in senescent spring wheat. Agricultural and Forest Meteorology, 93, 95–109.

Guo J, Trotter CM (2004) Estimating photosynthetic light-use efficiency using the photochemical reflectance index: variations among species. Functional Plant Biology 31 255-265.

Guo JM, Trotter CM (2006) Estimating photosynthetic light use efficiency using the photochemical reflectance index: the effects of short term exposure to elevated CO2 and low temperature. International Journal of Remote Sensing 27 4677-4684.

Hager A, Holocher K (1994) Localization of the xanthophyll-cycle enzyme violaxanthin de-epoxidase within the thylakoid lumen and abolition of its mobility by a (light-dependent) pH decrease. Planta 192 581-589.

Hall A.E., Schulze E.-D., 1980. Stomatal response to environment and a possible interrelation between stomatal effects on transpiration and CO2 assimilation. Plant, Cell & Environment, 3, 467–474.

Hari P, Mäkelä A, Pohja T (2000) Surprising implications of the optimality hypothesis of stomatal regulation gain support in a field test. Australian Journal of Plant Physiology 27 77-80.

Havaux M (1996) Short-term responses of Photosystem I to heat stress. Photosynthesis Research 47 85-97.

Havaux M, Eyletters M (1991a) Is the in vivo Photosystem I function resistant to photoinhibition? An answer from photoacoustic and far-red absorbance measurements in intact leaves. Zeitschrift für Naturforschung 46c 1038-1044.

Havaux M, Greppin H, Strasser RJ (1991b) Functioning of photosystems I and II in pea leaves exposed to heat stress in the presence or absence of light. Planta 186 88-98.

Havaux M, Gruszecki WI (1993) Heat- and light-induced chlorophyll-a fluorescence changes in potato leaves containing high or low levels of the carotenoid zeaxanthin—indications of a regulatory effect of zeaxanthin on thylakoid membrane fluidity. Photochemistry & Photobiology 58 607-614.

Haxeltine, A., I. C. Prentice, and I. D. Creswell, (1996), A coupled carbon and water flux model to predict vegetation structure (BIOME2). J. Veg. Sci., 7, 651–666.

Hazarika, M. K., Y. Yasuoka, A. Ito, and D. Dye (2005), Estimation of net primary productivity by integrating remote sensing data with an ecosystem model, Remote Sensing of Environment, 94, 298-310, doi:10.1016/j.rse.2004.10.004

He D, Edwards GE (1996) Evaluation of the potential to measure photosynthetic rates in C3 plants (Flaveria pringlei and Oryza sativa) by combining chlorophyll fluorescence analysis and a stomatal conductance model. Plant Cell and Environment 19 1272-1280.

Hendrickson L, Furbank RT, Chow WS (2004) A simple alternative approach to assessing the fate of absorbed light energy using chlorophyll fluorescence. Photosynthesis Research 82 73-81.

Hickler, T., Smith, B., Sykes, M.T., Davis, M.B., Sugita, S., Walker, K., (2004). Using a generalized vegetation model to simulate vegetation dynamics in northeastern USA. Ecology, 85 (2), 519–530.

Hilker T, Coops NC, Hall FG, Black AT, Krishnan P, Chen B, Wulder MA, Nesic Z, Huemmrich KF, Middleton EM, Margolis HA, Drolet G, Cheng Y (2007) Monitoring stand level photosynthesis from spectral reflectance. Eos Trans. AGU, 88(52), Fall Meet. Suppl.

Hilker T, Coops NC, Hall FG, Black TA, Wulder MA, Nesic Z, Krishnan P (2008) Separating physiologically and directionally induced changes in PRI using BRDF models. Remote Sensing of Environment, doi:10.1016/j.rse.2008.01.011.

Holt NE, Zigmantas D, Valkunas L, Li X-P, Niyogi KK, Fleming GR (2005) Carotenoid cation formation and the regulation of photosynthetic light harvesting. Science 307 433-436.

Houlès V., Guérif M., Mary B., 2007. Elaboration of a nitrogen nutrition indicator for winter wheat based on leaf area index and chlorophyll content for making nitrogen recommendations. European Journal of Agronomy, 27(1), 1-11.

Hsieh CI, Katul G, Chi TW, 2000. An approximate analytical model for footprint estimation of scalar fluxes in thermally stratified atmospheric flows. Advances in Water Resources, 23, 765–772.

Huemmrich KF, Middleton EM, Hall FG, Knox RG, Walter-Shea E, Verma SB (2006) Using reflectance measurements to determine ecosystem light use efficiency. Eos Trans. AGU, 87(36), Jt. Assem. Suppl.

Inoue Y, PeZuelas J, Miyata A, Mano M (2008) Normalized difference spectral indices for estimating photosynthetic efficiency and capacity at a canopy scale derived from hyperspectral and CO2 flux measurements in rice. Remote Sensing of Environment 112 156-172.

Inoue Y. and J. Peñuelas, (2006). Relationship between light use efficiency and photochemical reflectance index in soybean leaves as affected by soil water content, International Journal of Remote Sensing 27, 5249–5254.

Inoue Y., Moran M.S. & Horie T. (1998). Analysis of spectral measurements in rice paddies for predicting rice growth and yield based on a simple crop simulation model. Plant Production Science 1: 269-279.

Inoue, Y., Olioso A., (2006). Estimating the dynamics of ecosystem CO2 flux and biomass production in agricultural fields on the basis of synergy between process models and remotely sensed signatures. Journal of Geophysical Research., 111, D24, D24S91, doi: 10.1029/2006JD007469

Inoue, Y., Olioso A., 2006. Estimating the dynamics of ecosystem CO2 flux and biomass production in agricultural fields on the basis of synergy between process models and remotely sensed signatures. Journal of Geophysical Research, 111(D24), D24S91, doi: 10.1029/2006JD007469

Intergovernmental Panel on Climate Change (2001) Climate Change 2001. Impacts, Adaptation and Vulnerability. Cambridge University Press, Cambridge.

Jacobs, C.M.J., (1994). Direct impact of atmospheric CO2 enrichment on regional transpiration. Ph.D. Thesis. Agricultural University, Wageningen.

Jacobs, C.M.J., van den Hurk, B.J.J.M., de Bruin, H.A.R., (1996). Stomatal behaviour and photosynthetic rate of unstressed grapevines in semi-arid conditions. Agric. For. Meteorol. 80, 111–134.

Jacquemoud S, Ustin SL, Verdebout J, Schmuck G, Andreoli G, Hosgood B (1996) Estimating leaf biochemistry using the PROSPECT leaf optical properties model. Remote Sensing of Environment 56 194-202.

Jacquemoud S., F. Baret, 1990. PROSPECT: a model of leaf optical properties spectra. Remote Sensing of Environment, 34, 75-91.

Jahns P, Heyde S (1999) Dicyclohexylcarbodiimide alters the pH dependence of violaxanthin de-epoxidation. Planta 207 393-400.

Jain S, Nath S (2000) Kinetic model of ATP synthase: pH dependence of the rate of ATP synthesis. FEBS Letters 476 113-117.

Janssens IA, Freibauer A, Ciais P, et al (2003) Europe's terrestrial biosphere absorbs 7 to 12% of European anthropogenic CO2 emissions. Science 300 1538-1542.

Jarvis PG, McNaughton KG (1986) Stomatal control of transpiration: scaling up from leaf to region. Advances in Ecological Research 15 1-49.

Ji, J.J., (1995). A climate–vegetation interaction model: simulating physical and biological processes at the surface. J. Biogeogr. 22, 445–451.

Johnson R. C., Mornhinweg D. W., Ferris D.M., Heitholt J.J., 1987. Leaf Photosynthesis and Conductance of Selected Triticum Species at Different Water Potentials. Plant Physiol., 83, 1014-1017.

Justes, E., Mary, B., Meynard, J.M., Machet, J.M., Thelier-Huché, L., (1994). Determination of a critical nitrogen dilution curve for winter wheat crops. Ann. Bot. 74, 397–407.

Justes, E., Mary, B., Meynard, J.M., Machet, J.M., Thelier-Huché, L., 1994. Determination of a critical nitrogen dilution curve for winter wheat crops. Ann. Bot. 74, 397–407.

Kaminski, T., W. Knorr, P. Rayner, and H. Heimann (2002), Assimilating atmospheric data into a terrestrial biosphere model: A case study of the seasonal cycle, Global Biogeochemical Cycles, 16(4), 1066, doi:10.1029/2001GB001463

Kattge J, Knorr W (2007) Temperature acclimation in a biochemical model of photosynthesis: a reanalysis of data from 36 species. Plant Cell and Environment 30 1176-1190.

Kim, Y., Wang, G., (2005), Modeling seasonal vegetation variation and its validation against Moderate Resolution Imaging Spectroradiometer (MODIS) observations over North America. J. Geophys. Res., 110, D04106, doi:10.1029/2004JD005436.

Kitajima M, Butler WL (1975) Quenching of chlorophyll fluorescence and primary photochemistry in chloroplasts by dibromothymoquinone. Biochimica et Biophysica Acta 376 105-115.

Kornyeyev D, Hendrickson L (2007) Energy partitioning in photosystem II complexes subjected to photoinhibitory treatment. Functional Plant Biology 34 214-220.

Kramer DM, Johnson G, Kiirats O, Edwards GE (2004) New fluorescence parameters for the determination of Q(A) redox state and excitation energy fluxes. Photosynthesis Research 79 209-218.

Kramer K, Leinonen I, Bartelink HH, et al (2002) Evaluation of 6 process-based forest growth models based on eddy-covariance measurements of CO2 and H2O fluxes at 6 forest sites in Europe. Global Change Biology 8 213-230.

Krause GH, Weis E (1991) Chlorophyll fluorescence and photosynthesis: the basics. Annual Review of Plant Physiology and Plant Molecular Biology 42 313-349.

Krinner G, Viovy N, Noblet-Ducoudre N, et al (2005) A dynamic global vegetation model for studies of the coupled atmosphere-biosphere system. Global Biogeochemical Cycles 19 .

Krinner, G., N. Viovy, N. de Noblet-Ducoudré, J. Ogée, J. Polcher, P. Friedlingstein, P. Ciais, S. Sitch, and I. C. Prentice (2005), A dynamical global vegetation model for studies of the coupled atmosphere-biosphere system, Global Biogeochem. Cycles, 19, GB1015, doi:10.1029/2003GB002199.

Kucharik C. J., C. C. Barford , M. El Maayar, S. C. W. R. K. Monson, & D. D. Baldocchi (2006), A multiyear evaluation of a Dynamic Global Vegetation Model at three AmeriFlux forest sites: Vegetation structure, phenology, soil temperature, and CO2 and H2O vapour exchange. Ecological Modelling, 196, 1–31

Kucharik, C.J., Foley, J.A., Delire, C., Fisher, V.A., Coe, M.T., Gower, S.T., Lenters, J., Molling, C., Norman, J.M., Ramankutty, N., (2000). Testing the performance of a dynamic global ecosystem model: water balance, carbon balance, and vegetation structure. Global Biogeochem. Cycles, 14 (3), 795–825.

Laisk A, Eichelmann H (1989) Towards understanding oscillations: a mathematical model of the biochemistry of photosynthesis. Philosophical Transactions of the Royal Society of London, Series B 323 369-384.

Laney SR, Letelier RM, Abbott MR (2005) Parameterizing the natural fluorescence kinetics of Thalassiosira weissflogii. Limnology and Oceanography 50 1499-1510.

Lavergne J, Trissl HW (1995) Theory of fluorescence induction in photosystem II: derivation of analytical expressions in a model including exciton-radical-pair equilibrium and restricted energy transfer between photosynthetic units. Biophysical Journal 68 2474-2492.

Lawrence DM, Slingo JM (2004) An annual cycle of vegetation in a GCM. Part II: global impacts on climate and hydrology. Climate Dynamics 22 107-122.

Lazar D (1999) Chlorophyll a fuorescence induction. Biochimica et Biophysica Acta 1412 1-28.

Leakey ADB, Press MC, Scholes JD (2003) High-temperature inhibition of photosynthesis is greater under sunflecks than uniform irradiance in a tropical rain forest tree seedling. Plant Cell and Environment 26 1681-1690.

Lemaire, G., Gastal, F. (1997), N uptake and distribution in plant canopies. In: Lemaire, G. (Ed.), Diagnosis of the Nitrogen Status in Crops. Springer, Berlin, pp. 3–43.

Lemaire, G., Gastal, F., 1997. N uptake and distribution in plant canopies. In: Lemaire, G. (Ed.), Diagnosis of the Nitrogen Status in Crops. Springer, Berlin, pp. 3–43.

Leuning R (1995) A critical appraisal of a combined stomatal-photosynthesis model for C3 plants. Plant Cell and Environment 18 339-355.

Leuning R (1997) Scaling to a common temperature improves the correlation between the photosynthesis parameters Jmax and Vcmax. Journal of Experimental Botany 48 345-347.

Leuning R., 2002. Temperature dependence of two parameters in a photosynthesis model. Plant, Cell & Environment, 25(9), 1205–1210.

Leuning R., F. M. Kelliher, D.G.G. de Pury, E.-D. Schulze, 1995. Leaf nitrogen, photosynthesis, conductance and transpiration: scaling from leaves to canopies. Plant, Cell & Environment, 18(10), 1183-1200.

Leuning R., F.X. Dunin, Y.-P. Wang, 1998. A two-leaf model for canopy conductance, photosynthesis and partitioning of available energy. II. Comparison with measurements. Agricultural and Forest Meteorology, 91 (1-2), 113-125.

Lichtenthaler HK, Hak R, Rinderle U (1990) The chlorophyll fluorescence ratio F690/F730 in leaves of different chlorophyll content. Photosynthesis Research 25 295-298.

Lichtenthaler HK, Rinderle U (1988) The role of chlorophyll fluorescence in the detection of stress conditions in plants. CRC Critical Reviews in Analytical Chemistry 19 29-85.

Liu HQ, Huete AR (1995) A feedback based modification of the NDVI to minimize canopy background and atmospheric noise. IEEE Trans. Geosci. Remote Sens. 33 457-465.

Liu LY, Zhang YJ, Wang JH, Zhao CJ (2005) Detecting solar-induced chlorophyll fluorescence from field radiance spectra based on the Fraunhofer line principle. IEEE Transactions in Geoscience and Remote Sensing 43 827-832.

Liu, J., J. M. Chen, J. Cihlar, and W.M. Park (1997), A process-based boreal ecosystem productivity simulator using remote sensing inputs, Remote Sensing of Environment, 62, 158-175

Lloyd J, Taylor JA (1994) On the temperature dependence of soil respiration. Functional Ecology 8 315-323.

Lloyd J., Farquhar G.D. 1994. 13C discrimination during CO2 assimilation by the terrestrial biosphere. Oecologia, 99(3-4).

Logan BA, Adams III WW, Demmig-Adams B (2007) Avoiding common pitfalls of chlorophyll fluorescence analysis under field conditions. Functional Plant Biology 34 853-859.

Long SP, Bernacchi CJ (2003) Gas exchange measurements, what can they tell us about the underlying limitations to photosynthesis? Procedures and sources of error. Journal of Experimental Botany 54 2393-2401.

Loreto F, Harley PC, Di Marco G, Sharkey TD (1992) Estimation of mesophyll conductance to CO2 flux by three different methods. Plant Physiology 98 1437-1443.

Louis J, Ounis A, Ducruet J-M, et al (2005) Remote sensing of sunlight-induced chlorophyll fluorescence and reflectance of Scots pine in the boreal forest during spring recovery. Remote Sensing of Environment 96 37-48.

Louis J, Ounis A, Ducruet J-M, Evain S, Laurila T, Thum T, Aurela M, Wingsle G, Alonso L, Pedros R, Moya I (2005) Remote sensing of sunlight-induced chlorophyll fluorescence and reflectance of Scots pine in the boreal forest during spring recovery. Remote Sensing of Environment 96 37-48.

Louis, J., Ounis, A., Ducruet, J. M., Evain, S., Laurila, T., Thum, T., et al. (2005). Remote Sensing of sunlight-induced chlorophyll fluorescence and reflectance of Scots pine in the boreal forest during spring recovery. Remote Sensing of Environment, 96, 37–48.

Loustau, D., A. Bosc, et al. (2005). Modeling climate change effects on the potential production of French plains forests at the sub-regional level. Tree Physiology 25(7): 813-823.

Lu, L., R. A. Pielke Sr., G. E. Liston, W. J. Parton, D. Ojima, and M. Hartman, (2001). Implementation of a two-way interactive atmospheric and ecological model and its application to the central United States, J. Clim., 14, 900–919.

Lucht, W., Prentice, I.C., Myneni, R.B., Sitch, S., Friedlingstein, P., Cramer, W., Bousquet, P., Buermann, W., Smith, B., (2002). Climatic control of high-latitude vegetation greening trend and Pinatubo effect., Science, 296, 1687–1689.

Lüdeke, M.K.B., Ramge, P.H., Kohlmaier, G.H., (1996). The use of satellite NDVI data for the validation of global vegetation phenology models: application to the Frankfurt Biosphere Model. Ecol. Model. 91, 255–270.

Magnani F, Dayyoub A (2009) Modelling chlorophyll fluorescence under ambient conditions. New Phytologist in preparation .

Mahfouf J.F., A.O. Manzi, J. Noilhan, H. Giordani and M. Déqué, 1995. The land surface scheme ISBA within the Météo-France climate model ARPEGE. Part I. Implementation and preliminary results. Journal of Climate, 8, 2039–2057.

Mahfouf, J.-F., and J. Noilhan (1991), Comparative study of various formulations of evaporation from bare soil using in situ data, Journal of Appied. Meteorology., 30, 1354-1365

Mahfouf, J.-F., Noilhan, J., (1996), Inclusion of gravitational drainage in a land surface scheme based on the force restore method, J. Appl. Meteorol., 35(6), 987-992.

Massad RS, Tuzet A, Bethenod O (2007) The effect of temperature on C4-type leaf photosynthesis parameters. Plant Cell and Environment 30 1191-1204.

Matorin DN, Antal TK, Ostrowska M, Rubin AB, Ficek D, Majchrowski R (2004) Chlorophyll fluorimetry as a method for studying light absorption by photosynthetic pigments in marine algae. Oceanologia 46 519-531.

Maxwell K, Johnson GN (2000) Chlorophyll fluorescence. A practical guide. Journal of Experimental Botany 51 659-668.

McCloy, K.R., Lucht, W., (2004). Comparative evaluation of seasonal patterns in long time series of satellite image data and simulations of a global vegetation model. IEEE Trans. Geosci. Remote Sens. 42 (1), 140–153.

McFarlane J.C., Watson R.D., Theisen A.F., Jackson R.D., Ehrler W.L., Pinter Jr. P.J., Idso S.B., Reginato R.J. (1980). Plant stress detection by remote measurement of fluorescence. Applied Optics, 19, 3287-3289.

Medlyn B.E., E. Dreyer, D. Ellsworth, M. Forstreuter, P. C. Harley, M. U. F. Kirschbaum, X. Le Roux, P. Montpied, J. Strassemeyer, A. Walcroft, K. Wang, D. Loustau, 2002. Temperature response of parameters of a biochemically based model of photosynthesis. II. A review of experimental data. Plant, Cell & Environment, 25(9), 1167–1179.

Medrano H, Escalona JM, Bota J, Gulias J, Flexas J (2002) Regulation of photosynthesis of C3 plants in response to progressive drought. Stomatal conductance as a reference parameter. Annals of Botany 89 895-905.

Meroni M, Colombo R (2006) Leaf level detection of solar induced chlorophyll fluorescence by means of a subnanometer resolution spectroradiometer. Remote Sensing of Environment 103 438-448.

Méthy, M., Lacaze, B., Olioso, A., (1991). Perspectives et limites de la fluorescence pour la télédétection de l'état hydrique d'un couvert végétal : cas d'une culture de soja. International Journal of Remote Sensing, 12, 223-230.

Méthy, M., Olioso, A., Trabaud, L., (1994). Chlorophyll fluorescence as a tool for management of plant resources. Remote Sensing of Environment, 47, 2-9.

Mitsunori I, Tsuneo M, Masayuki T (2006) An application of the alternative PRI derived from the ground observation data to MODIS data. Proceedings of the Conference of the Remote Sensing Society of Japan 41 211-212.

Mohanty N, Gilmore AM, Yamamoto HY (1995) Mechanism of non-photochemical chlorophyll fluorescence quenching. II. Resolution of rapidly reversible absorbance changes at 530 nm and fluorescence quenching by the effects of

Monteith JL (1972) Solar radiation and productivity in tropical ecosystems. Journal of Applied Ecology 9 747-766.

Moorcroft, P.R., (2003). Recent advances in ecosystem–atmosphere interactions: an ecological perspective. Proc. R. Soc. Lond., B, 270, 1215–1227.

Morales P, Sykes MT, Prentice IC, et al (2005) Comparing and evaluating process-based ecosystem model predictions of carbon and water fluxes in major European forest biomes. Global Change Biology 11 2211-2233.

Moran M.S., Maas S.J., Clarke T.R., Pinter Jr P.J., Qi J., Mitchell T.A., Kimball B.A. & Neale C.M.U. (1996). Modeling/Remote Sensing Approach for Irrigation scheduling. In Evapotranspiration and Irrigation Scheduling (San Antonio, Texas), C. Camp, E. Sadler, et R. Yoder, Eds., ASAE-IA-ICID, ASAE, pp. 231-238.

Mougin, E., Lo Seen, D., Rambal, S., Gaston, A., Hiernaux, P. (1995). A regional Sahelian grassland model to be coupled with multispectral satellite data. I. Model description and validation., Rem. Sens. Environ. 52, 181–193.

Moulin, S., A. Bondeau, and R. Delécolle, (1998). Combining agricultural crop models and satellite observations: from field to regional scales, International Journal of Remote Sensing, 19 (6), 1021-1236.

Moya I, Camenen L, Evain S, et al (2004) A new instrument for passive remote sensing. 1. Measurements of sunlight-induced chlorophyll fluorescence. Remote Sensing of Environment 91 186-197.

Moya I, Camenen L, Latouche G, Mauxion C, Evain S, Cerovic ZG (1999) An instrument for the measurement of sunlight excited plant fluorescence. In: Proceedings of the XIth International Congress on Photosynthesis (ed Garab G), pp. 4265-4370. Kluwer Academic Publishers, Dordrecht.

Moya I, Guyot G, Goulas Y (1992) Remotely sensed blue and red fluorescence emission for monitoring vegetation. ISPRS Journal of Photogrammetry and Remote Sensing 47 205-231.

Moya, I., Daumard, F., Moise, N., Ounis, A., Goulas, Y., 2006. First airborne multiwavelength passive chlorophyll fluorescence measurements over La Mancha (Spain) fields. Proceedings of the 2nd International Symposium on Recent Advances in Quantitative Remote Sensing (RAQRS'II), 25-29 September 2006, Torrent, Spain. Pages 820-825.

Müller P, Li XP, Niyogi KK (2001a) Non-photochemical quenching. A response to excess light energy. Plant Physiology 125 1558-1566.

Müller P, Li XP, Niyogi KK (2001b) Non-photochemical quenching. A response to excess light energy. Plant Physiology 125 1558-1566.

Munekage Y, Hashimoto M, Miyake C, et al (2004) Nature 429 579-582.

Munoz-Sabater J. M., L. Jarlan, J.-C. Calvet, F. Bouyssel and P. de Rosnay, (2007). From near-surface to root-zone soil moisture using different assimilation techniques, Journal of Hydrometeorology, 8, 194-206.

Myneni, R. B., S. Hoffman, Y. Knyazikhin, J. L. Privette, J. Glassy, and Y. Tian (2002), Global products of vegetation leaf area index and fraction absorbed PAR from year one of MODIS data, Remote Sens. Environ., 83, 214–231.

Nakaji T, Ide R, Oguma H, Saigusa N, Fujinuma Y (2007a) Utility of spectral vegetation for estimation of gross CO2 flux under varied sky conditions. Remote Sensing of Environment 109 274-284.

Nakaji T, Ide R, Takagi K, Kosugi Y, Ohkubo S, Nasahara KN, Saigusa N, Oguma H (2007b) Utility of spectral vegetation indices for estimation of light conversion efficiency in coniferous forests in Japan. Agricultural and Forest Meteorology doi:10.1016/j.agrformet.2007.11.006.

Nakaji T, Takeda T, Fujinuma Y, Oguma H (2005) Effect of autumn senescence on the relationship between the PRI and LUE of young Japanese larch trees. Phyton 45 535-542.

Nelder, J.A., & Mead, R., 1965. A simplex method for function minimization.Computer Journal, 7, 398–313.

Nichol CJ, Huemmrich KF, Black TA, et al (2000a) Remote sensing of photosynthetic-light-use efficiency of boreal forest. Agricultural & Forest Meteorology 101 131-142.

Nichol CJ, Huemmrich KF, Black TA, et al (2000b) Remote sensing of photosynthetic-light-use efficiency of boreal forest. Agricultural and Forest Meteorology 101 131-142.

Nichol CJ, Huemmrich KF, Black TA, Jarvis PG, Walthall CL, Grace J, Hall FG (2000) Remote sensing of photosynthetic-light-use efficiency of boreal forest. Agricultural and Forest Meteorology 101 131-142.

Nichol CJ, Lloyd J, Shibistova O, Arneth A, R`ser C, Knohl A, Matsubara S, Grace J (2002) Remote sensing of photosynthetic-light-use efficiency of a Siberian boreal forest. Tellus 54B 677-687.

Nichol, C. J., Rascher, U., Matsubara, S., & Osmond, B. (2006). Assessing photosynthetic efficiency in an experimental mangrove canopy using remote sensing and chlorophyll fluorescence. Trees, 20, 9−15

Noilhan, J. and Planton, S. (1989). A simple parameterization of land surface processes for meteorological models. Monthly Weather Review, 117, 536–549.

Noilhan, J., Mahfouf, J.-F., (1996). The ISBA land surface parameterisation scheme. Global Planetary Changes, 13, 145-159.

Olioso A., H. Chauki, D. Courault and J.P. Wigneron (1999), Estimation of evapotranspiration and photosynthesis by assimilation of remote sensing data into SVAT models, Remote Sens. Environ., 68, 341-356,

Olioso A., Taconet O. & Ben Mehrez M. (1996). Estimation of heat and mass fluxes from IR brightness temperature. IEEE Transactions on Geoscience and Remote Sensing 34: 1184-1190.

Olioso, A, Sòria, G., Sobrino, J.A., Duchemin, B., 2007. Evidences of low land surface thermal infrared emissivity in presence of dry vegetation. IEEE-Geosciences and Remote Sensing Letters, 4 (1), 112-116. doi: 10.1109/LGRS.2006.885857.

Olioso, A., 1992. Simulation des échanges d'énergie et de masse d'un couvert végétal, dans le but de relier la transpiration et la photosynthèse aux mesures de réflectance et de température de surface. Thèse de doctorat, Université Montpellier II. 264 pages.

Olioso, A., 1995. Simulating the relationship between thermal emissivity and the Normalized Difference Vegetation Index. International Journal of Remote Sensing, 16, 3211-3216.

Olioso, A., Inoue, Y., Ortega-Farias, S., Demarty, J., Wigneron, J.-P.,Braud, I., Jacob, F., Lecharpentier, P., Ottlé, C., Calvet, J.-C., Brisson, N., (2005). Future directions for advanced evapotranspiration modeling: assimilation of remote sensing data into crop simulation models and SVAT models. Irrigation and Drainage Systems, 19, 377-412.

Olioso, A., Inoue, Y., Ortega-Farias, S., Demarty, J., Wigneron, J.-P.,Braud, I., Jacob, F., Lecharpentier, P., Ottlé, C., Calvet, J.-C., Brisson, N., 2005. Future directions for advanced evapotranspiration modeling: assimilation of remote sensing data into crop simulation models and SVAT models. Irrigation and Drainage Systems, 19, 377-412.

Olioso, A., Méthy, M., Lacaze, B., (1992). Simulation of canopy fluorescence as a function of canopy structure and leaf fluorescence. Remote Sensing of Environment, 41, 239-247.

Olioso, A., Rivalland, V., Faivre, R., Weiss, M., Demarty, J., Wassenaar, T., Baret, F., Cardot, H., Rossello, P., Jacob, F., Hasager, C.B., Inoue, Y., (2006). Monitoring Evapotranspiration over the Alpilles Test Site by Introducing Remote Sensing Data at Various Spatial Resolutions into a Dynamic SVAT Model. In Actes de la conférence 'Earth observation for vegetation monitoring and water management', Napoli, 24-25 Octobre 2005. AIP Conference proceedings, Volume 852 (American Institute of Physics). ISBN: 0-7354-0346-5. G. D'Urso, M. A. Osann Jochum, J. Moreno, editeurs. pp. 234-241.

Olioso, A., Y. Inoue, J.P. Wigneron, S. Ortega-Farias, P. Lecharpentier, M. Pardé, J.C. Calvet, and O. Inizan (2001), Using a coupled crop-SVAT model to assess crop canopy processes from remote sensing data, in IGARSS, Sydney, Australia

Osmond CB (1994) What is photoinhibition? Some insights from comparisons of shade and sun plants. In: Photoinhibition of Photosynthesis. From Molecular Mechanisms to the Field (eds Baker NR, Bowyer JR), pp. 1-24. BIOS Scientific, Oxford.

Osmond CB, Kramer DM, Luettge U (1999) Reversible, water stress-induced non-uniform chlorophyll fluorescence quenching in wilting leaves of Potentilla reptans may not be due to patchy stomatal responses. Plant Biology 1 618-624.

Pänke O, Rumberg B (1996) Kinetic modelling of the proton translocating CFoCF1-ATP synthase from spinach. FEBS Letters 383 196-200.

Pänke O, Rumberg B (1999) Kinetic modeling of rotary CF0F1-ATP synthase: storage of elastic energy during energy transduction. Biochimica et Biophysica Acta 1412 118-128.

Papageorgiou, G. C. and Govindjee (Eds.) (2006) Chlorophyll a Fluorescence. A Signature of Photosynthesis. Springer, Dordrecht.

Parton W., J. Stewart and C. Cole (1988) Dynamics of C, N, P, and S in grassland soil: A model, Biogeochemistry, 5, 109-131

Pedros RI, Moya I, Goulas Y, Jacquemoud S (2008) Chlorophyll fluorescence emission spectrum inside a leaf. Photochemical and Photobiological Sciences 7 498-502.

Peguero-Pina JJ, Morales F, Flexas J, Gil-Pelegrin E, Moya I (2008) Photochemistry, remotely sensed physiological reflectance index and de-epoxidation state of the xanthophyll cycle in Quercus coccifera under intense drought. Oecologia 156 1-11.

Penuelas J, Gamon JA, Fredeen AL, Merino J, Field CB (1994) Reflectance indices associated with physiological changes in nitrogen- and water-limited sunflower leaves. Remote Sensing of Environment 48 135-146.

Peñuelas J, Inoue Y (2000) Reflectance assessment of canopy CO2 uptake. International Journal of Remote Sensing 21 3353-3356.

Penuelas J.; Inoue Y. (2000). Reflectance assessment of canopy CO2 uptake. International Journal of Remote Sensing, 21, 3353-3356.

Perez-Priego O, Zarco-Tejada PJ, Miller JR, Sepulcre-Canto G, Fereres E (2005) Detection of water stress in orchard trees with a high-resolution spectrometer through chlorophyll fluorescence in-filling of the O-2-A band. IEEE Transactions in Geoscience and Remote Sensing 43 2860-2869.

Peterson RB, Oja V, Laisk A (2001) Chlorophyll fluorescence at 680 and 730 nm and leaf photosynthesis. Photosynthesis Research 70 185-196.

PeZuelas J, Baret F, Filella I (1995a) Semi-empirical indices to assess carotenoids/chlorophyll a ratio from leaf spectral reflectance. Photosynthetica 31 221-230.

PeZuelas J, Filella I, Llusia J, Siscart D, PiZol J (1998) Comparative field study of spring and summer leaf gas exchange and photobiology of the Mediterranean trees Quercus ilex and Phyllyrea latifolia. Journal of Experimental Botany 49 229-238.

PeZuelas J, Llusia J, PiZol J, Filella I (1997) Photochemical reflectance index and leaf photosynthetic radiation-use-efficiency assessment in Mediterranean trees. International Journal of Remote Sensing 18 2863-2868.

PeZuelas, J., I. Filella, J.A. Gamon (1995b) Assessment of photosynthetic radiation-use efficiency with spectral reflectance. New Phytologist 131 291-296.

Pfundel EE, Dilley RA (1993) The pH dependence of violaxanthin deepoxidation in isolated pea chloroplasts. Plant Physiology 101 65-71.

Piao S., P. Friedlingstein, P. Ciais, N. Viovy & J. Demarty (2007), Growing season extension and its effects on terrestrial carbon flux in the Northern Hemisphere over the past 2 decades, Global Biogeochemical Sciences, 21(3), GB 3018

Plascyk JA (1975) The MK II Fraunhofer line discriminator (FLD-II) for airborne and orbital remote sensing of solar-stimulated luminescence. Optical Engineering 14 339-346.

Porcar-Castell A, Bäck J, Juurola E, Hari P (2006) Dynamics of the energy flow through photosystem II under changing light conditions: a model approach. Functional Plant Biology 33 229-239.

Porcar-Castell A, Pfundel E, Korhonen JFJ, Juurola E (2008) A new monitoring PAM fluorometer (MONI-PAM) to study the short- and long-term acclimation of photosystem II in field conditions. Photosynthesis Research 96 173-179.

Potter, C. S., et al., (1993). Terrestrial ecosystem production: A process model based on global satellite and surface data (CASA), Global Biogeochem. Cycles, 7(4), 811–841.

Rabinowich E, Govindjee (1969) Photosynthesis. John Wiley and Sons, New York.

Raddi S, Cortes S, Pippi I, Magnani F (2005) Estimation of vegetation photochemical processes: an application of the photochemical reflectance index at the San Rossore test site. Proc. of the 3rd ESA CHRIS/Proba Workshop, 21-23 March, ESRIN, Frascati, Italy, (ESA SP-593, June 2005).

Raddi S, Cortes, Vicinelli E, Magnani F (2006) Remote sensing of photosynthetic processes by photochemical reflectance index (PRI). AIP Conf. Proc. 852 227-233.

Raddi S, Magnani F (2002) Evaluation of leaf energy dissipation by the Photochemical Reflectance Index. Effects of species and leaf photosynthetic potential. Proc. 1st Workshop on Remote Sensing of Solar Induced Vegetation Fluorescence. ESTEC, 19-20 June, 2002.

Rahman AF, Cordova VD, Gamon JA, Schmid HP, Sims DA (2004) Potential of MODIS ocean bands for estimating CO2 flux from terrestrial vegetation: a novel approach. Geophysical Research Letters 31 .

Rahman AF, Gamon JA, Fuentes DA, Roberts D, Prentiss D, Qiu H (2000) Modeling CO2 flux of boreal forests using narrow band indices from Aviris imagery. European Space Agency reference. Summaries of the Ninth JPL Airborne Earth Science Workshop. February 23-25, 2000. Jet Propulsion Laboratory, Pasadena, CA. http://vcsars.calstatela.edu/boreas/aviris00/modeling/faiz_aviris_paper.htm

Rahman AF, Gamon JA, Fuentes DA, Roberts DA, Prentiss D (2001) Modeling spatially distributed ecosystem flux of boreal forest using hyperspectral indices from AVIRIS imagery. Journal of Geophysical Research 106(D24) 33579-33591.

Rahman AF, Gamon JA, Sims DA, Schmidts M (2003) Optimum pixel size for hyperspectral studies of ecosystem function in southern California chaparral and grassland. Remote Sensing Environment 84 192-207.

Rayner, P. J., M. Scholze, W. Knorr, T. Kaminski, R. Giering, and H. Widmann (2005), Two decades of terrestrial carbon fluxes from a carbon cycle data assimilation system (CCDAS), Global Biogeochemical Cycles, 19, GB2026, doi:10.1029/2004GB002254

Reichle R.H., McLaughlin D.B. and Entekhabi D. (2001), Variational data assimilation of microwave radiobrightness observations for land surface hydrology applications. IEEE Transactions on Geoscience and Remote Sensing, 39, 1708–1718.

Reichstein M., E. Falge, D. Baldocchi, D. Papale, M. Aubinet, P. Berbigier, C. Bernhofer, N. Buchmann, T. Gilmanov, A. Granier, T. Grünwald, K. Havrankova, H. Ilvesniemi, D. Janous, A. Knohl, T. Laurila, A. Lohila, D. Loustau, G. Matteucci, T. Meyers, F. Miglietta, J.-M. Ourcival, J. Pumpanen, S. Rambal, E. Rotenberg, M. sanz, J. Tenhunen, G. Seufert, F. Vaccari, T. Vesala, D. Yakir, R. Valentini, 2005. On the separation of net eocsystem exchange into assimilation and ecosystem respiration: review and improved algorithm. Global Change Biology, 11(9), 1424-1439.

Richardson AD, Aikens M, Berlyn GP, Marshall P. 2004. Drought stress and paper birch (Betula papyrifera) seedlings: Effects on an organic biostimulant on plant health and stress tolerance, and detection of stress effects with instrument-based, noninvasive methods. Journal of Arboriculture 30 52-60.

Richardson AD, Berlyn GP, Gregoire TG (2001) Spectral reflectance of Picea rubens (Pinaceae) and Abies balsamea (Pinaceae) needles along an elevational gradient, Mt. Moosilauke, New Hampshire, USA. American Journal of Botany 88 667-676.

Rie N, Yoshiko K, Shinjiro O, Kenro N, Hiroyuki O, Satoru T, Makoto T (2006) Seasonal changes of a spectral reflectance index, PRI (Photochemical Reflectance Index) in a temperate Japanese cypress forest. Journal of Japan Society of Hydrology & Water Resources 19 475-482.

Rosema A, Cecchi G, Pantani L, et al (1992) Monitoring photosynthetic activity and ozone stress by laser-induced fluorescence in trees. International Journal of Remote Sensing 13 737-751.

Rosema A, Snel JFH, Zahn H, Buurmeijer WF, Van Hove LWA (1998) The relation between laser-induced chlorophyll fluorescence and photosynthesis. Remote Sensing of Environment 65 143-154.

Rosema A, Snel JFH, Zahn H, et al. (1998).Title: The relation between laser-induced chlorophyll fluorescence and photosynthesis. Remote Sens. Environ., 65, 143-154.

Rosema, A., Verhoef, W., Schroote, J., and Snel, J.F.H. (1991), Simulating fluorescence light-canopy interaction in support of laser-induced fluorescence measurements. Remote Sens. Environ. 37, 117–130.

Ryan MG (1991) A simple method for estimating gross carbon budgets for vegetation in forest ecosystems. Tree Physiology 9 255-266.

Sailaja MV, Chandrasekhar Y, Rao DN, Das VSR (1997) Laser-induced chlorophyll fluorescence ratio in certain plants exhibiting leaf heliotropism. Australian Journal of Plant Physiology 24 159-164.

Sands PJ (1995) Modelling canopy production. I. Optimal distribution of photosynthetic resources. Australian Journal of Plant Physiology 22 593-601.

Schimel DS, House JI, Hibbard KA, et al (2001) Recent patterns and mechanisms of carbon exchange by terrestrial ecosystems. Nature 414 169-172.

Scholes, R.J., Walker, B.H., (1993). An African savanna. Synthesis of the Nylsvley study. Cambridge University Press, 306 pp.

Schönknecht G, Neimanis S, Katona E, Gerst U, Heber U (1995) Relationship between photosynthetic electron transport and pH gradient across the thylakoid membrane in intact leaves. Proceedings of the National Academy of Sciences of the United States of America 92 12185-12189.

Schreiber U, Bilger W (1987) Rapid assessment of stress effects on plant leaves by chlorophyll fluorescence measurements. In: Plant Response to Stress.Functional Analysis in Mediterranean Ecosystems (eds Tenhunen JD, Catarino FM, Lange OL, Oechel WC), pp. 27-53. Springer-Verlag, Berlin.

Schreiber U, Neubauer C (1990) O2 dependent electron flow, membrane energisation and the mechanism of non-photochemical quenching of chlorophyll fluorescence. Photosynthesis Research 25 279-293.

Schuurmans J.M., Troch P.A., Veldhuizen A.A., Bastiaanssen W.G.M. & Bierkens M.F.P. (2003). Assimilation of remotely sensed latent heat flux in a distributed hydrological model. Advances in Water Resources 26: 151-159.

Schymanski, S.J., Roderick, M.L., Sivapalan, M., Hutley, B.H., Beringer, J., 2008. A canopy-scale test of the optimal water-use hypothesis. Plant, Cell & Environment, 31(1), 97 - 111

Sellers, P.J., S.O. Los, C.J. Tucker, C.O. Justice, D.A. Dazlich, G.J.Collatz and D.A. Randall. (1996). A revised land surface parameterization (SiB2) for atmospheric GCMs. II. The generation of global fields of terrestrial biophysical parameters from satellite data, Journal of Climate, Vol. 9, No 4, pp. 706-735.

Shuttleworth, W.J., J.S. Wallace, 1985. Evaporation from sparse crops - an energy combination theory. Q. J. R. Meteorol. Soc., 111, 839-855.

Sims DA, Gamon JA (1999) Estimating anthocyanin, chlorophyll, and carotenoid concentrations using hyperspectral reflectance. Annual Meeting of the Ecological Society of America, 8-12 August 1999, Spokane, WA.

Sims DA, Gamon JA (2002) Relationships between leaf pigment content and spectral reflectance across a wide range of species, leaf structures and developmental stages. Remote Sensing of Environment 81 337-354.

Sims DA, Luo H, Hastings S, Oechel WC, Rahman AF, Gamon JA (2006) Parallel adjustments in vegetation greenness and ecosystem CO2 exchange in response to drought in a Southern California chaparral ecosystem. Remote Sensing of Environment 103 289-303.

Sitch S., B. Smith, I.C. Prentice, A. Arneth, A; Bondeau, et al. (2003), Evaluation of ecosystem dynamics, plant geography and terrestrial carbon cycling in the LPJ dynamic vegetation model, Global Change Biology, 9, 161-185

Smith, B., Prentice, I.C., Sykes, M.T., (2001). Representation of vegetation dynamics in the modeling of terrestrial ecosystems: comparing two contrasting approaches within European climate space. Global Ecol. Biogeogr. 10, 621–637.

Soer G.J.R. (1980). Estimation of regional evapotranspiration and soil moisture conditions using remotely sensed crop surface temperature. Remote Sensing of Environment. 9, 27–45.

Somersalo S, Krause GH (1989) Photoinhibition at chilling temperature. Planta 177 409-416.

Soussana, J.-F., Casella, E., Loiseau, P., (1996). Long-term effects of CO2 enrichment and temperature increase on a temperate grass sward. II. Plant nitrogen budgets and root fraction. Plant and Soil, 182, 101–114.

Srivastava A, Guissé B, Greppin U, Strasser RJ (1997) Regulation of antenna structure and electron transport in photosystem II of Pisum sativum under elevated temperature probed by the fast polyphasic chlorophyll a fluorescence transient: OKJIP. Biochimica et Biophysica Acta 1320 95-106.

Strachan IB, Pattey E, Boisvert JB (2002) Impact of nitrogen and environmental conditions on corn as detected by hyperspectral reflectance. Remote Sensing of Environment 80 213-224.

Stylinski C, Gamon J, Oechel W (2002) Seasonal patterns of reflectance indices, carotenoid pigments and photosynthesis of evergreen chaparral species. Oecologia 131 366-374.

Stylinski CD, Oechel WC, Gamon JA, Tissue DT, Miglietta F, Raschi A (2000a) Effects of lifelong [CO2] enrichment on carboxylation and light utilisation of Quercus pubescens Willd. examined with gas exchange, biochemistry and optical techniques. Plant Cell & Environment 23 1353-1362.

Stylinski CD, Oechel WC, Gamon JA, Tissue DT, Miglietta F, Raschi A (2000b) Effects of lifelong [CO2] enrichment on carboxylation and light utilisation of Quercus pubescens Willd. examined with gas exchange, biochemistry and optical techniques. Plant Cell and Environment 23 1353-1362.

Su<rez L, Zarco-Tejada PJ, Sepulcre-Cant\ G, PJrez-Priego O, Miller JR, JimJnez-MuZoz JC, Sobrino (2008) Assessing canopy PRI for water stress detection with diurnal airborne imagery. Remote Sensing of Environment 112 560-575.

Suárez, L. ,P.J. Zarco-Tejada, G. Sepulcre-Cantó, O. Pérez-Priego, J.R. Miller, J.C. Jiménez-Muñoz, J. Sobrino (2008). Assessing canopy PRI for water stress detection with diurnal airborne imagery. Remote Sensing of Environment, 112, 560-575.

Sun P, Grignetti A, Liu S, Casacchia R, Salvatori R, Petrini F, Loreto F, Centritto M (2008) Associated changes in physiological parameters and spectral reflectance indices in olive (Olea europaea) leaves in response to different levels of water stress. International Journal of Remote Sensing 29 1725-1743.

Taconet O. & Vidal-Madjar D. (1988). Application of a flux algorithm to a field-satellite campaign over vegetated area. Remote Sensing of Environment 26, 227–239.

Takizawa K, Kanazawa A, Kramer DM (2008) Depletion of stromal Pi induces high 'energy-dependent' antenna exciton quenching (qE) by decreasing proton conductivity at CFO-CF1 ATP synthase. Plant Cell and Environment 31 235-243.

Tambussi EA, Casadesus J, Munne-Bosch SM, Araus JL (2002) Photoprotection in water-stressed plants of durum wheat (Triticum turgidum var. durum): changes in chlorophyll fluorescence, spectral signature and photosynthetic pigments. Functional Plant Biology 29 35-44.

Thenot F, MJthy M, Winkel T (2002) The photochemical reflectance index (PRI) as a water-stress index. International Journal of Remote Sensing 23 5135-5139.

Thomas D, D Eamus, and D Bell, 1999b. Optimization theory of stomatal behaviour II. Stomatal responses of several tree species of north Australia to changes in light, soil and atomospheric water content and temperature. J. Exp. Bot., 50, 391 - 398.

Thomas D, D Eamus, D Bell, 1999a. Optimization theory of stomatal behaviour I. A critical evaluation of five methods of calculation. J. Exp. Bot., 50: 383 - 390.

Thomas DS, Eamus D (1999) The influence of predawn leaf water potential on stomatal responses to atmospheric water content at constant Ci and on stem hydraulic conductance and foliar ABA concentrations. Journal of Experimental Botany 50 243-251.

Trotter GM, Whitehead D, Pinkney EJ (2002) The photochemical reflectance index as a measure of photosynthetic light use efficiency for plants with varying foliar nitrogen contents. International Journal of Remote Sensing 23 1207-1212.

Valentini R, Cecchi G, Mazzinghi P, et al (1994) Remote sensing of chlorophyll a fluorescence of vegetation canopies: 2. Physiological significance of fluorescence signal in response to environmental stresses. Remote Sensing of Environment 47 29-35.

Valentini R, Epron D, De Angelis P, Matteucci G, Dreyer E (1995) In situ estimation of net CO2 assimilation, photosynthetic electron flow and photorespiration in Turkey oak (Quercus cerris L.) leaves : diurnal cycles under different levels of water supply. Plant Cell and Environment 18 631-640.

van de Griend, A.A., and P.E. O'Neill, discrimination of soil hydraulic properties by combined thermal infrared and microwave remote sensing,, in IGARSS'86 Symposium, edited by S.-. ESA, ESA Publications division, Zürich, 8-11 September 1986, 1986.

van der Tol C, Verhoef W, Rosema A (2008) A model for chlorophyll fluorescence and photosynthesis at leaf scale. Agricultural and Forest Meteorology in press.

van der Tol, C. , A. J. Dolman, M. J. Waterloo, and K. Raspor, 2007b. Topography induced spatial variations in diurnal cycles of assimilation and latent heat of Mediterranean forest. Biogeosciences, 4, 137–154.

van der Tol, C., 2007a. A model for chlorophyll fluorescence and photosynthesis at leaf scale. In: Proceedings of the 3nd international workshop on remote sensing of vegetation fluorescence, 7-9 February 2007, Florence, Italy. ESA Noordwijk 2007. 4 p.

van der Tol, C., Verhoef, W., Timmermans, J., Verhoef, A., Su, Z., 2009. An integrated model of soil-canopy spectral radiance observations, photosynthesis, fluorescence, temperature and energy balance. Biogeosciences Discuss., 6, 6025-6075.

van Wijk MT, Dekker SC, Bouten W, et al (2000) Modeling daily gas exchange of a Douglas-fir forest: comparison of three stomatal conductance models with and without a soil water stress function. Tree Physiology 20 115-122.

Verhoef W. & Bach H. (2003). Remote sensing data assimilation using coupled radiative transfer models. Physics and Chemistry of the Earth 28, 3-13.

Verhoef W., van der Tol C., 2008. Integration of 4SAIL radiative transfer model with the canopy energy balance, photosynthesis and fluorescence

Verhoef, W., (2005). Extension of SAIL to model solar-induced canopy fluorescence spectra. In: Second International Workshop on Remote Sensing of Vegetation Fluorescence, 17–19 November 2004, Montreal, Canada.

Verhoef, W., 1998. Theory of radiative transfer models applied in optical remote sensing of vegetation canopies. PhD thesis, Wageningen University, Wageningen, The Netherlands.

Verhoef, W., Jia, L., Xiao, Q., Su, Z., 2007. Unified optical-thermal four-stream radiative transfer theory for homogeneous vegetation canopies. IEEE Transactions on Geoscience and Remote Sensing, 45(6), 1808-1822.

Wang YP, Leuning R (1998) A two-leaf model for canopy conductance, photosynthesis and partitioning of available energy. I. Model description and comparison with a multi-layered model. Agricultural and Forest Meteorology 91 89-111.

Weiss, M., Troufleau, D., Baret, F., Chauki, H., Prévot, L., Olioso, A., Bruguier, N., Brisson, N., 2001. Coupling canopy functioning and radiative transfer models for remote sensing data assimilation. Agricultural and Forest Meteorology, 108, 113-128.

Weng JH, Chen YN, Liao TS (2006) Relationships between chlorophyll fluorescence parameters and photochemical reflectance index of tree species adapted to different temperature regimes. Functional Plant Biology 33 241-246.

Wigneron J.-P., Chanzy A., Calvet J.-C., Olioso A. & Kerr Y. (2002). Modeling approaches to assimilating L-band passive microwave observations over land surfaces. Journal of Geophysical Research 107(D14): 10.1029/2001JD000958.

Wigneron J.-P., Olioso A., Calvet J.-C. & Bertuzzi P. (1999). Estimating root-zone soil moisture from surface soil moisture data and soil-vegetation-atmosphere transfer modeling. Water Resources Research 35, 3735-3745.

Wigneron, J.-P., Calvet, J.-C., Olioso, A., Chanzy, A., Bertuzzi, P., (1999). Estimating the root-zone soil moisture from the combined use of time series of surface soil moisture and SVAT modeling. Physics and Chemistry of the Earth, Part B, 24(7), 837-843.

Williams, J.R., Jones, C.A., Kiniry, J.R., Spanel, D.A., (1989). The EPIC crop growth model. Trans. ASAE. 32, 497-511.

Wilson KB, Baldocchi D, Falge E, et al (2003) Diurnal centroid of ecosystem energy and carbon fluxes at FLUXNET sites. Journal of Geophysical Research 108 Doi 10.1029/2001JD001349.

Wilson, K.B., Baldocchi, D.D., Hanson, P.J., 2000. Spatial and seasonal variability of photosynthetic parameters and their relationship to leaf nitrogen in a deciduous forest. Tree Physiology, 20, 565–578.

Wong SC, Cowan IR, Farquhar GD (1979) Stomatal conductance correlates with photosynthetic capacity. Nature 282 424-426.

Woodward F.I., M. R. Lomas & R.A. Betts, (1998), Vegetation-climate feedbacks in a greenhouse world. Philos.Trans. R. Soc. Lond. Ser. B. 353, 29–38.

Wullschleger SD (1993) Biochemical limitations to carbon assimilation in C3 plants. A retrospective analysis of the A/Ci curves from 109 species. Journal of Experimental Botany 44 907-920.

Xing J, Liao JC, Oster G (2005) Making ATP. Proceedings of the National Academy of Sciences of the USA 102 16539-16546.

Xu L., Baldocchi D.D., 2003. Seasonal trends in photosynthetic parameters and stomatal conductance of blue oak (Quercus douglasii) under prolonged summer drought and high temperature. Tree Physiology, 23, 865–877.

Zarco-Tejada PJ, Miller JR, Mohammed GH, Noland TL, Sampson PH (2000) Chlorophyll fluorescence effects on vegetation apparent reflectance: II. Laboratory and airborne canopy-level measurements with hyperspectral data. Remote Sensing of Environment 74 596-608.

Zarco-Tejada PJ, Miller JR, Pedros R, et al. (2006). FluorMODgui V3.0: A graphic user interface for the spectral simulation of leaf and canopy chlorophyll fluorescence. Computers & Geosciences. 32, 577-591.

Zarco-Tejada PJ, Miller JR, Pedros R, Verhoef W, Berger M (2006) FluorMODgui V3.0: A graphic user interface for the spectral simulation of leaf and canopy chlorophyll fluorescence. Computers & Geosciences 32 577-591.

Zarco-Tejada PJ, Pushnik JC, Dobrowski S, Ustin SL (2003) Steady-state chlorophyll a fluorescence detection from canopy derivative reflectance and double-peak red-edge effects. Remote Sensing of Environment 84 283-294.

Zhao C, Zhou Q, Wang J, Huang W (2004) Spectral indices redefined in detecting nitrogen availability for wheat canopy. Communications in Soil Science and Plant Analysis 35 853-864.

Zhu XG, Govindjee, Baker NR, deSturler E, Ort DR, Long SP (2005) Chlorophyll a fluorescence induction kinetics in leaves predicted from a model describing each discrete step of excitation energy and electron transfer associated with photosystem II. Planta 223 114-133.

10. APPENDICES

10.1. Appendix 1. Team Composition

Unit	Principal investigator(s)	Institution	Acronym	Role
1	Prof. Federico Magnani	Dipartimento di Colture Arboree Alma Mater Studiorum Università di Bologna Viale G. Fanin 46, I-40127 Bologna, Italy Ph. +39 51 2096400 Fax +39 51 2096401	UNIBO	project manager; modification and application of MLFL model for the generation of synthetic datasets. Functional analysis of PRI signal
2	Dr. Albert Olioso	INRA – Climat Sol et Environnement Site Agroparc, 84914 Avignon Cedex 9 -France Phone +33 (0) 4 32 72 24 06 Fax +33 (0) 4 32 72 23 63	INRA	Modification and application of MLFL and FluorMOD model for the generation of synthetic datasets
3	Dr. Marie Weiss	NOVELTIS Site Agroparc, 84914 Avignon Cedex 9 -France Phone +33 (0) 4 32 72 23 79 Fax +33 (0) 4 32 72 23 63	NOVELTIS	Modification and application of Dynamic Vegetation Model, assimilation of fluorescence data. Atmospheric radiative transfer modelling
4	Prof. Ismaël Moya	Equipe Fluorescence et Télédétection Laboratoire de Météorologie Dynamique, CNRS - UMR 8359, Ecole Polytechnique 91128 Palaiseau Cedex - FRANCE ismael.moya@lmd.polytechnique.fr Phone +33 (0) 1 6933 2862 (4356) Fax +33 (0) 1 6933 3005	CNRS	Definition of functional relationship between fluorescence and photosynthetic processes, leaf and canopy level (from laboratory experiments, SIFLEX and Sentinel-2 studies). Functional analysis of PRI signal
5	Dr. Giovanna Cecchi Dr. Giovanni Agati	Istituto di Fisica Applicata "Nello Carrara" - Consiglio Nazionale delle Ricerche Via Madonna del Piano 10, I-50019 Sesto Fiorentino, Italy Phone +390555226338 Fax. +390555226328	CNR	Definition of functional relationship between fluorescence and photosynthetic processes, leaf and canopy level. Analysis of F680/F730 fluorescence ratio

Unit	Principal investigator(s)	Institution	Acronym	Role
6	Dr. Wout Verhoef	National Aerospace Laboratory NLR P.O. Box 153, 8300 AD Emmeloord, Netherlands Phone +31 (527) 248253 Fax +31 (527) 248210	NLR	Canopy radiative transfer modelling in FluorMOD and in MLFL model; atmospheric radiative transfer modelling
7	Dr. Pablo Zarco-Tejada	Instituto de Agricultura Sostenible (IAS) Consejo Superior de Investigaciones Científicas Alameda del Obispo, 14004 Córdoba, Spain Phone +(34) 957 499 280 ; +(34) 676 954 937 Fax +(34) 957 499 252	CSIC	Definition of functional relationship between fluorescence and photosynthetic processes, leaf and canopy level

10.2. Appendix 2: Presentations and publications from FLEX-DVM project

Dayyoub A., Raddi S., van der Tol C., Magnani F. 2009. A model of the functional relationship between photosynthesis and ambient chlorophyll fluorescence. Chlorophyll Fluorescence: From Theory to (Good) Practice. Pisa, 25-26 May, 2009

Magnani F, Dayyoub A (2009) Modelling chlorophyll fluorescence under ambient conditions. *New Phytologist* in preparation .

Moreno J., Goulas Y., Middleton E., Miglietta F., North P., Verhoef W., Rascher U., Svanberg S., Berger M., Drusch M., Gascon F., Carnicero B., BezyJ.L., Guanter L., Magnani F. 2009. Fluorescence Explorer (FLEX): A new technique for the observation of global vegetation photosynthesis. IGARSS 2009, July 12-17, 2009, Cape Town, South Africa

Moreno J, Moya I, Miglietta F, *et al* (2008) Assessing gross primary production from solar-induced chlorophyll fluorescence: field results and integration into biogeophysical models. *Geophysical Research Abstracts* 10 07911.

Suarez L, Zarco-Tejada PJ, Berni JAJ, Gonzalez-Dugo V, Fereres E (2009) Modelling PRI for water stress detection using radiative transfer models. *Remote Sensing of Environment* 113 730-744.

Suarez L, Zarco-Tejada PJ, Sepulcre-Canto G, *et al* (2008) Assessing canopy PRI for water stress detection with diurnal airborne imagery. *Remote Sensing of Environment* 112 560-575.

van der Tol C, Verhoef W, Rosema A (2008) A model for chlorophyll fluorescence and photosynthesis at leaf scale. *Agricultural and Forest Meteorology* 149 96-105.

10.3. Appendix 3. FLEX-DVM project team meetings

The following meetings have been held during the project, as documented by meeting minutes uploaded on the project web page:

- Negotiation Meeting: ESA-ESTEC, Noordwijk, The Netherlands, 19 April, 2007
- 1st Progress Meeting: telephone conference, 28 June, 2007
- 2nd Progress Meeting: ESA-ESTEC, Noordwijk, The Netherlands, 16 January, 2008
- Mid-Term Presentation: ESA-ESTEC, Noordwijk, The Netherlands, 5 May, 2008
- 3rd Progress Meeting: University of Valencia, Valencia, Spain, 10 September, 2008
- Final Meeting: ESA-ESTEC, Noordwijk, The Netherlands, 3 April, 2009

10.4. Appendix 4. Project Tasks and Scientist Responsibilities

According to the original proposal, responsibility for individual Tasks and Workpackages was partitioned between Partners as follows:

Task	**Task manager**	**Institution**
1	Dr. Albert Olioso	INRA
2	Dr. Albert Olioso	INRA
3	Prof. Federico Magnani	UNIBO
4	Dr. Marie Weiss	NOVELTIS
5	Prof. Federico Magnani	UNIBO

Workpackage	**WP manager**	**Institution**
WP0	Prof. Federico Magnani	UNIBO
WP1	Dr. Albert Olioso	INRA
WP2	Prof. Federico Magnani	UNIBO
WP3	Dr. Giovanni Agati	CNR
WP4	Dr. Wout Verhoef	NLR
WP5	Prof. Federico Magnani	UNIBO
WP6	Dr. Albert Olioso	INRA
WP7	Dr. Pablo Zarco-Tejada	CSIC
WP8	Dr. Albert Olioso	INRA
WP9	Dr. Marie Weiss	NOVELTIS
WP10	Prof. Federico Magnani	UNIBO

Responsibility for project deliverables can be attributed to individual Partners as detailed in the following table:

Deliverable	*Description*	*Responsible Research Unit*
DL 1.1	Description of Dynamic Vegetation Model requirements and available modelling options	INRA
DL 1.2	Description of selected Dynamic Vegetation Model	INRA
DL 2.1	Description of functional model requirements and available modelling options	UNIBO
DL 2.2	Source code and description of selected functional model	UNIBO
DL 3.1.1	SIF and chlorophyll: estimation and corrections	CSIC
DL 3.1.2	SIF and photosynthesis: absolute SIF values	CNRS
DL 3.1.3	SIF and photosynthesis: peak ratio	CNR
DL 3.2	Algorithms for the inclusion of fluorescence and leaf optical properties in functional models at leaf level	UNIBO

Deliverable	*Description*	*Responsible Research Unit*
DL 3.3.1	Test of proposed algorithms against experimental data already available at the leaf level: SIF and chlorophyll: estimation and corrections	CSIC
DL 3.3.2	Test of proposed algorithms against experimental data already available at the leaf level: SIF and photosynthesis: absolute SIF values	CNRS and UNIBO
DL 3.3.3	Test of proposed algorithms against experimental data already available at the leaf level: SIF and photosynthesis: peak ratio	CNR
DL 4.1	Software to include leaf and soil thermal radiances in multi-layer model	NLR
DL 4.2	Description of incorporation of thermal infrared radiation in canopy model	NLR
DL 4.3	Code of multi-layer Farquhar-Leuning (MLFL) model	UNIBO
DL 4.4.1	Modified FluorMOD model for the assimilation of functional variables (multi-layer for MLFL)	NLR
DL 5.1	Database of environmental parameters for each selected site	UNIBO
DL 6.1.1	Database of MLFL model parameters for each selected PFT	UNIBO
DL 6.1.2	Database of DVM model parameters for each selected PFT	INRA
DL 6.2.1	Dataset of simulated annual canopy gas exchange at the selected sites using MLFL	UNIBO
DL 6.2.2	Dataset of simulated annual canopy gas exchange at the selected sites using DVM	INRA
DL 6.3.1	Dataset of simulated canopy radiance (inclusive of reflectance and fluorescence) for selected days at the canopy site using MLFL model	UNIBO
DL 6.3.2	Dataset of simulated canopy radiance (inclusive of reflectance and fluorescence) for selected days at the canopy site using DVM	INRA
DL 7.1	Review of parameters that can be extracted from modelled canopy fluorescence, based on (i) empirical comparison of modelled GPP and SIF and (ii) literature data	CNR
DL 7.2	Review of parameters that can be extracted from modelled canopy reflectance, based on (i) empirical comparison of modelled GPP and reflectance and (ii) literature data	CSIC
DL 9.0	Report on DVM sensitivity analysis	NOVELTIS
DL 10.1	Summary analysis: canopy fluorescence fields and relationship with canopy gas-exchange	UNIBO
DL 10.2	Summary analysis: impact of fluorescence assimilation on DVM predictive ability	UNIBO
DL 10.3	Recommendations: future needs for the preparation of a space-borne SI vegetation fluorescence mission and for the exploitation of the resulting data	UNIBO

10.5. Appendix 5. SCOPE Version 1.2User Manual (Christiaan van der Tol (tol@itc.nl) - April 2009

The original MatLab code of the model in its different versions has been provided to the agency as an attachment to this report.

Introduction

SCOPE is an integrated model for *soil-canopy spectral radiance observations, photosynthesis and energy balance* of the vegetated land surface.

The aim of the model is to link top of canopy (TOC) observations of radiance with land surface processes. Radiance includes the thermal and the optical part, with a module dedicated to chlorophyll fluorescence. Land surface processes include photosynthesis, net radiation, sensible and latent heat flux and soil heat flux.

The model is a 1D vertical model, which means that horizontal variations in surface characteristics are ignored. In the vertical direction, leaf layers are distinguished. In addition, discrete leaf angle classes, wavelengths and time steps are distinguished.

The model was developed at the ITC International Institute for Geo-Information Science and Earth Observation in The Netherlands, in the framework the ECO-RTM project, funded by the Netherlands Organisation for Scientific Research (NWO-SRON-EO71).

An overview paper of SCOPE will be submitted to Biogeosciences soon (the discussion paper should be available no later than June 2009):

Van der Tol, C., Verhoef, W., Timmermans, J. Verhoef, A. and Su, Z. "An integrated model of soil-canopy spectral radiance observations, photosynthesis, fluorescence, temperature and energy balance". This paper describes the fundamentals of the model, as well as potential applications and limitations. The reader is referred to this paper for the theoretical aspects of the model. Users are requested to refer to this paper in publications.

Questions about the model can be addressed to Christiaan van der Tol (tol@itc.nl) and Wout Verhoef (verhoef@itc.nl).

1 - Software requirements

The model SCOPE_v1.2 is written in Matlab 7.6 (R2008a). The model also works with version 6.0 (R2006a), but not with version Matlab 5.1. No special toolboxes are required. There is no warranty that the model will work with different versions of Matlab.

2 - Getting started

SCOPE consists of several scripts and functions (hereafter called modules), which can be used separately or as parts of the integrated SCOPE model. When the models are used separately, then it is important to provide input and globals. When the integrated model is called, then the input and globals are automatically loaded using the modules described in Chapter 4. Each module can be called from the Matlab prompt. Basic knowledge of the use of Matlab is required to operate the model.

The application of the model involves the following steps:

1. **To unpack the zip file**

   Unpack the model, and leave the directory structure intact.

2. **To define the desired output**

   Before running the model, it is necessary to decide what the required output is, and what input data is available. It is probably not necessary to run the complete model. Perhaps it is sufficient to switch some of the options off. It is also possible to write a new script that uses only some of the modules. The model always works in forward mode, which means that it produces spectra and fluxes using prescribed parameter values and meteorological variables as input.

3. **To create a parameter file**

   Next, a parameter file must be completed (`parameters.m`). In this file, the user sets the parameters for the simulations, and specifies which modules to use. The user also indicates where the input data can be found.

4. **To prepare input files**

   The input files are text files, in ASCII. The format is prescribed. The user who wants more flexibility (for example by reading in Excel sheets), will need to adapt the module '`load_data.m`'.

5. **To execute the model**

   The complete model can be executed by calling '`master`' in the command window of Matlab. Alternatively, separate modules can be called, provided that the required input is given. The modules have a help text describing how to do this, which can be called by typing '`help` modulename', for example: '`help master`'. If master is used, then the output of each simulation is automatically saved in an output directory.

6. **To plot the output**

   An example of a module which creates graphs is provided with the model (`plots.m`). This is a no so clean function with a variety of graphs that could be made. It is up to the user to create a script for plotting results, or to use alternative software for creating graphs.

3 - Description of the modules

3.1 - Master

SCOPE starts by running the script '`master`'. This script loads physical constants, parameters, and input data, prepares files for output, runs the model, saves the output, and (if this option is set in the parameter file) plots graphs of the results.

Master carries out the following operations:

3.1.1 Load constants

Here, physical constants are loaded, such as molecular mass of air, speed of light, etc. The constants are described in the function '`constants.m`'

3.1.3 Load Parameters

Here, user specified parameters are loaded, such as PROSPECT parameters, photosynthesis parameters, locations of specific input files, etc. These parameters are specified in '`parameters.m`'

3.1.4 Define globals

Here, the globals are defined. The globals are needed to make sure that '`master`' has access to all parameters and constants that were loaded in steps 1 and 2.

3.1.5 Load the input data

Here, the input data for the model simulation are loaded. The function '`load_data.m`' is used.

3.1.6 Set initial conditions

In SCOPE_v1.2, only the soil surface temperature is set as an initial condition. Otherwise, the state of the surface has no 'memory'. If the initial soil surface temperature is unknown, it is recommended to use an arbitrary value, to simulate a time series, and to discard the first few hours' worth of simulations.

3.1.7 Create output files

A directory for output data and output files is created. The name of the directory has the name of the research site, and the date and time when the simulations were carried out in it.

3.1.8 Execute the actual model and to save the output

The actual model is called '`ebal.m`'. The model '`ebal.m`' is called for each time step separately. After the calculations for each time step, the results are saved in the output files with '`output_data.m`'

3.1.9 Plot the results

The results will be plotted, if the option '`makeplots`' in `parameters.m` is switched on. The function '`plots.m`' needs to be modified by the user to make it work for a particular purpose.

3.2 - Parameters

The function '`parameters.m`' contains the parameters for the model simulations. The function is subdivided into sections (0 to 8, and Appendices A to H). The user can enter parameter values for the simulations in sections 1 to 8. It is recommended not to change the other sections.

In the consecutive sections 1 to 8, the following information should be entered:

3.2.1 Simulation options

The user can specify desired optional calculations (for example: fluorescence), (decimal) start and end date of the simulations (in case a time series is simulated), and alternative methods to be used. The options are described in Section 4.12.

Note: the soil heat flux method mentioned in this section of '`parameters`' refers to the calculation of soil thermal inertia. If this parameter is 1, then an a priori soil intertia is used. If this parameter is 2, then soil thermal inertia is an empirical function of soil moisture content. It is recommended to use the a priori thermal inertia, until better techniques to estimate soil thermal inertia become operational.

3.2.2 Declare file names

The user can specify the path, directory name and file names of input files. The path is specified in section 2.1 of `parameters`. The default path is: '`../../data/input/`'. The directory name needs to be specified in section 2.2. By default, the model collects the data from the first directory (alphabetically) starting with the word: '`Dataset`'. This can be changed according to the wish of the user.

Most input files are compulsory, except for the following: CO2_file, z_file, LAI_file, hc_file, Vcmax_file, Jmax_file, Lambda_file and SMC_file. If these data are not available, then empty quotes should be entered (''). The format of the input files is explained in Chapter 5.

If a compulsory file is not present in the input directory, or misspelled in the parameter file, then the model will be aborted after execution and Matlab will give the following error message: '`Unable to read file ../../data/input/filename: No such file or directory.`'

3.2.3 Location

Here, the user can specify the longitude and latitude of the location for which the simulations are carried out (in decimal degrees). The longitude and latitude are, together with time, needed to calculate solar azimuth and zenith angles.

3.2.4 Numerical parameters

In this section, the number of leaf layers, number of azimuth classes, the maximum number of energy balance loop iterations, the maximum allowed energy balance error, and wavelength classes are specified. It is not necessary that these wavelength classes match with the wavelength classes of the input data.

3.2.5 Radiative transfer parameters

Here, the user can specify the parameters for the radiative transfer models. In Section 5.0 one can specify the observation zenith and azimuth angle. It is also possible to include the location and name of a file which contains a table of different angles. This is useful in case one wishes to repeat the calculations for different observation angles. In that case, the option 'calcdirectional' must be switched on in `parameters`. In that case, a folder dedicated to multi-directional observations will be created in the output. In Section 5.1 one specifies PROSPECT parameters, leaf inclination distribution and the reflectance and transmittance in the thermal infrared. *It is not yet possible to vary reflectance and transmittance spectrally in the thermal infrared*. In Section 5.2 the location and file name of a file containing a soil spectrum must be provided.

3.2.6 Input radiation spectrum

In this section, a TOC input radiation spectrum should be given. This spectrum can be generated with MODTRAN. This file should be an ASCII file containing three columns: (1) the wavelength in nm, (2) solar irradiance in W m^{-2} μm^{-1}, and sky irradiance in W m^{-2} μm^{-1}, covering the range from 0.4 to 50 µm.

3.2.7 Fluorescence matrix

In SCOPE_v1.2, two fluorescence matrices have to be given as input. These matrices translate an input spectrum of incident PAR into a fluorescence spectrum of an unstressed leaf in low light conditions, in energy units. The input should have a spectral resolution of 1 nm, one for the upper side of the leaf (Mba), and one for the lower side of the leaf (Mfa). The incident radiation runs from 400 to 750 nm, the output from 640 to 850 nm. Thus, the size of the matrices is 351 x 211. Example matrices are delivered with the model. The calculation of the matrices will be integrated in the model in the future, in a new module `fluspect`. In SCOPE_v1.2 this is not yet available.

3.2.8 Energy balance, micrometeorological and physiological parameters

In this section, vegetation and soil parameters are specified, including leaf biochemical parameters (Section 8.1), canopy structure parameters (Section 8.2), soil parameters (Section 8.3), and a priori aerodynamic resistances (Section 8.4).

3.2.9 Appendices

The appendices do not need to be changed. In the appendices, a number of calculations are carried out on the parameters, in order to prepare them to be used by the model. For example, the spectral

resolution is calculated, the canopy is divided into layers, PROSPECT is executed, and a leaf angle distribution is calculated.

3.3 - Prospect

The function '`prospect.m`' is used by `parameters` to calculate reflectance and transmittance of leaves.

3.4- Load input data

The function `load_data.m` loads the input data for SCOPE. This module does not require input. A number of globals are required from `parameters.m` and `constants.m`.

The structure of load_data is as follows:

0. Globals
1. Time and zenith angle
2. Radiation
3. Windspeed, air temperature, humidity and air pressure
4. Vegetation structure (measurement height, vegetation height and LAI)
5. Gas concentrations
6. Soil Moisture Content
7. Leaf biochemical parameters

Load_data can be called in the following way:

[year_, t_, tts_, Rin_, Rli_, p_, Ta_, ea_, u_, Ca_, Oa_, GAM_, LAI_, …

hc_, zo_, d_, z_, rss_, rbs_ ,Vcmo_, Jmo_, lam_] = Load_data

Table 1 Output of load_data

Symbol	Description	Unit	Dimension
year_	year (Julian)		[nt]
t_	time in decimal days		[nt]
tts_	solar angle	degrees	[nt]
Rin _	incoming shortwave radiation (<2.5 µm)	W m^{-2}	[nt]
Rli_	incoming longwave radiation (>2.5 µm)	mol m^{-2} s^{-1}	[nt]
p_	air pressure	hPa	[nt]
Ta_	air temperature	°C	[nt]
ea_	atmospheric vapour pressure	hPa	[nt]
u_	wind speed	m s^{-1}	[nt]
Ca_	CO2 concentration in the air	µmol m^{-3}	[nt]
Oa_	O2 concentration in the air	µmol m^{-3}	[nt]
GAM_	thermal inertia	J m^{-2} K^{-1} $s^{-1/2}$	[nt]
LAI_	one sided Leaf Area Index	m^2 m^{-2}	[nt]

Symbol	Description	Unit	Dimension
hc_	vegetation height	m	[nt]
zo_	roughness length for momentum	m	[nt]
d_	zero-plane displacement	m	[nt]
z_	height of meteorological measurements	m	[nt]
rss_	soil surface resistance	s m^{-1}	[nt]
rbs_	soil boundary resistance	s m^{-1}	[nt]
Vcmo_	max carboxylation capacity Vcmax	µmol m^{-2} s^{-1}	[nt]
Jmo_	max electron transport rate Jmax	µmol m^{-2} s^{-1}	[nt]
lam_	Cowan's stomatal parameter		

In Table 1, *nt* is the number of time steps. All data are vectors with length *nt*. Note that for carboxylation capacity and for maximum electron transport rate, the symbols Vcmo_ and Jmo_ are used instead of Vcmax and Jmax (as used in `parameters`). The reason is that the parameters Vcmax and Jmax are already reserved for the a priori values in `parameters`. The values from `load_data` are time series of Vcmax and Jmax, taken either from a table (if any exists), or from the a priori values of parameters. This enables the user to use either fixed parameter values or time series of parameter values.

3-5 - Energy balance model

The function `Ebal.m` executes the energy balance calculations and the radiative transfer modules. In addition, some optional calculations can be carried out. The optional calculations have to be specified by the user in `parameters.m`. Ebal calls a number of modules. The order of execution and the contents of each module have been described in detail in the reference paper.

The following calculations are carried out:

3.5.1 Radiative transfer of solar and sky radiation

Net radiation on leaf (and soil) level is calculated, as well as the spectrum of outgoing radiance with the module `RTMo.m`.

3.5.2 Initialisations for the iteration loop

An iteration is needed in order to solve the energy balance. Before the iteration takes place, a number of variables need to be initialised: the CO2 concentration in the stomata, leaf and soil temperatures, Monin-Obukhov length, etc.

3.5.3 Energy balance iteration loop

In the energy balance iteration loop, the radiative transfer module for internally generated thermal radiation (`RTMt_sb.m`), biochemical processes (`biochemical.m`) and the turbulent heat fluxes (`heatfluxes.m`) are calculated iteratively, until closure of the energy balance for all leaves and for the soil.

3.5.4 Spectral output, fluxes in observation direction

Here, the TOC spectra in observation direction are prepared for output.

3.5.5 Extra Options: Vertical profiles of fluxes and temperatures, Planck curve, Fluorescence

Additional, optional calculations can be carried out, such as vertical profiles within the canopy, or thermal output spectrum and/or chlorophyll fluorescence in observation direction.

3.5.6 Spectrally integrated energy, fluorescence, water and CO2 fluxes

Canopy level fluxes, bulk resistances and spectrally integrated radiance are calculated for output.

3.6 - Radiative transfer module for solar and sky radiation

The module `RTMo.m` calculates the spectrum of outgoing visible and thermal radiation in hemispherical and viewing direction, and net radiation and absorbed PAR at the leaf and soil level. The module is based on earlier versions of the SAIL model, but now including the calculation of net radiation.

The user needs to specify input and globals only. The globals are all defined in `parameters.m`. The module is structured as follows:

0. Preparations
   - 0.1 parameters
   - 0.2 initialisations
1. Geometric quantities
   - 1.1 general geometric quantities
   - 1.2 geometric factors associated with extinction and scattering
   - 1.3 geometric factors to be used later with rho and tau
   - 1.4 solar irradiance factors for all leaf orientations
   - 1.5 probabilities Ps, Po, Pso
2. Calculation of upward and downward fluxes
3. Outgoing fluxes, hemispherical and in viewing direction, spectrum
4. Net fluxes, spectral and total, and incoming fluxes

A1 functions J1 and J2 (introduced for stable solutions)

A2 function volscat

A3 function e2phot

RTMo can be called in Matlab in the following way:

```
function [Lout_, Lo_ , Ps, Po, Pso, K, Louto, Loutt, Eplu_, Emin_, Rnhs, Rnus, Rnhv, Rnuv, Pnh, Pnu, PARhv, PARuv] = RTMo(Esun_, Esky_,LAI,tts,tto,psi)
```

The variables between the [] are the output, the variables between the () are the input (Tables 2 and 3)

Table 2. Input of RTMo

Symbol	Description	Unit	Dimension
Esun_	direct solar radiation	W m^{-2} μm^{-1}	[nwl]
Esky_	diffuse sky radiation	W m^{-2} μm^{-1}	[nwl]

LAI	leaf area index	$m^2 m^{-2}$	[1]
tts	solar zenith angle	degrees	[1]
tto	viewing angle	degrees	[1]
psi	azimuth angle difference between solar and viewing position	degrees	[1]

Table 3. Output of RTMo

Symbol	Description	Unit	Dimension
Rnhs	Net radiation of shaded soil	W m^{-2}	[1]
Rnus	Net radiation of sunlit soil	W m^{-2}	[1]
Rnhc	Net radiation of shaded leaves	W m^{-2}	[nl]
Rnuc	Net radiation of sunlit leaves	W m^{-2}	[13,36,nl]
Pnh	Net PAR by shaded leaves	mol m^{-2} s^{-1}	[nl]
Pnu	Net PAR by sunlit leaves	mol m^{-2} s^{-1}	[13,36,nl]
Eplu_	Upward diffuse radiation	W m^{-1} μm^{-1}	[nl+1]
Emin_	Downward diffuse radiation	W m^{-1} μm^{-1}	[nl+1]
Louto	Total outgoing hemispherical rad (<=2.5 um)	W m^{-2}	[1]
Loutt	Total outgoing hemispherical rad (>2.5 um)	W m^{-2}	[1]
Lout_	Spectrum of outgoing hemispherical rad	W m^{-2} μm^{-1}	[nwl]
Lo_	Spectrum of outgoing radiance in viewing dir	W m^{-2} μm^{-1} sr^{-1}	[nwl]
PARhc	Incident PAR on shaded leaves	mol m^{-2} s^{-1}	[nl]
PARuc	Incident PAR on sunlit leaves	mol m^{-2} s^{-1}	[13,36,nl]
Ps	probability of sunlit leaves		[nl+1]
Po	probability of viewing a leaf or soil		[nl+1]
Pso	probability of viewing a sunlit leaf or sunlit soil		[nl+1]
K	extinction coefficient in viewing dir		[nl+1]

In Tables 2 and 3, nwl is the number of wavelengths, nl is the number of layers, 13 is a fixed number of leaf orientations and 36 is a fixed number of leaf azimuth angle classes.

3.7 - Radiative transfer modules for internally generated thermal radiation

The radiative transfer modules for internally generated thermal radiation calculate outgoing thermal hemispherical radiation and radiance in viewing direction, and net thermal radiation at the leaf and soil level. RTMt_sb calculates the broad band radiance, whereas RTMt_planck calculates the full spectrum on the thermal range. In the energy balance iteration loop, RTMt_sb is always used, which is much faster than RTMt_planck. The spectrum can be calculated afterwards with RTMt_planck as an option.

The user needs to specify input and globals. The globals are all defined in `parameters.m` and `constants.m`. The module is structured as follows:

0 preparations
- 0.0 globals
- 0.1 initialisations
- 0.2 parameters
- 0.3 geometric factors of Observer
- 0.4 geometric factors associated with extinction and scattering
- 0.5 geometric factors to be used later with rho and tau
- 0.6 fo for all leaf angle/azumith classes

1 calculation of upward and downward fluxes

2 total net fluxes

Appendix A. Stefan-Boltzmann

RTMt_sb can be called in Matlab in the following way:

```
[Rnhs,Rnus,Rnhc,Rnuc,Loutt,Lot,Eplu,Emin] = ...
    RTMt_sb(Tcu,Tch,Tsu,Tsh,LAI,Ps,Po,Pso,K,tto,psi)
```

The input and output is similar to that of RTMo (see Tables 2 and 3), but now the variables are related to internally generated thermal radiation. As input, leaf and soil temperatures are needed in addition (Table 4).

Table 4. Leaf and soil temperature as input of RTMt_sb

Symbol	Description	Unit	Dimension
Tcu	temperature sunlit leaves	°C	[13,36,nl]
Tch	temperature shaded leaves	°C	[nl]
Tsu	temperature sunlit soil	°C	[1]
Tsu	temperature shaded soil	°C	[1]

RTMt_planck is similar to RTMt_sb, except that the output is a spectrum. Moreover, net radiation is not calculated. The usage of RTMt_planck is as follows:

```
[Loutt_,Lot_,Eplu,Emin] =  RTMt_planck(Tcu,Tch,Tsu,Tsh,LAI,Ps,Po,Pso,K,tto,psi)
```

3.8 - Radiative transfer module for chlorophyll fluorescence

The module RTMf calculates the spectrum of outgoing fluorescence L in observation direction, in W m^{-2} sr^{-1} μm^{-1}.

The module is structured as follows:

0 preparations
- 0.0 globals
- 0.1 initialisations
- 0.2 geometric quantities
- 0.3 solar irradiance factor and ext. in obs dir for all leaf angle/azumith classes

1.0 calculation of fluorescence flux in observation direction

The user needs to specify the input. The usage of the module is as follows:

Ltot_ = RTMf2(Esun_,Emin_,Eplu_,F0,F1,LAI,Po,Pso,tts, tto)

Table 5. Input for RTMt_f

Symbol	Description	Unit	Dimension
Esun_	direct inc. PAR	W m^{-2} μm^{-1}	[nwlfi,nl+1]
Emin_	downward fluxes in the canopy, spectral	W m^{-2} μm^{-1}	[nwlfi,nl+1]
Eplu_	upward fluxes in the canopy, spectral	W m^{-2} μm^{-1}	[nwlfi,nl+1]
F0	fluorescence factor for shaded leaves		[nl]
F1	fluorescence factor for sunlit leaves		[13,36,nl]

In Table 5, nwlfi is the number of PAR wavelength classes (351) and nwlfo the number of fluorescence wavelength classes (211). The factors F0 and F1 represent the fluorescence as a fraction of that of an unstressed leaf in low light conditions. These factors are calculated with `biochemical.m`.

3.9 - Turbulent heat fluxes

The function `heatfluxes.m` calculates sensible (H) and latent heat (lE) flux. The user needs to provide the input. The module use a number of globals defined in `constants.m`.

The usage of heatfluxes is as follows:

[lE, H] = heatfluxes(ra,rs,Tc,ea,Ta,e_to_q,PSI)

The required input is given in Table 5.

Table 6 Input for heatfluxes

Symbol	Description	Unit	Dimension
ra	aerodynamic resistance for heat	s m^{-1}	arbitrary
rs	surface resistance	s m^{-1}	arbitrary
Tc	surface temperature	°C	arbitrary
ea	vapour pressure above canopy	hPa	arbitrary
Ta	air temperature above canopy	°C	arbitrary
e_to_q	conversion from vapour pressure to absolute humidity	kg kg^{-1} hPa^{-1}	arbitrary
PSI	leaf or soil water potential	J kg^{-1}	arbitrary

Note: SCOPE_v1.2 uses PSI=0 for leaves, and a user defined, a priori value for PSI of the soil (see `parameters.m`). The value of PSI has a minor effect on H and lE. In theory, it is possible to include a pedotransfer function to calculate PSI of the soil from soil moisture content. This is not part of the current SCOPE model.

3.10 - Resistances

The function '`resistances`' calculates aerodynamic resistances, boundary and surface resistances for soil and vegetation according to Figure 4-1. The usage of resistance is as follows:

[ustar, raa, rawc, raws, rss, uz0, rai,rar, rac, rbc,rwc, rbs,rws, Kh] = resistances(u,L,LAI,rbs,rss,rwc,z0m,d,zr,h).

With:

$$r_{aa} = r_a^i + r_a^r + r_a^c$$
$$r_{awc} = r_w^c + r_b^c$$
$$r_{aws} = r_w^s + r_b^s$$

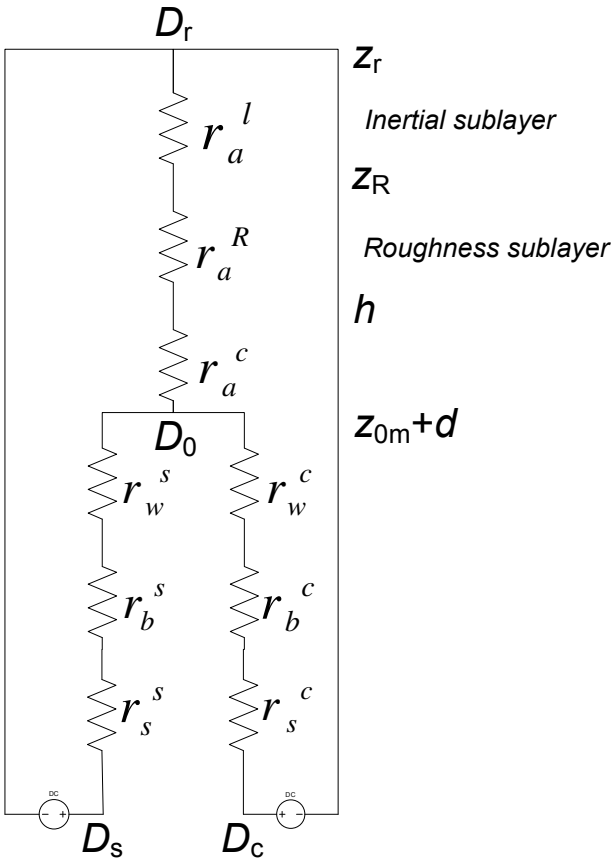

Figure 1. Schematic representation of the aerodynamic resistance model.

Table 7. Input of resistances

Symbol	Description	Unit	Dimension
u	windspeed	m s^{-1}	arbitrary
L	Monin-Obukhov length	m	arbitrary
LAI	Leaf Area Index	m^2 m^{-2}	arbitrary
rbs	Boundary Resistance of soil	s m^{-1}	arbitrary
rss	Surface resistance of soil for vapour transport	s m^{-1}	arbitrary
rwc	Within canopy Aerodynamic Resistance canopy	s m^{-1}	arbitrary

z0m	Roughness lenght for momentum for the vegetation	m	arbitrary
d	Displacement height (Zero plane)	m	arbitrary
zr	Measurement height	m	arbitrary
h	Vegetation height	m	arbitrary

Table 8. Output of resistances

Symbol	Description	Unit	Dimension
ustar	Friction velocity	m s^{-1}	arbitrary
raa	Aerodynamic resistance above the canopy	s m^{-1}	arbitrary
rawc	Total resistance within the canopy (canopy)	s m^{-1}	arbitrary
raws	Total resistance within the canopy (soil)	s m^{-1}	arbitrary
rai	Aerodynamic resistance in inertial sublayer	s m^{-1}	arbitrary
rar	Aerodynamic resistance in roughness sublayer	s m^{-1}	arbitrary
rac	Aerodynamic resistance in canopy layer (above z0+d)	s m^{-1}	arbitrary
rbc	Boundary layer resistance (canopy)	s m^{-1}	arbitrary
rwc	Aerodynamic Resistance within canopy(canopy)	s m^{-1}	arbitrary
rbs	Boundary layer resistance (soil)	s m^{-1}	arbitrary
rws	Aerodynamic resistance within canopy	s m^{-1}	arbitrary
rss	Surface resistance vapour transport	s m^{-1}	arbitrary
uz0	windspeed at z0	m s^{-1}	arbitrary
Kh	Diffusivity for heat	m^2 s^{-1}	arbitrary

3.11 Biochemical

The module `biochemical.m` calculates:

- Stomatal resistance at leaf (needle) level rsw (s m^{-1})
- Photosynthesis at leaf (needle) level A (µmol m^{-2} s^{-1})
- Fluorescence of a leaf (needle) as a fraction of that of an unstressed leaf at low irradiance F

The model is based on Van der Tol *et al*. (2009)

The use of biochemical is as follows:

function [A,F,rcw] = biochemical(C,Q,T,eb,O,p,option,gcmethod)

Table 9. Input for biochemical

Symbol	Description	Unit	Dimension
C	conc. of CO2 in leaf boundary layer	µmol m^{-3}	arbitrary
Q	net radiation, PAR	µmol m^{-2} s^{-1}	arbitrary
T	leaf temperature	°C or K	arbitrary
eb	vapour pressure in leaf boundary layer	hPa	arbitrary
O	concentration of O2	mmol m^{-3}	arbitrary
p	air pressure	Pa	arbitrary

Symbol	Description	Unit	Dimension
option	vegetation type, binary (1: C4, ~1: C3)		[1]
gcmethod	stomatal resistance model, binary (0: Leuning (1995), ~0: Cowan (1977)		[1]

Biochemical uses a number of globals, both from `constants.m` and from `parameters.m`.

The module can handle temperatures expressed in Kelvin and Celsius equally well. Input in Kelvin is automatically converted into Celsius. The range of input values is used to detect the unit. The module may confuse the units when erroneous data are provided with extremely high or low temperatures.

In SCOPE_v1.2, the temperature corrections of the parameters Vcmax, Jmax and Rdopt are switched off by default. They can easily be switched on by changing Line 119 into: `dT = T - Tref`.

3.12 Optional calculations

The module `optional_calculations.m` carries out the optional calculations options specified in `parameters`. They include the following:

- Vertical profiles of fluxes, absorbed PAR, temperature (option calcvertprofile)
- A spectrum of radiance in observation direction for the thermal part (option calcplanck)
- Chlorophyll fluorescence (option calcfluor)
- Spectra of radiance in many different observation directions (option calcdirectional)

The results of the calculations are stored in structures, with the following names: Vertical, Planck, Fluorescence and Directional. Tables 4.9 to 4.12 list the main variables stored in these structures.

Note: depending on the computing power, the model can be slow if all optional calculations are switched on at the same time.

Table 10. Content of structure Vertical

Symbol	Description	Unit	Dimension
Tc0	Temperature of shaded leaves	°C	[nl]
Tc11d	Temperature of sunlit leaves	°C	[nl]
Tc1d	Temperature of sunlit & shaded leaves	°C	[nl]
Hc1d	Sensible heat flux	W m^{-2}	[nl]
lEc1d	Latent heat flux	W m^{-2}	[nl]
A1d	Photosynthesis	µmol m^{-2} s^{-1}	[nl]
F_Pn1d	Product of aPAR and fluorescence factor	µmol m^{-2} s^{-1}	[nl]
Pn1d	aPAR	µmol m^{-2} s^{-1}	[nl]
Rn1d	Net radiation	W m^{-2}	[nl]

Table 11. Content of structure Planck

Symbol	Description	Unit	Dimension
wl	wavelength	µm	[nwl]
iwlt	index of thermal wavelengths		[nwlt]
Loutt_	Spectrum of hemispherical radiance	W m^{-2} $µm^{-1}$ sr^{-1}	[nwl]
Lot_	Spectrum of radiance in observation direction	W m^{-2} $µm^{-1}$ sr^{-1}	[nwl]
Tbright_	Brightness temperature in observation direction	°C	[nwl]

Table 12. Content of structure Fluorescence

Symbol	Description	Unit	Dimension
wl	wavelength	µm	[nwl]
iwlfi	index of incident PAR wavelengths		[nwli]
iwlfo	index of fluorescence wavelengths		[nwlo]
Lof_	Spectrum of radiance in observation direction	W m^{-2} μm^{-1} sr^{-1}	[nwl]

Table 13. Content of structure Directional

Symbol	Description	Unit	Dimension
wl	wavelength	µm	[nwl]
tts	solar zenith angle	degrees	[1]
tto	observer zenith angle	degees	[1]
psi	observer azimuth angle	degrees	[1]
iwlo	index of optical wavelengths		[nwlo]
iwlt	index of thermal wavelengths		[nwlt]
Lot	spectrally integrated thermal radiance in observation direction	W m^{-2} sr^{-1}	[1,noa]
Loo_	optical radiance in observation direction	W m^{-2} μm^{-1} sr^{-1}	[nwl.noa]
Lot_	thermal radiance in observation direction	W m^{-2} μm^{-1} sr^{-1}	[nwl.noa]
Lof_]	chlorophyll fluorescence radiance in observation direction	W m^{-2} μm^{-1} sr^{-1}	[nwl.noa]
brdf_	bi-directional reflectance in observation direction	μm^{-1}	[nwl.noa]

In tables 9-13, nwlt is the number of thermal wavelengths and nwlo the number of optical wavelengths, and noa the number of observation angles.

3.13 Output data

The module o`utput_data.m` saves the output of SCOPE in an output directory. In SCOPE, `output_data` is called after each calculation.

The data are stored in the following directory:

SiteName_yyyy-mm-dd-hh-mm

In which yyyy refers to the Julian year, mm to the month, dd the day, hh the hour and mm the minutes of the time when the simulation was started.

Table 14 shows the output files which are always created. Table 15 shows output files which are optionally created.

Table 14. Output files and their content. The columns in the output files refer to the variables in the table.

Filename	Variable	Description	Unit	Dim
fluxes.dat	timestep	time step counter		[nt]
	counter	number of iterations in energy balance		[nt]
	year	year		[nt]
	t	decimal DOY		[nt]
	Rntot	Total net radiation	W m^{-2}	[nt]
	lEtot	Total latent heat flux	W m^{-2}	[nt]
	Htot	Total sensible heat flux	W m^{-2}	[nt]

Filename	Variable	Description	Unit	Dim
	Rnctot	Net radiation of canopy	W m^{-2}	[nt]
	lEctot	Latent heat flux of canopy	W m^{-2}	[nt]
	Hctot	Sensible heat flux of canopy	W m^{-2}	[nt]
	Actot	Net photosynthesis of canopy	µmol m^{-2} s^{-1}	[nt]
	Rnstot	Net radiation of soil	W m^{-2}	[nt]
	lEstot	Latent heat flux of soil	W m^{-2}	[nt]
	Hstot	Sensible heat flux of soil	W m^{-2}	[nt]
	Gtot	Soil heat flux	W m^{-2}	[nt]
	Resp	Respiration rate	µmol m^{-2} s^{-1}	[nt]
	Pntot	absorbed PAR	µmol m^{-2} s^{-1}	[nt]
surftemp.dat	timestep	time step counter		[nt]
	year	year		[nt]
	t	decimal DOY		[nt]
	Ta	Air temperature above the canopy	°C	[nt]
	Tss(1)	Surface temperature of shaded soil	°C	[nt]
	Tss(2)	Surface temperature of sunlit soil	°C	[nt]
	Tcave	Average canopy temperature	°C	[nt]
	Tsave	Average soil temperature	°C	[nt]
aerodyn.dat	raa	total aerodynamic resistance above canopy	s m^{-1}	[nt]
	rawc	aerodynamic resistance below canopy for canopy	s m^{-1}	[nt]
	raws	aerodynamic resistance below canopy for soil	s m^{-1}	[nt]
	ustar	friction velocity	m s^{-1}	[nt]
radiation.dat	timestep	time step counter		[nt]
	year	year		[nt]
	t	decimal DOY		[nt]
	Louto	hemisph. outgoing radiation, shortwave (<2.5 µm)	W m^{-2}	[nt]
	Loutt	hemisph. outgoing radiation, long wave (>2.5 µm)	W m^{-2}	[nt]
	Lout	total hemispherical outgoing radiation	W m^{-2}	[nt]
fc.dat	Fc	fraction of shaded leaves, per layer		[nt,nl]
spectrum_hemis.dat	Lout_	hemispherical outgoing radiation	W m^{-2}	[nt,nwl]
spectrum_obsdir.dat	Lo_	outgoing radiance in observation direction	W m^{-2} sr^{-1}	[nt,nwl]
wl.dat	wl	wavelengths	µm	[nwl]

Table 15. Optional output files: for vertical profiles

File	Variable	Description	Unit	Dim
leaftemp	Tc11d', Tc0', Tc1d'	sunlit leaf temperature, shaded leaf temperature average leaf temperature	°C	[nt, 3 x nl]
layer_h	Hc1d', Hstot	sensible heat flux of leaf layers and soil	W m^{-2}	[nt, nl+1]
layer_le	lEc1d', lEstot	latent heat flux of leaf layers and soil	W m^{-2}	[nt, nl+1]
layer_a	A1d' Resp	photosynthesis of leaf layers and soil respiration	W m^{-2}	[nt, nl+1]
layer_f	F_Pn1d' 0	fluorescence of leaf layers (and soil)	µmol m^{-2} s^{-1}	[nt, nl+1]
layer_pn	Pn1d' 0	aPAR of leaf layers (and dummy for soil)		[nt, nl+1]
layer_rn	Rn1d' Rnstot	net radiation of leaf layers and soil	W m^{-2}	[nt, nl+1]

3.14 Plots

`Plots.m` is no more than an example of plots of the data. It is recommended to create one's own `plots`.

3.15 Other functions

SCOPE_v1.2 includes a number of smaller modules:

1. Brightness_T: is the inverse of Stefan-Boltzmann's equation for a black body
2. Calczenithangle: calculates the solar zenith angle from longitude, latitude and time of the day. In addition, the zenith angle relative to the surface slope can be calculated.
3. Constants: this file contains physical constants. The values are globals
4. Create_output_files: initializes the output files
5. Integration: integrates a quantity over leaf zenith and azimuth angles
6. Leafangles: calculates leaf angles from LIDFa and LIDFb
7. Planck_int: integrates Planck curve between two wavelengths
8. Satvap: calculates saturated vapour pressure deficit from air temperature
9. Soil_respiration: calculates soil respiration. Note: this script is not finished yet. Currently, soil respiration is an a-priori, fixed value of 0.5 umol m^{-2} s^{-1} per unit leaf area.
10. zo_and_d: calculates z0m and d from leaf area index and vegetation height according to Verhoef, McNaughton & Jacobs (1997), HESS 1, 81-91.

4. Input data format

The model is supplied with an example data set of the Speulderbos site in the Netherlands, collected during the EAGLE field campaign. This chapter explains how to work with the data, the directory structure and file types, etc. It is possible to add new datasets.

After unzipping the files, the directory 'data' can be found at the same hierarchal level as SCOPE_v1.2. It is possible to locate the data anywhere, as long as the location is indicated in `parameters.m`. The default directory structure of the data is as follows:

input
- dataset speulderbos
- directional
- fluormatrix
- prospect_parameters
- radiationdata
- soil_spectrum

measured
- dataset speulderbos

All data in directory 'input' are input files for SCOPE. All data in directory 'measured' are not input files, but validation data. They have been separated for reasons of transparency.

4.1 - Input data

4.1.2 Directory 'dataset *'

Dataset speulderbos contains time series of meteorological data. In this case, half-hourly data are provided. It is possible to work with any time interval, but due to the thermal inertia of the soil, the calculation of soil temperature may not be accurate when the time interval is longer than one hour.

It is recommended to name your own dataset '`dataset` sitename'.

The directory contains the following compulsory files (all in ASCII format):

- A time vector ('t_.dat'): a vertical array of time values, in decimal days of the year [1:366.99]. For example, 10 January 2009, 12:00 would be: 10.5. All other files (see below) should correspond to this time vector (and thus have the same size).
- A year vector ('year_.dat'): the year corresponding to the time vector. For example, 10 January 2009, 12:00 would be: 2009
- TOC incoming shortwave radiation ('Rin_.dat'): a broadband (0.4 to 2.5 µm) measurement of incoming shortwave radiation (W m^{-2}), perpendicular to the surface.
- TOC incoming long wave radiation ('Rli_.dat'): a broadband (2.5 to 50 µm) measurement of incoming long wave radiation (W m^{-2}), perpendicular to the surface.
- Air pressure ('p_.dat'): air pressure (hPa or mbar)
- Air temperature measured above the canopy ('Ta_'): Air temperature above the canopy in °C.
- Vapour pressure measured above the canopy (hPa or mbar).
- Wind speed ('u_.dat'): wind speed measured above the canopy (m s^{-1})

The following additional files (not compulsory) can be added:

- Carbon dioxide concentration measured above the canopy (mg m^{-3})

And the following tables (not compulsory):

- Leaf area index ('LAI_.dat')
- Measurement height ('z_.dat') (m)
- Vegetation height ('h_.dat') (m)
- Maximum carboxylation capacity (Table_Vcmax_.dat')
- Maximum electron transport capacity (Table_Jmax_.dat')

- Cowan's stomatal coefficient (Table_Lambda_.dat')

If a table is not present, then the corresponding a priori value specified in the `parameter` file is used instead. It is only useful to create the tables LAI_dat etc. if the leaf area index, measurement height, vegetation height etc. **change with time** during the measurement period.

A table has a slightly different format than the other input files. A table has two columns: the first column contains the decimal DOY, the second column contains the value of the variable. The reason why tables have a different format is that the variables in the table are usually not measured at the same time interval as the meteorological input. For example, the LAI may be measured only once per month.

An example of a table can be found in 'dataset speulderbos'.

The measurement height is only relevant for wind speed, vapour pressure and the carbon dioxide concentration. It is currently not possible to specify separate measurement heights for each of these variables.

The carbon dioxide concentration must be provided in mg m^{-3}. This is a commonly used unit in most data sets. SCOPE automatically converts this to ppm and to umol m^{-3} internally. If the carbon dioxide concentration file is not provided, SCOPE assumes a constant concentration corresponding to 380 ppm.

Note: it is important that all files have equal length, and that all measurements correspond to the time vector. A Julian calendar is used. The time should be that of the nearest 15-degree interval of the median, excluding daylight saving hour. Input files should be comma separated, space separated or tab separated ASCII files. They should not contain empty lines or comment lines.

4.1.3 Directory 'directional'

De input in the directory 'directional' is only used for multi-angle simulations (if the option 'directional' is switched on in `parameters`. In this directory one can provide the observer's zenith and azimuth angles. The files in this directory have two columns: the first column is the observer's zenith angle, the second the observer's azimuth (relative to that of the sun, counterclockwise), both in degrees. If the option 'directional' is switched on, SCOPE will calculate the radiance spectrum in all directions given in the input file.

4.1.4 Directory 'fluormatrix'

In this directory, two fluorescence input-output matrices should be given with a size 351 x 211, one for the upper side and one for the lower side of a leaf. The matrices represent the fluorescence response to irradiance. The 351 rows indicate the irradiance wavelength between 400 and 750 µm, the 211 columns the corresponding response between 640 and 850 µm. The unit is (W m^{-2} μm^{-1} sr^{-1}) / (W m^{-2} sr^{-1}).

In future versions of SCOPE, it will not be necessary to provide the spectra as input. The calculation of the spectra will be incorporated in the model.

4.1.5 The directory 'Prospect_parameters'

In this directory, absorption spectra of different leaf components are provided, according to PROSPECT 3.1.

4.1.6 The directory 'radiationdata'

In this directory, the input spectrum of solar and sky radiation is provided. The data have been calculated with MODTRAN4. The ASCII file in this directory consists of three columns containing the following. The first column contains the wavelength in nm, the second column the solar radiation in W m^{-2} μm^{-1}, and the third column the sky radiation in W m^{-2} μm^{-1}.

Only one input spectrum is present currently. Note that in the input data (Section 5.1.1), the broadband input radiation is provided. SCOPE linearly scales the input spectra of the optical and the thermal domain in such a way, that the spectrally integrated input shortwave and long wave radiation matches with the measured values. A limitation of this approach is that the same *shape* of the input spectrum is used independent on the atmospheric conditions.

4.1.7 The directory 'soil_spectrum'

In this directory, the soil spectrum is provided. The ASCII file in this directory consists of two columns containing the following: The first column contains the wavelength in µm, the second column the reflectance as a percentage of irradiance.

4.2 - Validation data

The validation data are stored in directory 'measured'. It is up to the user to organize this directory. In the example dataset, the files are provided in the same format as the input files (same size, same time intervals, etc.). This makes it easier to plot modelled versus measured data. The validation data are only used in the function '`plots.m`'. The validation data are optional, and they are not used by '`ebal.m`'.

10.6. Appendix 6 : Appendix to Chapter 7

10.6.1. Avignon crop datasets

The Avignon 'crane' site ('Flux and Remote Sensing Observation Site') has been set up at the INRA Research Center near Avignon, France for acquiring data helping in elaborating and testing crop models, soil-vegetation-atmosphere transfer models, procedures to estimate crop and soil biophysical variables from remote sensing data and procedures to assimilate remote sensing data into crop and SVAT models. It is located at N 43° 55' 00"; E 4° 52' 47" (center of the crane railway). A continuous monitoring of crop and soil processes is performed over a 1.8 ha flat agricultural field, including energy balance, H_2O and CO_2 surface-atmosphere exchanges, crop structure and biomass, soil moisture and temperature, agricultural interventions, surface temperature and canopy reflectances. Data have been acquired since 1998 and the site has been included in the CARBOEUROPE-IP network since 2004. A crane (21 m high) makes it possible to operate heavy remote sensing system along a 120 m transect. Instruments such as the MIRAS interferometric radiometer in 1999, in preparation of the SMOS mission, were set on the crane (Bayle et al. 2002). Starting in spring 2008, a new version of the AIRFLEX sensor (Moya et al. 2006) has been installed for monitoring crop solar induced fluorescence along the crop season (I.Moya's LMD team). The region is characterized by a typical Mediterranean climate. The crops were grown on a silty clay loam soil. Irrigation is performed when required using an irrigation ramp assuring a complete coverage of the field in 8 hours with a very good homogeneity.

In the present study we have selected the period from October 2005 to October 2007 covering two consecutive crop cycles: a C3 crop, wheat, in 2005-2006 and a C4 crop, sorghum, in 2007. The main characteristics of both crop cycles are given in Table A- 1.

Table A- 1. Main characteristics of the two crop cycles used in this study.

	Wheat		Sorghum	
Cultivar	Durum wheat, Acalou		Solarium	
Sowing	27 October 2005		10 May 2007	
Harvest	26 June 2006		16 October 2007	
Previous crop	Peas		Durum wheat	
Irrigation	22/05/06	20 mm	16/05/07 21/05/07 25/05/07	20 mm 20 mm 20 mm
Fertilization	Yes (twice 66 qN/ha)			
Yield	45 to 60 q/ha		52 q/ha	

10.6.2. Measurements

Micrometeorological measurements

Incident radiations and other meteorological variables were recorded on field as half-hourly average using the instruments described in Table A- 2. An adjacent meteorological station from the INRA-Agroclim network (http://www.avignon.inra.fr/agroclim) was used to gap-fill data when missing data occurred. This occurred for less than 0.5 % of the data when vegetation was present. Specific procedures for checking the validity of the recorded data were used (cross-checking data from several instruments, comparison to standard and statistical models). Careful calibrations of the instruments were performed, using several calibration laboratories after linking the reference instruments to international standard: INRA calibration laboratory (Ta, Tsol, RH), Météo-France radiometric center, and other accredited companies.

Energy balance measurements were performed using the instruments described in Table A- 2. As the field size was not very large (1.8 ha), the positions for eddy-covariance measurements were optimized in order to reduce effects of advection by considering the directions of major wind regimes and by setting the instruments around 1 meter above the canopy top. A footprint analysis indicated that 90% of the fluxes originated from the field, accounting for more than 90% of the data acquired in diurnal conditions (Hsieh et al. 2000). At night, because of the stable conditions, footprints were often larger than the field (60% of the data). However, less than 15% of the cumulated latent heat fluxes in the flux data did not originate from the field. Sensible heat flux, latent heat flux and CO_2 flux were computed from the sonic anemometer and the open-path analyser measurements using the Eddy-covariance calculation methodology proposed by CARBOEUROPE-IP (e.g. Aubinet et al. 1999; see http://www.bgc-jena.mpg.de/bgc-processes/ceip/products/files/Grasslands-Guidelines-v2.doc). We used the EDIRE software (University of Edinburgh, Scotland; see: http://www.geos.ed.ac.uk/abs/research/micromet/EdiRe/). Due to the low setting height of the eddy-correlation system, a careful analysis for the capture of very high frequency and low frequency signals was performed. Filtering and gap-filling were realized using the ECPP software (Eddy Covariance Post Processing, Pierre Béziat, CESBIO, Toulouse, France). Ground heat flux was computed from the measurements by the ground heat flux sensors set at 5 cm depth in the soil and a correction factor accounting for heat storage in the soil layer between the surface and the sensors. Soil temperature and soil moisture measured in this layer were used to compute the correction term.

Meteorological fields and energy fluxes

Atmospheric measurements performed during the considered period (only for the wheat cycle for the fluxes) are presented in Figures (Figure A- 1 and Figure A- 2).

Table A- 2. Characteristics of the micrometeorological instruments used in Avignon on the 'flux and remote sensing observation site.

Variable	Symbol	Instrument	Company and Model	setting height	Calibration / processing software
Incident solar radiation	Rg	Pyranometer	Kipp& Zonen CMP21		Linked to Météo-France standard
Incident longwave radiation	Ra	Pyrgeometer	Kipp& Zonen CG4		Linked to Météo-France standard
Air temperature	Ta	Platinium probe	Vaisala HMP35D	2 m above canopy top	Calibrated at INRA linked to AOIP[1] standard
Air relative humidity	HR	Capacitive probe	Vaisala HMP35D	2 m above canopy top	Calibrated at INRA linked to CETIAT[2] standard
Horizontal wind speed	Ua	Cup anemometer	Vector Inst. A100L2	2 m above canopy top	Maintained to optimal
Atmospheric pressure	Pa	Barometer	Vaisala PTB101B		Calibrated at Mesura Engineering[3]
Rain	RR	Rain gauge			AGROCLIM network
Sol temperature	Tsol		PT100	2 sensors at soil surface, 2 sensors at 2.5 cm 1 sensor at 5 cm	Calibrated at INRA linked to AOIP standard
Surface soil moisture	Wg	Capacitive probe	Decagon EC-H2O10	3 sensors integrating the 0-5 cm top soil layer	Compared to gravimetric sampling
Sensible heat flux	H	Sonic anemometer	Young 81000	1 m above canopy top	Original manufacturer setting
CO_2 and H_2O atmospheric concentration	$[CO_2]$ $[H_2O]$	Open-path analyser	LI-Cor LI7500	1 m above canopy top	Original manufacturer setting + test against standard gas bottle
Ground heat flux	G	Heat flux sensor	REBS HFT-3	4 replications at 5 cm depth	Original manufacturer setting
Net radiation	Rn	pyradiometer	Kipp& Zonen CNR1	1.5 – 2 m above canopy top	At manufacturer every two years and against CMP21 and CG4 sensors

[1] AOIP: company furnishing instruments, accredited for thermometer calibration by COFRAC (COmité FRançais d'Accréditation).

[2] CETIAT: Centre Technique des Industries Aérauliques et Thermiques, accredited for hygrometer calibration by COFRAC

[3] Mesura Engineering: engineering company in metrology and maintenance (not accredited at the time of calibration)

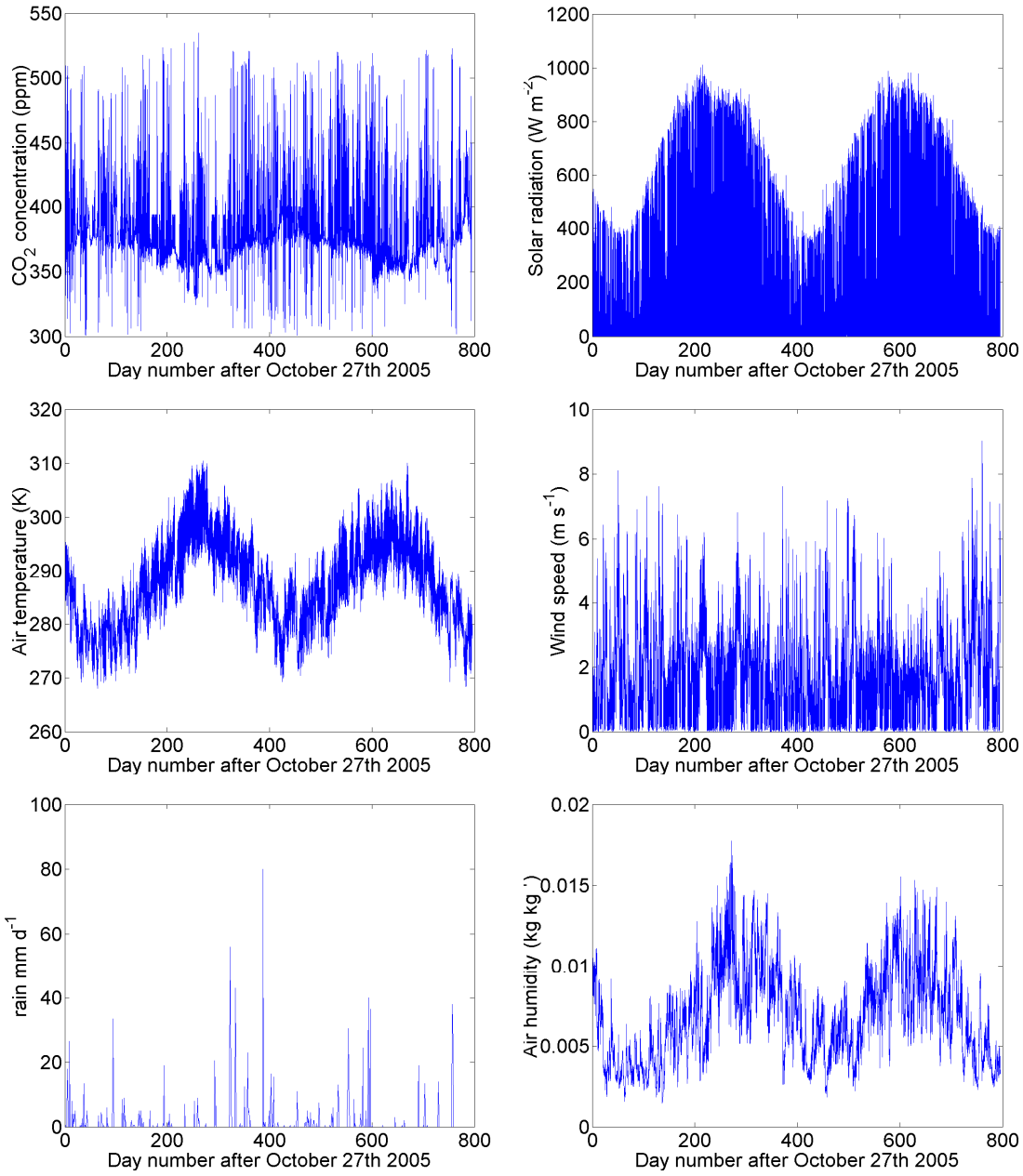

Figure A- 1. Evolution of atmospheric variables during the wheat and the sorghum crop cycles

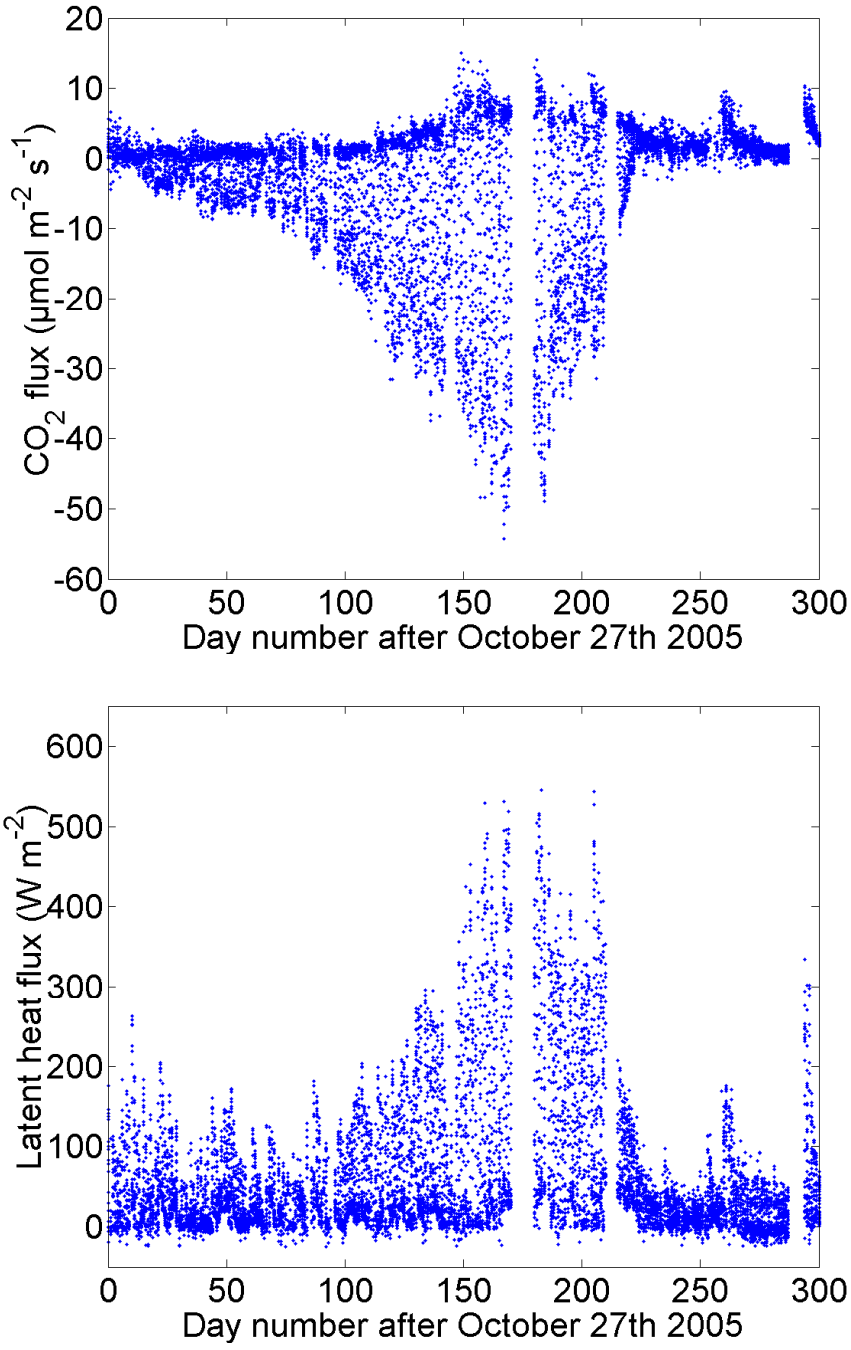

Figure A- 2. Evolution of CO_2 and H_2O surface – atmosphere exchanges along the wheat crop cycle.

Plant and soil measurements:

LAI was measured several times along the crop cycle using a LICOR 3000 planimeter and hemispherical photographs processed with the Can-Eye software (developed at INRA Avignon, see http://www.avignon.inra.fr/can_eye/). Vegetation height (hc) was estimated almost once a week as the average height of 15 individual plants. Biomass was measured every month. Three to six samples of 0.25 m^2 size were cut in the field. The samples were weighted after being dried for 48 hours at 80°C in a ventilated drying oven. Plant nitrogen content was measured at some occasions (above ground parts only) and leaf nitrogen content estimated by assuming a nitrogen ration of 0.33 between stems and leaves.

Soil moisture was measured every week with three replicates using a neutron probe from 0.2 m to 1.80 m depth in the soil. These measurements were complemented by collecting surface measurements using Decagon EC-H2O10 sensors set vertically in the soil between 0 and 5 cm depth.

Vegetation measurements (interpolated LAI), interpolated soil moisture measurements (down to 1.3 m) and leaf nitrogen related variables are presented in figures Figure A- 3 and Figure A- 4.

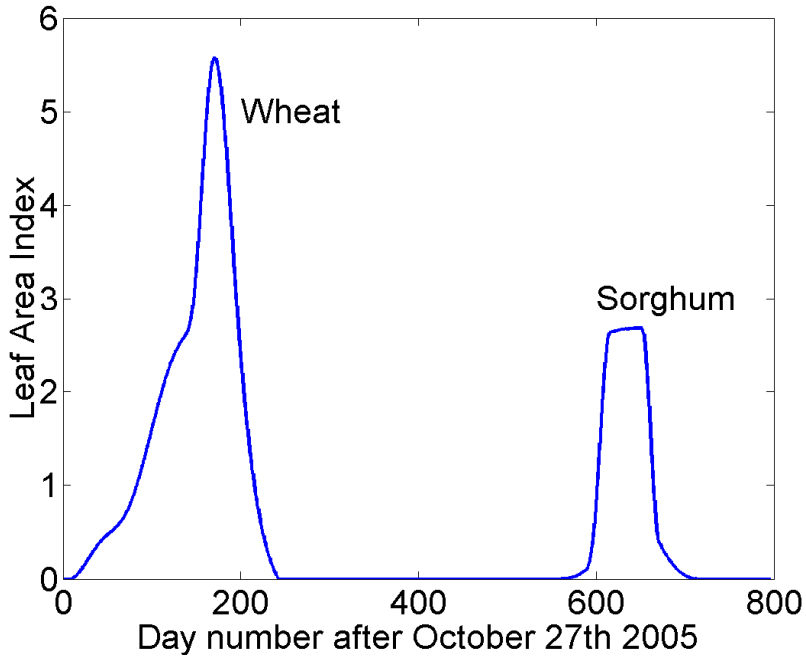

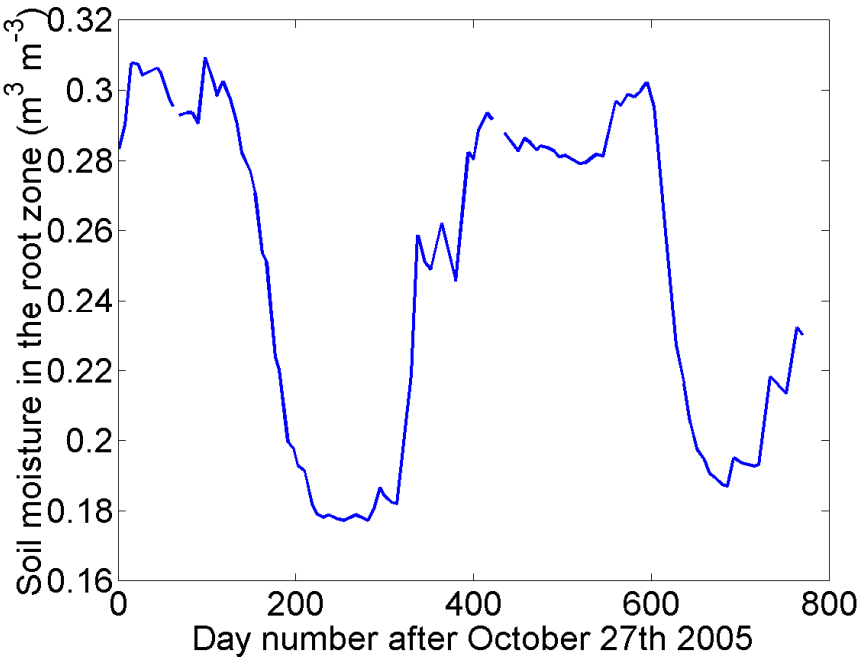

Figure A- 3. Evolution of LAI and soil moisture in the root zone (down to 1.3 m).

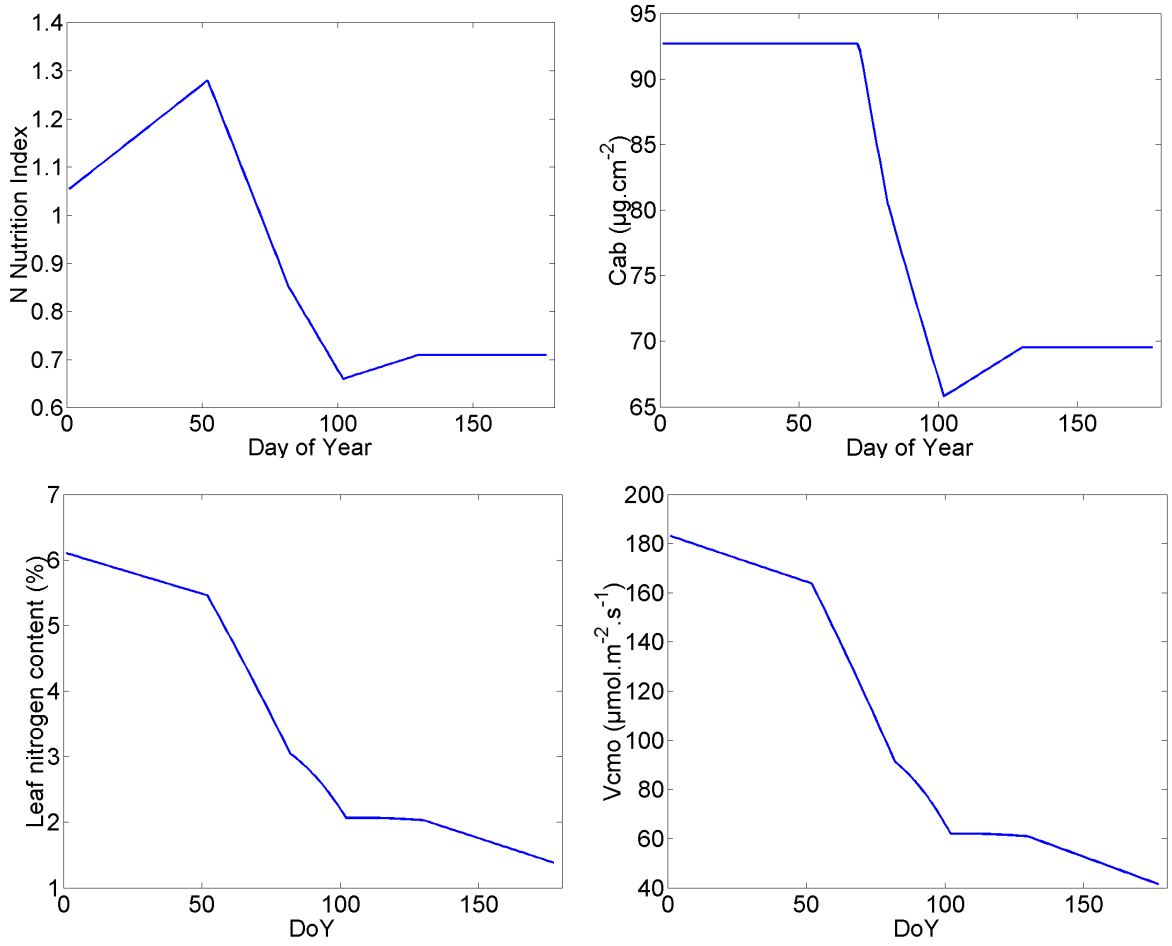

Figure A- 4. Evolution of leaf nitrogen related variables, as computed with Eq. 7.1. & 7.3; leaf nitrogen content was derived from plant nitrogen content using an allometric relationship with biomass.